

Distribution Agreement

In presenting this thesis or dissertation as a partial fulfillment of the requirements for an advanced degree from Emory University, I hereby grant to Emory University and its agents the non-exclusive license to archive, make accessible, and display my thesis or dissertation in whole or in part in all forms of media, now or hereafter known, including display on the world-wide web. I understand that I may select some access restrictions as part of the online submission of this thesis or dissertation. I retain all ownership rights to the copyright of the thesis or dissertation. I also retain the right to use in future works (such as articles or books) all or part of this thesis or dissertation.

Signature:

Travis Michael Rotterman

Date

The role of neuroinflammation in motor circuit synaptic plasticity within the spinal cord
following peripheral nerve injury

By

Travis Michael Rotterman
Doctor of Philosophy

Graduate Division of Biological and Biomedical Science
Neuroscience

Francisco J. Alvarez, Ph.D.
Advisor

Arthur English, Ph.D.
Committee Member

Shawn Hochman, Ph.D.
Committee Member

Malú G. Tansey, Ph.D.
Committee Member

Timothy C. Cope, Ph.D.
Committee Member

Peter Wenner, Ph.D.
Committee Member

Accepted:

Lisa A. Tedesco, Ph.D.
Dean of the James T. Laney School of Graduate Studies

Date

The role of neuroinflammation in motor circuit synaptic plasticity within the spinal
cord following peripheral nerve injury

By

Travis M. Rotterman
B.S., Wright State University, 2010

Advisor: Francisco J. Alvarez, Ph.D.

An abstract of a dissertation submitted to the Faculty of the James T. Laney
School of Graduate Studies of Emory University in partial fulfillment of the
requirements for the degree of Doctor of Philosophy in Neuroscience
2018

The role of neuroinflammation in motor circuit synaptic plasticity within the spinal
cord following peripheral nerve injury

By

Travis Michael Rotterman

Information regarding limb position is transmitted through Ia afferents and is integrated into spinal circuit networks to modulate motor output in response to environmental perturbations. However, following peripheral nerve injuries, a neuroinflammatory response occurs in the ventral horn that coincides with Ia afferent synapse degradation. The outcome after nerve regeneration depends on the type of injury; nerve transection causes permanent loss of Ia synapses and the reflex, while both recover after nerve crush. Our goal was to find causal relationships between spinal neuroinflammation and Ia synaptic losses. We further hypothesized that modulation of neuroinflammation properties could adjust synaptic plasticity to various levels according to injury severity. To test these hypotheses, we performed different types of nerve injuries in transgenic mouse models that allowed us to study resident microglia activation (CX3CR1-GFP mice) and infiltration of peripheral CCR2-expressing macrophages (CCR2-RFP mice), combined with various global and cell-specific knockout models to investigate signaling pathways that triggered the immune response and their relation to Ia synapse loss. Sciatic nerve transection results in long-lasting microglia activation and differentiation towards CCL2-releasing, pro-inflammatory phenotypes. This did not occur after sciatic nerve crush. Only after transection was there significant infiltration of CD45/CCR2 cells, including T-cells, monocyte/macrophages, and dendritic cells. CCL2-CCR2 signaling was especially critical for monocyte infiltration, some of which appear to transform into microglia-like cells by morphology and genetic lineage labeling. Lack of these cells in CCR2 global KOs correlated with better preservation of ventral horn Ia synapses after nerve transection. Moreover, CCR2 cell entry is graded to the location of injury with injuries to more distal nerves causing less CCR2 infiltration and less Ia synapse plasticity. In conclusion, promoting CCR2+ monocyte infiltration amplifies Ia synapse losses, and the properties of spinal neuroinflammation after different nerve injuries is under fine control by signaling between axotomized MNs, microglia and penetrating blood-derived CCR2+ immune cells.

The role of neuroinflammation in motor circuit synaptic plasticity within the spinal
cord following peripheral nerve injury

By

Travis M. Rotterman
B.S., Wright State University, 2010

Advisor: Francisco J. Alvarez, Ph.D.

A dissertation submitted to the Faculty of the James T. Laney School of
Graduate Studies of Emory University in partial fulfillment of the requirements for
the degree of Doctor of Philosophy in Neuroscience
2018

Table of Contents

<u>Chapter 1: Introduction to spinal cord circuitry and plasticity following peripheral nerve injury</u>	1
1.1 Introduction.....	2
1.2 Organization and function of spinal cord motor circuitry	3
1.2.1 Motoneurons.....	3
1.2.2 Ia afferent connections.....	7
1.2.3 Stretch reflex and reciprocal inhibition.....	11
1.3 Peripheral nerve injury.....	14
1.3.1 Type and prevalence of nerve injuries.....	16
1.3.2 Peripheral degeneration and reinnervation.....	19
1.3.3 Clinical intervention and patient outcomes.....	24
1.3.4 Functional deficits in the Ia stretch circuit.....	28
1.4 Synaptic stripping vs axon retraction and transganglionic anterograde degeneration of sensory afferents injured in the periphery.....	35
1.4.1 History of synaptic stripping.....	37
1.4.2 Evidence of anterograde transganglionic degeneration of sensory axons and synapses after PNI.....	39
1.4.3 Mechanisms involved.....	44
1.5 Neuroinflammation.....	51
1.5.1 Microglia.....	53
1.5.2 Macrophage recruitment and infiltration into the CNS.....	63
1.5.3 Role of macrophages/microglia in synaptic stripping and retraction.....	68
1.5.4 Astrocytes.....	71
1.5.5 T-cells in PNI.....	75
1.6 Dissertation overview.....	76
References.....	83

<u>Chapter 2: Normal distribution of VGLUT1 synapses on spinal motoneuron dendrites and their reorganization after nerve injury</u>	104
2.1 Abstract.....	105
2.2 Introduction.....	106
2.3 Methods.....	108
2.3.1 Peripheral nerve transection and repair.....	108
2.3.2 Electrophysiology.....	110
2.3.3 Histological processing and immunohistochemistry.....	111
2.3.4 Confocal imaging and neuron reconstruction.....	113
2.3.5 Neuron reconstructions.....	114
2.3.6 Analyses.....	114
2.3.7 Statistics.....	117
2.4 Results.....	117
2.4.1 Basic physiological and morphological properties do not differ between control and regenerated motoneurons.....	117
2.4.2 VGLUT1-IR synapses are lost in injured and regenerated MG motoneurons.....	121
2.4.3 VGLUT1 contacts accumulate on proximal dendrites.....	123
2.4.4 Proximal VGLUT1 contacts are preferentially lost after nerve injury.....	125
2.4.5 VGLUT1 contact groupings are dispersed after peripheral nerve injury.....	128
2.4.6 VGLUT1-IR contacts show a preference for dendrite territories located dorso-medially with respect to the cell body and this preferred location becomes more apparent after injury.....	130
2.5 Discussion.....	134
2.5.1 VGLUT1 synapses concentrate in proximal dendrites.....	134
2.5.2 Significance of VGLUT1 synapses remaining after nerve injury.....	136
2.5.3 Relationship between synaptic reorganization and Ia afferent input strength.....	138
References.....	165

<u>Chapter 3: Motor circuit synaptic plasticity after peripheral nerve injury depends on a central neuroinflammatory response and a CCR2 mechanism</u>	169
3.1 Abstract.....	170
3.2 Introduction.....	171
3.3 Methods.....	173
3.3.1 Transgenic models.....	174
3.3.2 Motoneuron labeling and peripheral nerve injury procedures.....	176
3.3.3 Harvesting tissue for histological analysis.....	178
3.3.4 Histological processing and immunohistochemistry.....	178
3.3.5 Densitometric analysis of VGLUT1 and GFP fluorescence.....	180
3.3.6 Analysis of VGLUT1 synaptic bouton densities on motoneurons.....	180
3.3.7 Quantification of microglia cells.....	181
3.3.8 Microglia morphological analysis.....	182
3.3.9 Motoneuron cell body coverage by microglia cell processes.....	182
3.3.10 RFP cell quantification.....	183
3.3.11 Quantification of Iba1 cells after injury that are not derived from resident microglia.....	183
3.3.12 Analysis of CCL2 expression inside the spinal cord after nerve injuries.....	184
3.3.13 Statistical analysis for histological analyses.....	185
3.3.14 Peripheral blood mononuclear cell (PBMC) isolation and spinal cord tissue dissociation for myeloid cell analysis.....	187
3.3.15 Flow cytometry.....	188
3.4 Results.....	189
3.4.1 Animal model and experimental design.....	189
3.4.2 VGLUT1 synapse depletions on motoneurons following tibial or sciatic nerve injury in mice.....	192
3.4.3 Microglia responses differ between tibial and sciatic nerve injuries.....	197

3.4.4 Microglia undergo similar morphological changes after sciatic or tibial nerve injuries but become more tightly associated to motoneuron cell bodies after sciatic injuries.....	199
3.4.5 The number of CCR2-RFP+ cells infiltrating the spinal cord ventral horn depends on the type of injury and is tightly correlated to overall VGLUT1 loss.....	201
3.4.6 Heterogeneity of CCR2+ cells infiltrating the spinal cord after nerve injury.....	203
3.4.7 Flow cytometry characterization of CCR2+ cells.....	206
3.4.8 VGLUT1 synapses are preserved on motoneuron dendrites of CCR2 knockout mice.....	209
3.4.9 CCL2 is upregulated inside the spinal cord by axotomized motoneurons and activated microglia but with different time courses.....	212
3.5 Discussion.....	213
3.5.1 Different mechanisms control plasticity of VGLUT1 synapses on dendrites and cell bodies of motoneurons and the role of microglia.....	214
3.5.2 CCR2 monocyte entry is critical for VGLUT1 synapse plasticity.....	217
References.....	248

Chapter 4: The effect of axon regeneration efficiency in spinal motor circuit plasticity following peripheral nerve injury and the role neuroinflammation plays.....

4.1 Abstract.....	257
4.2 Introduction.....	258
4.3 Methods.....	261
4.3.1 Transgenic mouse models.....	261
4.3.2 Motoneuron labeling and peripheral nerve injury procedures.....	262
4.3.3 Harvesting tissue for histological analysis.....	263
4.3.4 Histological processing and immunohistochemistry.....	264
4.3.5 Densitometric analysis of VGLUT1 and GFP immunofluorescence.....	265

4.3.6 Neuromuscular junction analysis.....	266
4.3.7 Motoneuron reinnervation.....	266
4.3.8 Edu injections and Ki-67 labeling.....	267
4.3.9 Quantification of microglia cells.....	268
4.3.10 CCR2-RFP cell quantification.....	269
4.3.11 Experimental design and statistical analysis.....	269
4.4 Results.....	270
4.4.1 VGLUT1 synapse depletion on motoneurons following sciatic nerve cut-repair or sciatic nerve crush.....	270
4.4.2 Rate and specificity of peripheral nerve regeneration and reinnervation predict the permanency of VGLUT1 loss.....	274
4.4.3 The activation and proliferation of microglia cells in the ventral horn of the spinal cord after nerve injury.....	278
4.4.4 The release of CCL2 and the recruitment of peripheral CCR2+ myeloid cells following sciatic injury.....	281
4.5 Discussion.....	283
4.5.1 Success of peripheral regeneration determines permanency of VGLUT1 loss.....	283
4.5.2 CCL2 release from microglia results in a robust infiltration of peripheral CD45+ cells.....	286
References.....	305

Chapter 5: General Discussion and Future Directions.....309

5.1 Discussion.....	310
5.1.1 Distribution of VGLUT1 synapses on motoneurons and their permanent loss after nerve injury.....	312
5.1.2 The permanent removal of Ia afferents is dependent on CCR2 mechanisms.....	316
5.1.3 The importance of peripheral nerve regeneration efficiency and the permanency of Ia synaptic loss.....	321
5.2 Future directions.....	324
5.2.1 CCL2 Removal from MNs and microglia.....	324
5.2.2 Microglia activation by CSF1.....	325
5.2.3 CCR2 lineage tracing experiments.....	327

5.2.4 Live cell imaging.....	327
5.2.5 Physiology.....	328
References.....	331

Appendix I- VGLUT1 synapses and p-boutons on regenerating

<u>motoneurons after nerve crush.....</u>	335
6.1 Abstract.....	336
6.2 Introduction.....	337
6.3 Methods.....	342
6.3.1 Nerve injury and injections of retrograde tracers.....	342
6.3.2 Histology and immunocytochemistry.....	343
6.3.3 Antibody characterization.....	344
6.3.4 Confocal imaging and neuron reconstruction.....	345
6.3.5 Surface-to-surface analysis.....	346
6.3.6 Statistical analyses.....	347
6.3.7 Figure composition.....	347
6.4 Results.....	348
6.4.1 Technical considerations and data interpretation.....	348
6.4.2 Nerve crush causes only a small loss of VGLUT1 contacts on proximal dendrites and cell bodies of regenerating motoneuron.....	350
6.4.3 Reduction in P-bouton coverage of VGLUT1 boutons following nerve crush.....	354
6.5 Discussion.....	358
6.5.1 Differences in stretch reflex synaptic circuit plasticity after different kinds of nerve injury.....	359
6.5.2 Presynaptic inhibition of Ia afferents after nerve crush injuries.....	362
References.....	380

<u>Appendix II- Two-photon live imaging of microglia dynamics after nerve injury in an adult spinal cord slice</u>	384
7.1 Abstract.....	385
7.2 Introduction.....	386
7.3 Methods.....	389
7.3.1 Animals.....	389
7.3.2 Injury model.....	390
7.3.3 aCSF preparation.....	390
7.3.4 Spinal cord dissection.....	391
7.3.5 Sectioning.....	391
7.3.6 Imaging parameters.....	392
7.3.7 Analysis.....	393
7.3.8 Statistics.....	394
7.3.9 Tips and tricks.....	394
7.4 Results.....	394
7.5 Discussion.....	398
References.....	408

Figure Index

Table 1.1: Medical research council grading system.....	80
Table 1.2: Antibodies for microglia detection.....	81
Figure 1.1: Summary model.....	79
Figure 1.2: Complement expression around axotomized MNs.....	82

Table 2.1: Electrical properties of control and regenerated motoneurons.....	140
Table 2.2: Morphological properties of the cell bodies and dendritic arbors.....	141
Table 2.3: COM coordinates of VGLUT1-IR synaptic distributions and random synaptic distributions.....	142
Figure 2.1: Control and regenerated medial gastrocnemius (MG) motoneurons (MNs) one year after nerve injury display similar general electrophysiological and morphological characteristics.....	143
Figure 2.2: VGLUT1-IR contacts on cell bodies and different proximo-distal segments of dendrites.....	146
Figure 2.3: VGLUT1-IR contacts on MN dendrites display the active zone markers Bassoon.....	149
Figure 2.4: VGLUT1-IR synapses are lost along the dendrites of injured MNs; they also become de-clustered and more homogeneously distributed.....	151
Figure 2.5: Quantification of VGLUT1-IR contact proximo-distal distribution in control and regenerated MNs.....	153
Figure 2.6: Sholl analyses also reveals a proximal bias in VGLUT1-IR contacts in control MNs and a preferential loss of proximal synapses in regenerated MNs...	157
Figure 2.7: Center of Mass Analyses reveal a preferential loss of VGLUT1-IR in ventrolateral quadrants of the dendritic trees.....	160
Figure 2.8: The COM of VGLUT1-IR synaptic distributions moves to dorso-medial positions in regenerated MNs.....	163

Table 3.1: Transgenic mice.....	222
Table 3.2: Antibodies used for immunohistochemistry.....	223
Table 3.3: Morphological characteristics of reconstructed motoneurons and VGLUT1 numbers.....	224
Table 3.4: Sholl analysis.....	225

Figure 3.1: Peripheral nerve injury experimental design and mouse model	226
Figure 3.2: Permanent VGLUT1 synaptic loss on motoneurons after nerve injury	228
Figure 3.3: Microglia activation around injured motoneurons.....	231
Figure 3.4: Microglia morphological changes around axotomized motoneurons	234
Figure 3.5: CCR2+ cells infiltrate the ventral horn of the spinal cord after nerve injury.....	237
Figure 3.6: Heterogeneity of CCR2-RFP+ cells infiltrating the spinal cord ventral horn.....	239
Figure 3.7: Flow cytometry analysis of CCR2+ cells inside the spinal cord and in the blood in CCR2 hets and CCR2 KOs 21 days after bilateral sciatic nerve injuries.....	242
Figure 3.8: Microgliosis, CCR2-RFP cells and VGLUT1 synapses in CCR2 KOs after injury and sources of CCL2 within the spinal cord.....	245
<hr/>	
Table 4.1: Antibodies used for immunohistochemistry.....	289
Figure 4.1: VGLUT1 synapses recover following a sciatic nerve crush but are permanently removed following a sciatic nerve cut.....	290
Figure 4.2: Motor axons regenerate faster after a SC compared to a SR injury.....	294
Figure 4.3: Motor axons regenerate with greater specificity after a SC compared to a SR injury.....	297
Figure 4.4: The microglial response in the ventral horn is longer following sciatic nerve cut compared to crush.....	300
Figure 4.5: CCR2-RFP+ cells infiltrate the ventral horn following SR and are recruited by CCL2 release from microglia.....	303
<hr/>	
Figure 5.1: Mechanism of synaptic removal following a sciatic nerve cut.....	329
Figure 5.2: Mechanism for the recovery of synaptic inputs following a nerve crush.....	330

Table 6.1: Primary antibody characterization.....	366
Table 6.2: Somatic and dendritic surfaces in CTb-labeled MG motoneurons...	367
Table 6.3: VGLUT1 boutons analyzed and percentage coverage by GAD65 P-boutons.....	368
Figure 6.1: VGLUT1 inputs in control and regenerating motoneurons.....	369
Figure 6.2: VGLUT1 synaptic density on the surface of control and regenerating motoneuron cell bodies.....	371
Figure 6.3: VGLUT1 synaptic densities on control and regenerating motoneuron dendrites.....	373
Figure 6.4: Presynaptic GAD65 P-boutons on VGLUT1 bouton contacts on retrogradely labeled motoneurons.....	375
Figure 6.5: Coverage of VGLUT1 boutons by GAD65 P-boutons.....	378

Figure 7.1: Imaging and quantification of microglia dynamics in an adult spinal cord slice preparation using two photon microscopy.....	400
Figure 7.2: Microglia interactions with axotomized motoneurons (MNs) and sensory Ia afferent axons/synapses in the ventral horn of the spinal cord.....	402
Supplemental table 7.1: The artificial cerebral spinal fluid (aCSF) recipe.....	405
Supplemental figure 7.1: Spinal cord quality control experiment.....	406

Chapter 1:

Introduction to spinal cord circuitry and plasticity following peripheral nerve injury

1.1 Introduction

Every single year millions of individuals suffer from nerve injuries, ranging from a simple crush to complete transections in which the nerve is entirely severed. These injuries can be sustained from traumatic events including automobile accidents, sports injuries, surgical errors, or war. Nerve injuries cause axotomy of both sensory and motor axons. Interestingly, in the peripheral nerve, these axons have the capacity to regenerate given the right conditions. However, axon guidance cues that allow these axons to find their targets during development are not present in adults resulting in axon misdirection and inefficient reinnervation in the periphery. Patients are left with sensory abnormalities, including pain, and significant motor dysfunction. We will focus on the motor aspects. Deficits in regeneration are frequently cited to be the cause of poor recovery of motor function in patients. However, years of accumulating evidence, including the work in this document, have found that reorganization of essential spinal motor circuits can at least partially explain these abnormalities. These spinal motor circuits are not “hardwired” but undergo plasticity following nerve injury ultimately resulting in abnormal motor control. The changes we will focus on explicitly relate to the permanent loss of proprioceptive Ia afferent inputs into the ventral horn and that is manifested by a loss of stretch reflexes, inter-joint discoordination, and muscle co-contraction, all of which impair and disrupt normal daily activities. In this thesis, we will characterize in detail the loss of this input over the dendritic arbor of motoneurons (Chapter 1). Then we will examine potential mechanisms that trigger spinal circuit plasticity, more specifically the role neuroinflammation plays in this

process (Chapter 2). Finally, we will compare nerve lesions with better or worse outcomes in regeneration efficiency and specificity and compare their differences in central spinal cord neuroinflammation resulting in different levels of Ia afferent input loss. Furthermore, we will provide a perspective on essential genes and signaling molecules involved in initiating the central neuroimmune response. This will uncover mechanisms that can be interfered with to prevent inflammation within the ventral horn and preserve these motor circuitries.

1.2 Organization and function of spinal cord motor circuitry

1.2.1: Motoneurons

Motoneurons (MNs) are arguably one of the most critical cell types in the central nervous system (CNS). These powerhouse cells are the largest of all the neurons and are essential for motor function being the “final common path” of the CNS for sending motor commands to the muscle (Sherrington, 1906). To provide context to their massive size the average CA1 pyramidal neuron in the hippocampus of an adult rat has an average surface of $59,000 \pm 29,000 \mu\text{m}^2$ (Scorcioni et al., 2004) while a spinal alpha MN has an average surface area of $204,482 \pm 7,365 \mu\text{m}^2$ (Rotterman et al., 2014). Their extensive dendritic arbors integrate information from the periphery (proprioceptors), spinal cord circuitries and descending motor commands and transform these inputs into the motor output that controls our muscles. Without motoneurons, the CNS has no way to communicate with the body leaving one wholly trapped in one’s own body and with

no possibility of interaction with the external world (for example amyotrophic lateral sclerosis).

There are two main types of motoneurons (MNs) within the spinal cord of mammals: alpha and gamma MNs. The cell bodies (soma) of both classes are located in the ventral horn of the spinal cord, specifically in lamina IX (Rexed, 1952). Alpha MNs have large cell bodies and massive dendritic arbor that spans the whole ventral horn receiving somewhere around 50,000 synaptic inputs from a variety of sources (Brannstrom, 1993; Fyffe, 2001). Some reports have even suggested as many as 100,000 synaptic inputs per MN in the cat (Ulfhake and Cullheim, 1988).

Traditionally, using electron microscopy (EM) synapses onto MNs have been classified into one of four categories based on their shape and structural components (Uchizono, 1966; Conradi, 1969b; Bodian, 1970; McLaughlin, 1972; Conradi et al., 1979; Kandel and Siegelbaum, 2000): 1) S-type bouton which contains spherical synaptic vesicles and thought to be excitatory, 2) F-type bouton which contains flattened or pleomorphic synaptic vesicles and is inhibitory, 3) M-type synapses that are large spherical boutons, similar to S-types, but are surrounded by several p-boutons (presynaptic inhibitory) terminals (Conradi, 1969a; Conradi et al., 1979). These synapses originate from large sensory type I (or type II) fibers. 4) C-boutons which are cholinergic and are distinguished based on their unique post-synaptic cisternae structure (Lewis and Shute, 1966; Conradi, 1969a; Conradi and Skoglund, 1969; Deardorff et al., 2014). The distribution and density of these different synapses vary depending on the species (i.e., cat vs. rat),

muscle target innervated, and location of the MN cell body within the spinal cord. A study by Conradi et al., estimated the synaptic coverage of different boutons on the soma and proximal dendrites of alpha MNs in the lumbar segment 7 (L7) region of the cat. They found that each type of terminal covered the following proportion of the total soma surface covered by synapses: S = 8.7%, F = 71.3%, and C = 20.0% and on the proximal dendrite: S = 15.5%, F = 65.2%, C = 16.0%, M = 3.3% (Conradi et al., 1979). These data do not exactly reflect the percentage of synaptic boutons at each location, just their relative soma coverage, since each type of synapse has different sizes (S<F<C=M). Also, synaptic distributions vary depending on location (rostral – caudal, medial – lateral) and functional type of MN investigated (FF-type, FR-type, and S-type). In a thorough, comparative analysis performed by Thomas Brannstrom of cat MNs giving rise to each of the three types of motor units, the percentage of F and S terminals to all synapses on the cell body of FF, FR and S-type MNs was respectively 57.5% (F) and 31.3% (S), 52.1% (F) and 32.3% (S), 70.1 (F) and 27.5% (S). However, in the dendrites, the proportion of S terminals increased. For example, in dendrite segments at a distance between 300 and 700 μm from the cell body, the proportion of F and S terminals in FF, FR and S-type MNs was 40.0% (F) and 56.6% (S), 34.7% (F) and 58.3% (S), 50.9% (F) and 44.5% (S) (Brannstrom, 1993). In this study, M and C terminals were denominated “L”, for large (apposition length > 4 μm). It should be noted that C-terminals are only present on the cell body and most proximal dendrites, while proprioceptive synapses target mainly the dendrite and can be characterized ultrastructurally as M or S depending on the angle of the cross-section. In

summary, excitatory synapses (including likely Type I and II proprioceptive inputs) target mainly the dendrites.

Each MN contains a single myelinated axon that extends from the soma all the way to a peripheral muscle target where it innervates extrafusal muscle fibers and can elicit a contraction of each innervated muscle fiber. Together, the MN and all the muscle fibers it innervates is known as the motor unit (Liddell and Sherrington, 1925). The electrical signal necessary for this contraction is initiated in the initial segment of the motor axon containing a high density of voltage-gated sodium channels that cluster along this region in part by Ankyrin-G (Zhou et al., 1998) (reviewed in (Rasband, 2010)). The electrical signal travels down the axon to the presynaptic terminal of the axon, wherein a calcium-dependent manner, synaptic vesicles release acetylcholine into the synaptic cleft. The acetylcholine then binds to postsynaptic nicotinic acetylcholine receptors that are cation channels permeable to sodium (Na) and potassium (K) (K rushes out while Na rushes in, $E_{rev} = 0$) (Millar, 2003). This depolarizes the muscle membrane into an end-plate potential (EPP) that triggers a Na-dependent muscle action potential to occur which then provides the depolarization necessary to initiate a muscle contraction.

Among all the MNs, in the cat and rodent ventral horn, about one-third are classified as gamma MNs (Burke et al., 1977; Friese et al., 2009). These cells are much smaller than alpha motoneurons in their overall surface area (Alvarez et al., 1997). Their average soma cross-sectional area is rodents of $331 \pm 77 \mu\text{m}^2$ compared to an average of $755 \pm 220 \mu\text{m}^2$ for alpha MNs (Shneider et al., 2009)

(These data were collected from the adult mouse). Gamma MNs receive much fewer synaptic inputs compared to alphas, and this is true across different mammalian species (Johnson, 1986). However, gamma MNs are critical to proper motor control in that they extend their axons to the periphery and innervate the intrafusal muscle fibers in the muscle spindles (discussed in detail below) (Kuffler et al., 1951). This is important for modulating muscle spindles sensitivity to stretch.

1.2.2: *Ia afferent connections*

Sensory fibers are classified based on their diameter and myelination, both of which influence their conduction velocities and help to distinguish them. For this particular project, we will focus on the largest diameter and more heavily myelinated sensory axons, thus with the fastest conduction velocities. This was named group 1 fibers (Lloyd, 1943), and more specifically the Ia's (Brown and Fyffe, 1978a) and innervate the muscle spindle.

Sometimes referred to as the “sixth sense” proprioception is the biological system responsible for encoding information about the body’s position in space. This “sensation” necessitates of detailed information from the skeleto-muscular system (static and velocity changes in length and force of muscle and the position of our joints), and it is encoded in part by proprioceptor Ia and II afferent fibers (muscle length information, both static and dynamic, arising from the muscle spindle). Additional information is provided by type Ib afferents (force signals) and cutaneous afferents, all integrated together to provide proprioception.

Ia afferents are pseudounipolar sensory neurons located in the dorsal root ganglia and extend a single axon split into two directions from the cell body. One branch is directed towards the periphery where it forms annulo-spiral endings surrounding intrafusal muscle fibers in muscle spindles, the other end projects centrally entering into the spinal cord. The central axons project rostrally in the white matter and transmit sensory information to ascending neural pathways while extending collaterals that enter the spinal cord gray matter and project ventrally where they modulate spinal motor circuitries. We will examine plasticity in these ventral projecting spinal cord collaterals as a consequence of injury to the peripheral branch of the peripheral nerve. Muscle spindles are present in all load-bearing muscles, but are lacking in muscles that do not carry loads, like facial or oculomotor muscles. We will focus on the afferents that innervate ankle extensors in the lower hindlimb.

Ia axons innervating muscles in the hindlimbs are typically 12-20 μm in diameter in cat peripheral nerves (Lloyd, 1943) and upon entry through the dorsal root these fibers bifurcate in the dorsal column where one branch ascends to Clarke's Nucleus in thoracic and upper lumbar segments of the spinal cord (T1-L2) (Rethelyi, 1970). Here Ia axons synapse onto dorsal spinocerebellar tract (DSCT) neurons that project to the cerebellum (Lundberg, 1964). Many axon collaterals stem from dorsal column Ia parent axons and enter the spinal cord forming synaptic arborizations in medial lamina V/VI and in lamina VII. At these locations they synapse onto a variety of premotor interneurons (Hultborn et al., 1971a, b; Jankowska and Lindstrom, 1972). These collaterals then project down

to the MNs located in lamina IX (Sprague, 1958; Iles, 1976; Brown and Fyffe, 1978b; Brown, 1981; Brown and Fyffe, 1981). The dendritic arbors of MNs are so massive they span into lamina VII and receive some innervation by Ia afferents here as well. It is important to note that even though there is one main Ia branch that enters the spinal cord, there are several collaterals that project from this branch at different rostrocaudal levels forming a high density of synaptic boutons with interneurons and MNs through several lumbar segments. These synaptic boutons are M-type or S-type, based on Contradi's classification, and contain glutamate which upon activation provide excitation to their target sources, typically through non-NMDA receptors such as AMPA channels (Jahr and Yoshioka, 1986; Maxwell et al., 1990; Walmsley and Bolton, 1994). When interpreting electron microscopy data, one must be aware of classification ambiguities during identification of M-and S-boutons at the ultrastructural level. M boutons are characterized by receiving axo-axonic synapses from small inhibitory GABAergic P-boutons, but these can be missed depending on the cross-sectional level and orientation of ultrathin sections used for EM. In this case, the synaptic cross-section could appear as an S-bouton. M and S boutons display the same morphological type of synaptic vesicle. Recently, it was shown that the synaptic vesicles of proprioceptive synapses contain the vesicular glutamate transporter 1 isoform (see below), permitting their identification at the ultrastructural level in the ventral horn (Alvarez et al., 2004).

Our primary interest in this project is the monosynaptic connections between Ia afferents and MNs in lamina IX and lamina VII. Single triceps surae

HRP-filled Ia afferent collaterals were estimated to establish an average of 8.5 ± 6.7 contacts on the surface of individual MNs (Burke and Glenn, 1996). Moreover, a single Ia axon gives approximately 10 collaterals, so there is an estimated 1,000 - 2,000 Ia afferent synapses on MNs in the cat (Brown and Fyffe, 1978a; Ishizuka et al., 1979; Munson and Sybert, 1979). The majority of these synaptic inputs are on the MN dendritic arbor, with only about 5-10% of them targeting the soma (Iles, 1976; Brown and Fyffe, 1981). Earlier studies by Mendell and Henneman showed that each Ia distributes functional synaptic connections to virtually all homonymous MNs (>90%) (Mendell and Henneman, 1971) and to more than half of heteronymous synergist MNs (Scott and Mendell, 1976).

For many years it was difficult to quantify all Ia afferent inputs innervating MNs because there were no specific antibodies or techniques to distinguish glutamatergic synapses derived from Ia's or other sources. The previous quantification of Ia afferent synaptic density on MNs was estimated based on intraxonally filling individual Ia axons or from physiological studies (Brown and Fyffe, 1978a). One advance in the identification of these synapses was the recognition that they express the vesicular glutamate transporter isoform 1 (VGLUT1) (Todd et al., 2003; Alvarez et al., 2004). VGLUT1 is one of three different glutamate vesicular transporter isoforms expressed through the CNS (though only 1 and 2 are highly expressed in the spinal cord) and shows high immunoreactivity in lamina III/IV, V/VI, and in IX (Alvarez et al., 2004). VGLUT1 synapses in the spinal cord can originate in descending corticospinal axons, low-threshold cutaneous mechanoreceptors, and muscle proprioceptors. Todd et al.

(2003) and Alvarez et al. (2004) demonstrated the primary afferent origin of the overwhelming majority of VGLUT1 synapses in the ventral horn and lamina IX using a variety of techniques that include anterograde transganglionic transport of the cholera toxin subunit b (CTB), co-localization in sensory axons with parvalbumin (a marker of proprioceptors), and their disappearance after dorsal rhizotomy. Alvarez et al. (2011) directly confirmed that all electrophysiological identified Ia afferent boutons contain VGLUT1. Alvarez et al. (2004) explicitly showed that VGLUT1 is contained in S- and M- terminals at the EM level in the ventral horn.

Within the spinal cord, VGLUT1 is only expressed in DSCT neurons, but the axons of these neurons do not leave synaptic boutons inside the spinal cord (Hantman and Jessell, 2010). We also know, through genetic knock out experiments, that at least in lamina IX, where we have the highest density of Ia projections, VGLUT1 is a specific marker for proprioceptor afferents, including Ia's (Siembab et al., 2016) and maybe type II (Vincent et al., 2017). VGLUT1 synaptic boutons originated in low threshold cutaneous mechanoreceptors, or corticospinal tract axons do not project directly to lumbar MNs (Alvarez et al., 2004; Alvarez et al., 2011). Lastly, VGLUT1 has a functional significance by being primarily responsible for packaging and accumulating glutamate into presynaptic vesicles that will be released into the synaptic space (Hnasko and Edwards, 2012).

1.2.3: Stretch reflex and reciprocal inhibition

The connectivity and physiological understanding of spinal reflexes has been a topic of investigation for over 100 years, starting with Sir Charles Sherrington and John Eccles (Sherrington, 1906; Sherrington, 1909; Brock et al., 1952; Eccles et al., 1957; Hultborn, 2006), and will only be reviewed briefly in this section. One of the significant functional outcomes of this early work is that muscle stretch can produce a monosynaptic reflex directly in MNs (Liddell and Sherrington, 1924; Hammond, 1955) and type I afferents are responsible for this response (Eccles et al., 1957; Lundberg and Winsbury, 1960), specifically Ia afferents (Mendell and Henneman, 1971). This reflex is a direct indicator of the efficacy of the Ia afferent input into the ventral horn circuitry. Simplistically explained, any change in muscle length is detected by stretch sensitive receptors located in the muscle spindles, and fires Ia afferent axons. This electrical signal travels centrally and is monosynaptically transmitted to essentially all the homonymous, and some heteronymous, MNs in the ventral horn (Mendell and Henneman, 1971). These same MNs then elicit an action potential resulting in the release of acetylcholine at the NMJ and ultimately resulting in the contraction that counteracts the lengthening of the muscle. The gamma MNs, described above, are also involved in this processes by maintaining sensitivity to stretch.

The Ia afferents that are engaged during muscle stretch also project to heteronymous MNs as well (Eccles et al., 1957). An elegant, comprehensive study by Scott and Mendell demonstrate the connectivity of individual Ia afferents on homonymous and heteronymous MNs in the triceps surae muscle group of an adult cat (Scott and Mendell, 1976). This is of particular interest to us as this is the

muscle group/motor pool we are investigating. The authors of this paper stimulated individual Ia afferents from either the lateral gastrocnemius (LG), medial gastrocnemius (MG), or soleus (SOL) and recorded the excitatory postsynaptic potentials (EPSPs) in all three motor pools. They found that EPSPs were always significantly larger in homonymous MNs, i.e., stimulation of an LG Ia afferent will produce the greatest EPSP in LG MNs (Scott and Mendell, 1976). This was true for each afferent group. It is important to note that EPSPs detected in heteronymous MNs had a decrease in maximum amplitude by 17-65% compared to the homonymous connections.

This reflex, however, is only one of the many functions the Ia afferent input has on the modulation of MN and spinal circuitry activity. The functional consequence of Ia afferent disconnection with MNs was described in a 2000 study by Arber et al. (Arber et al., 2000). The authors knocked out (KO) an essential transcription factor, *Er81*, which is expressed in proprioceptor DRG cell bodies and by MNs at different times points through development and is critical for the formation of Ia synapses in the ventral horn (Lin et al., 1998). KO animals had almost no Ia afferent projections in the ventral horn and were utterly ataxic displaying abnormal flexor-extensor coordination and resulting in their death by 3–5 weeks after birth (Arber et al., 2000). These data highlight the importance of preserving this circuitry within the spinal cord.

Additionally, Ia afferents also provide reciprocal inhibition to antagonist MNs through a disynaptic pathway (Bradley et al., 1953; Bradley and Eccles, 1953; Eccles et al., 1956; Eccles and Lundberg, 1958) via the Ia inhibitory interneurons

located in lamina VII (Jankowska and Lindstrom, 1972). Ia afferents provide synaptic drive to these inhibitory interneurons which then project to antagonist MNs and elicit an inhibitory postsynaptic potential (IPSP). This reflex pathway inhibits antagonists and provides for flexor – extensor alternations to promote smooth movement and motor control (Kiehn, 2016). Modulation of Ia inhibitory interneuron activity can then control the level of co-contraction around single joints (Bawa et al., 2000). Co-contraction is a useful mechanism; it stiffens muscle joints in specific behaviors, but if it is not tightly modulated, it can provoke “spastic” movements.

In summary, loss of Ia afferent synapses in the spinal cord ventral horn will deafferent MNs and also critical interneurons necessary for normal spinal motor control.

1.3 Peripheral nerve injury

The peripheral nerve is considered the “conducting unit” between the periphery and the central nervous system (Sunderland, 1991) which carries both afferent sensory information into the spinal cord and efferent motor commands back out to the periphery (note: sympathetic fibers are also part of the peripheral nerves though we will not focus on these fibers in this thesis). One could consider this as a two-way highway in which traffic is moving in both directions. Quite amazingly the sensory and motor components of the nerve and its function as a conduit between central and peripheral structures were carefully dissected and

described in the 3rd century B.C by a Greek physician known as Herophilus (Lee and Wolfe, 2000).

Nerve fibers are complex structures composed of many integral components aiding in its function, and we will highlight a few of these in this thesis to provide context to the studies we performed. For a full anatomical overview, please see Sunderland 1991. In brief, the motor and sensory axons we are studying are both heavily myelinated fibers however it is important to note that sensory axons can vary in the myelin coverage depending on the fiber type. Looking inside out, the axons of both Ia afferents and MNs are ensheathed by Schwann Cells (Schwann, 1839) which are glial cells derived from the neural crest that form the myelin around individual axons leaving small segments of axonal exposure to the environment, known as the Nodes of Ranvier. By difference to the oligodendrocytes in the CNS, each Schwann Cell wraps only one axon and express little protrusions that extend out and interlock with one another forming a sheet-like structure over the nodes (Sunderland, 1991). Schwann Cells are covered by a thin basal lamina made of connective tissue known as the endoneurium (Causey and Barton, 1959). There are several other layers of specialized cell types and connective tissue on top of the endoneurial sheath that forms the nerve fascicles and that are known as perineurium. All nerve fascicles are then bundled together and with blood vessels, fatty tissue and connective tissue by the epineurium that forms the nerve trunk.

Peripheral nerves are subject to trauma and damage resulting in permanent disability by impairment of motor function and/or sensory abnormalities, such as

chronic pain leaving individuals with a low quality of life (Lundborg, 2003; Siemionow and Brzezicki, 2009). In the following section of this thesis we will review the prevalence, surgical intervention, and patient outcomes following different types of nerve injuries. In addition, I will review the most recent findings in the field to promote regeneration and reinnervation to peripheral targets that may enhance the functional outcomes for the patient population affected by these injuries.

1.3.1: Type and prevalence of nerve injuries

It can be somewhat difficult to quantify and accurately report PNI prevalence as the type and severity of an injury can vary so greatly (more on this in 1.3.2). Here I will review several seminal studies investigating the prevalence of nerve injury and the different classifications of nerve injuries. It is important to point out that these studies and statistics are based only on reported injuries. However, it is suspected that some individuals who experience mild to medium nerve trauma may never be seen at a clinic or their injuries go unreported most likely resulting in underestimation of PNI prevalence in the literature.

PNI encompasses a broad range of injuries. H.J. Seddon proposed a classification system in 1947 (Seddon, 1947) based on three categories: 1) Neurapraxia: this is a very mild injury in which the myelin surrounding axons is damaged, typically from compression; however, neither sensory nor motor axons are damaged directly. 2) Axonotmesis: a slightly more severe injury in which the

axons are damaged, but the surrounding connective tissue remains intact, typically from a crush injury. 3) Neurotmesis: This is the most severe injury in which the axons and surrounding connective tissue are completely severed and transected.

In 1951 Sir Sydney Sunderland expanded on Seddon's classification to more accurately describe the diversity of nerve injuries (Sunderland, 1951) (for a comprehensive review and comparison, please see (Grinsell and Keating, 2014)). In brief, he used a Type 1 – Type 6 classification system. He described the neurapraxia as a Type 1 injury. The axonotmesis category was divided into Type 2 (severed intraneural axons), Type 3 (severed endoneurium), and Type 4 (severed intra-axons, endoneurium, and perineurium but maintenance of the epineurium). He called neurotmesis a Type 5 injury and described a Type 6 injury as a mix combination of Types 2 – 4 injuries (Sunderland, 1951). The major problem, as pointed out by Grinsell and Keating, is that you can't distinguish Type 2 – 4 clinically and can only use this type of classification *posthoc* by performing histological analyses of the nerve tissue. Therefore, Mackinnon and Dellon used non-invasive techniques such as nerve conduction velocity and electromyographic (EMG) recordings to classify which type of injury was sustained (Mackinnon and Dellon, 1988). This was done to allow diagnostic assessment of injury severity in the clinic without the need to perform histological analysis of tissue.

Currently, it is reported that approximately 20 million Americans are suffering from PNI (Lundborg, 2003) resulting in \$150 billion being spent on these patients every single year! (Taylor et al., 2008; Grinsell and Keating, 2014). One comprehensive study published in 1998 provides a good overview of the

prevalence and nature of PNI. Noble et al., looked at a population of 5,777 patients that visited a level 1 trauma emergency room between 1986 and 1996 (Noble et al., 1998). They found that approximately 2.8% of all patients that visited the ER had some form of nerve trauma, with 61% affecting the upper extremities (radial, medial, ulnar) and the remaining 39% the lower extremities (sciatic, femoral, peroneal, or tibial nerves) (Noble et al., 1998). However, when they accounted for plexus or nerve root injuries up to 5% of all ER patients fell into a nerve injury category. Lastly, they found that the most prevalent cause of injury was from motor vehicle accidents (46%). Another study, published in 2006, by Kouyoumdjian looked at 456 nerve injury patients with a total of 557 nerve lesions identified over a 16-year period expanding from 1989 to 2004 (Kouyoumdjian, 2006). Some patients had multiple nerves severed in a single accident (17% of patients reported). He found that the most common pair of nerves injured together was the ulnar and medial nerves of the arm and the tibial and peroneal of the leg (Kouyoumdjian, 2006). There was a wide range of accidents leading to a nerve injury but, again, the most common was from motor vehicle accidents, accounting for 43.9% of all cases, with a particular emphasis on motorcycle accidents. Other causes of PNI were blunt trauma (20.6%), falls (13.3%) gunshot wounds (8.5%), and sports-related injuries (2.7%) (Kouyoumdjian, 2006). Lastly, Kouyoumdjian described the patient population as 74% male with an average age of 32.4 but ranging from 4 to 79 years old.

In summary, PNI is very prevalent and costly, and they have a tremendous diversity of causes and severities. We will address the consequences of different

types of injuries resulting in differences in reinnervation efficiency and specificity in the periphery.

1.3.2: Peripheral degeneration and reinnervation

One of the unique defining features of peripheral axons is that they can regenerate and reinnervate peripheral targets given the right conditions. Many factors can influence this capacity such as the type and location of the nerve trunk injured, the age of the individual, and severity of the injury. This is however entirely different to CNS axons, for example after spinal cord or optic nerve injuries, in which glial scarring and inhibiting molecules prevent axon regeneration from occurring. In fact, the peripheral nerve promotes axon growth and regeneration as can be demonstrated by bridging CNS lesions with peripheral nerve grafts (Richardson et al., 1980; Cote et al., 2011; Hanna et al., 2011).

The peripheral nerve undergoes a series of well-orchestrated changes after a lesion. Immediately following axonal injury (Sunderland's Type 2 – 6) axons become destabilized through a calcium-calpain mediated process (George et al., 1995) and phagocytosed by local Schwann cells and recruited peripheral macrophages, a process known as Wallerian degeneration (Waller, 1850; Stoll and Muller, 1999; Navarro et al., 2007; Brushart, 2011; Wang et al., 2012). Local Schwann Cells de-differentiate, proliferate, and change their phenotype from a myelinating function to a growth-promoting state by releasing a number of critical trophic factors and cytokines, including the chemokine known as monocyte

chemoattractant protein 1 (MCP-1/ also known as CCL2) that is responsible for the recruitment and migration of peripheral macrophages to the site of injury (Martini et al., 2008). These professional macrophages are more efficient at myelin and axon debris cleanup compared to the Schwann Cells and therefore aid in the speedy removal of axon segments distal to the injury and disconnected from the cell body. The entire separated distal segment is fully degraded and removed within 48 – 72 hours post injury (reviewed in (DeFrancesco-Lisowitz et al., 2014). A similar degradation process occurs up to the first Node of Ranvier of the intact axon on the proximal side of the injury. This “cleanup” mechanism is necessary for allowing rapid axon regeneration as demonstrated with mutations that prevent distal axon breakdown (slow Wallerian degeneration *Wld^s*) (Lunn et al., 1989) or phagocytosis of peripheral axons (Rosenberg et al., 2012).

As these axons undergo degeneration, there are significant changes in the cell body of sensory and motor neurons. Traditionally, the changes in the soma of the MN and the cell bodies of DRG cells, were described morphologically as chromatolysis. During this reaction, the Nissl bodies become dissolved, the cells undergo hypertrophy, and the nucleus moves to a peripheral location (Lloyd, 1900; Cragg, 1970; Lieberman, 1971). Many signals from the injury site travel centrally to the cell body to provoke these alterations and more importantly, change gene expression. Immediately after the axons are severed, there is a spike in calcium that propagates back to the cell body of the injured neurons. Local translation and auto-phosphorylation at the injury site of importins and transcription factors such as ERK, JNK, STAT3 result in their retrograde transport back to the cell body and

signaling injury (reviewed in (DeFrancesco-Lisowitz et al., 2014; Mar et al., 2014)). The calcium wave increases local cAMP levels to promote regeneration. Moreover, calcium-dependent intracellular signaling pathways in conjunction with the arrival of injury signals carried by a number of transcription factors modified at the injury site ultimately results in upregulation of early immediate genes in the cell body (including JUN, ATF3, and FOS) as well as a number of regenerative associated genes (RAGs) including GAP-43 (Skene and Willard, 1981; Jenkins et al., 1993; Tsujino et al., 2000; Reynolds et al., 2001; Hyatt Sachs et al., 2007; DeFrancesco-Lisowitz et al., 2014; Mar et al., 2014; Rishal and Fainzilber, 2014). This finally results in the formation of a growth cone at the end of the severed axons that can be guided to reinnervate peripheral targets (Kato and Ide, 1994) and the modification of protein synthesis machinery in MNs and sensory neurons towards promoting axon elongation.

Once the cleanup phase has been completed in the periphery, there must be a switch in the local environment from a pro-inflammatory to a growth-promoting one. Previous studies have shown that local Schwann cells and myeloid cells have the capacity to release a whole host of supporting factors including, but not limited to, nerve growth factor (NGF), brain-derived neurotrophic factor (BDNF), transforming growth factor beta (TGF- β), glial-derived neurotrophic factor (GDNF) (Fu and Gordon, 1997; Brushart, 2011; Gordon and Sulaimain, 2012). Additionally, the reactive Schwann cells release glycoproteins and adhesion molecules allowing them to form a scaffold inside the endoneurial sheath called the “bands of Büngner” which promote axon regeneration (Büngner, 1891; Fu and Gordon,

1997; Gordon and Sulaimain, 2012). Taken together, the axotomized neurons switch from transmitting to a regenerative phenotype, and the periphery develops a growth promoting environment. Axons regenerate at a rate of 1 – 4 mm/day depending on the severity of the injury, age of the individual and time after injury, being regenerative capacity progressively decreased as time passes (Grafstein, 1971; Hoffman and Lasek, 1980; Verdu et al., 2000; Navarro et al., 2007; Hoke and Brushart, 2010).

The rate at which regeneration takes place very much depends on where the injury occurred and how far the axon has to travel to its target. For example, it will take much longer for a single axon to reach the LG muscle in a sciatic nerve transection compared to a tibial nerve transection. In addition, the type of injury impacts the rate of regeneration as well (see chapter 5 for more information). In general, it takes somewhere between 3 – 20 days post-injury for a growth cone to pass over the injury site and begin its journey down the endoneurial tube to its target destination, being the initiation of growth usually faster after crush (endoneurial tube and axon continuity preserved through the injury) than after full transection (the axon has to find an enter an endoneurial tube in the distal stump) (Sunderland, 1991). Many studies have focused on interventions and mechanisms that promote speed of regeneration including applying scaffolds, neurotrophic factors and very importantly examining the effects of activity and exercise (Gordon and English, 2016).

A second major problem in peripheral regeneration is the specificity of target reinnervation. A single MN and proprioceptor neuron innervate specific muscles in

the periphery and the connectivity in the spinal cord that modulates MN firing is based on the muscle it innervates, i.e., a MN innervating the lateral gastrocnemius (LG) receives monosynaptic connections from Ia fibers innervating the same muscle and reciprocal inhibition during contraction of the antagonist, for example, the tibialis anterior (TA) muscle. If, after axotomy, motor or sensory axons that originally innervated the LG now regenerate un-specifically into the TA, a disorganization of motor pool specificity by Ia inputs can occur. Controlling specific target reinnervation has been a significant obstacle and could result in major motor deficits (Rotterman et al., 2017).

The reinnervation target of the primary axon branch is primarily determined at the site of injury during initial regeneration and depending on which endoneurial tube the axon enters. This tube guides the axon through and will specify the ultimate target (Brown and Hopkins, 1981; Hoke and Brushart, 2010; Brushart, 2011). The success of peripheral regeneration is very much dependent on the type of injury sustained as well. During a crush injury, injured axons remain with their original endoneurial tubes, and the axon follows specific paths back to their original targets (Nguyen et al., 2002). However, when the nerve is completely severed and rejoined, the sensory (Brushart and Mesulam, 1980b) or motor axons may enter endoneurial tubes at random and end up innervating targets different from the original (Brushart and Mesulam, 1980a; Brushart et al., 1983; Bodine-Fowler et al., 1997; Valero-Cabre et al., 2004).

We will, therefore, analyze how neuroinflammation and central synaptic plasticity of the Ia afferent – MN connection are controlled depending on the type of injury.

1.3.3: Clinical intervention and patient outcomes

Some of the earliest data we have on PNI dates back to the American Civil War. Dr. John K. Mitchell followed, between 1890 and 1895 men who had experienced traumatic nerve injuries during the war from 1863-65 (Mitchell, 1895). For soldiers with minor injuries in which the nerve remained intact, he closed the external wound and insisted on rest (page 223). However, when the nerve was completely severed, he recommended immediate rejoining of end-to-end via suture to promote regeneration (page 225) (Mitchell, 1895). He describes the persistent motor deficits these later patients had 25-30 years after the injury, providing the first thorough data set on the motor consequences of PNI. Dr. Mitchell also mentions the extraordinary pain many of these patients' experience. He recommended injecting a cocktail of morphine and cocaine directly into the wound site!

Another seminal study was published in 1956 by Woodhall and Beebe in which they performed a 5 – 10-year follow-up of 2,720 men who had a combined 3,656 nerve injuries reported during WWII (injuries sustained from 1943 until the end of the war) (Woodhall and Beebe, 1956). This approximately 700-page report goes into great depth of motor, sensory, and autonomic outcomes from these

patients, however, for this project I will briefly review the motor results. These data related to patients who had a complete nerve transection (Sunderland type 5) followed by a successful repair via suture. Of course, the authors point out that the gap between nerve stumps had a significant impact on regeneration which can account for the variability in data. At this time in history, the patients were evaluated and scored on a 1 – 5 rating system: 1: No voluntary contraction, 2: Only perceptible voluntary contraction, 3: Movement but not against gravity, 4: Movement against gravity but not applied resistance, and 5: Movement against gravity (page 73). They found that 64% of patients had 12% or less in overall muscle strength in the affected limb compared to the control side with 19.5% having absolutely no muscle contraction at all (Woodhall and Beebe, 1956). Again, the main point here is that even with successful regeneration, patients report persistent motor deficits that never return.

The history of nerve repair was recently reviewed by Sunderland (Sunderland, 1991). Essentially, towards the end of WWII between 1943 and 1945, Seddon (Seddon et al., 1943) and Sunderland (Sunderland, 1945), independently, published papers describing technical approaches to nerve repair and these have only been slightly revised in the past 70 or so years (Kurze, 1964; Smith, 1964; Millesi, 1973) (reviewed in (Grinsell and Keating, 2014)).

As mentioned above, the primary technique for nerve repair, when possible, is the end-to-end suture method. This technique relies on correctly aligning the two stumps, as best as possible, and with as little tension as possible, the superficial epineurium is brought together and loosely sutured together (Sunderland, 1991).

However, this may be difficult in tiny nerves or small animal models. Therefore, the fibrin glue method was introduced as an alternative method of repair. This technique requires that the nerve endings be aligned end-to-end, but instead of sutures, fibrin glue mixture is used to adhere the ends together. This was initially proposed in by Young and Medawar in 1940 but had a short life in the clinic as the adhesion strength did not seem suited for patients. However, in 1988 Narakas published a paper with a fibrin glue recipe mixed with thrombin that has been very successful clinically (Narakas, 1988) and later in 1997 Guest et al., published a recipe with thrombin and fibronectin (Guest et al., 1997). Throughout our studies, we used the latter thrombin and fibronectin mixture to repair sciatic nerves in mice.

If the injury is severe enough, it may not be possible to realign the ends of the stump. In this case, a nerve autograft may be required to promote nerve regeneration. Millesi pioneered this approach in the early 1970's (Millesi et al., 1972). Typically, nerve autografts are used if the space between nerve stumps is > 3 cm and is still considered a preferred method of repair even today (Pfister et al., 2011). This technique entails taking a donor nerve from the patient, typically the sural nerve, and placing it between the gap in an inverted orientation and then connecting each nerve stump together either through sutures or by fibrin glue (Lee and Wolfe, 2000). One of the major downsides to this method is the need for a section of an intact and correctly functioning nerve from the host which could result in other complications. An alternative, although not used as frequently, is implanting an allograft from a donor body instead of using a host nerve. This technique has mixed reviews and is not considered to be a superior method

compared to the allograft. Typically, patients have to be immunosuppressed for up to two years to ensure acceptance of the donor nerve (Moore et al., 2009; Grinsell and Keating, 2014). Even with these precautions as “standard of care,” only 40% of patients regain near-normal function (Lee and Wolfe, 2000). This has encouraged a substantial investment in bioengineered conduits to promote successful regeneration by using synthetic nerve conduits to reconnect nerve stumps (Colen et al., 2009; Mokarram et al., 2017). The idea here is to use a growth promoting biomaterial that contains neurotrophic factors like NGF, GDNF, and NT-3 that would enhance axon regeneration and favor reinnervation of peripheral targets. A recent study has shown an alternative approach. Injecting the chemokine known as fractalkine into the conduit recruits pro-healing macrophages to the implant site resulting in significantly higher numbers of axons growing through (Mokarram et al., 2017). This topic remains a very active area of research.

Investing in ways to measure functional outcomes is critical to evaluate therapeutic interventions. The most straightforward appraisal is through a motor recovery exam using a scoring system, almost identical to Sunderland’s method discussed above. This method was adopted by the Medical Research Council (in the UK) and then separated into a motor and sensory evaluation (Table 1, adapted from (Lee and Wolfe, 2000)). A more quantitative measure to evaluate the success of a peripheral nerve repair is utilizing electrophysiological methodologies. One of the most common techniques is using electromyography (EMG) to record compound motor unit action potentials (CMAPs) resulting from muscle

contractions (Campbell, 2008). In brief, when a motor unit is activated, and acetylcholine is released onto nicotinic receptors at the NMJ, a muscle action potential occurs and can be recorded using fine electrodes placed on the muscle. In essence, a severed nerve with complete axon degeneration to the muscle will result in no EMG signal. When axons begin to reinnervate muscle fibers, small desynchronized potentials can be detected, and after complete muscle reinnervation full synchronized compound potentials reappear. Electromyography can be applied in longitudinal studies allowing one to record the initial extent of the injury when reinnervation begins and to what extent it proceeds. Another alternative method is the measurement of nerve conduction velocity (CV) recordings. This technique involves electrically stimulating the nerve at two spots, one proximal to the injury site and one distal to the injury site, and then recording the electrical potentials in the muscle (Aminoff, 2004; Campbell, 2008). The increase in EMG signal and CV together indicates axon regeneration and muscle reinnervation. Furthermore, this method allows localizing the injury site. Stimulation proximal to the injury within the first few days after injury will result in reduced or no muscle activation, as axons begin to degenerate and are not capable of transmitting a signal across the injury site (Aminoff, 2004). As Wallerian degeneration proceeds, the efficiency of muscle activation after stimulation of distal ends decreases further. In contrast, as reinnervation advances muscle activation by proximal stimulation increases.

1.3.4: Functional deficits in the Ia stretch circuit

It is not sufficient to get axons to regrow. Of course, this is the first step in restoring function, but this is not good enough and does not mean that normal motor control and function will return. For example, in experimental situations in which speed and specificity of regeneration can be controlled, there are still functional motor deficits that remain after regeneration and reinnervation in the periphery is complete. One significant consequence of PNI and the focus of this thesis is that there is also plasticity of central motor circuits in the spinal cord that occur after axotomy and that these are, at least partially, responsible for the motor deficits experienced by patients. The most prevalent and well-studied deficit is the loss of the stretch reflex, which occurs even when efficient and specific reinnervation occurs. For example, after transection and repair of the MG nerve, sensory and motor axons regenerate and reinnervate the MG in a complete and precise manner, but still the stretch reflex in the MG muscle never recovers (Cope et al, 1994).

A pioneering study by Barker and Young in 1947, investigated the stretch reflex in rabbits who had undergone either a complete transection or a crush of different hindlimb nerves. They developed a clever way to measure the knee-jerk reflex by placing the rabbits on their back in a supine position and placing the foot underneath a horizontal bar. When they tapped the patellar tendon, the foot pushed out the bar that would move up, and the maximum height was measured. They showed in 9 out of 11 cases the knee-jerk reflex never returned when the entire crural nerve was severed and reunited; however, the reflex returned in all animals following a crural nerve crush (Barker and Young, 1947).

With the introduction of intracellular recording techniques in the cat spinal cord preparation, Eccles and colleagues went on to demonstrate that the aggregated Ia EPSPs amplitude in axotomized MNs was significantly reduced and their rise and fall times slowed during electrical stimulation (Eccles et al., 1958). These early studies provided insight into the central synaptic plasticity of the monosynaptic Ia afferent stretch reflex following PNI. Later, Mendell and colleagues thoroughly investigated connectivity between Ia afferents and MNs and how it changed after nerve injury (Mendell et al., 1974, 1976). Early studies using the spike-triggered averaging (STA) technique found that a single Ia afferent synapses with approximately 94% of homonymous MNs (Mendell and Henneman, 1971), however, 29 days after axotomy only 9 out of 29 MNs responded to stimulation of a single Ia afferent, demonstrating a reduction to just a 30% connectivity (Mendell et al., 1974). Furthermore, they reported a decrease in the EPSP rise time that returned to near normal following peripheral regeneration (Mendell et al., 1974). This was interpreted as specific deficits in proximal synapses on axotomized MNs. Based on the fact that a few years earlier the phenomenon of “synaptic stripping” (see below) had been described with electron microscopy over the cell bodies of axotomized facial MNs (Blinzinger and Kreutzberg, 1968) and then extended to spinal MNs (Chen, 1978), they hypothesized that the functional deficits of the Ia input could be explained by a transient removal of Ia synapses from the surface of cell bodies and proximal dendrites of axotomized MNs. These synapses were then recovered after MNs reinnervated peripheral targets. Two critical errors of interpretation resulted in the

erroneous conclusion of “transient plasticity” of the Ia afferent input: 1) All of these studies are based on electrical stimulation of the peripheral nerve, and none tested the stretch reflex using natural stimulation, 2) the anatomical interpretation was based on comparing the structural plasticity of excitatory synapses on axotomized MNs, but the synapses investigated in structural studies, for the most part, had nothing to do with Ia afferents.

By difference to Mendell’s results and interpretation, the stretch reflex never recovers after nerve transection, and this was rediscovered by Cope, Bonasera, and Nichols in 1994 (Cope et al., 1994). Cope et al., investigated the ability to produce a stretch response in cats who had the LG and peroneal nerves severed and rejoined. These animals were allowed to survive for 3 years after injury! A time at which regeneration and reinnervation were complete, as demonstrated by the return of single motor unit twitches in all MNs recorded and fired. Nevertheless, the muscles were unable to produce muscle contractions in response to stretch (Cope et al., 1994). Regardless of the absence of the stretch reflex, the electrical properties of the MNs return to normal levels (Bichler et al., 2007) as well as the ability for most Ia afferents to respond with stretch evoked potentials and encode normal firing to stretch (Cope et al., 1994). It must be noted that if the Ia afferents failed to reinnervate muscle spindles correctly or end up in a different end organ, they would not respond to stretch (Scott, 1996); however, this seems not to be the case. These papers demonstrate that the loss of the stretch reflex is not a failure of Ia afferents spindle reinnervation or the possibility that regenerated MNs are incapable of producing an action potential in response to synaptic input. They

strongly suggest a permanent deficit in connectivity between Ia synapses and MNs after regeneration in the periphery was successful and complete.

Similar experiments were performed in rats, and the results were consistent with the observations in the cat. Haftel et al. showed that injured Ia afferents regenerate into muscle and regain their ability to respond to muscle stretch after they reinnervate muscle spindles (Haftel et al., 2005). To prove this, they used a paradigm in which the muscle tendon is attached to a servomotor and is stretched 1mm at a rate of 20mm/s, held for 1 s and then released. This technique is called ramp-hold-release. They measured the response in Ia afferents between 9 – 14 months after either an MG or LGS nerve transection and repair. They recorded the stretch response in 40 Ia afferents and all responded to muscle stretch, and recovered stretch transduction capabilities, suggesting that they have reinnervated the muscle spindles in the muscle (Haftel et al., 2005). All recordings were performed in the dorsal root proving further that this information was entering into the spinal cord. They then went on to record, intracellularly, stretch synaptic potentials (SSPs) in MNs using an *in vivo* spinal cord preparation adapted to the rat. Normal healthy MNs depolarize as the muscle is stretched with a waveform that matches the dynamic and steady-state level of firing of the Ia afferent (Westbury, 1972). However, in reinnervated MNs 13 of 22 MNs recorded had absolutely no response to stretch (Haftel et al., 2005). A follow-up study by Bullinger et al., found a very similar result, with 40% of MNs having no response to stretch and the remaining 60% had a significantly smaller amplitude (Bullinger et al., 2011). This study also used STA to estimate connectivity between Ia

afferents and MNs in the MG homonymous connections and reported a drop from 97% connectivity to 17%. This drop in connectivity is similar to that reported by Mendell and colleagues in the cat after an acute injury (Mendell et al., 1974, 1976), except that in this new experiment the MNs and Ia afferents are no longer disconnected in the periphery, but have regenerated and reinnervated the muscle. Thus, Mendell's results on reduced connectivity in the cat are in fact permanent and not transient as initially reported.

The loss of the stretch reflex and the significant decrease in SSPs recorded from MNs is very much dependent on the type of injury sustained. Lack of recovery appears to be specific for a complete nerve transection. When the peripheral nerve is crushed the stretch-reflex is however capable of returning (Barker and Young, 1947; Seburn and Cope, 1998). This was more recently investigated by Prather et al., who analyzed SSPs and the stretch-reflex in cats that had undergone an MG nerve crush (Prather et al., 2011). They found that SSPs recovered in MNs but were about 70% of normal strength compared to the sham un-operated side and, interestingly, the stretch-reflex not only returned but was enhanced to 145% - 157% compared to the control side (Prather et al., 2011).

The reason for this permanent deficit in connectivity was investigated through a collaboration of the Alvarez and Cope labs, using VGLUT1 as a marker of Ia synapses. They found that the majority of VGLUT1 Ia afferents that project into lamina IX and synapse on the soma and proximal dendrites of MNs are permanently removed and never return even after peripheral regeneration is complete (Alvarez et al., 2010; Alvarez et al., 2011). This process was entirely

different to synaptic stripping followed by recovery of synapses labeled with alternative synaptic markers like VGLUT2, VGAT, and VACHT (Alvarez et al., 2011). Furthermore, they found that it is not just the disconnection of Ia synapses, but the complete removal of the entire Ia axonal branch that projects into lamina VII and IX what ultimately explains the permanent reduction in SSPs and a complete absence of the stretch reflex after peripheral regeneration (Alvarez et al., 2011).

This conclusion is opposite to the interpretation of Ia synapse plasticity after injury as an extension of the “synaptic stripping” phenomenon (Mendell, 1984). These results not only prove this interpretation to be incorrect but open a new area of investigation on the mechanisms of this permanent Ia afferent synapse and axon removal. Moreover, in the published study described in Appendix I (Schultz et al., 2017) we also show that removal of Ia afferent synapses on MNs is incomplete after nerve crush in parallel to the physiological experiments in the Cope lab. We therefore seek in this thesis to uncover possible mechanisms that induce more or less removal of the synaptic circuitry depending on the type of lesion in the periphery. We hypothesize that the neuroinflammatory response triggered centrally inside the spinal cord after peripheral nerve injury could be designed in part to remove inappropriate connections after more or less ambiguous regeneration in the periphery. In the following section(s) I will review the differences between Ia afferent synaptic plasticity and the synaptic stripping phenomenon and later I will review the neuroinflammation inside the spinal cord in response to nerve injury.

1.4 Synaptic stripping vs axon retraction and transganglionic anterograde degeneration of sensory afferents injured in the periphery

After nerve injury or motor neurodegenerative diseases there is a displacement of presynaptic terminals from axotomized or diseased MNs (Gonzalez-Forero and Moreno-Lopez, 2014). For the purpose of this thesis we will specifically focus on the synaptic plasticity after PNI and the mechanisms involved in this process. The term synaptic detachment or synaptic stripping refers to the temporary displacement of presynaptic terminals from the surface of MNs following axotomy (Blinzinger and Kreutzberg, 1968; Chen, 1978; Graeber et al., 1991; Alvarez et al., 2011). The majority of these synapses return to the MN surface following peripheral nerve regeneration when MNs reinnervate muscle. I want to make clear the difference between this classical synaptic stripping and the removal of Ia synapses. As described above, following PNI the synaptic inputs from Ia afferents are displaced from the MN surface, however these inputs never return even after peripheral reinnervation is completed. This is because entire ventrally projecting Ia collaterals die-back towards the dorsal horn and largely disappear from laminae IX and VII. The critical difference is that the majority of synapses removed from the MN surface during synaptic stripping originate from local spinal interneurons and descending inputs that are undamaged by the nerve injury. Therefore, their removal from the MN surface solely depends on the injury (axotomy) of the postsynaptic MN. Moreover, their removal was described as “stripping” or “lifting” and not as phagocytic. Once these MNs reinnervate their targets the “lifted boutons” have the capacity to re-establish synapses with the MN

surface. However, Ia afferents are directly affected by PNI and their removal is permanent. In this case the synaptic deletion depends on injury to the presynaptic element since Ia inputs from injured afferents are also removed from uninjured heteronymous MNs and uninjured ventral horn interneurons. Moreover, because the mechanism implies removal of the full collateral from the ventral horn, Ia synapses are lost in both the cell soma and the dendrites (as fully characterized in chapter 1), causing significant deficits since the majority of the input targets the dendritic arbor. In contrast, “synaptic stripping” of axotomized MNs is focused to the cell body and the very proximal primary dendrites.

Also, importantly, the deficit in the Ia afferent projections seems restricted to the ventral horn while other targets in the dorsal horn and Clarke’s Nucleus are better preserved (Alvarez et al., 2011). This implies that proprioceptive information can still be carried to the cerebellum and cerebral cortex through ascending sensory pathways. Moreover, proprioceptive information can also reach the ventral horn through polysynaptic pathways, although in this case, it might carry additional information, for example from Ib afferents, and therefore the pathways are not as specific to Ia information as the original monosynaptic stretch reflex and disynaptic reciprocal inhibitory pathways. The objective of this thesis is to provide insight into the mechanisms that remove Ia synaptic collaterals from the ventral horn after a peripheral nerve injury and should not be confused with the classical synaptic stripping mechanism. This error has been the cause of much confusion in the literature.

1.4.1: History of synaptic stripping

Synaptic displacement after PNI was first described in a seminal study by Blinzinger and Kreutzberg in 1968. They performed a complete transection of the facial nerve and investigated changes in synaptic density on the surface of axotomized MNs 4 days after injury. They found, using electron microscopy (EM), an 80% reduction of synaptic boutons on the MN perikarya and proximal dendritic arbor (Blinzinger and Kreutzberg, 1968). Importantly they noted that the detached synapses did not appear to be degenerating but merely were retracted from the MN surface. Lastly, this study became a keystone in the field because for the first time the authors involucre microglia in a synaptic plasticity mechanism. Later authors re-interpreted this study as to suggest microglia phagocytosis of synaptic terminals, but this was never mentioned in the study. The evidence presented is based on the ultrastructural observation that microglia processes interpose between synapses and the MN surface and the images were interpreted as “lifting” of synapses. Ultrastructural evidence for synaptic lifting or “stripping” was then confirmed by many authors (Sumner and Sutherland, 1973; Sumner, 1975; Chen, 1978; Graeber et al., 1993). It should be noted that the phenomenon affects synapses on the cell body and a small proportion of these might be Ia afferent synapses when studying spinal MNs; however, these synapses do not exist in the cranial nuclei where the synaptic lifting phenomenon was initially first reported and confirmed (facial and hypoglossal MNs).

Sumner and Sutherland performed time course experiments and went on to demonstrate that the majority of detached synaptic boutons returned to the MN

when peripheral regeneration and reinnervation occurred (Sumner and Sutherland, 1973). They performed a complete transection of the hypoglossal nerve in adult rats and investigated the synaptic density on the soma and proximal dendrites of axotomized MNs at different time points between 5 days and 12 weeks after injury. As expected, they found a major depletion in synaptic boutons on the soma and proximal dendrites of axotomized MNs starting 5 days after injury all the way out to 5 weeks postinjury, however by 12 weeks post injury the majority of synapses had returned (Sumner and Sutherland, 1973). In these cranial nerves (facial and hypoglossal) PNI only affects motor axons indicating that this synaptic retraction is dependent on injury to the axon of postsynaptic MNs. Similarly, the earliest EM analysis of synaptic stripping of axotomized spinal MNs, by ventral root avulsion, found a very similar phenomenon in which synaptic boutons were temporarily stripped and returned to the MN upon peripheral nerve reinnervation (Chen, 1978). After ventral root avulsion, sensory fibers remained intact and uninjured.

Synaptic “stripping” does not affect equally all synaptic boutons. Sumner published another study in 1975 that demonstrated that the primary synapses affected by axotomy were the S-type glutamatergic boutons which made up 72 – 89% of all the synaptic boutons on the MN soma in normal healthy hypoglossal MNs (Sumner, 1975) (note that this synaptic organization on the cell body is different to what was reviewed before for spinal MNs). A similar preference for detachment of excitatory synapses was later confirmed in spinal MNs after proximal intramedullary axotomy (Linda et al., 2000). They showed that the F-type

inhibitory synapses made up the majority of the remaining somatic boutons and were resistant to detachment. These data also fit well with the Blinzinger and Kreutzberg study in the facial nucleus that showed an 80% detachment of synapses, a majority of these most likely S-type and most of the remaining 20% being F-type.

From a clinical relevance perspective, it is important to point out that synaptic stripping has been confirmed in human MNs. A case report from Graeber et al., described one patient who presented with damage to the hypoglossal nerve and died 3 months after the nerve damage for unrelated reasons (Graeber et al., 1993). In this patient, the authors demonstrate a high density of synaptophysin-immunoreactive boutons innervating the MNs contralateral to the injury and a significant depletion of these synapses on the ipsilateral side (Graeber et al., 1993). These data are the first to demonstrate synaptic displacement after nerve injury in humans.

1.4.2: Evidence for anterograde transganglionic degeneration of sensory axons and synapses after PNI

Anterograde transganglionic degeneration refers to the central degradation of the Ia afferent axon that occurs after the peripheral branch of the nerve is severed. This is an interesting phenomenon where the peripheral axons can regenerate while their central projections are actively degenerating. One potential explanation for the decrease in Ia afferent synaptic density is the death of the Ia

afferents after injury. Many studies have investigated cell death of dorsal root ganglia (DRG) neurons following PNI and have reported many contradicting conclusions and confusing results. It seems that species, injury type, the location of the injury, and age are all important factors that can influence the survival of sensory neurons in the DRG. Here I will review a few select studies that may be pertinent to our project by mostly focusing on the nerves of the hindlimb and injuries performed in adult animals (unless otherwise noted). Furthermore, we will review the survival of DRG neurons and the central projecting axons that enter into the dorsal root independently as it is possible to have central degeneration of a primary sensory neuron axon and the cell still survive in the DRG.

The data on sensory neuron cell loss in dorsal root ganglia (DRG) seems relatively consistent across rats, cats, and guinea pigs with approximately a 10 – 30% loss in DRG cells following sciatic nerve injury (Risling et al., 1983; Rich et al., 1984; Johnson and Yip, 1985; Arvidsson et al., 1986; Otto et al., 1987; Rich et al., 1987; Schmalbruch, 1987) (Comparison table in (Tandrup et al., 2000)). Though, as time has passed entered a time in scientific discovery where mouse models have become prevalent. The most thorough study in mouse, to my knowledge, is that performed by Shi et al., in 2001. The authors of this paper transected the sciatic nerve and counted the number of DRG cells at 7 and 28 days post-injury. They found that at 7 days there was a 24% decrease in cell number and by 28 days this number had a reduction by 54%, both of which were significant compared to controls (Shi et al., 2001). These decreases seem much higher than what has been reported in other mammalian species.

However, not all injuries affect DRG cells equally. An interesting study was by Rich et al., compared sciatic nerve cut versus crush in the adult rat. They found that after crush there was a 12% loss in DRG neurons and this loss significantly increased to 18% after transection (Rich et al., 1989). Moreover, complete transection, without regeneration (ligated), results in an even more significant decline in DRG neurons with a percent loss of around 37% at 32 weeks post-injury (Tandrup et al., 2000) and a 50% loss in a ligation model with no direct axotomy (note: this ligature was placed just distal to the L5 DRG and not directly on the sciatic nerve) (Lekan et al., 1997). Another interesting study was performed by Ygge where he compared the amount of cell death in the DRG after either a sciatic nerve transection (proximal injury) versus a tibial and common peroneal transection (distal injury) in the adult rat (Ygge, 1989). The DRGs from the L4-L6 region were compared between the axotomized and control side around 120 days post-injury. Ygge found that after complete sciatic nerve transection there was an average of 27% neuronal loss compared to controls, however, after tibial/peroneal transection there was only a 7% loss in DRG neurons (Ygge, 1989). These data suggest that proximity of the injury to the DRG influences the number of DRG neurons lost after injury.

Not all DRG neurons are equally susceptible to cell death. Small and large DRG cell bodies are respectively associated with unmyelinated C-fibers carrying nociceptive and temperature information from skin, muscles and internal organs (some even carry skin mechanoreception or “social touch”) and myelinated A-fibers that carry cutaneous low-threshold mechanoreception and muscle

proprioception (Ia, Ib, and II). The consensus is that small size DRG neurons are the ones susceptible to cell death, while large DRG neurons are mostly unaffected (Tandrup et al., 2000; Shi et al., 2001). This is also true following sciatic nerve transection in kittens (Aldskogius and Risling, 1983). This is relevant to our study as we analyzed connectivity of Ia afferents which are amongst the larger sensory neurons in the DRG and have the largest diameter and more heavily myelinated axons. This reinforces the point that the substantial loss in Ia afferent synaptic inputs is not from dying DRG cells and supports the hypothesis that there are central mechanisms at work in the degeneration of ventrally projecting Ia afferent axon collaterals.

Additional experiments quantified changes in myelinated and unmyelinated axons entering the spinal cord through dorsal roots after PNI. A distinction needs to be made between quantifying the number of sensory neurons in the DRG and the number of sensory axons in the dorsal root, since as mentioned previously, it is possible to have degeneration of central projecting sensory axons while preserving DRG cells. A thorough study was performed by Coggeshall and colleagues who investigated the number of myelinated and unmyelinated fibers entering through lumbar 4 and 5 dorsal roots in rats following sciatic nerve cut-ligation or crush injuries (Coggeshall et al., 1997). They study different time points ranging from 2 weeks to 32 weeks. Interestingly they found no matter which injury or time point they investigated the number of significant myelinated fibers was always unaffected (Coggeshall et al., 1997). However, in both cut and crush, there

is approximately a 50% decrease in the number of unmyelinated fibers compared to the uninjured contralateral side by 32 weeks post-injury.

In conclusion, large sensory neurons, likely including proprioceptors do not die after nerve injuries and their myelinated axons are preserved in dorsal roots. Nevertheless, their synapses inside the spinal cord were found in some instances to be degenerating. Some early reports described primary sensory axon degeneration in the trigeminal area (Grant and Arvidsson, 1975) as well as the sensory axons innervating the vibrissae (Arvidsson, 1986) after trigeminal nerve injury. In the spinal cord degenerating fibers were located in lamina III and IV 14 and 30 days after a sciatic nerve transection in the rat (Arvidsson et al., 1986). This region is occupied by the synaptic termination of A-type myelinated cutaneous mechanoreceptors. Interestingly, though not discussed in detail in their manuscript, further evidence of degenerating fibers was found in lamina IX of the L4-L5 segment (figure 1 in (Arvidsson et al., 1986)). This was not detected in any other lumbar region following sciatic nerve transection. The changes identified in the central synaptic terminals of sensory axons injured in the peripheral nerves was then named “transganglionic anterograde degeneration” and reviewed by Aldskogius, Arvidsson, and Grant in 1985 (Aldskogius et al., 1985), but little attention has been paid to this phenomenon in the following 30 years, and nothing is known about its mechanisms.

Transganglionic anterograde degeneration fits well with what we know about Ia afferent plasticity after nerve injury. Evidence for the preservation of stretch-sensitive afferents in the dorsal root after nerve injury and regeneration

was found with electrophysiology (Mendell et al., 1974; Bullinger et al., 2011) and anatomically (Alvarez et al., 2011). Moreover, this later paper performed intra-axonal fills of single Ia afferents and demonstrates that one year after injury these afferents were still present in lamina V/VI but had retracted entirely from lamina IX and were reduced in LVII (Alvarez et al., 2011). These data support the notion that Ia sensory neurons do not die in the DRG and that their axons still travel in dorsal roots and enter the spinal cord projecting to the dorsal horn, but with decreased projections to the ventral horn implying secondary degeneration as a consequence of injury to the peripheral branch in the nerve.

1.4.3: Mechanisms involved

One of the first steps that must occur during synaptic displacement is the destabilization and detachment of the presynaptic bouton. A proposed mechanism is through the production of nitric oxide (NO) (Yu, 1994; Sunico et al., 2005). NO is a gaseous messenger molecule known to be involved in many intracellular signaling pathways and is produced upon activation of the enzyme nitric oxide synthase (NOS) (Yu, 1994). Following axotomy, MNs upregulate the inducible form of neuronal NOS (nNOS) by 3 days post injury with a peak around 14 days; expression remains elevated for up to 28 days before returning to control levels (Yu, 1994, 1997) (reviewed in (Moreno-Lopez, 2010)). This time course is very much dependent on the type and location of the injury as demonstrated by Yu (Yu, 1997). In these studies, the number of NO-producing neurons was estimated based on the NADPH diaphorase histochemistry, following a crush, cut, or avulsion

of the hypoglossal nerve. The maximum number of MNs with NADPH diaphorase activity was approaching 24% in crush (3 days, approx. 20% at 14 days), 60% after the cut (14 days), and around 92% after avulsion (14 days) in hypoglossal MNs (Yu, 1997). nNOS expression remains elevated until axon regeneration and muscle reinnervation is completed in the periphery (Sunico et al., 2005) suggesting that perhaps signals from the muscle downregulate the expression of nNOS.

Sunico et al. described a molecular pathway linking NO release and synaptic detachment (Sunico et al., 2010). They propose that NO produced in axotomized motoneurons diffuses into presynaptic boutons where NO activates Rho-associated protein kinase ROCK and GTPase kinase Rho-A increasing phosphorylation of myosin light chain protein and ultimately destabilizing the peripheral cytoskeleton of presynaptic terminals inducing synapse detachment (Sunico et al., 2010; Gonzalez-Forero and Moreno-Lopez, 2014).

Interestingly, and very fitting with the synaptic stripping phenomenon, this process seems to be specific to the excitatory synapses. Sunico et al., performed another exciting experiment by injecting a virus vector carrying the nNOS gene (AAV-nNOS) into the tongue of injured rats and then looked at changes in synaptic inputs on MNs in the hypoglossal nucleus. They found that by just expressing nNOS in the MNs they induced a significant 34.6% reduction in VGLUT2 (excitatory) synaptic inputs on MNs while VGAT (inhibitory) synapses were unaffected (Sunico et al., 2010).

One proposed mechanism for the difference in inhibitory versus excitatory synaptic loss is through the major histocompatibility complex (MHC) class I

pathway. This pathway has been shown to be critical in eliminating synapses in the developing CNS (Huh et al., 2000). In a study by Linda et al., they investigated the regulation of MHC I expression in the rat spinal cord following a complete transection of the sciatic nerve (Linda et al., 1998). They found an IFN- γ mediated pathway that upregulates the association protein $\beta 2$ – microglobulin in axotomized MNs between 3 – 21 days following injury (Linda et al., 1998). Microglobulin protein associates with MHC I to allow proper antigen presentation. Furthermore, there was a rapid increase in MHC I around the MNs in what appeared to be microglia cells, though this was not confirmed in the study. A follow-up study from Oliveira et al., hypothesized that in the injured adult CNS this MHC I pathway could also be mediating synaptic elimination (Oliveira et al., 2004). They went on to perform complete sciatic nerve transections and compare them to sham controls in $\beta 2$ -microglobulin KO adult mice and measured the changes in synaptic density around lesioned MNs. They found a higher loss of synaptic inputs on MNs following injury specifically affecting inhibitory synapses (Oliveira et al., 2004). The decline in excitatory synaptic inputs was similar as in the WT mice. This study concluded that MHC I upregulation after injury prevents the loss of inhibitory synapses following axotomy while having no impact on excitatory inputs. However, the exact relationship between inhibitory synaptic loss and MHC I expression is not clear. The authors argue that it is necessary to remove excitatory inputs when MNs switch from a transmitting to a regenerative state after axotomy to prevent neurotoxicity and suggest that preservation of inhibitory synapses might further contribute in protecting from excitotoxicity axotomized MNs. However, there is no

evidence to support this claim. Moreover, axotomized MNs decrease their expression of KCC2 around cell bodies, which is essential for maintaining the chloride gradient necessary for an IPSP to occur in response to GABA or glycine release from F-type boutons (Erica T. Akhter, Arthur W. English and Francisco J. Alvarez, unpublished observations). Without KCC2 expression, the chloride gradient will be disrupted, and inhibitory synapses will now become depolarizing, as seen early in development (Doyon et al., 2016). In the β 2-microglobulin KO mice, peripheral nerve regeneration is delayed compared to WT mice, suggesting that preservation of inhibitory synapse mechanisms may be necessary for promoting axon growth (Oliveira et al., 2004).

In addition to the actual detachment of synapses, there must be a mechanism in place that targets particular synapses for permanent degradation while not eliminating others. A potential mechanism for permanent synaptic elimination is through neuroinflammation and complement-mediated pathways. Complement is a set of proteins that when expressed on synaptic terminals marks them for recognition and degradation through lysis or phagocytosis (Esser, 1991; Kinoshita, 1991; Stevens et al., 2007; Perry and O'Connor, 2008; Ramaglia et al., 2008; Schafer et al., 2012). This process is known as opsonization and allows specific cells or synapses to be tagged for removal by elements of the immune system. This mechanism was shown to be critical for synaptic pruning in the developing CNS and during neurodegeneration in the mature system (Bonifati and Kishore, 2007; Stevens et al., 2007). The “classical complement cascade” is initiated by the accumulation of C1q protein on the surface of the targeted synapse

by binding to extracellular domains of synapses membrane proteins. Once linked, through a series of enzymatic and cleavage processes, C3 and C5 proteins may be expressed that can promote synaptic elimination (Perry and O'Connor, 2008). These proteins can coat the surface of the target synapses making them recognizable for destruction by effector cells, typically a macrophage such as a microglia cell or blood-derived macrophage.

Complement is also known to be expressed around MNs following PNI. An early study by Svensson and Aldskogius showed, in adult rats, that 7 and 14 days after complete transection of the hypoglossal nerve there was a significant increase in perineuronal expression of C3 (Svensson and Aldskogius, 1992). Furthermore, spinal microglia cells are activated after PNI and upregulate the C3 receptor (CD11b, OX-42). These cells then migrate and surround axotomized MNs. Later studies found complement proteins C1q and C3 in the dorsal horn and gracile nucleus of the spinal cord following sciatic nerve transection in the rat (Liu et al., 1995) and the ventral horn of the mouse (Berg et al., 2012). We have performed some preliminary experiments and have also found strong expression of C1q around axotomized MNs one week following sciatic nerve transection (unpublished, figure 1.1).

To investigate the role of complement in synaptic removal, Berg et al. performed a sciatic nerve transection in mice lacking either C1q or C3 (Berg et al., 2012). They found that 7 days after transection there was a 32.3% reduction in synaptophysin immunoreactivity around axotomized MNs in WT mice but only a 6.2% reduction in C3 KO mice. Furthermore, the inhibitory synaptic inputs, defined

by expression of the vesicular inhibitory amino acid transporter (VIAAT), were the primary synaptic inputs rescued in the C3 KO mice with only a trend towards the preservation of glutamatergic inputs (VGLUT2+), but this was not significant (Berg et al., 2012). There was no difference in synaptic removal or preservation in the C1q KO mice compared to control. While this study provides some insight into complement involvement in the elimination of inhibitory synapses, this study is also incomplete and presents some conflicting data. First, we know that the primary synaptic inputs that are removed from axotomized MNs are the excitatory glutamatergic inputs and that the inhibitory inputs are mostly unaffected (Sumner, 1975; Linda et al., 2000). It was unclear how the preservation in the C1q KO could be specific to synaptic inputs that are largely unaffected. Secondly, the authors only investigated VGLUT2+ synapses and did not look at VGLUT1+ inputs from the Ia afferents. These may be the primary synaptic inputs that are opsonized considering these are, most likely, the only inputs targeted for permanent degradation. The earliest EM data from Blinzinger and Kreutzberg suggested that the terminals that detach are not degraded, but just withdrawn from the MN surface (Blinzinger and Kreutzberg, 1968). These data would support the notion that VGLUT2+ synapses retract but are not tagged with complement for permanent degradation, as the majority return to the MN. However, this is not the case for the Ia VGLUT1 afferent inputs which are entirely removed from the ventral horn, involving both their synapses and pre-terminal axons.

Taken together these data demonstrate that complement proteins are expressed following nerve injury and could be involved in the degradation of Ia

afferent axons and synapses in adults after PNI, though this remains to be explored. It is worth mentioning a recent report by Vasek et al., provide evidence for target VGLUT1 synaptic removal dependent on complement expression in the hippocampus after exposure to West Nile Virus (Vasek et al., 2016). The authors of this paper found that C3d and C1q co-localized with VGLUT1 synapses 7 days after viral exposure and these synapses were targeted for removal by activated microglia cells (Vasek et al., 2016). Interestingly, in the C3 KO, they prevented synaptic loss. A similar mechanism for removal may be occurring in our model.

To summarize this section, there is a clear difference between a temporary synaptic stripping of boutons on axotomized MNs versus the complete degradation of the Ia afferent synapses and their parent axon collaterals. The initiation of synaptic detachment may be similar amongst the two in that they both could detach from the surface of MNs in a NO-dependent process. However, axotomized Ia afferents differ in that they are recognized as being injured and their ventral collaterals targeted for removal whereas other glutamatergic synapses are only temporarily retracted from the surface and then return upon peripheral regeneration. One possible mechanism these synapses can be targeted for destruction is through a complement-dependent pathway capable of distinguishing injured Ia's from uninjured synaptic inputs. This mechanism links Ia afferent loss with neuroinflammation and this might be tightly regulated depending on the kind of injury since the permanency of the Ia input loss is dependent on the type of injury in the periphery. Central neuroinflammation involves activation of microglia but also frequently recruitment of peripherally derived immune cells that can

infiltrate the spinal cord and exacerbate inflammation. In the following section, we will discuss the neuroinflammatory reaction that occurs in the spinal cord after nerve injury and discuss potential involvement of different immune cells in synapse plasticity and degradation.

1.5 Neuroinflammation

Inflammation, as defined by the reaction of living tissue to injury (Robbins et al., 1981) has become a topic of great interest as there is increasing evidence that inflammation inside the CNS may be responsible for promoting neural deficits in many different neurodegenerative conditions including Alzheimer's, Parkinson's, Amyotrophic Lateral Sclerosis, spinal cord injury, and PNI (Streit, 2004; Streit et al., 2004; Frank-Cannon et al., 2009; Kempuraj et al., 2016). PNI results in a massive immune reaction within the spinal cord ipsilateral to the injury. This immune reaction is primarily localized in two distinct regions. The dorsal horn superficial lamina where the terminations of injured cutaneous afferents are localized and the ventral horn around motor pools containing the cell bodies of axotomized MNs. This is quite interesting as the injury itself is outside the CNS. The central microglia cells first respond by swelling their cell bodies and retracting their extensive processes. These cells increase in cell number and populate the ventral horn around axotomized MNs and sensory axon projections. In addition, peripherally derived myeloid cells can, in some situations, infiltrate the CNS and migrate to the dorsal and ventral horn (Echeverry et al., 2011; Gu et al., 2016). The primary focus of this thesis is built around the neuroinflammatory response that

occurs in the spinal cord after nerve injury. How this can drive permanent changes in motor circuitry connectivity, specifically the degradation of Ia afferent synaptic inputs on MNs, and how this mechanism is regulated according to the severity of the injury in the periphery.

It is important to note that whether inflammation is adaptive or maladaptive is an open question and likely depends on the conditions and types of injuries and neurodegenerative processes. The consensus is that inflammation after direct injury to the CNS may be necessary for cleaning up dead cells, clearing plaques, and degrading any cellular debris within the CNS; however, when these immune processes go awry, and control mechanisms are overwhelmed, then devastating consequences may follow. A balanced immune reaction is necessary for keeping homeostasis and neuronal health, but the scale can easily tip during injury and disease. For many years, the CNS was considered an “immune privileged” space in that the peripheral immune system could not influence the CNS due to the presence of a blood-brain barrier (BBB), or blood-spinal cord barrier (BSCB). We now know that this is not true, and this barrier can become leaky during inflammation allowing trafficking of elements of the innate and adaptive immune system into the CNS (Zlokovic, 2008).

During acute inflammation, there is an immediate immune response in which the central microglia cells, the native macrophages of the CNS, can respond by changing their activation state and releasing a whole host of different cytokines and signaling molecules that can exacerbate inflammation or signal to other immune cells in the body. Additionally, local injured neurons may release signaling

molecules that activate the microglia cells or assist in recruiting additional immune cells.

The types of cells that are activated and recruited varies widely depending on the injury as well as the overall neuroinflammatory time course. For the remainder of this section, I will focus on critical immune cells known to be relevant after PNI. After reviewing the neuroinflammation literature during my Ph.D., the complexity of neuroinflammation has become apparent, and the involvement of inflammation in different disease states can vary greatly and should not be generalized.

1.5.1: Microglia

The field of glia (Greek for glue) research started with the German scientist Rudolf Virchow who in 1846 who first described it as a type of connective tissue in the spinal cord and brain and coined the term neuroglia (Virchow, 1846; Virchow, 1858; Garcia-Marin et al., 2007). At this early time, Virchow was not able to distinguish the different types of neuroglia as the methodology wasn't available yet. We now know neuroglia is composed of two different classes of cells: 1) microglia (mesodermal origin) and 2) macroglia (ectodermal origin), which can be divided into astrocytes and the myelin-forming oligodendrocytes inside the CNS, and Schwann cells in the PNS. Other types of glial cells are ependymal cells lining the ventricles or satellite cells and the more recently discovered NG2 progenitors.

Each one of these cell types has a unique history of discovery, but for this section, we will focus on microglia.

In the early 20th century Franz Nissl and Alois Alzheimer described a unique rod-shaped cell, or as they called it in German Stäbchenzellen, in the brains of patients who had been diagnosed with neurodegenerative or psychiatric illness, but the function of these cells remained unknown (Nissl, 1904; Alzheimer, 1910; Wolf et al., 2017). Two Spanish researchers deserve credit for our current understanding of the microglia cell, Nicolás Achúcarro, and his student Pío del Río-Hortega. Both worked under Cajal and were the first to fully characterize microglia and coin the name (Tremblay et al., 2015; Sierra et al., 2016). Achúcarro, who actually worked with Alzheimer in Germany for a while, developed a new staining technique using ammoniacal silver nitrate which labeled and distinguished phagocytic microglia cells, though at the time he called them granuloalipose cells to distinguish them from other glial cells such as astrocytes (Achúcarro, 1911; Achúcarro, 1913; Tremblay et al., 2015). Achúcarro was making significant progress and became a leader in this area of research, but unfortunately, shortly after starting these studies, he became sick and died in 1915 from lymphoma. At this time Cajal encouraged Río-Hortega to pursue the pioneering work of Achúcarro and follow up on these newly described cells. It was the development of a novel staining technique by Río-Hortega that allowed him to investigate these cells in full detail. He came up with the silver carbonate staining method that, for the first time, showed a complete detailed structure of the microglia cell (Tremblay et al., 2015). It should be noted that for some unknown reason this labeling method

works best in sheep brain (Streit, 2012). He published three seminal papers in 1919 describing the full morphological characteristics of these cells and their ability to change morphology in response to injury. Furthermore, he proposed that these cells were of mesodermal origin (Río-Hortega, 1919a; Río-Hortega, 1919b, c) (for a brief review and an English translation with commentary of all three papers, please see (Sierra et al., 2016)). For many years after the work of Río-Hortega, not much was added to the field of microglia research until the work of George Kreutzberg in the late 1960's. This was the start of the modern field of research and understanding of microglia (Blinzinger and Kreutzberg, 1968). The number of papers published every single year involving microglia has been on the rise ever since with almost 3,000 articles published in 2016 with the keyword “microglia” (Pubmed search).

Microglia cells are tissue-specific macrophages, and they have a mesodermal origin that was confirmed with modern lineage tracing techniques (Ginhoux et al., 2010). Microglial are derived from yolk-sac fetal macrophages that invade the developing CNS at approximately 8 – 8.5 days post conception in the mouse (Ginhoux et al., 2010; Prinz et al., 2011; Streit, 2012). These progenitors then differentiate into microglia by expression of the colony stimulating factor 1 receptor, CD34, and the transcription factors PU.1 and Irf8 (Davoust et al., 2006; Ginhoux et al., 2010; Saijo and Glass, 2011; Kierdorf et al., 2013). A long-standing debate existed on whether peripherally derived monocytes could contribute to the resident microglia pool in the CNS or if microglia cells were self-sustainable and continued to divide maintaining the whole population in the CNS through

development and maturity. Based on the current data, the latter case seems to be the better supported. Ginhoux et al., using lineage tracing techniques found that in healthy conditions hematopoietic progenitors do not infiltrate the postnatal CNS and therefore do not contribute to the resident microglia population (Ginhoux et al., 2010).

By difference to most other CNS cells, microglial can undergo cell division allowing them to distribute and populate the CNS (Kettenmann et al., 2011). In the adult CNS these cells have a long half-life with only about 0.05% of microglia dividing at any one time (Lawson et al., 1992). Once microglia distribute throughout the CNS they make up 5% - 20% of all the glial cells in the CNS (Streit, 2012); that is equal to about 6,000 – 8,000 cells/mm³ (Kirchhoff, 2012). These cells spread relatively uniformly throughout the CNS with a slightly higher density in the ventral pallidum (165 ± 9 cells/mm²) and lower density in the molecular region of the cerebellum (21 ± 3 cells/mm²) (Note: these data come from adult female BALB/c mice and were quantified in 2D projection images) (Lawson et al., 1990). Total estimates put them at 3.5 million microglia cells in the brain.

Microglia cells have a small cell body with several highly branched processes extending into the environment and covering spherical territories of about 50 – 60 μ m in diameter per cell (Kirchhoff, 2012). These processes are covered by small filopodia that are constantly surveying the environment looking for any disruption in homeostasis. Unlike neurons in the CNS these cells are highly dynamic, continuously extending and retracting their processes at a rate of about 1 – 3 μ m/minute. It is estimated that the entire surface of the CNS is surveyed by

microglia processes and filopodia at a rate of 3 – 4 times per day and every single synapse is contacted about once every hour (Wolf et al., 2017)! Their cell bodies are relatively stationary with only minimal migratory movements (Nimmerjahn et al., 2005; Kirchhoff, 2012).

During early development, microglia cells appear “activated” meaning that they are more amoeboid in shape and more phagocytic. I use quotes around the word “activated” as this is somewhat ambiguous when discussing microglia. We are referring to these cells as activated based on their change in phenotype and function from a surveying and homeostatic role. Throughout the literature, some classify activated microglia as M1 (inflammatory) or M2 (anti-inflammatory), but we now know this is a gross simplification (Ransohoff, 2016). First, microglia cells are activated along a spectrum of phenotypes that include upregulation of different combinations of genes with pro- or anti-inflammatory properties in different proportions and levels. Second, microglia cells in the same area can show a diversity of gene activation patterns. Lastly, all of these factors can change through time in a single microglia cell. To more precisely classify microglia, single-cell transcriptome analysis would need to be performed, and each cell analyzed individually as their gene expression can vary significantly from one cell to the next (Fonseca et al., 2016; Gosselin et al., 2017).

Back to the point, during early development, microglia cells have shorter processes and an amoeboid phenotype associated with increased activity and phagocytosis. One of the most critical functions of microglia during this time is the pruning of synaptic connections. One example is the developing visual system.

The laboratory of Beth Stevens elegantly demonstrated that synapses in the retinogeniculate pathway are selectively eliminated during development by microglia cells in a complement-dependent manner (Stevens et al., 2007; Schafer et al., 2012). Microglia are also responsible for a wide range of activities including cleaning cellular debris via phagocytosis, eliminating aberrant synaptic inputs, cytokine release including chemokines that signal and recruit peripheral immune cells, and they can present antigens to T-cells (Kettenmann et al., 2011; Saijo and Glass, 2011).

These cells have become of particular interest during neurodegeneration and after injury. I will review a few actions of microglia cells in disease, but this is not a comprehensive review by any means. It is safe to say that if there is ANY degeneration, injury, or infection that affects the CNS, microglia will be involved in one way or another at the center of an inflammatory response. For example, microglia have been implicated in the clearance of amyloid- β in Alzheimer's Disease and slowing progression of the disease (Lee and Landreth, 2010), while others have reported that microglia activation exacerbates, in some situations, neuronal cell death in Alzheimer's (Fuhrmann et al., 2010). In experimental autoimmune encephalitis (EAE), a model of multiple sclerosis, depletion of native microglia cells reduces disease onset and clinical symptoms, suggesting that the early microglia reaction may initiate or exacerbate the disease (Bogie et al., 2014; Wolf et al., 2017). These examples illustrate the double-edge properties of microglia activation in disease being at the same time beneficial and detrimental depending on differences in activation and progression of the disease.

One handicap of microglia research has been developing adequate criteria for identification. Through the years we made a lot of progress moving from the old silver carbonate staining to developing more specific antibodies for immunohistochemistry and using novel transgenic tools to identify microglia. One of the major hurdles has been distinguishing central native microglia from infiltrating macrophages that could differentiate into microglia-like cells during injury or neurodegeneration. This has been a particularly tricky area as microglia share about 70% homology with peripheral immune cells (Hickman et al., 2013). I have provided a list of some of the most common antibodies used to detect microglia, and in some cases other macrophage cells, in the CNS in table 2.

For this section, I will focus on one specific gene, the fractalkine receptor or CX3CR1. This gene will be used as the principal means of microglia identification in this project. The root CX3C is a class of chemokines that have a cysteine with three amino acids in between (X3) another cysteine residue, and in this case, the R1 is for receptor 1 (CX3CR1) (Harrison et al., 1998). While CX3CR1 is a reliable marker for detection of central microglia cells (Mizutani et al., 2012), there are also some macrophage cells, including meningeal, choroid plexus and perivascular macrophages, that also express various levels of CX3CR1 (Prinz et al., 2011). Fortunately, these other cells have either a precise location and/or a unique phenotype allowing them to be distinguished from the more prominent CX3CR1 expressers in the CNS, the microglia.

This chemokine receptor is a seven-transmembrane G-coupled protein receptor that binds to its unique ligand CX3CL1 or fractalkine and signals through

a $G_{\alpha i}$ coupled pathway which in turn inhibits cyclic AMP production, mobilizes calcium and can activate further intracellular signaling pathways (Ransohoff and El Khoury, 2015). The ligand, fractalkine or CX3CL1, is produced by neurons in the CNS and used in a rather interesting manner as there are two possibilities for its signaling mechanism: 1) Neuronal fractalkine can be membrane bound and bind directly to microglia CX3CR1 through direct cell-to-cell interactions resulting in a robust intracellular calcium signal, which is not what is expected from a $G_{\alpha i}$ pathway. 2) Membrane fractalkine can be released through cleavage of a proteolytic domain and interactions of CX3CR1 with soluble fractalkine decreases calcium signaling (Harrison et al., 1998). These signaling pathways need to be considered with caution, as there are some discrepancies in the literature about the role of membrane-bound versus soluble fractalkine on microglia dynamics and the specific intracellular signaling pathways activated may be context dependent to disease, time and condition (Ransohoff and El Khoury, 2015). For example, Harrison et al., 1998 reported no change in calcium dynamics when 50 nM of soluble fractalkine was applied to rat primary microglia cultures, however a study by Maciejewski-Lenoir et al., 1999 found that 10 nM of soluble fractalkine to similar cultures increased calcium and changed cytoskeletal structure triggering cell migration (Harrison et al., 1998; Maciejewski-Lenoir et al., 1999; Paolicelli et al., 2014).

Perhaps the most crucial point to consider with these early experiments is that they were all done in culture. This could introduce experimental biases that modify actual responses since microglia cells are known to be very sensitive to

their environment and take on very different phenotypes depending on culture conditions. Cell culture work, therefore, needs to be interpreted carefully such that the observed results do not lead to false conclusions about the behavior of microglia *in vivo*. For a thorough review of the pros and cons of cultured microglia see (Biber et al., 2014). More recently *in vivo* studies have suggested that fractalkine signaling may act preferentially as an inhibitory molecule that prevents the overactivation and migration of microglia cells (Biber et al., 2007; Limatola and Ransohoff, 2014). Several studies have shown that when CX3CR1 is genetically knocked out, microglia can become overactive and exacerbate neurotoxicity during neurodegeneration (Wolf et al., 2013; Biber et al., 2014). For example, Cardona et al., injected MPTP in a mouse model to mimic Parkinson's Diseases and found that in CX3CR1 KO mice there was a greater loss in dopaminergic neurons compared to heterozygous mice (Cardona et al., 2006). There may be other instances in which more active microglia might be beneficial to improve repair. A recent study by Freria et al., showed that CX3CR1 KO mice had enhanced recovery following spinal cord injury by promoting axon sprouting and synaptogenesis (Freria et al., 2017). The authors of this report found significantly more glutamatergic (both VGLUT1 and VGLUT2) and serotonergic (5HT) synaptic connections in these KO mice compared to WT mice which correlated with significantly higher levels of anti-inflammatory cytokines such as TGF β 1, IGF1, and FGF2 (Freria et al., 2017). Taken together, we still do not have a crystal-clear answer to the role CX3CL1-CX3CR1 signaling plays in microglia function and the importance of this pathway in injury and degeneration. I think it is important to

remember the complexity of this pathway and interpret different results contextually without trying to over-generalize or apply results from one study to a different condition or disease.

One of the advantages we have with the discovery of the CX3CR1 gene is the generation of transgenic mouse models in which the first 390 bp region of the first exon was replaced with an *enhanced green fluorescent protein* (EGFP) (Jung et al., 2000). This animal model has been an excellent tool for visualizing microglia in health and disease and has led to greater insights into the physiology of these cells. However, we need to remember when analyzing EGFP⁺ expressing cells in this animal that other immune cells can upregulate CX3CR1 expression, such as natural killer cells, T-cells, and circulating monocytes and macrophages (Imai et al., 1997; Jung et al., 2000; Shi and Pamer, 2011). More recently a CX3CR1-Cre^{ER} mouse was generated which expresses a Cre recombinase and human estrogen receptor 1 fusion gene under the control of the CX3CR1 promoter. (Yona et al., 2013). In this model Cre recombination is controlled by tamoxifen injections and adjusting the timing of a single Cre recombination event (with one dose of tamoxifen) allows specific labeling and targeting of microglia cells avoiding other CX3CR1 expressing cells with shorter life-spans and replenishing at faster rates than the long-lived microglia (Goldmann et al., 2013; Tay et al., 2017). Rapidly renewing monocytes (originated from CX3CR1 non-expressing progenitors) will lose their genetic labeling as they turn over while long-lived microglia retain their labels. We will further use this second model in some of the studies described here.

1.5.2: *Macrophage recruitment and infiltration into the CNS*

Macrophages consist of a broad class of different types of cells, some of which are tissue-specific, like microglia, and others are derived from circulating monocytes. For this project, I will focus on the Ly6C^{hi} bone-marrow derived monocytes that can be recruited to a site of inflammation and differentiate into an active macrophage cell and can even take on a “microglia-like” phenotype in some instances (Shi and Pamer, 2011). Recruitment into specific tissues as well as emigration into circulation from the bone marrow are both thought to be dependent on chemokine signaling through activation of a receptor known as cysteine-cysteine receptor 2 (CCR2) (Geissmann et al., 2003; Serbina and Pamer, 2006; Tsou et al., 2007).

One major advance in understanding these macrophage cells was the development of a transgenic mouse model in which a red fluorescent protein (RFP) was knocked in and replaced the first 279 base pairs of the amino terminus of the CCR2 gene (Saederup et al., 2010). This allowed researchers to study the infiltration of these cells into the CNS during a time of disease or injury, as these cells are not present in the healthy CNS. Additionally, this model has been helpful in distinguishing central microglia from infiltrating monocytes/macrophages because some of these infiltrating cells can upregulate low or sporadic levels of CX3CR1 during trans-differentiation into local macrophages. For example, the use of dual heterozygous CX3CR1 GFP/+ and CCR2 RFP/+ mice provided the tools to for the first time definitively conclude that CX3CR1 expression and not CCR2 characterizes microglia throughout development (Mizuno et al., 2012). Moreover,

dual color mice have been used since to distinguish contributions between resident microglia (CX3CR1-GFP+) from infiltrating macrophages (CCR2-RFP+) in a variety of diseases (Evans et al., 2014; Morganti et al., 2014; Yamasaki et al., 2014; Kohno et al., 2015; Umekawa et al., 2015; Gu et al., 2016). It must be noted here that not all CCR2+ cells are monocytes that differentiate into macrophages. While these monocytes/macrophages appear to be the dominant expresser of CCR2, other cells of the myeloid lineage can also express CCR2. These include T-cells, B-cells and dendritic cells (Frade et al., 1997; Kurihara et al., 1997; Kuziel et al., 1997; Banchereau et al., 2000; Reichel et al., 2006). One last important feature of this mouse model is that in homozygosis it is a functional knock out because the RFP insert renders the *ccr2* gene dysfunctional.

The primary ligand for CCR2 is CCL2, also referred to monocyte chemoattractant protein 1 (MCP1). CCL2 is a 13 kDa chemokine protein produced and released from a variety of different cell types, including neurons, astrocytes, and microglia during insult to the CNS (Deshmane et al., 2009). There are additional ligands that can bind to CCR2 including CCL7, CCL8, CCL12, CCL13, and CCL16 (Deshmane et al., 2009). To analyze which cell upregulates CCL2 and might contribute to facilitating entry of CCR2-dependent cells we will use a more recently developed mouse that reports CCL2 expression. In this mouse loxp sites flank exons 2-3 of *cc/2* and in addition the 3' end of exon 3 contains a red fluorescent protein gene (Shi et al., 2011). Thus, in these mice, RFP reports the expression of *cc/2* and when crossed with cre lines will remove both *cc/2* and RFP from cre expressing cells. Therefore, these mice, denominated *Ccl2-RFP^{flox}*, are

used for both reporting *cc/2* expression and also deleting *cc/2* in a cell-type specific manner using cre-lox recombination.

CCR2 macrophages are of particular interest in neurodegeneration and injury. CCR2⁺ cells have been well studied in the context of MS using the EAE model, mentioned above. An interesting study performed by Yamasaki et al., used dual heterozygous CX3CR1^{EGFP/+}::CCR2^{RFP/+} mice to study the differential role of each cell type in the disease (Yamasaki et al., 2014). They found that monocyte-derived macrophages that infiltrate from the periphery seem to initiate the demyelination process and using EM they were able to show that more than half of these cells contained myelin debris that was being actively phagocytosed (Yamasaki et al., 2014). Even more interestingly when they did these experiments in CCR2 KO mice they were able to delay the onset of disease, and they found a significant decrease in the demyelination within the spinal cord, again pointing to the importance of these peripherally derived macrophages in neurodegeneration.

CCR2 cells have also been shown to infiltrate the spinal cord in the context of chronic pain following partial constriction nerve injuries, a well-known model that induces long-lasting hyperalgesia (Gu et al., 2016). One of the main driving forces behind pain hypersensitivity after nerve injury is the inflammatory response in the dorsal horn of the spinal cord, in which microglia cells become activated and peripherally derived immune cells infiltrate the CNS (Ellis and Bennett, 2013; Tsuda, 2016). One study by Zhang et al., transplanted GFP⁺ bone marrow stem cells to irradiated adult mice then performed a partial sciatic ligation injury (Zhang et al., 2007). After the injury they found bone-marrow derived macrophages

invaded the spinal cord dorsal horn; the recruitment of these cells was dependent on MCP1 release. Furthermore, this infiltration was abolished in CCR2 KO mice (Zhang et al., 2007). Lastly, the authors showed, using von Frey testing, that WT mice developed hypersensitivity to stimulation following nerve injury and this was entirely attenuated in CCR2 KO mice (Zhang et al., 2007). There are, however, two important caveats when interpreting these data. 1) The authors claim that the intrathecal injection of MCP1 caused local microgliosis. This is somewhat suspicious as native microglia cells do not express CCR2 (Mizutani et al., 2012). However, it could be possible that after injury native microglia cells begin to express CCR2 or that the cells they were describing were peripherally derived cells or that the injections itself caused microgliosis. 2) The authors of this study used irradiation experiments which are known to break down the BBB and BSCB. This could affect the infiltration rate of blood derived cells. In fact, following studies that did not use experimental irradiation failed to detect infiltration of CCR2 cells in the dorsal horn. In any case, a number of studies have implicated CCL2-CCR2 signaling in contributing to hyperalgesia after partial constriction nerve injuries (Abbadie et al., 2009; Thacker et al., 2009).

This raises the question of the role of BSCB permeability changes during infiltration of peripheral myeloid cells. A thorough study by Echeverry et al. studied this question using adult rats in the sciatic nerve partial ligation model (Echeverry et al., 2011). The authors of this paper injected Evans Blue into the tail vein of injured animals at different time points and found a significant increase in BSCB leakage in the lumbar region 3 days after injury. The BSCB remained significantly

leaky for up to one month after injury. Interestingly, they found that the permeability of the barrier is dependent on the central release of MCP1, which was proposed to be upregulated after injury in sensory neurons and MNs (Zhang and De Koninck, 2006). The authors then injected MCP1 intrathecally into naïve animals and found leakage that resembled that of injured animals. Furthermore, this leakage was prevented in injured rats that were injected with a neutralizing antibody against MCP1 (Echeverry et al., 2011). There have been no studies that have investigated CCL2-CCR2 signaling and infiltration of CCR2 cells in the ventral horn in response to nerve injury and their potential role in synaptic plasticity.

1.5.3: Role of macrophages/microglia in synaptic stripping and retraction

Since the seminal paper by Blinzinger and Kreutzberg microglia have been implicated in the displacement of synaptic boutons from the surface of MNs (Blinzinger and Kreutzberg, 1968). However, through the years there has been significant debate about the exact role of these cells and if they have a direct role in the removal of synapses. Furthermore, distinguishing infiltrating peripheral macrophages from central microglia in this process has been difficult considering the similarities between the two cell types. We must also consider, in current and past literature, that the techniques used to define microglia may include both native central microglia and newly infiltrated peripheral derived cells that might have taken on a microglia-like phenotype. Also, the activation of microglial cells may be a key regulator in initiating the recruitment of peripheral myeloid cells to the CNS.

Immediately following axotomy the MNs, and perhaps primary afferents, can release many factors that can activate microglia by inducing their proliferation, change in phenotype, and also direct their migration. Once microglia receive an injury signal, they begin to retract their processes to become more amoeboid in shape as well as change their gene expression profile. For example, they are known to increase expression of the complement receptor 3 (CD11b) and produce pro-inflammatory cytokines such as TNF- α and IFN- γ (Aldskogius, 2011). They proliferate, migrate towards sites releasing tropic signals, and surround axotomized MNs in the ventral horn. Interestingly, they seem to specifically target the cell body of MNs after PNI though the exact signaling mechanism for tropism is yet unknown (chapter 3). One example of such factors is ATP which directs dynamic movement of microglia processes through P2Y₁₂ receptor activation (Inoue, 2008). Another critical factor during activation of microglia, as will be explored in chapter 5, is through the release of the colony stimulating factor 1 (CSF-1) which could potentially be released from axotomized MNs, or even from microglia themselves, and regulate local proliferation and activation (Raivich et al., 1994b; Raivich et al., 1994a).

Electron microscopy work has repeatedly shown that these microglia cells pry their fine processes in-between synaptic terminals and the post-synaptic neuron. (Blinzinger and Kreutzberg, 1968; Reisert et al., 1984; Svensson and Aldskogius, 1993b). These images were interpreted as microglia actively displacing synaptic terminals. However, controversy arose about the exact role of microglia as follow-up studies demonstrated that pharmacological blockage of

microglia proliferation (Svensson and Aldskogius, 1993a, b) or genetic manipulation at their activation mechanism had no effect on synaptic removal (Kalla et al., 2001; Berg et al., 2013a). These studies must be interpreted carefully as there is also evidence for microglia-independent synaptic detachment mechanisms, for example through NO release from the MN surface as reviewed above. However, the majority of studies casting doubt on the involvement of microglia have looked at plasticity of generalized synaptic inputs through immunoreactivity to markers such as synaptophysin. These studies do not distinguish specific synapses, like for example Ia synapses from others.

Therefore, a possible role of microglia in the permanent removal of Ia afferent synapses and their axon collaterals has not yet been studied. Moreover, permanent removal of full axon synaptic arbors most involve some degradative mechanism and not solely physical displacement. We know that during general “synaptic stripping” excitatory synapses retract and return after the MNs reinnervate muscle, so it makes sense that microglia are not involved in the full removal of these inputs since they are not permanently deleted but only transiently displaced. The microglia may contribute (although they might not be entirely necessary) in physically detaching synapses but not phagocytosing them. This may be very different to what occurs with the Ia afferent inputs that are known to be permanently deleted and completely removed from the ventral horn of the spinal cord. Furthermore, the total synaptic input provided by the Ia’s on the surface of the MN is somewhere around 2-3% (Fyffe, 2001), so would not be detected when using a general synaptic marker like synaptophysin. The mechanisms that drive

temporary synaptic stripping and the permanent removal of the Ia afferent synaptic input are most likely different.

Motoneurons-microglia interactions have been the focus when looking at synaptic detachment, but it is also possible that the primary afferents themselves are vital in signaling microglia or peripherally derived macrophages in their disappearance. This would make sense as it is necessary to be able to distinguish a synaptic terminal coming from axotomized afferents from those that have their axons intact in the periphery or are originated in undamaged spinal interneurons. This is interesting as microglia have been found to engulf and phagocytose synaptic terminals in the dorsal horn (Huang et al., 2007) and trigeminal nucleus after a sensory nerve axotomy (Arvidsson, 1979, 1986; Bjelke et al., 1996; Aldskogius, 2011). Another study that I find very interesting is one by Eriksson et al., where they looked at the microglia reaction in the regions of the spinal cord that primary sensory afferents project after a sciatic nerve transection injury in the rat (Eriksson et al., 1993). The authors quantified the expression of OX-42 immunoreactivity 12 hours to 14 weeks after injury. They found, in addition to microgliosis in lamina IX, microglia activation also significantly elevated one week after injury in the gracile nucleus, spinal trigeminal nucleus, and both superficial and deep dorsal horn (LIV-V) (Eriksson et al., 1993). What I found most interesting about this study is that they also observed a significant increase in microglia activity in Clarke's Column, located in L1 of the spinal cord. Many of these regions receive projections from Ia afferents but lack injured postsynaptic neurons. These

data suggest that the central terminations of primary afferents injured in the periphery might also release signals capable of activating microglia.

1.5.4: Astrocytes

In this section, I would like to at least mention one of the primary macroglial cells of the CNS, the astrocyte, which was recognized before the microglia cell in 1895 by Lenhossek (Lenhossek, 1895). For this thesis, we did not investigate the role of these cells in PNI, but it must be noted they do respond to axotomy and have the capacity to interact with microglia cells. Astrocytes can be broken down into two main groups: the fibrous astrocyte located in the white matter and the protoplasmic astrocytes located in the grey matter, which are the cells we will discuss here (Matyash and Kettenmann, 2010). As the name may imply, the cytoskeletal structure is star-shaped with a central cell body and numerous processes extending out radially, as can be seen with a glial fibrillary acidic protein (GFAP). However, this is not the full story the image provided by GFAP is somewhat incomplete since it only labels the cytoskeleton and these cells have rather large lamellar branches that extend out and occupy a much more considerable space than their GFAP labeling would suggest.

Physiologically these cells have a vast repertoire of functions, and I will only brush the surface of what these cells are capable of as it may relate to this specific thesis. A critical role of astrocytes is sealing the BBB/BSCB. This barrier is formed by brain capillary endothelial cells surrounded by a basal lamina and pericytes all

encased by the end feet of astrocytes (Janzer and Raff, 1987; Abbott et al., 2006; Krizbai et al., 2013). This complex is necessary for regulating the exchange of blood compounds with the CNS, it governs nutrient and ion influx to maintain the required CSF fluid osmolarity, but most relevant for this project, it tightly restricts immune cell trafficking from the blood into the CNS (Pachter et al., 2003; Abbott et al., 2006; Galea et al., 2007). The astrocyte endfeet that project to the barrier has some unique features such as the ability to tighten the BBB during a time of attack by the release and accumulation of a protein known as agrin (Wolburg et al., 2009).

However, this barrier can become leaky and permeable to peripheral immune cells as a result of neuroinflammation, particularly after PNI. As mentioned above, the release of CCL2/MCP1 can result in the breakdown of the BBB/BSCB. Echeverry et al., showed that three essential proteins in tight junction formation at the BBB (ZO-1, occludin, and caveolin-1), all had significantly lower protein expression 3 days after sciatic nerve injury ultimately increasing the permeability of this barrier (Echeverry et al., 2011). They also showed that infusion of TGF- β 1 inhibited CCL2/MCP1 release and rescued the tight junction proteins preserving the integrity of the BBB (Echeverry et al., 2009). Once the BBB becomes permeable, peripherally derived, immune cells have the capacity to be recruited centrally where they can exacerbate neuroinflammation and promote degeneration.

Another interesting function of astrocytes is their interaction with synapses. Usually, the pre and postsynaptic elements are surrounded by astrocytic processes in what has been denominated the tripartite synapse (Halassa et al.,

2007). Astrocytes can detect synaptic transmission and in return respond by increasing their intracellular calcium concentration, which can spread through gap junctions to other astrocytes. Increases in intracellular calcium can lead to transmitter release from the astrocyte, including glutamate, GABA, ATP, and others, back onto the pre- and postsynaptic targets (De Pitta et al., 2016). This modulation of synaptic transmission can either modulate synaptic function ultimately strengthening or weakening connectivity between neurons. Furthermore, astrocytes can eliminate weakened synapses through phagocytosis by a MEGF10 and MERTK pathway (Chung et al., 2013).

Astrocytes also respond to neurological disease and injury and they can become reactive and neurotoxic. This reactivity seems to be dependent, at least in part, on microglia activation. An interesting study by Liddel et al., looked at the induction of neurotoxic astrocytes by microglia activation via LPS (Liddel et al., 2017). The authors of this paper showed that when microglia activation is prevented in CSF1R KOs, astrocytes did not become reactive after LPS treatment. Furthermore, they found that astrocyte reactivity was induced by production of interleukin 1- α , tumor necrosis factor and complement C1q protein from microglia cells after LPS stimulation (Liddel et al., 2017). Additionally, they were able to prevent astrocytic reactivity by producing triple KOs for the three factors mentioned above. These data are of great interest because they demonstrate one of the downstream effects of microglia activation is astrocyte activation and these could further contribute to synapses elimination.

Astrocytes were also investigated in the seminal 1968 paper by Blinzinger and Kreutzberg on synaptic displacement after facial nerve axotomy. They concluded that astrocytes were not directly involved in the stripping process but were merely interacting with microglia cells (Blinzinger and Kreutzberg, 1968). Follow up studies, however, found that the lamellae processes of astrocytes were capable of intervening between microglia, synapses, and neurons, suggesting possible roles in the removal of synaptic terminals (Reisert et al., 1984). Astrocytes responded to facial nerve axotomy in the rat by becoming hypertrophic starting around 3 days post-injury and lasting for approximately 3 weeks, based on their expression of GFAP (Graeber and Kreutzberg, 1986; Tetzlaff et al., 1988), but these cells do not undergo mitosis as microglia cells do (Graeber et al., 1988). Furthermore, they increase their production of gap junction protein connexin-43 (Rohlmann et al., 1994), NMDA receptors (Popratiloff et al., 1996), and many other factors that enhance their responsiveness within the CNS.

One study by Emirandetti et al., looked at the extent of GFAP reactivity following sciatic nerve transection in two different strains of mice, the A/J and C57BL/6J (Emirandetti et al., 2006). The authors found a correlation between the amount of GFAP immunoreactivity and the degree of synaptophysin puncta removed around the soma of axotomized MNs; A/J mice had significantly greater GFAP expression and a more substantial depletion of synaptic boutons around the MNs (Emirandetti et al., 2006). However, this study was purely correlative and did not investigate mechanisms or other immune cell differences between the two strains of mice. Others have examined synaptic stripping and axon regeneration

in mice that were KOs for GFAP and another intermediate filament protein known as vimentin (*GFAP^{KO}:Vimentin^{KO}*) (Berg et al., 2013b). As expected, there was no GFAP or vimentin immunoreactivity following axotomy in these double-KO mice. The authors of this paper used EM to quantify differences in synaptic density around the soma of axotomized MNs 7 days after sciatic nerve injury and found a 35% better preservation of synapses in double KO mice compared to WT controls. These results further suggest a role for astrocytes in synaptic stripping after nerve injury (Berg et al., 2013b).

1.5.5: T-cells in PNI

There are a variety of other immune cells that have been implicated in the synaptic plasticity of spinal circuits after nerve injury, as well as in the survival of axotomized MNs. One particular cell type of interest has been T-lymphocytes (Raivich et al., 1998). A study by Serpe et al., found that the survival of axotomized MNs in the facial nucleus is dependent on CD4⁺ T-cell infiltration following nerve transection, and independent of CD8 T-cells, natural killer cells, and B-cells (Serpe et al., 1999; Serpe et al., 2003). The authors of this paper found that in WT mice about 86% of MNs survive when CD4⁺ T-cells are present, but only about 60% survive in CD4 KO mice. Why some MNs survive and others die in the same motor pool seems to be a topic of debate without any clear answer still. CD4⁺ T-cells can be pro-inflammatory (Th1) or anti-inflammatory (Th2) depending on their environment. Further studies have shown that CD4⁺ T-cells in the facial nucleus fall under the Th2 category as they are known to produce the anti-inflammatory

cytokine IL-4 (Deboy et al., 2006). The survival of MNs is also dependent on IL-10, though this has been shown not to come from CD4+ T-cells (Xin et al., 2011). Importantly, for induction of this Th2 response, T-cells must be primed by an MHCII mechanism dependent on microglia presentation. The current working model suggests that through this MHCII dependent interaction, IL-10 is released from microglia, which then in turn recruit's astrocytes that provide trophic support to the MNs for survival (Jones et al., 2015). It should also be noted that this massive infiltration of T-cells in the facial nucleus may be specific to mice since it was found to occur at a much lesser extent in rats (Raivich et al., 1998). Lastly, I want to point out that CD4+ and CD8+ T-cells also infiltrate the spinal cord after injury though we will not extensively show these data and we did not test what might be the role of these cells. It is known in mice a proportion of spinal MNs die following sciatic nerve injury. This MN death could potentially be exacerbated by the presence of CD8 T-cells.

1.6: Dissertation overview

The primary goal of this thesis is to elucidate the role neuroinflammation in the permanent degeneration of proprioceptive Ia afferents after peripheral nerve injury. The literature demonstrates a large and diverse immune response in the spinal cord after nerve injury with several different immune cells potentially involved. Throughout this thesis, we will dissect various components of this response and investigate how this impacts Ia afferent connectivity. We will start by describing the extent of Ia afferent inputs loss on the entire dendritic arbor of rat

axotomized MNs. Then we switched animal models to mice. These allowed us to use genetic manipulations to genetically label different cell types and described in detail the neuroinflammatory response to different kinds of injuries. Moreover, it allowed us to analyze global knockouts or cell-specific gene deletions in the spinal cord to test the roles of CX3CR1, CCR2, CCL2, and CSF1 in triggering the microglia reaction, promoting CCR2 immune cell infiltration and analyzing the consequences of alteration of these mechanisms for Ia afferent synapse stability. Lastly, we compared how the severity of nerve injury and success of peripheral regeneration can influence the properties of neuroinflammation and the overall density of Ia afferent synapses on regenerated MNs.

Hypotheses:

- 1) Ia afferent synapses are removed, by difference to synaptic stripping, throughout the dendritic arbor of MNs. (Chapter 1)
- 2) Sciatic nerve injuries causing a larger loss of Ia afferent VGLUT1 synapses should correlate with stronger local neuroinflammation assessed by microglia activation and CCR2 cell infiltration. Thus, sciatic nerve transection should display a neuroinflammatory phenotype more intense than more distal injuries (tibial nerve) or after nerve crush. (Chapters 2 and 3)
- 3) Preventing infiltration of peripheral macrophages preserves VGLUT1 synapses on MNs. Thus, a CCR2 mechanism is necessary for permanent removal of Ia afferent synapses. (Chapter 2)
- 4) Nerve transection and nerve crush both results in activation of microglia cells in the ventral horn of the spinal cord, but only nerve transection (causing a more substantial permanent synaptic loss) will recruit CCR2 peripheral myeloid cells. (Chapter 3)

In summary, the ultimate goal of the thesis is to test the idea of whether triggering graded neuroinflammation inside the spinal cord is a mechanism that induces more or less plasticity after nerve injuries of different severity and therefore different predictable outcomes in the efficiency and specificity of nerve regeneration.

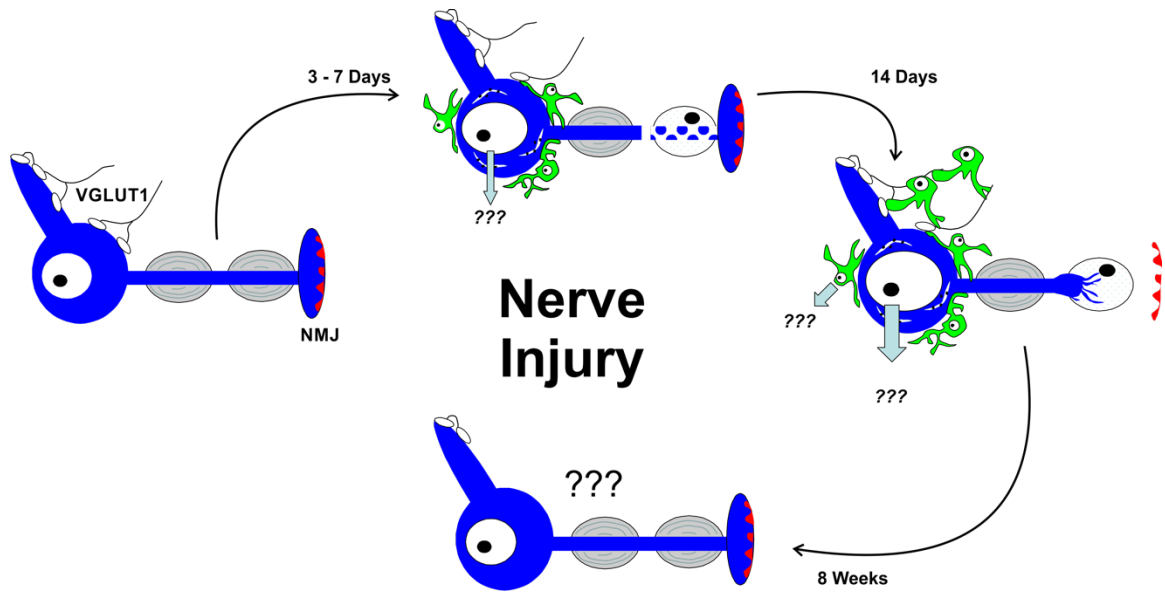


Figure 1.1: Summary Figure. The overall theme of this thesis is to investigate the mechanism(s) that initiate the neuroinflammatory response after nerve injury and explore what role this response have in the removal of VGLTU1 synapses following peripheral nerve injury.

Medical Research Council Grading System	
<i>Motor Recovery</i>	
M0	No contraction
M1	Return of contraction of proximal muscle
M2	Return of contraction in both proximal and distal muscles
M3	Function in proximal and distal muscles returns to a degree in which the limb can counteract the forces of gravity
M4	Muscles act against an applied resistance force. Some independent movement of the limb
M5	Full recovery of muscles and function

Table 1.1: Medical Research Council evaluation scoring system of peripheral nerve injury. Exam is used both pre- and post- regeneration to evaluate the success of surgical intervention. *Adopted from (Lee and Wolfe, 2000).*

Molecular Target	Detection/Description	Reference
F4/80	Epidermal growth factor (EGF) transmembrane 7 (TM7)	(Austyn and Gordon, 1981)
CD11b (OX-42)	Against the $\alpha_M\beta_2$ integrin protein: recognizes the complement receptor 3 (CR3).	(Robinson et al., 1986)
Iba1	Ionized calcium binding adaptor molecule 1: EF hand protein	(Imai et al., 1996)
CX3CR1	G-protein coupled receptor	(Harrison et al., 1998)
Tmem119	Cell surface single-pass transmembrane protein 119.	(Bennett et al., 2016)
P2RY12 (clone S16007D)	Purinergic receptor highly specific for microglia centrally	(Orr et al., 2009)

Table 1.2: Antibodies for microglia identification using immunohistochemistry

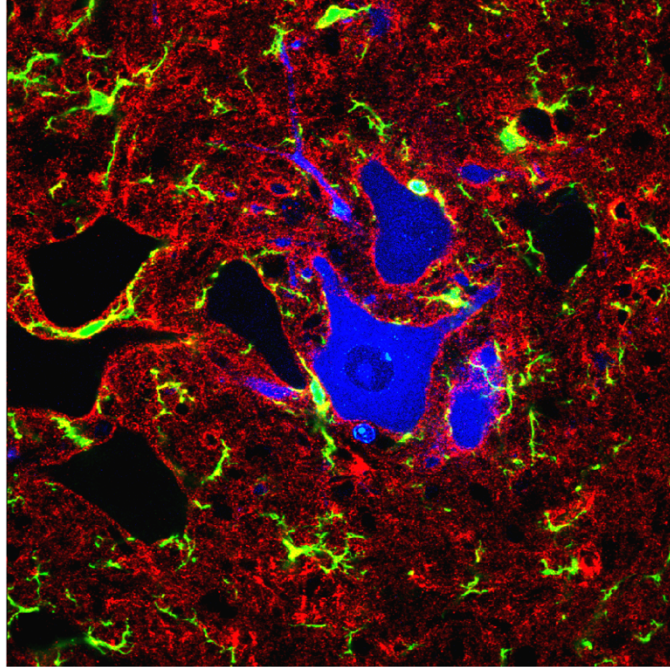


Figure 1.2: Complement expression around axotomized MNs 7 days following sciatic nerve transection. LG Fast Blue labeled MNs (blue), microglia (green), C1q expression (red).

References:

- Abbadie C, Bhangoo S, De Koninck Y, Malcangio M, Melik-Parsadaniantz S, White FA (2009) Chemokines and pain mechanisms. *Brain research reviews* 60:125-134.
- Abbott NJ, Ronnback L, Hansson E (2006) Astrocyte-endothelial interactions at the blood-brain barrier. *Nature reviews Neuroscience* 7:41-53.
- Achúcarro N (1911) Nuevo método para el estudio de la neuroglia y del tejido conjuntivo. *Boletín de la Sociedad Española de Biológica* 1.
- Achúcarro N (1913) Notas sobre la estructura y funciones de la neuroglia y en particular de la neuroglia de la corteza cerebral humana *Trabajos del laboratorio de investigaciones biológicas: de la Universidad de Madrid* 3.
- Aldskogius H (2011) Mechanisms and consequences of microglial responses to peripheral axotomy. *Frontiers in bioscience* 3:857-868.
- Aldskogius H, Risling M (1983) Preferential loss of unmyelinated L7 dorsal root axons following sciatic nerve resection in kittens. *Brain research* 289:358-361.
- Aldskogius H, Arvidsson J, Grant G (1985) The reaction of primary sensory neurons to peripheral nerve injury with particular emphasis on transganglionic changes. *Brain research* 357:27-46.
- Alvarez FJ, Dewey DE, Harrington DA, Fyffe RE (1997) Cell-type specific organization of glycine receptor clusters in the mammalian spinal cord. *The Journal of comparative neurology* 379:150-170.
- Alvarez FJ, Villalba RM, Zerda R, Schneider SP (2004) Vesicular glutamate transporters in the spinal cord, with special reference to sensory primary afferent synapses. *The Journal of comparative neurology* 472:257-280.
- Alvarez FJ, Bullinger KL, Titus HE, Nardelli P, Cope TC (2010) Permanent reorganization of Ia afferent synapses on motoneurons after peripheral nerve injuries. *Annals of the New York Academy of Sciences* 1198:231-241.
- Alvarez FJ, Titus-Mitchell HE, Bullinger KL, Kraszpulski M, Nardelli P, Cope TC (2011) Permanent central synaptic disconnection of proprioceptors after nerve injury and regeneration. I. Loss of VGLUT1/IA synapses on motoneurons. *Journal of neurophysiology* 106:2450-2470.
- Alzheimer A (1910) Beiträge zur Kenntnis der pathologischen Neuroglia und ihrer Beziehungen zu den Abbauvorgängen im Nervengewebe. . In: *Histologische und Histopathologische Arbeiten über die Grosshirnrinde mit besonderer Berücksichtigung der pathologischen Anatomie der Geisteskrankheiten*, ed. F Nissl, A Alzheimer pp 401-562: Verlag Gustav Fischer.
- Aminoff MJ (2004) Electrophysiologic testing for the diagnosis of peripheral nerve injuries. *Anesthesiology* 100:1298-1303.
- Arber S, Ladle DR, Lin JH, Frank E, Jessell TM (2000) ETS gene Er81 controls the formation of functional connections between group Ia sensory afferents and motor neurons. *Cell* 101:485-498.

- Arvidsson J (1979) An ultrastructural study of transganglionic degeneration in the main sensory trigeminal nucleus of the rat. *Journal of neurocytology* 8:31-45.
- Arvidsson J (1986) Transganglionic degeneration in vibrissae innervating primary sensory neurons of the rat: a light and electron microscopic study. *The Journal of comparative neurology* 249:392-403.
- Arvidsson J, Ygge J, Grant G (1986) Cell loss in lumbar dorsal root ganglia and transganglionic degeneration after sciatic nerve resection in the rat. *Brain research* 373:15-21.
- Austyn JM, Gordon S (1981) F4/80, a monoclonal antibody directed specifically against the mouse macrophage. *European journal of immunology* 11:805-815.
- Banchereau J, Briere F, Caux C, Davoust J, Lebecque S, Liu YJ, Pulendran B, Palucka K (2000) Immunobiology of dendritic cells. *Annual review of immunology* 18:767-811.
- Barker D, Young JZ (1947) Recovery of stretch reflexes after nerve injury. *Lancet* 1:704-707.
- Bawa P, Chalmers GR, Jones KE, Sogaard K, Walsh ML (2000) Control of the wrist joint in humans. *Eur J Appl Physiol* 83:116-127.
- Bennett ML, Bennett FC, Liddel SA, Ajami B, Zamanian JL, Fernhoff NB, Mulinyawe SB, Bohlen CJ, Adil A, Tucker A, Weissman IL, Chang EF, Li G, Grant GA, Hayden Gephart MG, Barres BA (2016) New tools for studying microglia in the mouse and human CNS. *Proceedings of the National Academy of Sciences of the United States of America* 113:E1738-1746.
- Berg A, Zelano J, Thams S, Cullheim S (2013a) The extent of synaptic stripping of motoneurons after axotomy is not correlated to activation of surrounding glia or downregulation of postsynaptic adhesion molecules. *PloS one* 8:e59647.
- Berg A, Zelano J, Pekna M, Wilhelmsson U, Pekny M, Cullheim S (2013b) Axonal regeneration after sciatic nerve lesion is delayed but complete in GFAP- and vimentin-deficient mice. *PloS one* 8:e79395.
- Berg A, Zelano J, Stephan A, Thams S, Barres BA, Pekny M, Pekna M, Cullheim S (2012) Reduced removal of synaptic terminals from axotomized spinal motoneurons in the absence of complement C3. *Experimental neurology* 237:8-17.
- Biber K, Owens T, Boddeke E (2014) What is microglia neurotoxicity (Not)? *Glia* 62:841-854.
- Biber K, Neumann H, Inoue K, Boddeke HW (2007) Neuronal 'On' and 'Off' signals control microglia. *Trends in neurosciences* 30:596-602.
- Bichler EK, Carrasco DI, Rich MM, Cope TC, Pinter MJ (2007) Rat motoneuron properties recover following reinnervation in the absence of muscle activity and evoked acetylcholine release. *The Journal of physiology* 585:47-56.
- Bjelke K, Aldskogius H, Arvidsson J (1996) Short- and long-term transganglionic changes in the central terminations of transected vibrissal afferents in the

- rat. Experimental brain research Experimentelle Hirnforschung
Experimentation cerebrale 112:268-276.
- Blinzinger K, Kreutzberg G (1968) Displacement of synaptic terminals from
regenerating motoneurons by microglial cells. Zeitschrift fur Zellforschung
und mikroskopische Anatomie 85:145-157.
- Bodian D (1970) An electron microscopic characterization of classes of synaptic
vesicles by means of controlled aldehyde fixation. The Journal of cell
biology 44:115-124.
- Bodine-Fowler SC, Meyer RS, Moskovitz A, Abrams R, Botte MJ (1997)
Inaccurate projection of rat soleus motoneurons: a comparison of nerve
repair techniques. Muscle & nerve 20:29-37.
- Bogie JF, Stinissen P, Hendriks JJ (2014) Macrophage subsets and microglia in
multiple sclerosis. Acta neuropathologica 128:191-213.
- Bonifati DM, Kishore U (2007) Role of complement in neurodegeneration and
neuroinflammation. Molecular immunology 44:999-1010.
- Bradley K, Eccles JC (1953) Strychnine as a depressant of primary inhibition.
Nature 171:1061-1062.
- Bradley K, Easton DM, Eccles JC (1953) An investigation of primary or direct
inhibition. The Journal of physiology 122:474-488.
- Brannstrom T (1993) Quantitative synaptology of functionally different types of
cat medial gastrocnemius alpha-motoneurons. The Journal of comparative
neurology 330:439-454.
- Brock LG, Coombs JS, Eccles JC (1952) The recording of potentials from
motoneurons with an intracellular electrode. The Journal of physiology
117:431-460.
- Brown AG (1981) Organization in the Spinal Cord London Springer
- Brown AG, Fyffe RE (1978a) Synaptic contacts made by identified Ia afferent
fibres upon motoneurons [proceedings]. The Journal of physiology
284:43P-44P.
- Brown AG, Fyffe RE (1978b) The morphology of group Ia afferent fibre collaterals
in the spinal cord of the cat. J Physiol 274:111-127.
- Brown AG, Fyffe RE (1981) Direct observations on the contacts made between
Ia afferent fibres and alpha-motoneurons in the cat's lumbosacral spinal
cord. The Journal of physiology 313:121-140.
- Brown MC, Hopkins WG (1981) Role of degenerating axon pathways in
regeneration of mouse soleus motor axons. The Journal of physiology
318:365-373.
- Brushart T (2011) Nerve Repair Oxford University Press.
- Brushart TM, Mesulam MM (1980a) Alteration in connections between muscle
and anterior horn motoneurons after peripheral nerve repair. Science
208:603-605.
- Brushart TM, Mesulam MM (1980b) Transganglionic demonstration of central
sensory projections from skin and muscle with HRP-lectin conjugates.
Neuroscience letters 17:1-6.

- Brushart TM, Tarlov EC, Mesulam MM (1983) Specificity of muscle reinnervation after epineurial and individual fascicular suture of the rat sciatic nerve. *J Hand Surg Am* 8:248-253.
- Bullinger KL, Nardelli P, Pinter MJ, Alvarez FJ, Cope TC (2011) Permanent central synaptic disconnection of proprioceptors after nerve injury and regeneration. II. Loss of functional connectivity with motoneurons. *Journal of neurophysiology* 106:2471-2485.
- Büngner OV (1891) On the regeneration and degeneration of nerve-processes to injury. *Beitr Path Anat Allg Path* 10:321-393.
- Burke RE, Glenn LL (1996) Horseradish peroxidase study of the spatial and electrotonic distribution of group Ia synapses on type-identified ankle extensor motoneurons in the cat. *The Journal of comparative neurology* 372:465-485.
- Burke RE, Strick PL, Kanda K, Kim CC, Walmsley B (1977) Anatomy of medial gastrocnemius and soleus motor nuclei in cat spinal cord. *Journal of neurophysiology* 40:667-680.
- Campbell WW (2008) Evaluation and management of peripheral nerve injury. *Clinical neurophysiology : official journal of the International Federation of Clinical Neurophysiology* 119:1951-1965.
- Cardona AE, Pioro EP, Sasse ME, Kostenko V, Cardona SM, Dijkstra IM, Huang D, Kidd G, Dombrowski S, Dutta R, Lee JC, Cook DN, Jung S, Lira SA, Littman DR, Ransohoff RM (2006) Control of microglial neurotoxicity by the fractalkine receptor. *Nature neuroscience* 9:917-924.
- Causey G, Barton AA (1959) The cellular content of the endoneurium of peripheral nerve. *Brain : a journal of neurology* 82:594-598.
- Chen DH (1978) Qualitative and quantitative study of synaptic displacement in chromatolyzed spinal motoneurons of the cat. *The Journal of comparative neurology* 177:635-664.
- Chung WS, Clarke LE, Wang GX, Stafford BK, Sher A, Chakraborty C, Joung J, Foo LC, Thompson A, Chen C, Smith SJ, Barres BA (2013) Astrocytes mediate synapse elimination through MEGF10 and MERTK pathways. *Nature* 504:394-400.
- Coggeshall RE, Lekan HA, Doubell TP, Allchorne A, Woolf CJ (1997) Central changes in primary afferent fibers following peripheral nerve lesions. *Neuroscience* 77:1115-1122.
- Colen KL, Choi M, Chiu DT (2009) Nerve grafts and conduits. *Plastic and reconstructive surgery* 124:e386-394.
- Conradi S (1969a) Ultrastructure and distribution of neuronal and glial elements on the surface of the proximal part of a motoneuron dendrite, as analyzed by serial sections. *Acta Physiol Scand Suppl* 332:49-64.
- Conradi S (1969b) Observations on the ultrastructure of the axon hillock and initial axon segment of lumbosacral motoneurons in the cat. *Acta Physiol Scand Suppl* 332:65-84.
- Conradi S, Skoglund S (1969) Observations on the ultrastructure of the initial motor axon segment and dorsal root boutons on the motoneurons in the

- lumbosacral spinal cord of the cat during postnatal development. *Acta Physiol Scand Suppl* 333:53-76.
- Conradi S, Kellerth JO, Berthold CH (1979) Electron microscopic studies of serially sectioned cat spinal alpha-motoneurons. II. A method for the description of architecture and synaptology of the cell body and proximal dendritic segments. *The Journal of comparative neurology* 184:741-754.
- Cope TC, Bonasera SJ, Nichols TR (1994) Reinnervated muscles fail to produce stretch reflexes. *Journal of neurophysiology* 71:817-820.
- Cote MP, Amin AA, Tom VJ, Houle JD (2011) Peripheral nerve grafts support regeneration after spinal cord injury. *Neurotherapeutics* 8:294-303.
- Cragg BG (1970) What is the signal for chromatolysis? *Brain research* 23:1-21.
- Davoust N, Vuillat C, Cavillon G, Domenget C, Hatterer E, Bernard A, Dumontel C, Jurdic P, Malcus C, Confavreux C, Belin MF, Nataf S (2006) Bone marrow CD34+/B220+ progenitors target the inflamed brain and display in vitro differentiation potential toward microglia. *FASEB journal : official publication of the Federation of American Societies for Experimental Biology* 20:2081-2092.
- De Pitta M, Brunel N, Volterra A (2016) Astrocytes: Orchestrating synaptic plasticity? *Neuroscience* 323:43-61.
- Deardorff AS, Romer SH, Sonner PM, Fyffe RE (2014) Swimming against the tide: investigations of the C-bouton synapse. *Frontiers in neural circuits* 8:106.
- Deboy CA, Xin J, Byram SC, Serpe CJ, Sanders VM, Jones KJ (2006) Immune-mediated neuroprotection of axotomized mouse facial motoneurons is dependent on the IL-4/STAT6 signaling pathway in CD4(+) T cells. *Experimental neurology* 201:212-224.
- DeFrancesco-Lisowitz A, Lindborg JA, Niemi JP, Zigmond RE (2014) The neuroimmunology of degeneration and regeneration in the peripheral nervous system. *Neuroscience*.
- Deshmane SL, Kremlev S, Amini S, Sawaya BE (2009) Monocyte chemoattractant protein-1 (MCP-1): an overview. *Journal of interferon & cytokine research : the official journal of the International Society for Interferon and Cytokine Research* 29:313-326.
- Doyon N, Vinay L, Prescott SA, De Koninck Y (2016) Chloride Regulation: A Dynamic Equilibrium Crucial for Synaptic Inhibition. *Neuron* 89:1157-1172.
- Eccles JC, Fatt P, Landgren S (1956) Central pathway for direct inhibitory action of impulses in largest afferent nerve fibres to muscle. *Journal of neurophysiology* 19:75-98.
- Eccles JC, Eccles RM, Lundberg A (1957) The convergence of monosynaptic excitatory afferents on to many different species of alpha motoneurons. *The Journal of physiology* 137:22-50.
- Eccles JC, Libet B, Young RR (1958) The behaviour of chromatolysed motoneurons studied by intracellular recording. *The Journal of physiology* 143:11-40.
- Eccles RM, Lundberg A (1958) The synaptic linkage of direct inhibition. *Acta Physiol Scand* 43:204-215.

- Echeverry S, Shi XQ, Rivest S, Zhang J (2011) Peripheral nerve injury alters blood-spinal cord barrier functional and molecular integrity through a selective inflammatory pathway. *J Neurosci* 31:10819-10828.
- Echeverry S, Shi XQ, Haw A, Liu H, Zhang ZW, Zhang J (2009) Transforming growth factor-beta1 impairs neuropathic pain through pleiotropic effects. *Mol Pain* 5:16.
- Ellis A, Bennett DL (2013) Neuroinflammation and the generation of neuropathic pain. *British journal of anaesthesia* 111:26-37.
- Emirandetti A, Graciele Zanon R, Sabha M, Jr., de Oliveira AL (2006) Astrocyte reactivity influences the number of presynaptic terminals apposed to spinal motoneurons after axotomy. *Brain research* 1095:35-42.
- Eriksson NP, Persson JK, Svensson M, Arvidsson J, Molander C, Aldskogius H (1993) A quantitative analysis of the microglial cell reaction in central primary sensory projection territories following peripheral nerve injury in the adult rat. *Experimental brain research Experimentelle Hirnforschung Experimentation cerebrale* 96:19-27.
- Esser AF (1991) Big MAC attack: complement proteins cause leaky patches. *Immunol Today* 12:316-318; discussion 321.
- Evans TA, Barkauskas DS, Myers JT, Hare EG, You JQ, Ransohoff RM, Huang AY, Silver J (2014) High-resolution intravital imaging reveals that blood-derived macrophages but not resident microglia facilitate secondary axonal dieback in traumatic spinal cord injury. *Experimental neurology* 254:109-120.
- Fonseca GJ, Seidman JS, Glass CK (2016) Genome-Wide Approaches to Defining Macrophage Identity and Function. *Microbiol Spectr* 4.
- Frade JM, Mellado M, del Real G, Gutierrez-Ramos JC, Lind P, Martinez AC (1997) Characterization of the CCR2 chemokine receptor: functional CCR2 receptor expression in B cells. *Journal of immunology* 159:5576-5584.
- Frank-Cannon TC, Alto LT, McAlpine FE, Tansey MG (2009) Does neuroinflammation fan the flame in neurodegenerative diseases? *Mol Neurodegener* 4:47.
- Freria CM, Hall JC, Wei P, Guan Z, McTigue DM, Popovich PG (2017) Deletion of the Fractalkine Receptor, CX3CR1, Improves Endogenous Repair, Axon Sprouting, and Synaptogenesis after Spinal Cord Injury in Mice. *J Neurosci* 37:3568-3587.
- Friese A, Kaltschmidt JA, Ladle DR, Sigrist M, Jessell TM, Arber S (2009) Gamma and alpha motor neurons distinguished by expression of transcription factor *Err3*. *Proceedings of the National Academy of Sciences of the United States of America* 106:13588-13593.
- Fu SY, Gordon T (1997) The cellular and molecular basis of peripheral nerve regeneration. *Molecular neurobiology* 14:67-116.
- Fuhrmann M, Bittner T, Jung CK, Burgold S, Page RM, Mitteregger G, Haass C, LaFerla FM, Kretschmar H, Herms J (2010) Microglial *Cx3cr1* knockout prevents neuron loss in a mouse model of Alzheimer's disease. *Nature neuroscience* 13:411-413.

- Fyffe RE (2001) Spinal Motoneurons: Synaptic Inputs and Receptor Organization In: Motor Neurobiology of the Spinal Cord (Cope TC, ed), pp 21-46: CRC Press
- Galea I, Bechmann I, Perry VH (2007) What is immune privilege (not)? Trends in immunology 28:12-18.
- Garcia-Marin V, Garcia-Lopez P, Freire M (2007) Cajal's contributions to glia research. Trends in neurosciences 30:479-487.
- Geissmann F, Jung S, Littman DR (2003) Blood monocytes consist of two principal subsets with distinct migratory properties. Immunity 19:71-82.
- George EB, Glass JD, Griffin JW (1995) Axotomy-induced axonal degeneration is mediated by calcium influx through ion-specific channels. J Neurosci 15:6445-6452.
- Ginhoux F, Greter M, Leboeuf M, Nandi S, See P, Gokhan S, Mehler MF, Conway SJ, Ng LG, Stanley ER, Samokhvalov IM, Merad M (2010) Fate mapping analysis reveals that adult microglia derive from primitive macrophages. Science 330:841-845.
- Goldmann T, Wieghofer P, Muller PF, Wolf Y, Varol D, Yona S, Brendecke SM, Kierdorf K, Staszewski O, Datta M, Luedde T, Heikenwalder M, Jung S, Prinz M (2013) A new type of microglia gene targeting shows TAK1 to be pivotal in CNS autoimmune inflammation. Nature neuroscience 16:1618-1626.
- Gonzalez-Forero D, Moreno-Lopez B (2014) Retrograde response in axotomized motoneurons: nitric oxide as a key player in triggering reversion toward a dedifferentiated phenotype. Neuroscience 283:138-165.
- Gordon T, Sulaimain OAR (2012) Nerve Regeneration in the Peripheral Nervous System. In: Neuroglia 3Edition. New York, NY, USA: Oxford University Press
- Gordon T, English AW (2016) Strategies to promote peripheral nerve regeneration: electrical stimulation and/or exercise. The European journal of neuroscience 43:336-350.
- Gosselin D, Skola D, Coufal NG, Holtman IR, Schlachetzki JCM, Sajti E, Jaeger BN, O'Connor C, Fitzpatrick C, Pasillas MP, Pena M, Adair A, Gonda DD, Levy ML, Ransohoff RM, Gage FH, Glass CK (2017) An environment-dependent transcriptional network specifies human microglia identity. Science 356.
- Graeber MB, Kreutzberg GW (1986) Astrocytes increase in glial fibrillary acidic protein during retrograde changes of facial motor neurons. Journal of neurocytology 15:363-373.
- Graeber MB, Streit WJ, Kreutzberg G (1991) The glial response to motor neuron axotomy: role of microglia and astrocytes. In: Proceedings of the XIth International Congress of Neuropathology, Supplement 4 pp 282-287. Kyoto: Japanese Society for Neuropathology
- Graeber MB, Bise K, Mehraein P (1993) Synaptic stripping in the human facial nucleus. Acta neuropathologica 86:179-181.

- Graeber MB, Tetzlaff W, Streit WJ, Kreutzberg GW (1988) Microglial cells but not astrocytes undergo mitosis following rat facial nerve axotomy. *Neuroscience letters* 85:317-321.
- Grafstein B (1971) Role of slow axonal transport in nerve regeneration. *Acta neuropathologica* 5:Suppl 5:144-152.
- Grant G, Arvidsson J (1975) Transganglionic degeneration in trigeminal primary sensory neurons. *Brain research* 95:265-279.
- Grinsell D, Keating CP (2014) Peripheral nerve reconstruction after injury: a review of clinical and experimental therapies. *Biomed Res Int* 2014:698256.
- Gu N, Peng J, Murugan M, Wang X, Eyo UB, Sun D, Ren Y, DiCicco-Bloom E, Young W, Dong H, Wu LJ (2016) Spinal Microgliosis Due to Resident Microglial Proliferation Is Required for Pain Hypersensitivity after Peripheral Nerve Injury. *Cell reports* 16:605-614.
- Guest JD, Hesse D, Schnell L, Schwab ME, Bunge MB, Bunge RP (1997) Influence of IN-1 antibody and acidic FGF-fibrin glue on the response of injured corticospinal tract axons to human Schwann cell grafts. *Journal of neuroscience research* 50:888-905.
- Haftel VK, Bichler EK, Wang QB, Prather JF, Pinter MJ, Cope TC (2005) Central suppression of regenerated proprioceptive afferents. *The Journal of neuroscience : the official journal of the Society for Neuroscience* 25:4733-4742.
- Halassa MM, Fellin T, Haydon PG (2007) The tripartite synapse: roles for gliotransmission in health and disease. *Trends Mol Med* 13:54-63.
- Hammond PH (1955) Involuntary activity in biceps following the sudden application of velocity to the abducted forearm. *The Journal of physiology* 127:23-25P.
- Hanna AS, Cote MP, Houle J, Dempsey R (2011) Nerve grafting for spinal cord injury in cats: are we close to translational research? *Neurosurgery* 68:N14-15.
- Hantman AW, Jessell TM (2010) Clarke's column neurons as the focus of a corticospinal collateral circuit. *Nature neuroscience* 13:1233-1239.
- Harrison JK, Jiang Y, Chen S, Xia Y, Maciejewski D, McNamara RK, Streit WJ, Salafranca MN, Adhikari S, Thompson DA, Botti P, Bacon KB, Feng L (1998) Role for neuronally derived fractalkine in mediating interactions between neurons and CX3CR1-expressing microglia. *Proceedings of the National Academy of Sciences of the United States of America* 95:10896-10901.
- Hickman SE, Kingery ND, Ohsumi TK, Borowsky ML, Wang LC, Means TK, El Khoury J (2013) The microglial sensome revealed by direct RNA sequencing. *Nature neuroscience* 16:1896-1905.
- Hnasko TS, Edwards RH (2012) Neurotransmitter corelease: mechanism and physiological role. *Annu Rev Physiol* 74:225-243.
- Hoffman PN, Lasek RJ (1980) Axonal transport of the cytoskeleton in regenerating motor neurons: constancy and change. *Brain research* 202:317-333.

- Hoke A, Brushart T (2010) Introduction to special issue: Challenges and opportunities for regeneration in the peripheral nervous system. *Experimental neurology* 223:1-4.
- Huang Z, Ha GK, Petitto JM (2007) IL-15 and IL-15R alpha gene deletion: effects on T lymphocyte trafficking and the microglial and neuronal responses to facial nerve axotomy. *Neuroscience letters* 417:160-164.
- Huh GS, Boulanger LM, Du H, Riquelme PA, Brotz TM, Shatz CJ (2000) Functional requirement for class I MHC in CNS development and plasticity. *Science* 290:2155-2159.
- Hultborn H (2006) Spinal reflexes, mechanisms and concepts: from Eccles to Lundberg and beyond. *Progress in neurobiology* 78:215-232.
- Hultborn H, Jankowska E, Lindstrom S (1971a) Recurrent inhibition from motor axon collaterals of transmission in the Ia inhibitory pathway to motoneurons. *The Journal of physiology* 215:591-612.
- Hultborn H, Jankowska E, Lindstrom S (1971b) Recurrent inhibition of interneurons monosynaptically activated from group Ia afferents. *The Journal of physiology* 215:613-636.
- Hyatt Sachs H, Schreiber RC, Shoemaker SE, Sabe A, Reed E, Zigmond RE (2007) Activating transcription factor 3 induction in sympathetic neurons after axotomy: response to decreased neurotrophin availability. *Neuroscience* 150:887-897.
- Iles JF (1976) Central terminations of muscle afferents on motoneurons in the cat spinal cord. *The Journal of physiology* 262:91-117.
- Imai T, Hieshima K, Haskell C, Baba M, Nagira M, Nishimura M, Kakizaki M, Takagi S, Nomiya H, Schall TJ, Yoshie O (1997) Identification and molecular characterization of fractalkine receptor CX3CR1, which mediates both leukocyte migration and adhesion. *Cell* 91:521-530.
- Imai Y, Ibata I, Ito D, Ohsawa K, Kohsaka S (1996) A novel gene *iba1* in the major histocompatibility complex class III region encoding an EF hand protein expressed in a monocytic lineage. *Biochemical and biophysical research communications* 224:855-862.
- Inoue K (2008) Purinergic systems in microglia. *Cell Mol Life Sci* 65:3074-3080.
- Ishizuka N, Mannen H, Hongo T, Sasaki S (1979) Trajectory of group Ia afferent fibers stained with horseradish peroxidase in the lumbosacral spinal cord of the cat: three dimensional reconstructions from serial sections. *The Journal of comparative neurology* 186:189-211.
- Jahr CE, Yoshioka K (1986) Ia afferent excitation of motoneurons in the in vitro new-born rat spinal cord is selectively antagonized by kynurenate. *The Journal of physiology* 370:515-530.
- Jankowska E, Lindstrom S (1972) Morphology of interneurons mediating Ia reciprocal inhibition of motoneurons in the spinal cord of the cat. *The Journal of physiology* 226:805-823.
- Janzer RC, Raff MC (1987) Astrocytes induce blood-brain barrier properties in endothelial cells. *Nature* 325:253-257.
- Jenkins R, McMahon SB, Bond AB, Hunt SP (1993) Expression of c-Jun as a response to dorsal root and peripheral nerve section in damaged and

- adjacent intact primary sensory neurons in the rat. *The European journal of neuroscience* 5:751-759.
- Johnson EM, Jr., Yip HK (1985) Central nervous system and peripheral nerve growth factor provide trophic support critical to mature sensory neuronal survival. *Nature* 314:751-752.
- Johnson IP (1986) A quantitative ultrastructural comparison of alpha and gamma motoneurons in the thoracic region of the spinal cord of the adult cat. *Journal of anatomy* 147:55-72.
- Jones KJ, Lovett-Racke AE, Walker CL, Sanders VM (2015) CD4 + T Cells and Neuroprotection: Relevance to Motoneuron Injury and Disease. *Journal of neuroimmune pharmacology : the official journal of the Society on NeuroImmune Pharmacology* 10:587-594.
- Jung S, Aliberti J, Graemmel P, Sunshine MJ, Kreutzberg GW, Sher A, Littman DR (2000) Analysis of fractalkine receptor CX(3)CR1 function by targeted deletion and green fluorescent protein reporter gene insertion. *Mol Cell Biol* 20:4106-4114.
- Kalla R, Liu Z, Xu S, Koppius A, Imai Y, Kloss CU, Kohsaka S, Gschwendtner A, Moller JC, Werner A, Raivich G (2001) Microglia and the early phase of immune surveillance in the axotomized facial motor nucleus: impaired microglial activation and lymphocyte recruitment but no effect on neuronal survival or axonal regeneration in macrophage-colony stimulating factor-deficient mice. *The Journal of comparative neurology* 436:182-201.
- Kandel ER, Siegelbaum SA (2000) Synaptic Integration. In: *Principles of Neural Science*, pp 207-228. New York: McGraw-Hill.
- Kato S, Ide C (1994) Axonal sprouting at the node of Ranvier of the peripheral nerve disconnected with the cell body. *Restorative neurology and neuroscience* 6:181-187.
- Kempuraj D, Thangavel R, Natteru PA, Selvakumar GP, Saeed D, Zahoor H, Zaheer S, Iyer SS, Zaheer A (2016) Neuroinflammation Induces Neurodegeneration. *J Neurol Neurosurg Spine* 1.
- Kettenmann H, Hanisch UK, Noda M, Verkhratsky A (2011) Physiology of microglia. *Physiol Rev* 91:461-553.
- Kiehn O (2016) Decoding the organization of spinal circuits that control locomotion. *Nature reviews Neuroscience* 17:224-238.
- Kierdorf K et al. (2013) Microglia emerge from erythromyeloid precursors via Pu.1- and Irf8-dependent pathways. *Nature neuroscience* 16:273-280.
- Kinoshita T (1991) Biology of complement: the overture. *Immunol Today* 12:291-295.
- Kirchhoff F (2012) Role of microglia in the normal brain. In: *Neuroglia* pp 605-613. New York, NY Oxford University Press
- Kohno H, Koso H, Okano K, Sundermeier TR, Saito S, Watanabe S, Tsuneoka H, Sakai T (2015) Expression pattern of Ccr2 and Cx3cr1 in inherited retinal degeneration. *Journal of neuroinflammation* 12:188.
- Kouyoumdjian JA (2006) Peripheral nerve injuries: a retrospective survey of 456 cases. *Muscle & nerve* 34:785-788.

- Krizbai I, Wilhelm I, Bauer H-C, Bauer H (2013) The role of glia in the formation and function of the blood-brain barrier In: Neuroglia 3Edition, pp 417-419. New York, NY Oxford University Press
- Kuffler SW, Hunt CC, Quilliam JP (1951) Function of medullated small-nerve fibers in mammalian ventral roots; efferent muscle spindle innervation. *Journal of neurophysiology* 14:29-54.
- Kurihara T, Warr G, Loy J, Bravo R (1997) Defects in macrophage recruitment and host defense in mice lacking the CCR2 chemokine receptor. *The Journal of experimental medicine* 186:1757-1762.
- Kurze T (1964) Microtechniques in neurological surgery. *Clin Neurosurg* 11:128-137.
- Kuziel WA, Morgan SJ, Dawson TC, Griffin S, Smithies O, Ley K, Maeda N (1997) Severe reduction in leukocyte adhesion and monocyte extravasation in mice deficient in CC chemokine receptor 2. *Proceedings of the National Academy of Sciences of the United States of America* 94:12053-12058.
- Lawson LJ, Perry VH, Gordon S (1992) Turnover of resident microglia in the normal adult mouse brain. *Neuroscience* 48:405-415.
- Lawson LJ, Perry VH, Dri P, Gordon S (1990) Heterogeneity in the distribution and morphology of microglia in the normal adult mouse brain. *Neuroscience* 39:151-170.
- Lee CY, Landreth GE (2010) The role of microglia in amyloid clearance from the AD brain. *J Neural Transm (Vienna)* 117:949-960.
- Lee SK, Wolfe SW (2000) Peripheral nerve injury and repair. *J Am Acad Orthop Surg* 8:243-252.
- Lekan HA, Chung K, Yoon YW, Chung JM, Coggeshall RE (1997) Loss of dorsal root ganglion cells concomitant with dorsal root axon sprouting following segmental nerve lesions. *Neuroscience* 81:527-534.
- Lenhossek MV (1895) Der feinere Bau des Nervensystems im Lichte neuester Forschungen In: Fisher's Medicinische Buchhandlung H. Kornfeld 2 Edition.
- Lewis PR, Shute CC (1966) The distribution of cholinesterase in cholinergic neurons demonstrated with the electron microscope. *Journal of cell science* 1:381-390.
- Liddell EGT, Sherrington CS (1924) Reflexes in response to stretch (myoatic reflexes). *Proc R Soc Lond B*:212-242.
- Liddell EGT, Sherrington CS (1925) Recruitment and some factors of reflex inhibition. *Proc R Soc London Ser B* 97:488-518.
- Liddel SA et al. (2017) Neurotoxic reactive astrocytes are induced by activated microglia. *Nature* 541:481-487.
- Lieberman AR (1971) The axon reaction: a review of the principal features of perikaryal responses to axon injury. *International review of neurobiology* 14:49-124.
- Limatola C, Ransohoff RM (2014) Modulating neurotoxicity through CX3CL1/CX3CR1 signaling. *Frontiers in cellular neuroscience* 8:229.

- Lin JH, Saito T, Anderson DJ, Lance-Jones C, Jessell TM, Arber S (1998) Functionally related motor neuron pool and muscle sensory afferent subtypes defined by coordinate ETS gene expression. *Cell* 95:393-407.
- Linda H, Hammarberg H, Cullheim S, Levinovitz A, Khademi M, Olsson T (1998) Expression of MHC class I and beta2-microglobulin in rat spinal motoneurons: regulatory influences by IFN-gamma and axotomy. *Experimental neurology* 150:282-295.
- Linda H, Shupliakov O, Ornung G, Ottersen OP, Storm-Mathisen J, Risling M, Cullheim S (2000) Ultrastructural evidence for a preferential elimination of glutamate-immunoreactive synaptic terminals from spinal motoneurons after intramedullary axotomy. *The Journal of comparative neurology* 425:10-23.
- Liu L, Tornqvist E, Mattsson P, Eriksson NP, Persson JK, Morgan BP, Aldskogius H, Svensson M (1995) Complement and clusterin in the spinal cord dorsal horn and gracile nucleus following sciatic nerve injury in the adult rat. *Neuroscience* 68:167-179.
- Lloyd DPC (1943) Neuron patterns controlling transmission of ipsilateral hind limb reflexes in cat *Journal of neurophysiology* 6:293-315.
- Lloyd RE (1900) On chromatolysis in Deiters' nucleus after hemisection of the cord. *The Journal of physiology* 25:191-195.
- Lundberg A (1964) Ascending Spinal Hindlimb Pathways in the Cat. *Progress in brain research* 12:135-163.
- Lundberg A, Winsbury G (1960) Selective adequate activation of large afferents from muscle spindles and Golgi tendon organs. *Acta Physiol Scand* 49:155-164.
- Lundborg G (2003) Richard P. Bunge memorial lecture. Nerve injury and repair-- a challenge to the plastic brain. *Journal of the peripheral nervous system : JPNS* 8:209-226.
- Lunn ER, Perry VH, Brown MC, Rosen H, Gordon S (1989) Absence of Wallerian Degeneration does not Hinder Regeneration in Peripheral Nerve. *The European journal of neuroscience* 1:27-33.
- Maciejewski-Lenoir D, Chen S, Feng L, Maki R, Bacon KB (1999) Characterization of fractalkine in rat brain cells: migratory and activation signals for CX3CR-1-expressing microglia. *Journal of immunology* 163:1628-1635.
- Mackinnon SE, Dellon AL (1988) *Surgery of the Peripheral Nerve* In, 1 Edition. New York, NY, USA: George Thieme Verlag
- Mar FM, Bonni A, Sousa MM (2014) Cell intrinsic control of axon regeneration. *EMBO Rep* 15:254-263.
- Martini R, Fischer S, Lopez-Vales R, David S (2008) Interactions between Schwann cells and macrophages in injury and inherited demyelinating disease. *Glia* 56:1566-1577.
- Matyash V, Kettenmann H (2010) Heterogeneity in astrocyte morphology and physiology. *Brain research reviews* 63:2-10.

- Maxwell DJ, Christie WM, Short AD, Brown AG (1990) Direct observations of synapses between GABA-immunoreactive boutons and muscle afferent terminals in lamina VI of the cat's spinal cord. *Brain research* 530:215-222.
- McLaughlin BJ (1972) The fine structure of neurons and synapses in the motor nuclei of the cat spinal cord. *The Journal of comparative neurology* 144:429-460.
- Mendell LM (1984) Modifiability of spinal synapses. *Physiol Rev* 64:260-324.
- Mendell LM, Henneman E (1971) Terminals of single Ia fibers: location, density, and distribution within a pool of 300 homonymous motoneurons. *Journal of neurophysiology* 34:171-187.
- Mendell LM, Munson JB, Scott JG (1974) Connectivity changes of Ia afferents on axotomized motoneurons. *Brain research* 73:338-342.
- Mendell LM, Munson JB, Scott JG (1976) Alterations of synapses on axotomized motoneurons. *The Journal of physiology* 255:67-79.
- Millar NS (2003) Assembly and subunit diversity of nicotinic acetylcholine receptors. *Biochemical Society transactions* 31:869-874.
- Millesi H (1973) Microsurgery of peripheral nerves. *Hand* 5:157-160.
- Millesi H, Meissl G, Berger A (1972) The interfascicular nerve-grafting of the median and ulnar nerves. *The Journal of bone and joint surgery American volume* 54:727-750.
- Mitchell JK (1895) *Remote Consequence of Injuries of Nerves, and Their Treatment.*: Lea Brothers & Co. .
- Mizutani M, Pino PA, Saederup N, Charo IF, Ransohoff RM, Cardona AE (2012) The fractalkine receptor but not CCR2 is present on microglia from embryonic development throughout adulthood. *J Immunol* 188:29-36.
- Mokarram N, Dymanus K, Srinivasan A, Lyon JG, Tipton J, Chu J, English AW, Bellamkonda RV (2017) Immunoengineering nerve repair. *Proceedings of the National Academy of Sciences of the United States of America* 114:E5077-E5084.
- Moore AM, Ray WZ, Chenard KE, Tung T, Mackinnon SE (2009) Nerve allotransplantation as it pertains to composite tissue transplantation. *Hand (N Y)* 4:239-244.
- Moreno-Lopez B (2010) Local isoform-specific NOS inhibition: a promising approach to promote motor function recovery after nerve injury. *Journal of neuroscience research* 88:1846-1857.
- Morganti JM, Jopson TD, Liu S, Gupta N, Rosi S (2014) Cranial irradiation alters the brain's microenvironment and permits CCR2+ macrophage infiltration. *PLoS one* 9:e93650.
- Munson JB, Sybert GW (1979) Properties of single central Ia afferent fibres projecting to motoneurons. *The Journal of physiology* 296:315-327.
- Narakas A (1988) The use of fibrin glue in repair of peripheral nerves. *Orthop Clin North Am* 19:187-199.
- Navarro X, Vivo M, Valero-Cabre A (2007) Neural plasticity after peripheral nerve injury and regeneration. *Progress in neurobiology* 82:163-201.
- Nguyen QT, Sanes JR, Lichtman JW (2002) Pre-existing pathways promote precise projection patterns. *Nature neuroscience* 5:861-867.

- Nimmerjahn A, Kirchhoff F, Helmchen F (2005) Resting microglial cells are highly dynamic surveillants of brain parenchyma in vivo. *Science* 308:1314-1318.
- Nissl F (1904) Über einige Beziehungen zwischen Nervenzellenerkrankungen und gliösen Erscheinungen bei verschiedenen Psychosen. *Arch Psych* 32:1-21.
- Noble J, Munro CA, Prasad VS, Midha R (1998) Analysis of upper and lower extremity peripheral nerve injuries in a population of patients with multiple injuries. *The Journal of trauma* 45:116-122.
- Oliveira AL, Thams S, Lidman O, Piehl F, Hokfelt T, Karre K, Linda H, Cullheim S (2004) A role for MHC class I molecules in synaptic plasticity and regeneration of neurons after axotomy. *Proceedings of the National Academy of Sciences of the United States of America* 101:17843-17848.
- Orr AG, Orr AL, Li XJ, Gross RE, Traynelis SF (2009) Adenosine A(2A) receptor mediates microglial process retraction. *Nature neuroscience* 12:872-878.
- Otto D, Unsicker K, Grothe C (1987) Pharmacological effects of nerve growth factor and fibroblast growth factor applied to the transected sciatic nerve on neuron death in adult rat dorsal root ganglia. *Neuroscience letters* 83:156-160.
- Pachter JS, de Vries HE, Fabry Z (2003) The blood-brain barrier and its role in immune privilege in the central nervous system. *Journal of neuropathology and experimental neurology* 62:593-604.
- Paolicelli RC, Bisht K, Tremblay ME (2014) Fractalkine regulation of microglial physiology and consequences on the brain and behavior. *Frontiers in cellular neuroscience* 8:129.
- Perry VH, O'Connor V (2008) C1q: the perfect complement for a synaptic feast? *Nature reviews Neuroscience* 9:807-811.
- Pfister BJ, Gordon T, Loverde JR, Kochar AS, Mackinnon SE, Cullen DK (2011) Biomedical engineering strategies for peripheral nerve repair: surgical applications, state of the art, and future challenges. *Crit Rev Biomed Eng* 39:81-124.
- Popratiloff A, Kharazia VN, Weinberg RJ, Laonipon B, Rustioni A (1996) Glutamate receptors in spinal motoneurons after sciatic nerve transection. *Neuroscience* 74:953-958.
- Prather JF, Nardelli P, Nakanishi ST, Ross KT, Nichols TR, Pinter MJ, Cope TC (2011) Recovery of proprioceptive feedback from nerve crush. *The Journal of physiology* 589:4935-4947.
- Prinz M, Priller J, Sisodia SS, Ransohoff RM (2011) Heterogeneity of CNS myeloid cells and their roles in neurodegeneration. *Nature neuroscience* 14:1227-1235.
- Raivich G, Moreno-Flores MT, Muller JC, Kreutzberg GW (1994a) Regulation of microglial proliferation: colony-stimulating factors and their receptors. *Neuropathology and applied neurobiology* 20:209-211.
- Raivich G, Moreno-Flores MT, Moller JC, Kreutzberg GW (1994b) Inhibition of posttraumatic microglial proliferation in a genetic model of macrophage colony-stimulating factor deficiency in the mouse. *The European journal of neuroscience* 6:1615-1618.

- Raivich G, Jones LL, Kloss CU, Werner A, Neumann H, Kreutzberg GW (1998) Immune surveillance in the injured nervous system: T-lymphocytes invade the axotomized mouse facial motor nucleus and aggregate around sites of neuronal degeneration. *J Neurosci* 18:5804-5816.
- Ramaglia V, Daha MR, Baas F (2008) The complement system in the peripheral nerve: friend or foe? *Molecular immunology* 45:3865-3877.
- Ransohoff RM (2016) A polarizing question: do M1 and M2 microglia exist? *Nature neuroscience* 19:987-991.
- Ransohoff RM, El Khoury J (2015) *Microglia in Health and Disease*. Cold Spring Harb Perspect Biol 8:a020560.
- Rasband MN (2010) The axon initial segment and the maintenance of neuronal polarity. *Nature reviews Neuroscience* 11:552-562.
- Reichel CA, Khandoga A, Anders HJ, Schlondorff D, Luckow B, Krombach F (2006) Chemokine receptors Ccr1, Ccr2, and Ccr5 mediate neutrophil migration to postischemic tissue. *Journal of leukocyte biology* 79:114-122.
- Reisert I, Wildemann G, Grab D, Pilgrim C (1984) The glial reaction in the course of axon regeneration: a stereological study of the rat hypoglossal nucleus. *The Journal of comparative neurology* 229:121-128.
- Rethelyi M (1970) Ultrastructural synaptology of Clarke's column. *Experimental brain research Experimentelle Hirnforschung Experimentation cerebrale* 11:159-174.
- Rexed B (1952) The cytoarchitectonic organization of the spinal cord in the cat. *The Journal of comparative neurology* 96:414-495.
- Reynolds AJ, Hendry IA, Bartlett SE (2001) Anterograde and retrograde transport of active extracellular signal-related kinase 1 (ERK1) in the ligated rat sciatic nerve. *Neuroscience* 105:761-771.
- Rich KM, Disch SP, Eichler ME (1989) The influence of regeneration and nerve growth factor on the neuronal cell body reaction to injury. *Journal of neurocytology* 18:569-576.
- Rich KM, Luszczynski JR, Osborne PA, Johnson EM, Jr. (1987) Nerve growth factor protects adult sensory neurons from cell death and atrophy caused by nerve injury. *Journal of neurocytology* 16:261-268.
- Rich KM, Yip HK, Osborne PA, Schmidt RE, Johnson EM, Jr. (1984) Role of nerve growth factor in the adult dorsal root ganglia neuron and its response to injury. *The Journal of comparative neurology* 230:110-118.
- Richardson PM, McGuinness UM, Aguayo AJ (1980) Axons from CNS neurons regenerate into PNS grafts. *Nature* 284:264-265.
- Río-Hortega P (1919a) El "tercer elemento de los centros nerviosos." IV. Poder fagocitario y movilidad de la microglía. *Boletín de la Sociedad Española de Biológica* 8
- Río-Hortega P (1919b) El "tercer elemento" de los centros nerviosos. III Naturaleza probable de la microglía. *Boletín de la Sociedad Española de Biológica* 8:108-115.
- Río-Hortega P (1919c) El "tercer elemento" de los centros nerviosos. I. La microglía en estado normal. II. Intervención de la microglía en los

- procesos patológicos (células en bastoncito y cuerpos gránulo-adipose). Boletín de la Sociedad Española de Biología 8:69-109.
- Rishal I, Fainzilber M (2014) Axon-soma communication in neuronal injury. *Nature reviews Neuroscience* 15:32-42.
- Risling M, Aldskogius H, Hildebrand C, Remahl S (1983) Effects of sciatic nerve resection on L7 spinal roots and dorsal root ganglia in adult cats. *Experimental neurology* 82:568-580.
- Robbins SL, Angell M, Kumar V (1981) *Basic Pathology* Philadelphia: W.B. Saunders
- Robinson AP, White TM, Mason DW (1986) Macrophage heterogeneity in the rat as delineated by two monoclonal antibodies MRC OX-41 and MRC OX-42, the latter recognizing complement receptor type 3. *Immunology* 57:239-247.
- Rohlmann A, Laskawi R, Hofer A, Dermietzel R, Wolff JR (1994) Astrocytes as rapid sensors of peripheral axotomy in the facial nucleus of rats. *Neuroreport* 5:409-412.
- Rosenberg AF, Wolman MA, Franzini-Armstrong C, Granato M (2012) In vivo nerve-macrophage interactions following peripheral nerve injury. *J Neurosci* 32:3898-3909.
- Rotterman TM, Nardelli P, Cope TC, Alvarez FJ (2014) Normal distribution of VGLUT1 synapses on spinal motoneuron dendrites and their reorganization after nerve injury. *The Journal of neuroscience : the official journal of the Society for Neuroscience* 34:3475-3492.
- Rotterman TM, MacPherson KP, Chopra T, Fisher S, Tansey MG, Alvarez FJ (2017) Comparison between sciatic nerve transection and sciatic nerve crush: differences in regenerative outcomes peripherally, graded central neuroimmune response and differences in spinal circuit plasticity following injury. In: *Society for Neuroscience* Washington, D.C. .
- Saederup N, Cardona AE, Croft K, Mizutani M, Cotleur AC, Tsou CL, Ransohoff RM, Charo IF (2010) Selective chemokine receptor usage by central nervous system myeloid cells in CCR2-red fluorescent protein knock-in mice. *PloS one* 5:e13693.
- Saijo K, Glass CK (2011) Microglial cell origin and phenotypes in health and disease. *Nature reviews Immunology* 11:775-787.
- Schafer DP, Lehrman EK, Kautzman AG, Koyama R, Mardinly AR, Yamasaki R, Ransohoff RM, Greenberg ME, Barres BA, Stevens B (2012) Microglia sculpt postnatal neural circuits in an activity and complement-dependent manner. *Neuron* 74:691-705.
- Schmalbruch H (1987) Loss of sensory neurons after sciatic nerve section in the rat. *The Anatomical record* 219:323-329.
- Schultz AJ, Rotterman TM, Dwarakanath A, Alvarez FJ (2017) VGLUT1 synapses and P-boutons on regenerating motoneurons after nerve crush. *The Journal of comparative neurology*.
- Schwann T (1839) *Mikroskopische Untersuchungen über die Uebereinstimmung un der Struktur und dem Wachstum der Tiere und Pflanzen*. In: Berlin: Sander

- Scorcioni R, Lazarewicz MT, Ascoli GA (2004) Quantitative morphometry of hippocampal pyramidal cells: differences between anatomical classes and reconstructing laboratories. *The Journal of comparative neurology* 473:177-193.
- Scott JG, Mendell LM (1976) Individual EPSPs produced by single triceps surae Ia afferent fibers in homonymous and heteronymous motoneurons. *Journal of neurophysiology* 39:679-692.
- Scott JJ (1996) The functional recovery of muscle proprioceptors after peripheral nerve lesions. *Journal of the peripheral nervous system : JPNS* 1:19-27.
- Seburn KL, Cope TC (1998) Short-term afferent axotomy increases both strength and depression at Ia-motoneuron synapses in Rat. *J Neurosci* 18:1142-1147.
- Seddon HJ (1947) The use of autogenous grafts for the repair of large gaps in peripheral nerves. *The British journal of surgery* 35:151-167.
- Seddon HJ, Medawar PB, Smith H (1943) Rate of regeneration of peripheral nerves in man. *The Journal of physiology* 102:191-215.
- Serbina NV, Pamer EG (2006) Monocyte emigration from bone marrow during bacterial infection requires signals mediated by chemokine receptor CCR2. *Nature immunology* 7:311-317.
- Serpe CJ, Coers S, Sanders VM, Jones KJ (2003) CD4+ T, but not CD8+ or B, lymphocytes mediate facial motoneuron survival after facial nerve transection. *Brain, behavior, and immunity* 17:393-402.
- Serpe CJ, Kohm AP, Huppenbauer CB, Sanders VM, Jones KJ (1999) Exacerbation of facial motoneuron loss after facial nerve transection in severe combined immunodeficient (scid) mice. *J Neurosci* 19:RC7.
- Sherrington CS (1906) *The integrative action of the nervous system*. New York,: C. Scribner's sons.
- Sherrington CS (1909) On plastic tonus and proprioceptive reflexes. *Quarterly Journal of Experimental Physiology* 2:109-156.
- Shi C, Pamer EG (2011) Monocyte recruitment during infection and inflammation. *Nature reviews Immunology* 11:762-774.
- Shi C, Jia T, Mendez-Ferrer S, Hohl TM, Serbina NV, Lipuma L, Leiner I, Li MO, Frenette PS, Pamer EG (2011) Bone marrow mesenchymal stem and progenitor cells induce monocyte emigration in response to circulating toll-like receptor ligands. *Immunity* 34:590-601.
- Shi TJ, Tandrup T, Bergman E, Xu ZQ, Ulfhake B, Hokfelt T (2001) Effect of peripheral nerve injury on dorsal root ganglion neurons in the C57 BL/6J mouse: marked changes both in cell numbers and neuropeptide expression. *Neuroscience* 105:249-263.
- Shneider NA, Brown MN, Smith CA, Pickel J, Alvarez FJ (2009) Gamma motor neurons express distinct genetic markers at birth and require muscle spindle-derived GDNF for postnatal survival. *Neural Dev* 4:42.
- Siembab VC, Gomez-Perez L, Rotterman TM, Shneider NA, Alvarez FJ (2016) Role of primary afferents in the developmental regulation of motor axon synapse numbers on Renshaw cells. *The Journal of comparative neurology* 524:1892-1919.

- Siemionow M, Brzezicki G (2009) Chapter 8: Current techniques and concepts in peripheral nerve repair. *International review of neurobiology* 87:141-172.
- Sierra A, de Castro F, Del Rio-Hortega J, Rafael Iglesias-Rozas J, Garrosa M, Kettenmann H (2016) The "Big-Bang" for modern glial biology: Translation and comments on Pio del Rio-Hortega 1919 series of papers on microglia. *Glia* 64:1801-1840.
- Skene JH, Willard M (1981) Characteristics of growth-associated polypeptides in regenerating toad retinal ganglion cell axons. *J Neurosci* 1:419-426.
- Smith JW (1964) *Microsurgery of Peripheral Nerves*. Plastic and reconstructive surgery 33:317-329.
- Sprague JM (1958) The distribution of dorsal root fibres on motor cells in the lumbosacral spinal cord of the cat, and the site of excitatory and inhibitory terminals in monosynaptic pathways. *Proceedings of the Royal Society of London Series B, Containing papers of a Biological character Royal Society* 149:534-556.
- Stevens B, Allen NJ, Vazquez LE, Howell GR, Christopherson KS, Nouri N, Micheva KD, Mehalow AK, Huberman AD, Stafford B, Sher A, Litke AM, Lambris JD, Smith SJ, John SW, Barres BA (2007) The classical complement cascade mediates CNS synapse elimination. *Cell* 131:1164-1178.
- Stoll G, Muller HW (1999) Nerve injury, axonal degeneration and neural regeneration: basic insights. *Brain pathology* 9:313-325.
- Streit WJ (2004) Microglia and Alzheimer's disease pathogenesis. *Journal of neuroscience research* 77:1-8.
- Streit WJ (2012) Microglial Cells In: *Neuroglia* 3Edition, pp 86-97. New York, NY: Oxford University Press.
- Streit WJ, Mrak RE, Griffin WS (2004) Microglia and neuroinflammation: a pathological perspective. *Journal of neuroinflammation* 1:14.
- Sumner BE (1975) A quantitative analysis of the response of presynaptic boutons to postsynaptic motor neuron axotomy. *Experimental neurology* 46:605-615.
- Sumner BE, Sutherland FI (1973) Quantitative electron microscopy on the injured hypoglossal nucleus in the rat. *Journal of neurocytology* 2:315-328.
- Sunderland S (1945) The intraneural topography of the radial, median and ulnar nerves. *Brain : a journal of neurology* 68:243-299.
- Sunderland S (1951) The function of nerve fibers whose structure has been disorganized. *The Anatomical record* 109:503-513.
- Sunderland S (1991) *Nerve Injuries and their Repair* UK: Longman Group.
- Sunico CR, Portillo F, Gonzalez-Forero D, Moreno-Lopez B (2005) Nitric-oxide-directed synaptic remodeling in the adult mammal CNS. *J Neurosci* 25:1448-1458.
- Sunico CR, Gonzalez-Forero D, Dominguez G, Garcia-Verdugo JM, Moreno-Lopez B (2010) Nitric oxide induces pathological synapse loss by a protein kinase G-, Rho kinase-dependent mechanism preceded by myosin light chain phosphorylation. *J Neurosci* 30:973-984.

- Svensson M, Aldskogius H (1992) Evidence for activation of the complement cascade in the hypoglossal nucleus following peripheral nerve injury. *Journal of neuroimmunology* 40:99-109.
- Svensson M, Aldskogius H (1993a) Infusion of cytosine-arabioside into the cerebrospinal fluid of the rat brain inhibits the microglial cell proliferation after hypoglossal nerve injury. *Glia* 7:286-298.
- Svensson M, Aldskogius H (1993b) Synaptic density of axotomized hypoglossal motoneurons following pharmacological blockade of the microglial cell proliferation. *Experimental neurology* 120:123-131.
- Tandrup T, Woolf CJ, Coggeshall RE (2000) Delayed loss of small dorsal root ganglion cells after transection of the rat sciatic nerve. *The Journal of comparative neurology* 422:172-180.
- Tay TL, Mai D, Dautzenberg J, Fernandez-Klett F, Lin G, Sagar, Datta M, Drougard A, Stempf T, Ardura-Fabregat A, Staszewski O, Margineanu A, Sporbert A, Steinmetz LM, Pospisilik JA, Jung S, Priller J, Grun D, Ronneberger O, Prinz M (2017) A new fate mapping system reveals context-dependent random or clonal expansion of microglia. *Nature neuroscience* 20:793-803.
- Taylor CA, Braza D, Rice JB, Dillingham T (2008) The incidence of peripheral nerve injury in extremity trauma. *American journal of physical medicine & rehabilitation / Association of Academic Physiatrists* 87:381-385.
- Tetzlaff W, Graeber MB, Bisby MA, Kreutzberg GW (1988) Increased glial fibrillary acidic protein synthesis in astrocytes during retrograde reaction of the rat facial nucleus. *Glia* 1:90-95.
- Thacker MA, Clark AK, Bishop T, Grist J, Yip PK, Moon LD, Thompson SW, Marchand F, McMahon SB (2009) CCL2 is a key mediator of microglia activation in neuropathic pain states. *Eur J Pain* 13:263-272.
- Todd AJ, Hughes DI, Polgar E, Nagy GG, Mackie M, Ottersen OP, Maxwell DJ (2003) The expression of vesicular glutamate transporters VGLUT1 and VGLUT2 in neurochemically defined axonal populations in the rat spinal cord with emphasis on the dorsal horn. *The European journal of neuroscience* 17:13-27.
- Tremblay ME, Lecours C, Samson L, Sanchez-Zafra V, Sierra A (2015) From the Cajal alumni Achucarro and Rio-Hortega to the rediscovery of never-resting microglia. *Frontiers in neuroanatomy* 9:45.
- Tsou CL, Peters W, Si Y, Slaymaker S, Aslanian AM, Weisberg SP, Mack M, Charo IF (2007) Critical roles for CCR2 and MCP-3 in monocyte mobilization from bone marrow and recruitment to inflammatory sites. *The Journal of clinical investigation* 117:902-909.
- Tsuda M (2016) Microglia in the spinal cord and neuropathic pain. *Journal of diabetes investigation* 7:17-26.
- Tsujino H, Kondo E, Fukuoka T, Dai Y, Tokunaga A, Miki K, Yonenobu K, Ochi T, Noguchi K (2000) Activating transcription factor 3 (ATF3) induction by axotomy in sensory and motoneurons: A novel neuronal marker of nerve injury. *Molecular and cellular neurosciences* 15:170-182.

- Uchizono K (1966) Excitatory and inhibitory synapses in the cat spinal cord. *The Japanese journal of physiology* 16:570-575.
- Ulfhake B, Cullheim S (1988) Postnatal development of cat hind limb motoneurons. III: Changes in size of motoneurons supplying the triceps surae muscle. *The Journal of comparative neurology* 278:103-120.
- Umekawa T, Osman AM, Han W, Ikeda T, Blomgren K (2015) Resident microglia, rather than blood-derived macrophages, contribute to the earlier and more pronounced inflammatory reaction in the immature compared with the adult hippocampus after hypoxia-ischemia. *Glia* 63:2220-2230.
- Valero-Cabre A, Tsironis K, Skouras E, Navarro X, Neiss WF (2004) Peripheral and spinal motor reorganization after nerve injury and repair. *Journal of neurotrauma* 21:95-108.
- Vasek MJ et al. (2016) A complement-microglial axis drives synapse loss during virus-induced memory impairment. *Nature* 534:538-543.
- Verdu E, Ceballos D, Vilches JJ, Navarro X (2000) Influence of aging on peripheral nerve function and regeneration. *Journal of the peripheral nervous system : JPNS* 5:191-208.
- Vincent JA, Gabriel HM, Deardorff AS, Nardelli P, Fyffe REW, Burkholder TJ, Cope TC (2017) Muscle Proprioceptors in Adult Rat: Mechanosensory Signaling and Synapse Distribution in Spinal Cord. *Journal of neurophysiology:jn* 00497 02017.
- Virchow R (1846) Über das granuliertes ansehn der Wandungen der Gehirnvventrikel. *Allgemeine Zeitschrift für Psychiatrie* 3:242-250.
- Virchow R (1858) *Die Cellularpathologie in ihrer Begründung auf physiologische und pathologische Gewebelehre* Verlag von August Hirschwald.
- Waller A (1850) Experiments on the section of the glossopharyngeal and hypoglossal nerves of the frog, and observations of the alterations produced thereby in the structures of their primitive fibres. *Philosophical Transactions of the Royal Society of London* 140:423-429.
- Walmsley B, Bolton PS (1994) An in vivo pharmacological study of single group Ia fibre contacts with motoneurons in the cat spinal cord. *The Journal of physiology* 481 (Pt 3):731-741.
- Wang JT, Medress ZA, Barres BA (2012) Axon degeneration: molecular mechanisms of a self-destruction pathway. *The Journal of cell biology* 196:7-18.
- Westbury DR (1972) A study of stretch and vibration reflexes of the cat by intracellular recording from motoneurons. *The Journal of physiology* 226:37-56.
- Wolburg H, Noell S, Wolburg-Buchholz K, Mack A, Fallier-Becker P (2009) Agrin, aquaporin-4, and astrocyte polarity as an important feature of the blood-brain barrier. *The Neuroscientist : a review journal bringing neurobiology, neurology and psychiatry* 15:180-193.
- Wolf SA, Boddeke HW, Kettenmann H (2017) Microglia in Physiology and Disease. *Annu Rev Physiol* 79:619-643.
- Wolf Y, Yona S, Kim KW, Jung S (2013) Microglia, seen from the CX3CR1 angle. *Frontiers in cellular neuroscience* 7:26.

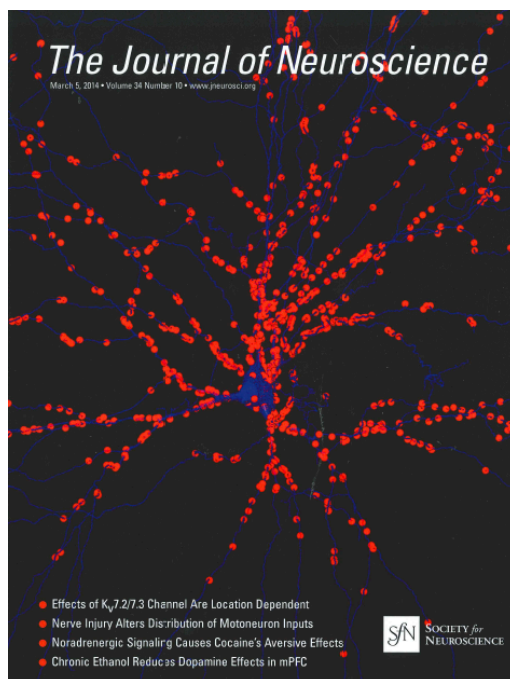
- Woodhall B, Beebe GW (1956) Peripheral Nerve Regeneration: A Follow-up Study of 3,656 World War II Injuries Washington, D.C. : U.S. Government Printing Office
- Xin J, Wainwright DA, Mesnard NA, Serpe CJ, Sanders VM, Jones KJ (2011) IL-10 within the CNS is necessary for CD4+ T cells to mediate neuroprotection. *Brain, behavior, and immunity* 25:820-829.
- Yamasaki R et al. (2014) Differential roles of microglia and monocytes in the inflamed central nervous system. *The Journal of experimental medicine* 211:1533-1549.
- Ygge J (1989) Neuronal loss in lumbar dorsal root ganglia after proximal compared to distal sciatic nerve resection: a quantitative study in the rat. *Brain research* 478:193-195.
- Yona S, Kim KW, Wolf Y, Mildner A, Varol D, Breker M, Strauss-Ayali D, Viukov S, Guilliams M, Misharin A, Hume DA, Perlman H, Malissen B, Zelzer E, Jung S (2013) Fate mapping reveals origins and dynamics of monocytes and tissue macrophages under homeostasis. *Immunity* 38:79-91.
- Yu WH (1994) Nitric oxide synthase in motor neurons after axotomy. *The journal of histochemistry and cytochemistry : official journal of the Histochemistry Society* 42:451-457.
- Yu WH (1997) Regulation of nitric oxide synthase expression in motoneurons following nerve injury. *Dev Neurosci* 19:247-254.
- Zhang J, De Koninck Y (2006) Spatial and temporal relationship between monocyte chemoattractant protein-1 expression and spinal glial activation following peripheral nerve injury. *Journal of neurochemistry* 97:772-783.
- Zhang J, Shi XQ, Echeverry S, Mogil JS, De Koninck Y, Rivest S (2007) Expression of CCR2 in both resident and bone marrow-derived microglia plays a critical role in neuropathic pain. *J Neurosci* 27:12396-12406.
- Zhou D, Lambert S, Malen PL, Carpenter S, Boland LM, Bennett V (1998) AnkyrinG is required for clustering of voltage-gated Na channels at axon initial segments and for normal action potential firing. *The Journal of cell biology* 143:1295-1304.
- Zlokovic BV (2008) The blood-brain barrier in health and chronic neurodegenerative disorders. *Neuron* 57:178-201.

Chapter 2:

Normal distribution of VGLUT1 synapses on spinal motoneuron dendrites and their reorganization after nerve injury

*Chapter Published: Rotterman TM, Nardelli P, Cope TC, Alvarez FJ (2014)
Normal Distribution of VGLUT1 Synapses on Spinal Motoneuron Dendrites and
Their Reorganization after Nerve Injury. J Neurosci 34:3475-3492.*

Permission granted from publisher for reproduction



2.1 Abstract

Peripheral nerve injury induces permanent alterations in spinal cord circuitries that are not reversed by regeneration. Nerve injury provokes the loss of many proprioceptive IA afferent synapses (VGLUT1-IR boutons) from motoneurons, the reduction of IA EPSPs in motoneurons and the disappearance of stretch reflexes. After motor and sensory axons successfully reinnervate muscle, lost IA VGLUT1 synapses are not re-established and the stretch reflex does not recover; however, electrically-evoked EPSPs do recover. The reasons why remaining IA synapses can evoke EPSPs on motoneurons but fail to transmit useful stretch signals are unknown. To better understand changes in the organization of VGLUT1 IA synapses that might influence their input strength we analyzed their distribution over the entire dendritic arbor of motoneurons before and after nerve injury. Adult rats underwent complete tibial nerve transection followed by microsurgical reattachment and one year later motoneurons were intracellularly recorded and filled with neurobiotin to map the distribution of VGLUT1 synapses along their dendrites. We found in control motoneurons an average of 911 VGLUT1 synapses; around 62% of them were lost after injury. In controls, VGLUT1 synapses were focused to proximal dendrites where they were grouped in tight clusters. After injury, most synaptic losses occurred in the proximal dendrites and remaining synapses were de-clustered smaller, and uniformly distributed throughout the dendritic arbor. We conclude that this loss and reorganization renders IA afferent synapses incompetent for efficient

motoneuron synaptic depolarization in response to natural stretch, while still capable of eliciting EPSPs when synchronously fired by electrical volleys.

2.2 Introduction

Functional recovery following repair of peripheral nerves remains disappointing for nearly one million people who suffer traumatic nerve injuries annually. Nine out of ten patients do not regain normal motor coordination and four of ten have difficulty achieving gross manual activity (Hoke and Brushart, 2010). Current consensus holds that this poor outcome is the result of connection errors made by regenerating sensory and motor axons with peripheral targets. Certainly, targeting errors hinder recovery after injury to major nerve trunks, however, functional impairments are also observed following injuries to terminal nerve branches and after reinnervation of the correct muscle (Abelew et al., 2000, Maas et al., 2007, Sabatier et al., 2011). In this case targeting errors are not possible and a different mechanism is needed to explain the permanency of disorders in gait, balance, and controlled reaching.

Changes in spinal cord circuitry triggered by the nerve injury also cause motor dysfunction (Navarro, 2009). Specifically, the stretch reflex is lost after nerve transection and muscle stretch fails to initiate or even modulate motoneuron (MN) firing; this alteration is permanent and remains after successful nerve regeneration and muscle reinnervation in the periphery (Cope et al., 1994, Huyghues-Despointes et al., 2003). This occurs even though nearly half of regenerated muscle spindle afferents successfully reconnect with spindle receptors and afferent responses to stretch can be readily recorded in dorsal

roots entering the spinal cord (Collins et al., 1986, Haftel et al., 2005). We found that these deficits are partially explained by the loss of a large fraction of IA afferent synapses on MNs (Alvarez et al., 2011, Bullinger et al., 2011).

Surprisingly, while muscle reinnervation does not induce recovery of lost IA synapses, it does partially reverse the profound depression of electrically-evoked monosynaptic EPSPs seen in the early weeks after injury (Mendell, 1988; Mendell et al., 1995), and it can restore and even amplify H-reflexes (Valero-Cabre and Navarro, 2001). These findings suggest a non-intuitive paradigm in which remaining IA synapses partially recover their capacity to depolarize the MN when electrically driven, but they are not competent to effectively transmit information about muscle stretch. One possibility is that the IA afferents that remain connected with MNs fail to reinnervate spindles peripherally (Banks and Barker, 1989); another is that their central synapses with MNs redistribute on the dendritic arbor in such a manner that weakens neurotransmission. The exact distribution of the IA afferent input on the whole dendritic arbor of MNs before and after injury is unknown. Therefore, this study had two main goals. First, determine the total IA afferent input onto single uninjured neurobiotin-filled MNs (using VGLUT1 as a marker; Alvarez et al., 2011) and second, map the location of IA synapses that remain after nerve injury and regeneration. Our results suggest that IA afferents are normally non-uniformly distributed along MN dendrites, being concentrated on proximal dendrites. After nerve injury there is preferential loss and structural changes in proximal synapses that could present

significant barriers for recovery of MN responses to muscle stretch and reflex function.

2.3 Methods

All studies were performed on adult female Wistar rats (225-300 g). All animal care, nerve surgeries and electrophysiological recordings in terminal experiments were prepared at Wright State University and approved by the institutional laboratory animal use committee at Wright State University.

2.3.1: Peripheral nerve transection and repair

Two to three-month-old Wistar rats were anesthetized with isoflurane until the animal achieved a surgical plane of anesthesia (induction 4-5%; maintenance 1-3%, both in 100% O₂). Nerves were exposed by a midline posterior incision (~1.5 cm) through the skin of the left leg at the popliteal fossa level. After retraction of the overlying biceps femoris, the tibial nerve (TN) was exposed, completely transected with scissors and immediately surgically rejoined to promote regeneration. Surgical nerve reunion was achieved by rejoining the cut nerve ends without tension using three 10-0 Ethilon sutures passed through the epineurium. After washing with 0.9% sterile saline, the wound was closed in layers and the animals were removed from anesthesia. A subcutaneous injection of buprenorphine (0.1 mg/kg) was delivered immediately and every 12 hours after surgery prophylactically to alleviate any possible pain, up to 2 days after surgeries. The animals never showed signs of distress (vocalization, lethargy,

weight loss, absence of grooming) and displayed normal exploratory and feeding behaviors soon after recovery from anesthesia.

Animal preparation for terminal recording sessions and collection of tissue: Electrophysiological studies were performed on two groups of rats *in vivo*: a control group of rats that were untreated and age matched to a second group which was treated with tibial nerve repair (described above) more than 12 months earlier in order to allow ample time for muscle reinnervation. These animals are all different from the animals we collected our previously published materials with this nerve injury model (Alvarez et al., 2011). In the terminal experiments, rats were deeply anesthetized by isoflurane throughout the experiment, beginning with induction in an enclosed chamber (4-5% in 100% O₂, inhalation in induction chamber) and continuing with delivery through a tracheal cannula (1-3% mixed in 100% O₂). The animal's condition was continuously monitored for respiratory rate (40-60 breaths per min), end tidal CO₂ (3-5%), oxygen saturation (>90%), heart rate (300-500 beats per min) and core temperature (36-38 °C). These levels were variously maintained by adjusting isoflurane concentration, radiant and water-pad heat sources, and subcutaneous injection of Ringer/dextrose solution. One hour after intracellular recording and labeling of MG MNs the animals received a lethal injection of euthasol (i.p. 150 mg/kg) and were perfusion-fixed through the left ventricle with 4% paraformaldehyde in 0.1M phosphate buffer (PB). The spinal cord tissue was then harvested and post-fixed overnight before histology.

2.3.2: Electrophysiology

Standard procedures were used to prepare the rat *in vivo* for electrophysiological recording of individual spinal MNs supplying the MG muscle (see Bullinger et al, 2011). Briefly, anesthetized rats were fixed to a rigid recording frame with the dorsal surface of the lumbosacral spinal cord exposed by a laminectomy and the left hind limb dissected to expose selected nerves and muscles. Skin flaps were used to construct pools of warm mineral oil over exposed tissues. The MG nerve was dissected and suspended in-continuity on a monopolar silver hook electrode for electrical stimulation at a site just distal to the lesion for rats in the regenerated group. Electrical stimulation yielded robust contraction of MG muscles, thereby verifying successful reinnervation in injured animals. All other nerves supplying the limb were crushed, including common peroneal, sural, and tibial nerve.

Motoneurons were searched, impaled and recorded intracellularly using borosilicate glass microelectrodes (1.2 mm OD, 7-10 M Ω DC resistance, 2 M K-acetate) advanced through the spinal cord using a stepping microdrive (Transvertex, Sweden). MG MNs were identified by antidromic action potentials elicited by electrical stimulation of the MG nerve (current strength 2.5X muscle contraction threshold, pulse duration 40 μ S). Glass microelectrodes contained 10% solution of Neurobiotin (Vector Labs, Burlingame, CA) for labeling. Only MNs with stable membrane potentials and action potential amplitudes of at least +60 mV were acceptable for further study. Motoneurons were injected with current through the micropipette to measure their intrinsic electrical properties:

rheobase current (depolarizing pulses 50 ms in duration at the lowest strengths capable of initiating action potentials), after hyperpolarization (AHP) (suprathreshold pulses 0.5 ms in duration), and input resistance (hyperpolarization produced by -1 and -3 nA current pulses 50 ms in duration). Possible differences in conduction velocity were estimated by comparing the delays of the antidromic action potentials after MG nerve stimulation. Positive current (5 nA), delivered as 400-ms pulses at 2 Hz for approximately 5 to 10 mins, were used to aid neurobiotin passage into the MN. Then we waited for about an hour, before sacrificing the animal, to allow neurobiotin to spread throughout the entire MN. Records of MN membrane potential, electrode current, muscle length, and muscle force were collected, digitized (20 kHz for all records except 1kHz for muscle length), stored and analyzed using CED (Cambridge Electronic Design) Power 1401 and Spike2 software. To optimize neurobiotin labeling and morphological analyses we deliberately kept our recordings short (< 30 mins). Therefore, these MNs did not undergo the thorough physiological characterization presented in Bullinger et al. (2011). Each filled MN was collected from a different rat with the exception of regenerated MNs 5 and 6 that were obtained from the same rat; MN#5 was more caudal than MN#6.

2.3.3: Histological processing and immunohistochemistry

Parasagittal longitudinal sections were obtained serially at 75 μm thickness on a vibratome (VT-1000) and processed to reveal neurobiotin and VGLUT1 immunofluorescence. The sections were collected free floating and

after blocking with 10% normal donkey serum for one hour they were incubated overnight in a solution containing streptavidin coupled to Alexa fluor 555 (SA-555, diluted 1:50; Invitrogen, Grand Island, NY, USA) and rabbit anti VGLUT1 antibodies (diluted 1:1,000; Synaptic Systems, 37079 Goettingen Germany) both diluted in 0.01M phosphate buffer with 0.9% NaCl and 0.3% Triton-X-100 (PBS-TX0.3). The following day the sections were washed in PBS and incubated for 2 hours in donkey anti-rabbit IgG antibodies conjugated to fluorescein isothiocyanate (FITC) (Jackson ImmunoResearch, West Grove, PA, USA) diluted 1:100 in PBS-TX0.3 and then washed (in PBS), mounted serially on glass slides and coverslipped with Vectashield (Vector labs).

To confirm the presence of synapses we estimated the percentage of VGLUT1 dendrite contacts that displayed a presynaptic active zone identified by immunoreactivity to bassoon. Sections containing a further neurobiotin-filled control MN (*cell #7*) were immunolabeled with VGLUT1 antibodies as described, but mixed with a mouse monoclonal antibody against bassoon (Enzo Life Sciences, Farmingdale, NY) diluted 1:4,000 in PBS-TX0.3. Bassoon and VGLUT1 immunoreactivities were detected with respectively DyLight 649- and FITC-coupled secondary antibodies raised in donkey against mouse or rabbit IgGs (Jackson-ImmunoResearch). Neurobiotin labeling was revealed with SA-555 as before. We randomly sampled 65 VGLUT1 contacts on neurobiotin-labeled dendrites and measured the three fluorescent signals (dendrite neurobiotin, bassoon-IR and VGLUT1-IR) along lines orthogonal to the dendrites and

VGLUT1 terminals. Sixty-three VGLUT1 contacts (or 95.4%) displayed a bassoon-IR active zone interposed between them and the dendrite (Figure 3).

2.3.4: Confocal imaging and neuron reconstruction

Every section containing either cell bodies, dendrites or axonal segments of intracellularly filled MNs was imaged first at low magnification with 10X and 20X objectives using an epifluorescence microscope (BX60 Olympus) coupled to RT-Spot camera (Diagnostic Instruments, Sterling Heights, Michigan, USA) and then at high magnification in an Olympus FV1000 confocal microscope using a 60X objective (NA, 1.35, immersion oil) with no digital zoom applied. Low mag images were superimposed in Image Pro Plus (ver. 7.0. Media Cybernetics) to render a first view of the overall organization of the dendrites and matching branches in serial sections (Figure 1, E1 and F1). High magnification was necessary to reveal the presence of synaptic contacts between VGLUT1-immunoreactive (IR) punctae and intracellularly filled dendrites. At high magnification the field of view includes only a small region of the whole dendritic arbor in the section, for that reason we imaged the whole section using overlapping image tiles, each containing a z-stack of all optical planes (z-step = 1 μ m). Up to 42 tiles were necessary in some sections to image all dendritic segments.

2.3.5: *Neuron reconstructions*

Sections were montaged in Neurolucida (ver 10.0, Microbrightfield, Williston, VT) from the z-stack image tiles and all labeled dendrites traced. Dendritic origins from the cell body were defined as the point of maximal convexity in each emerging dendrite. The numbers of points used to trace particular dendrites regions depended on the speed at which they changed in diameter, z-position or path tortuosity. We entered, on average, one tracing point per 1.4 μm of dendrite length (depending on MN size and dendrite tortuosity this represents between 50,000 to 77,000 points per neuron). The position of each synapse was labeled using a “marker” (filled circle) that was then “attached” to that dendritic position. The cell body was reconstructed through a series of contours traced in each optical plane. Sometimes cell body tracings expanded two sections. VGLUT1-IR synapses on the cell body were labeled with a different marker (filled triangles). Contacts were sometimes confirmed by rotating the images in 3D using Imaris software (ver. 7.2.2, Bitplane) (see Figure 2). The primary axon and all its collaterals were also traced (not shown). Once all labeled dendrite and axon segments were traced in single sections and their synapses marked, we reconstructed the whole neuron by manually splicing dendrite and axon pieces through serial sections.

2.3.6: *Analyses*

The traced neurons and their synaptic markers were analyzed using Neuroexplorer (ver10.0, Microbrightfield) and several custom-made MATLAB

(MathWorks) programs kindly donated by the laboratory of Dr. P. Kenneth Rose (Queen's University in Kingston, Ontario, Canada). All basic morphological features were measured. Cell body: surface, volume, aspect ratio and maximum, minimum and average diameters. Dendritic arbor: number of primary dendrites, and for each dendrite or all dendrites combined we calculated the overall surface, total length (path-lengths of all dendritic branched added), number of branches and dendrite segments, number of dendrites of different order, maximum path distance from the cell body and maximum branch order (Table 2). Dendrograms were constructed in Neuroexplorer for each dendrite. Only the most relevant measurements and analyses are reported. Two dendrograms are presented as examples (Figure 4).

The distribution of synapses was analyzed by obtaining the following measurements. 1) Overall VGLUT1 synaptic densities on dendrites and cell bodies were calculated by dividing the total number of synapses by the total dendritic or cell body surface. 2) VGLUT1 proximo-distal distributions were obtained by calculating total number of contacts, the total length and the total available membrane of all dendrite segments at defined dendrite path-distances from dendrite origins. Data were binned at 50 μm increasing distances to obtain a distribution of either linear (length) or surface density along the dendrite. 3) Sholl analysis was used to further test VGLUT1 distributions along dendrites. For this purpose, a series of concentric nested spheres were placed around the cell body to segment the dendritic arbor in 50 μm bins of incremental radial distance from the center of the cell body. The total number of synapses and the overall length

and/or surface of all dendrite segments contained in each Sholl bin were used to estimate the density of contacts according to dendritic length (linear) or surface area. 4) To analyze the clustering or spread of synapses a “nearest-neighbor” analysis was performed. Differences in next-neighbor distances provided an estimate of the spread of synapses in different regions of the dendritic arbor. 5) A *center of mass analysis* (COM) as reported by Grande et al. (2005) and Montague et al. (2012) was performed to test whether VGLUT1 synapses on control and injured MNs were randomly placed according to the distribution of available dendritic surface or if on the contrary VGLUT1 synapses displayed preferential placements on dendritic arbors.

Finally, we noted that VGLUT1-IR contacts remaining in regenerated MNs were smaller (particularly in the more proximal regions) than distally. Therefore, we divided each MN in three Sholl bins, proximal (<300 μm), mid-region (300-600 μm) and distal (>300 μm) and measured approximately 50 VGLUT1-IR contacts per dendritic compartment and per cell. We outlined each VGLUT1-IR cluster and measured their areas and ferret diameters but given the complexity of the VGLUT1-IR cluster we only analyzed their total area. It should be noted that the VGLUT1-IR cluster is a representation of the presynaptic vesicle cluster and not of the full synaptic bouton, as shown using intracellular fills of IA afferent fibers in Alvarez et al. (2011).

2.3.7: Statistics

All statistical tests were made using SigmaStat 12 (Jandel) and curve fitting was performed with Clampfit 10.2 (Axon Instruments). When possible, we used parametric comparisons based on t-tests (for pair comparisons, i.e., control vs. regenerated groups) or ANOVA (multiple comparisons, i.e., individual motoneurons, different motoneuron compartments). If normality was not fulfilled due to small sample sizes we used Mann-Whitney Wilcoxon rank-sum tests. Proportions were compared using Fisher's exact tests. Non-normally distributed samples were organized in cumulative probability functions and compared using Kolmogorov-Smirnov tests. Statistical significance was set at $p < 0.05$. Curve fitness was tested with standard regression.

2.4 Results

2.4.1: Basic physiological and morphological properties do not differ between control and regenerated motoneurons

Six adult medial gastrocnemius (MG) motoneurons (MNs) (control, *cells* #1 – 3; regenerated, *cells* #4 – 6) were identified *in vivo*, recorded intracellularly, filled with neurobiotin and successfully recovered histologically with their entire dendritic arbors fully labeled (see methods and Figure 1). Another control MN (*cell* #7) was only partially filled with neurobiotin. This cell was not fully reconstructed but used to confirm the precision of synapse identification using VGLUT1 immunoreactivity (see below). Rats in the regenerated group underwent

complete tibial nerve (TN) transection followed by immediate rejoining of the nerve to facilitate nerve regeneration and muscle reinnervation (Alvarez et al., 2011). MNs were recorded and labeled approximately one year after surgery, therefore, well after peripheral nerve regeneration and muscle reinnervation was completed. Reinnervated MG muscles recovered their original wet weight and readily contracted after electrical stimulation of the regenerated tibial nerve. No significant differences in action potential (AP) delay, resting membrane potential, AP amplitude, rheobase, input resistance, AHP amplitude, and AHP $\frac{1}{2}$ width were detected between control and regenerated MNs (Figures 1C-D; Table 1). These parameters were also similar to rat MG MNs analyzed previously and confirmed the restoration of electrical properties after MNs successfully reinnervate muscle (Haftel et al., 2005, Bichler et al., 2007, Bullinger et al., 2011).

After obtaining these electrophysiological data, the spinal cord blocks containing recorded neurons were sectioned in a parasagittal plane (Figure 1B). The sections were collected serially and immunostained for VGLUT1. Neurobiotin-labeled dendrite segments were sometimes located more than 1.5 mm apart from the cell body, therefore to image all labeled MN dendrites at a magnification high enough (60x objective) to resolve VGLUT1-IR contacts we used a motorized stage and automatic tiling of sequential confocal image stacks to fully sequentially image areas up to 2.5 mm² in single sections (up to 42 tiles of confocal image stacks). The tiled images were imported into NeuroLucida for section reconstruction and 3D tracing. All labeled dendrite segments in each

vibratome section were manually traced throughout all confocal optical planes (1 μm z-steps). The full dendritic arbor was reconstructed by stitching all traced dendrite segments through serial sections (from 13 to 20 sections per neuron) and then corrected for Z-axis shrinkage. MN cell bodies were reconstructed as a series of contours traced at all confocal optical planes. The cell bodies, with one exception, were fully contained within the thickness of single vibratome sections.

All MN cell bodies were located in spinal lumbar segments 4 and 5 (Figures 1E-F), as previously described for the rat Triceps Surae motor pool (Nicolopoulos-Stournaras and Iles, 1983, Chen and Wolpaw, 1994). Each cell body extended 6 to 11 primary dendrites with processes up to 1.77 mm from origin (i.e., *cell #4*). Dendrites were filled all the way to their terminal segments which displayed the characteristic beaded varicosities with thin intervaricose connections ($< 0.5 \mu\text{m}$ in diameter) that are typical of MN distal dendrite endings (Ulfhake and Kellerth, 1981) (Figure 2F-L). All six reconstructed MNs had dendritic branches that penetrated into the white matter, both ventrally and in a lateral orientation (Figures 4, 7 and 8). The amount of dendrite in the white matter appears dependent on the relative positions of the cell body to the white matter border. It should be noted that in our parasagittal planes of cut the ventral white matter border is accurately defined, but the exact position of the lateral border and the points of entry of laterally directed dendrites are more ambiguous. This prevented us from calculating the exact proportions of dendritic surface and length located in the white matter for each of the cells.

Overall morphological characteristics were compared between reconstructed control and regenerated MNs to determine any structural change that could influence synaptic densities or distributions (Table 2). The average mean soma diameter of regenerated MNs was slightly larger than in controls. This small difference did not reach statistical significance but was related to a more rounded cell body shape after injury (compare figures 2A and 2G). Thus, while maximum soma diameters did not significantly change, minimum soma diameters significantly increased in regenerated MNs ($p = 0.013$, t-test) and therefore aspect ratios (maximum diameter / minimum diameter) decreased significantly from 2.2 ± 0.2 in control MNs to 1.5 ± 0.1 in regenerated MNs ($p = 0.006$, t-test). This alteration could be the result of the earlier chromatolytic cell body reaction that axotomized MNs undergo to sustain metabolic demands and increase protein synthesis during regeneration (Lieberman, 1971). The change in shape, however, did not significantly (in our samples) affect the somatic surface available for synaptic contacts but did increase significantly total cell body volume ($p = 0.03$; Table 2).

There were no significant changes in overall dendritic arbor parameters, such as number of first order dendrites, dendrite segments, branch points or endings (Table 2). Our estimates of dendritic arbor total length and surface in control MG MNs are larger than previously reported by Chen and Wolpaw (1994). These differences could be due to dissimilar proportions in the type of motor units sampled. On average, F-motor units have a larger dendritic arbor than S-motor units (Cullheim et al., 1987) and the relatively brief and low

amplitude AHPs recorded in our control and experimental MNs suggest a sampling bias towards F-type motor units (Deardorff et al., 2013). Alternatively, differences in shrinkage correction, which were not reported in the previous work (Chen and Wolpaw, 1994), might have also contributed to this difference. Total dendritic length (corrected for z-axis shrinkage) decreased in regenerated MNs, on average, by 15% compared to controls (Table 2), but this trend did not reach significance in our relatively small samples ($p = 0.06$). The maximum dendrite length recorded in each cell was however unchanged and interestingly there was a 12% significant increase in surface area in regenerated MNs ($p = 0.03$). This increase in surface area is likely due to an overall increase in dendrite thickness and was correlated with a significant increase in dendrite volume. The increase in dendrite surface area was, however, too small to explain the large changes in synaptic densities described below in regenerated MNs.

2.4.2: VGLUT1-IR synapses are lost in injured and regenerated MG motoneurons

The density of VGLUT1-IR synapses decreased in lamina IX regions occupied by the cell bodies and dendrites of regenerated MNs (Figure 1G, H), suggesting a decreased overall input, as previously reported (Alvarez et al., 2011). VGLUT1-IR contacts occurred on the cell body, proximal and distal dendrites (Figures 2 and 4). VGLUT1-IR contacts were defined as punctae touching neurobiotin-filled dendrites or cell bodies. “Contacts” were confirmed, when necessary, in three-dimensional views (Figure 2) and mapped throughout

the dendritic arbor (Figure 4). To establish their synaptic nature, control *cell #7* was dually immunostained for VGLUT1 and bassoon, an active zone presynaptic protein (tom Dieck et al., 1998, Nishimune et al., 2004). Of 65 VGLUT1-IR contacts sampled on MN dendrites, 95.4% displayed a bassoon-IR active zone between dendrite and VGLUT1-IR, as revealed by fluorescence intensity profiles along lines drawn orthogonal to VGLUT1-IR contacts (Figure 3). This test population of VGLUT1-IR contacts was sampled from dendrites of different sizes and distances from the cell body. We conclude that with very few exceptions, “contacts” indeed represent synaptic sites. This particular MN was not fully reconstructed because neurobiotin labeling was incomplete.

Control MNs received an average of 911.0 ± 104.3 (\pm S.D.) VGLUT1-IR contacts over the entire dendritic arbor and an average of 25.0 ± 12.2 on the cell body. *Cells #1* and *#2* received a comparable number of VGLUT1-IR contacts (*cell #1* = 941, *cell #2* = 997) while control *cell #3* had a lower number (*cell #3* = 795). Interestingly, the cell body of *cell #3* was located more laterally than the other two; this resulted in a larger portion of the dendritic arbor in the white matter (see Figure 8D-F). Dendrites in the white matter received very few VGLUT1-IR contacts. Therefore, the dendritic surface located in the gray matter and that is available to receive VGLUT1-IR synapses was lower in *cell #3* compared to the other two control MNs. (Note that in this and other figures the border between white and grey matter is drawn at the plane of the cell body and can slightly change its exact position in other planes; thus, most VGLUT1-IR contacts close to this border in the 2D projection are in fact in the gray matter).

There were fewer VGLUT1-IR contacts on regenerated MNs (*cells #4-6*). On average they received 350.3 ± 79.5 VGLUT1-IR contacts (61.6% depletion from controls, $p=0.001$, Student's t-test). This depletion was larger than previously estimated when analyzing dendrites contained within single $50 \mu\text{m}$ thick sections oriented in the transverse plane (Alvarez et al., 2010, Alvarez et al., 2011). The most likely explanation is that the longitudinal orientation used in present analyses, coupled with obtaining full reconstructions, allowed sampling a larger proportion of dendrites contained in lamina IX, where the greatest loss of Ia afferent synapses occurs. Further support for this explanation comes from *cell #5* which extended the largest number of medially directed dendrites into LVII and retained the largest number of contacts in the regenerated group (442 compared to *cell #4*, 301 and *cell #6*, 308). The cell body of regenerated MNs also showed a large decrease in contacts with an average of 3.3 ± 2.1 VGLUT1 contacts per MN ($p = 0.03$; 86.8% fewer vs. control values). Next, we examined the distribution of synaptic losses on the dendritic arbor.

2.4.3: VGLUT1 contacts accumulate on proximal dendrites

The distribution of VGLUT1-IR synapses over the dendritic arbors of MNs has not been reported before. Contrary to previous conclusions on the distribution of Ia afferent synapses on MNs based on HRP intraxonal fills (Burke and Glenn, 1996), VGLUT1-IR contacts were found non-uniformly distributed on the dendrites of control MNs, with the highest numbers located proximal to the cell body (Figures 4A-D, 5A-B, 6A, C-D). In addition, proximal VGLUT1-IR

contacts were frequently clustered in groups, as shown more clearly in individual dendrograms (Figure 4C).

Proximal dendrites have the largest diameters and thus expose large surface areas available for synaptic inputs (i.e., “synaptic space”). Nevertheless, there were more VGLUT1-IR contacts in proximal dendritic segments than would correspond to their surface area. On average, 50% of all VGLUT1-IR contacts in control MNs were found within the proximal 300 μm of dendrite (calculated as path distance from dendrite origins on the cell body) despite this region representing only 25% of total dendritic surface (Figures 5A-D). Seventy-five percent of all VGLUT1-IR contacts were accumulated in the first 550 μm of dendrite, representing 56% of the entire dendritic surface. When the number of VGLUT1-IR contacts was divided by the available length of dendrites (linear density) or dendritic surface area (surface density) calculated densities were in both cases larger proximally than distally (Figures 5E-F). In control MNs, surface densities at 100 μm distance from dendrite origins were, on average, 11.5 ± 0.6 (\pm S.D.) VGLUT1-IR contacts per 1000 μm^2 and decreased to 4.8 ± 2.2 at a distance of 350 μm . Contact densities decreased further at more distal locations and also became more variable (at 800 μm distance from dendrite origins we calculated on average 2.1 ± 5.7 VGLUT1-IR contacts per 1000 μm^2). Even higher variability was found distal to 800 μm because differences in dendrite locations and thicknesses. While distal dendrites running medially towards lamina VII retain many VGLUT1-IR contacts, dendrites entering the white matter, either laterally or ventrally, display few or no VGLUT1-IR contacts (Figures 7 and 8). In

addition, the extreme and variable tapering of distal segments and the fact that fewer dendrite segments are sampled at the most distal regions generates large variability in calculated surface densities, even from a few VGLUT1-IR contacts (Figure 5F, distances greater than 1000 μm).

Similar conclusions were obtained using Sholl analyses in bins of 50 μm incremental distances from the cell body center (Figure 6). Close parallelism between path-distance and Sholl analyses are expected because MN dendrites fan out linearly in radial directions from the cell body center (Figure 6A, B). Thus, dendrite segments contained within a radius of 250 μm from the cell body center received, on average, 51% of all VGLUT1-IR contacts ($\pm 3\%$, S.D.) but represented only 19.7% of the total dendritic surface. Peak numbers of VGLUT1-IR contacts were found in Sholl bins at 100 to 250 μm distances in different control MNs (Figure 6C) and in all MNs VGLUT1-IR contact densities diminished from proximal to distal Sholl bins (Figure 6D). Sholl bins in the first 50 to 150 μm from the cell body averaged 11.0 ± 1.3 VGLUT1-IR contacts per 1000 μm^2 of available surface, while Sholl bins 350 to 500 μm from the cell body center displayed lower densities, on average 3.2 ± 0.2 (S.D.) contacts per 1000 μm^2 . Variability in contact numbers and calculated densities increased, as expected, in more distal Sholl bins.

2.4.4: Proximal VGLUT1 contacts are preferentially lost after nerve injury

Following peripheral nerve injury VGLUT1-IR contacts were reduced in number and reorganized along dendritic arbors. Proximal dendrites were the

most affected by synaptic losses (Figure 4C, D, G, H); approximately 77% ($\pm 7\%$, S.D.) of VGLUT1-IR contacts were lost in the first 300 μm of dendrite in regenerated MNs compared to the control average. The loss was around 50% ($\pm 17\%$, S.D.) between 300 and 1000 μm path distances and 12% ($\pm 35\%$, S.D.) in dendrite segments more distal than 1000 μm (Figure 4A). The increased variability in calculated percent losses with increased distance has several explanations. Variable synaptic losses in dendrite mid-regions are best explained by the different territories occupied by dendrites from different cells at 300 to 1000 μm distance from their origins. *Cell #5* displayed the lower loss in this region (31%) because the presence of many dendrite branches directed medio-dorsally into LVII (see Figure 7H, I). In contrast, the high variability in very distal segments is better explained by differing numbers of dendrite segments sampled distal to 1000 μm in different neurons.

The proximo-distal differences in the loss of VGLUT1-IR synapses, coupled to the similar amount of available dendrite at different distances from the cell body in control and regenerated MNs (Figures 5C, D), resulted in more uniform distributions of remaining VGLUT1-IR contacts on regenerated MNs compared to the steep proximo-distal gradients of VGLUT1-IR contact densities in control MNs. Up to 1000 μm distance from dendrite origins linear density estimates ranged from 0.2 to 3.1 VGLUT1-IR contacts per 100 μm in different proximo-distal bins of regenerated MNs (average 0.9 ± 0.5 (S.D.); Figures 5A, E). Surface densities ranged from 0.6 to 3.3 VGLUT1-IR contacts per 1000 μm^2 (average 1.4 ± 0.3 (S.D.); Figures 5F). The distribution of VGLUT1-IR contacts

changed significantly. While the cumulative probability of VGLUT1-IR contacts (up to a 1000 μm distance from the cell body) at increasing distances could be well fitted ($R^2=0.99$) by a single exponential in control MNs (i.e., increasingly lower numbers of contacts with distance), in regenerated MNs this was well fitted by a linear polynomial function ($R^2=0.97$; i.e., uniform distribution) (Figure 5B). Moreover, when the distribution of VGLUT1-IR contact densities in each cell was normalized to a uniform distribution of average density (inset in Figure 5F), the distribution in control MNs displayed densities higher than average values up to approximately 400 μm path-distance and lower than average density more distally. In contrast, the distribution of densities fluctuated around the uniform distribution throughout the dendritic arbor in regenerated MNs. In conclusion, the loss of VGLUT1-IR synapses in regenerated MNs does not result in scaled-down versions of control synaptic distributions but represents a reorganization of inputs such that the proximal bias is lost, and synapses become uniformly distributed. Similar to control MNs, VGLUT1-IR contacts in dendrite regions distal to 1000 μm were rare in regenerated MNs and calculated densities were also highly variable.

Sholl analyses lead to the same conclusion (Figure 6B). We identified three Sholl bins as roughly comparable to dendrite regions analyzed by path distance and designated them proximal ($< 300 \mu\text{m}$ Sholl bins), middle (300 - 600 μm), and distal ($> 600 \mu\text{m}$). We found an 80% depletion of VGLUT1-IR contacts within Sholl bins in the first 300 μm (Figure 6C). Sholl bins located between 300 and 600 μm showed depletions of 35.9 to 63.3%, with *cell #5* again having the lowest percent depletion. In regions greater than 600 μm , *cells #4* and *#5*

showed respectively 13.6 and 15.9% percent depletions. However, *cell #6* showed 59% fewer VGLUT1-IR contacts but this cell also displayed a shorter total dendrite length in this region. Similar to above, the changes in VGLUT1-IR contact numbers resulted in greatly diminished densities in proximal regions and in a low uniform density along Sholl distance bins (Figure 5D).

2.4.5: VGLUT1 contact groupings are dispersed after peripheral nerve injury

Dendrograms revealed a decreased incidence of clusters of VGLUT1-IR synaptic contacts in regenerated MNs (Figure 4C, G). Where clusters did occur, they contained fewer numbers of VGLUT1-IR contacts. A “near-neighbor” analysis was used to calculate the dendrite distance from each VGLUT1-IR contact to its closest neighbor and plot the frequency of contacts against their nearest neighbor distances (Figure 6E). Control MNs had the highest numbers of VGLUT1-IR contacts (36% \pm 2) with nearest neighbors at a distance of 2 to 5 μ m from their respective centers of apposition with the dendrite. Given that many VGLUT1-IR contacts are quite large (>2 μ m apposition along the dendrite), this implies that most of these terminals are tightly clustered. Most of these clusters occurred relatively proximal, while more distal VGLUT1-IR contacts were more dispersed. In contrast, only 17% \pm 3 of VGLUT1-IR synapses on regenerated MNs had a near neighbor at less than 5 μ m distance. When this did occur, it usually consisted of just two closely located synapses, whereas control MNs clusters always include more than 2 synapses. In regenerated MNs the majority of VGLUT1-IR contacts were dispersed, 50% \pm 8 had nearest neighbors at more

than 20 μm distance along the dendrites. In contrast, only $19\% \pm 3$ of VGLUT1-IR contacts in control MNs were this isolated.

We also noted that the remaining VGLUT1-IR contacts appeared smaller on regenerated MNs compared to controls and that in controls there was a proportion of very large synapses located on proximal dendrites. Therefore, we randomly measured in each cell 50 VGLUT1-IR contacts in each of the three different Sholl bins defined above (proximal, mid, distal). As shown previously (Alvarez et al., 2011), VGLUT1-immunofluorescence delimits the clusters of presynaptic vesicles and it is not identical to the full bouton size. This is because there are areas inside the boutons occupied by neurofilaments and mitochondria that are unlabeled by VGLUT1-immunofluorescence. Therefore, immunolabeled VGLUT1-IR synaptic vesicle clusters are frequently convoluted and have tortuous surfaces and for that reason are best described by their areas. Interestingly, in control MNs the distribution of areas is highly skewed because the presence of a proportion of very large VGLUT1-IR clusters concentrated in the proximal dendrites of control MNs (Fig. 6, inset). Thus, we analyzed their median areas rather than their average size. The average median area of VGLUT1-IR contacts significantly decreased in control MNs ($n=3$) from $4.7 \pm 0.1 \mu\text{m}^2$ (\pm SE) in proximal dendrites to $2.7 \pm 0.4 \mu\text{m}^2$ and $1.8 \pm 0.5 \mu\text{m}^2$ in the middle and distal regions, respectively (Fig. 6, ANOVA $p < 0.001$; Bonferroni t-tests, $p < 0.001$ between proximal and the two other compartments; $p < 0.043$ between mid and distal regions). The population of large VGLUT1-IR boutons disappeared in the proximal dendritic arbor of regenerated MNs such that their median area

was significantly reduced to less than half of controls ($2.3 \pm 0.1 \mu\text{m}^2$ average median VGLUT1-IR cluster area of regenerated MNs; $n=3$, $p<0.001$ Bonferroni corrected t-test). Interestingly, there were no significant differences ($p>0.05$) in average median area between the three proximo-distal compartments dendritic compartments in regenerated MNs or between the mid and distal compartments of regenerated MNs compared to controls.

In conclusion, after injury proximal VGLUT1-IR contacts are spread out on the dendrites and they are also reduced in size because of the disappearance of a population of large synapses. The resulting distribution of VGLUT1-IR synapses in regenerated MNs is therefore best described as small size de-clustered synapses distributed at uniform low-densities throughout the dendrites. This structural re-organization, in addition to the dramatic loss of proximal VGLUT1-IR synapses, likely significantly alters VGLUT1 input strength on regenerated MNs.

2.4.6: VGLUT1-IR contacts show a preference for dendrite territories located dorso-medially with respect to the cell body and this preferred location becomes more apparent after injury

To quantify preferences for VGLUT1-IR contact localization in different dendrite quadrants around cell bodies (i.e., dorso-medial, ventro-lateral, rostro-caudal) we used the recently described *Center of Mass* (COM) analysis (Grande et al., 2005, Montague et al., 2012). In this analysis each contact is assigned an X (rostro-caudal), Y (dorso-ventral) and Z (medio-lateral) coordinate with 0,0,0

representing the center of the cell body. Positive values indicate caudal, dorsal and medial to the cell body; negative values are rostral, ventral, and lateral to the cell body. Because synapse locations are necessarily affected by the distribution of available synaptic space on dendrites, the observed COMs are compared to synapse distributions generated randomly on the available dendritic arbors. For this purpose, we generated 1,000 random distributions of the same number of terminals counted for VGLUT1-IR contacts in each cell. The average COM of these random distributions was calculated and compared to estimate the probability that the observed VGLUT1-IR contacts were randomly distributed (Figure 7, Table 3).

Observed COMs in control and regenerated MNs suggest a VGLUT1-IR contact bias to dendrite regions located rostrally (6 of 6 cells), dorsally (5 of 6) and medially (6 of 6) to the cell body (Figures 7 and 8), but always close to the cell body (Table 3), suggesting relatively well-balanced distributions around the cell body. Differences between observed VGLUT1 and random COM coordinates in control MNs were usually small (50 μm or less) and not significant. When they did differ, the differences were not consistent among the three controls MNs (Table 3) and seem influenced by the cell body position, which in turn affected dendrite availability in different directions and proximity with the white matter. For example, the dorsal distribution of VGLUT1-IR contacts in two control MNs (*cells #1 and #3*) with relatively ventral cell bodies and extending more dendrite branches dorsally, did not differ from random distributions. In contrast, *cell #2* had a more dorsal cell body, more dendrite branches directed ventrally, and the

observed dorso-ventral COM coordinate of VGLUT1-IR contacts was significantly more dorsal than random distributions (Figure 7A-N, Table 3). This could suggest a dorsal bias that might be masked in other MNs because it coincides with more available “synaptic space” in dorsal dendrites. Analogous topographic considerations explain the medial coordinates of VGLUT1 and random COMs in control MNs. In this case proximity to the white matter exacerbates the medial bias because lateral dendrites entering the white matter lack VGLUT1-IR contacts and because the proportion of medially directed dendrites and branches increases when the cell body is located more laterally and closer to the white matter. For example, a medial preference of VGLUT1-IR contacts was particularly large in *cell #3* whose cell body was positioned close to the lateral white matter border and extended many medially oriented dendrites (Figure 8F).

In conclusion, VGLUT1-IR contacts on control MNs displayed a slight bias to dendrite territories located dorsal and medial to the cell body, but this was frequently matched by a larger amount of dendrite surface area in these regions. Whether this bias was significantly different from random synaptic distributions was dependent on the exact position of the cell body and dendrite distributions. A dorso-medial preference makes sense because incoming IA primary afferents from homonymous and close synergistic muscles course from dorso-medial to ventro-lateral territories in an approximately 45° angle (Ishizuka et al., 1979, Burke and Glenn, 1996). However, the fact that most VGLUT1-IR contacts are located on proximal dendrites likely obscures possible biases imposed by Ia afferent trajectories on more distal dendrites.

In regenerated MNs, VGLUT1 COMs were located more dorsally and medially; this was significantly different from random distributions (Figures 7 and 8, Table 3). This result suggests a relatively larger loss of VGLUT1-IR contacts in ventro-lateral dendrite territories which fits the suggested progressive retraction of Ia afferent branches (Alvarez et al., 2011). Alternatively, a possible dorso-medial bias in contact distribution in distal dendrites might be unmasked by the great loss of proximal synapses surrounding the cell body. It is likely that both effects contribute to the shift of observed COMs to dorso-medial locations after injury. Rostro-caudal distributions of VGLUT1-IR contacts did not change. In summary, this study demonstrates that injured MNs that successfully regenerate and reinnervate muscle nevertheless lose two thirds of their VGLUT1 synapses. Moreover, their distribution along MN dendrites changes such that the remaining VGLUT1 synapses are now smaller, more uniformly distributed along dendrites, de-clustered and preferentially preserved in dendrite branches located dorso-medial to the cell body. As discussed below this reorganization might weaken IA-VGLUT1 inputs on MNs.

2.5 Discussion

2.5.1: *VGLUT1 synapses concentrate in proximal dendrites*

A few studies previously analyzed the distribution of IA synapses on MN dendrites by mapping synapses between IA afferents and MN pairs, both intracellularly labeled with horseradish peroxidase (HRP) in the cat (Brown and Fyffe, 1981, Redman and Walmsley, 1983a, b, Burke and Glenn, 1996). In these analyses IA synapses were found widely distributed throughout the dendrites but with scarce somatic and juxtasomatic synapses. Detailed analyses of single IA fibers are lacking in rodents, but our study, using VGLUT1, provides the first analysis of the whole IA input on single rat MNs and by difference to previous conclusions (in cat), we found this input heavily biased towards the proximal dendritic tree. Species differences could explain these different conclusions. Alternatively, these mismatches could be due to undersampling of afferent arbors in HRP studies, as was documented by comparisons with neurobiotin-filled afferents (Koerber and Mirnics, 1995). The study of Glenn and Burke (1996) detected the larger number of synapses and reported on average 8.5 synapses from single IA afferents onto single MNs. If that was the case, the numbers of VGLUT1 synapses we report in rat MNs would predict a disparate large convergence from over 100 IA afferents. This is roughly two times the number of IA afferents estimated for triceps surae muscles in rat (Zelena, 1994). VGLUT1 also labels group IB and II synapses, but it is expected that contributions from these afferents will be minor compared to IAs (see Alvarez et al., 2011 for full justification). In cats, further support for a wide distribution of IA synapses, at low

density close to the soma also rests on decades of intracellular recordings of IA-MN EPSPs (Redman, 1979, Fleshman et al., 1988). This conclusion was based on interpretations of EPSP amplitude and rise times expected from passive spread of synaptic currents on dendrites. However, EPSPs produced by single IA afferents activated by muscle stretch in rat and cat MG MNs have similar rise times when recorded in comparable conditions in which passive membrane properties dominate (Mendell and Henneman, 1971, Watt et al., 1976, Bullinger et al., 2011). Assuming that EPSP rise times reflect synaptic location, then the distributions of IA synapses should be similar in cat and rat MNs, ruling out species differences.

Glenn and Burke also reported that several collaterals from single IA fibers contribute synapses to single MNs. Synapses originated in different collaterals were located far apart on the dendritic arbor, but synapses originated from single collaterals were closely spaced. These are likely represented in our study by clustered VGLUT1-IR synapses frequently linked by weakly immunolabeled intervaricose segments. Interestingly, VGLUT1 synaptic clusters do not exist in distal regions; therefore, a logical conclusion is that IA collaterals targeting proximal dendrites establish several closely spaced synapses, while those targeting distal branches establish single isolated synapses. The origins of this organization could be rooted in development. VGLUT1 synapses undergo intense proliferation during early postnatal maturation with differential capacity for generating additional synapses depending on their neuron targets (Siembab et al., 2010). Differential synaptic addition might also occur in different

compartments of the MN dendrite. Connections between IA afferents and MNs are initially established in embryo (Chen et al., 2003) before the postnatal maturation of the MN dendritic arbor (Kalb, 1994, Inglis et al., 1998). Proximal IA synapses are therefore formed first, expected to strongly couple with postsynaptic firing in relatively immature MNs with high input resistances and become subject to Hebbian-type strengthening, including *de novo* formation of synapses (Holtmaat and Svoboda, 2009). This might also result in larger synaptic boutons. In conclusion, the distribution of VGLUT1 synapses might be the result of developmental mechanisms that strengthen IA synapses targeting proximal dendrites and fail to strengthen distal IA synapses. Their distinct impact on MN firing could explain the malfunction of the monosynaptic reflex after nerve injury (Cope et al., 1994, Haftel et al., 2005, Bullinger et al., 2011) or spinal muscular atrophy (Mentis et al., 2011). Both are situations in which there is a large loss of proximal VGLUT1 synapses while preserving distal VGLUT1 synapses.

2.5.2: Significance of VGLUT1 synapses remaining after nerve injury

The loss of proximal VGLUT1 synapses after nerve injury results in a population of VGLUT1 synapses that are not clustered, smaller in size and are uniformly distributed at low density throughout the dendrites. It is well known that the stripping of synapses from axotomized motoneurons is more intense in proximal somatodendritic regions (Carlstedt and Cullheim, 2000, Cullheim and Thams, 2007) and maybe the distributions observed after injury result from this effect. However, we found important differences between the removal of IA

synapses and synaptic stripping (Alvarez et al., 2010, Alvarez et al., 2011). First, lost VGLUT1 synapses are not recovered after regeneration. Second, IA VGLUT1 synapse losses are a consequence of retraction of all IA fiber collaterals from LIX and therefore remaining synapses on LIX dendrites likely originate in nerves other than the injured tibialis nerve, which carries afferents from the homonymous MG and its closest synergists.

Homonymous IA connections are usually stronger than heteronymous IA inputs, and the strength of the latter varies according to the level of synergy between the IA afferent muscle of origin and the target motor pool (Eccles et al., 1957, Webb and Cope, 1992). It is therefore tempting to suggest that the proximal input with many clustered and large synapses is populated by homonymous and close synergist heteronymous connections, while distal VGLUT1 synapses (and to a certain extent isolated proximal synapses remaining after nerve injury) might originate from IA inputs less relevant for the MN and that are not involved in generating stretch reflexes from the homonymous muscle or its close synergists. Their sparse distribution probably reflects a weaker influence on MN firing. Nonetheless, some remaining VGLUT1 synapses must originate from injured axons since these are still capable of eliciting electrically-evoked EPSPs on MNs (Bullinger et al., 2011). The extensive retraction of IA afferents from LIX suggest these are preferentially located in dorso-medially directed LVII dendrites and likely responsible for biasing the distribution of VGLUT1 synapses after injury to the dorso-medial quadrant above the soma.

2.5.3: Relationship between synaptic reorganizations and IA afferent input strength

The retraction of proximal IA synapses agrees with early studies that found significantly reduced electrically-evoked homonymous IA EPSPs on MNs after nerve injury in a large number of different experimental conditions (Eccles et al., 1959, Mendell et al., 1974, Gallego et al., 1980). However, after muscle reinnervation electrically-evoked composite EPSPs recovered in amplitude and time-course (Gallego et al., 1980, Goldring et al., 1980, Foehring et al., 1986a,b). Although EPSPs produced by regenerated afferents did not fully recover their original amplitude and were smaller than in controls (Mendell et al., 1995), their significant functional recuperation was speculated to be due to synapse restoration (Mendell et al., 1988), but we confirm here that lost VGLUT1 synapses never recover, as previously suggested (Alvarez et al., 2011). This is in agreement with the permanent loss of the stretch reflex (Cope et al., 1994) and the poor recovery of stretch-evoked EPSPs in MNs (Haftel et al., 2005, Bullinger et al., 2011). One possibility is that injured IA afferents that remain connected to MNs do not re-innervate spindle receptors. Indeed, a proportion of proprioceptive axons fail to reconnect with appropriate receptors (Collins et al., 1988), but partial failure in peripheral reconnection cannot explain the large loss in synaptic transmission of stretch signals from affected muscles (Bullinger et al., 2011).

On the other hand, synaptic reorganizations after nerve injury result in a more distal and sparsely distributed synaptic input that could decrease synaptic efficacy at the cell body. Moreover, it has been shown that synaptic vesicle

cluster and bouton size correlate with variables that have significant effects on the synaptic current (Pierce and Mendell, 1993). Weaker synaptic currents and passive electrotonic attenuation should decrease IA input efficacy, but more importantly IA afferent input strength at the cell body strongly relies on amplification from dendritic active conductances known as persistent inward currents (PICs) that increase both the amplitude and time course of IA EPSPs on MNs (Schwindt and Crill, 1980, Hounsgaard et al., 1986, Hounsgaard and Kiehn, 1993, Lee and Heckman, 1998, Carlin et al., 2000, Hultborn, 2002, Heckman et al., 2008). Modeling studies demonstrated the necessity of spatial matching between synaptic inputs and PIC localization for optimal amplification (Elbasiouny et al., 2005, Bui et al., 2006, Grande et al., 2007) and depending on the study, they located PICs in mid-dendrite regions or proximally. It is thus possible that synaptic redistributions after injury might create a spatial mismatch between the localization of IA synapses and PICs. De-clustering and smaller synaptic currents might decrease further their efficacy to bring the membrane to PIC activation thresholds in situations in which the input is temporally dispersed (as occurs in response to natural stretch), but not so much after synchronous maximal activation of all remaining IA synapses after an electrical volley. Future modeling studies will be necessary to test these hypotheses.

Cell	Delay (ms)	V _m (mV)	AP Amp (mV)	Rheobase (nA)	R _{in} (MΩ)	AHP Amp (mV)	AHP ½ Width (ms)
Control Cell#1	1.7	60	79	12	2.9	1.0	13.2
Control Cell #2	1.6	X	63	4	2.6	1.9	10.5
Control Cell #3	1.5	62	78	7	2.0	0.8	8.7
Regenerated Cell #4	1.5	70	73	9	1.6	1.1	9.2
Regenerated Cell #5	1.6	68	72	10	1.4	1.4	6.6
Regenerated Cell #6	1.6	62	72	13	3.3	0.4	7.8
Control Cell #7	1.7	60	66	4	4	2.5	17
Control – Average (n=4)	1.6 ± 0.1	64.8 ± 4.6	70.9 ± 3.5	9.0 ± 3.7	2.6 ± 1.3	1.4 ± 0.9	10.2 ± 4.7
Regenerated – Average (n=3)	1.6 ± 0.1	60.8 ± 1.8	73.1 ± 9.2	7.7 ± 4.0	2.5 ± 0.8	1.2 ± 0.6	10.8 ± 2.3
P-Value*	1.000	0.329	0.662	0.670	0.941	0.851	0.836

Table 2.1: Electrical Properties of Control and Regenerated Motoneurons

* Student t-test

	Control Cell #1	Control Cell #2	Control Cell #3	Regenerated Cell #4	Regenerated Cell #5	Regenerated Cell #6	Average Control (S.D.)	Average Regen. (S.D.)	P-Value*
Soma									
Maximum Dia. (μm)	54.5	56.2	52.1	56.8	41.9	46.5	54.3 ± 2.1	48.4 ± 7.6	0.27
Minimum Dia. (μm)	27.2	23.7	23.0	34.6	30.3	32.0	24.6 ± 2.2	32.3 ± 2.2	0.01*
Mean Diameter (μm)	36.1	36.7	34.5	45.4	36.5	37.0	35.8 ± 1.1	39.6 ± 5.0	0.26
Surface Area (μm^2)	6,371.2	5,645.3	5,878.6	6,134.7	1,2981.8	7,768.45	5,965.0 ± 370.6	8,,961.6 ± 3576.1	0.22
Volume (μm^3)	34,952.8	29,838.6	26,505.1	38,212.4	40,942.0	45,814.5	30,432.2 \pm 4,255.0	41,656.3 \pm 3,851.1	0.03*
Dendrites									
Total Length (μm)	54,295	57,670	55,035	43,125	53,103	45,383	55,667 \pm 1,774	47,203 \pm 5,232	0.06
Surface Area (μm^2)	197,772	212,362	203,311	220,915	258,011	249,239	204,482 $\pm 7,365$	242,722 $\pm 19,388$	0.03*
Volume (μm^3)	80,320	94,431	74,422	127,273	134,535	143,630	83,057 $\pm 10,281$	135,146 $\pm 8,196$	0.002*
# of 1st order dendrites	7	8	6	8	10	11	7.0 ± 1.0	9.7 ± 1.5	0.06
# of Segments	226	228	250	196	299	241	234.7 ± 13.3	213.3 ± 51.6	0.74
# of branch points	125	109	121	93	141	114	118.3 ± 8.3	116.0 ± 24.1	0.88
# of Endings	135	118	128	102	157	126	127.0 ± 8.5	128.3 ± 27.6	0.96
Maximum Branch Order	11	9	10	10	10	9	10.0 ± 1.0	9.7 ± 0.6	0.65

Table 2.2: Morphological Properties of the Cell Bodies and Dendrite Arbors.

*Mann-Whitney Wilcoxon test

All values were obtained AFTER shrinkage correction

	Observed COM			Average Random COM			p-value*		
	Distance from Cell Body Center (μm)			Distance from Observed COM (μm) [#]					
	Rostro - Caudal	Dorso - Ventral	Medio - Lateral	Rostro - Caudal	Dorso - Ventral	Medio - Lateral	Rostro - Caudal	Dorso - Ventral	Medio - Lateral
Control Cell 1	-2.4	+112.8	+25.4	-52.8	+1.9	-28.3	0.0001	0.75	0.27
Control Cell 2	-42.8	-8.4	+75.6	+4.8	-48.4	+1.2	0.60	0.0001	0.77
Control Cell 3	-27.3	+27.0	+161.0	+20.6	-15.1	-19.3	0.01	0.31	0.003
Regen. Cell 4	-32.1	+68.3	+95.2	+32.8	-49.2	-44.0	0.06	0.0001	0.0001
Regen. Cell 5	-23.0	+21.3	+227.1	+1.3	-94.4	-191.9	0.67	0.0001	0.0001
Regen. Cell 6	-1.9	+56.8	+113.5	+22.6	-99.4	-58.1	0.06	0.0001	0.0001

Table 2.3: COM coordinates of VGLUT1-IR synaptic distributions and random synaptic distributions.

Bold numbers indicate those differences that were statistically different. A negative difference indicates that the COM coordinates of the observed VGLUT1-IR contact distribution were either more rostral, dorsal or medial than the average COM of random synaptic distributions.

*see Figure 7 for calculation of p-values.

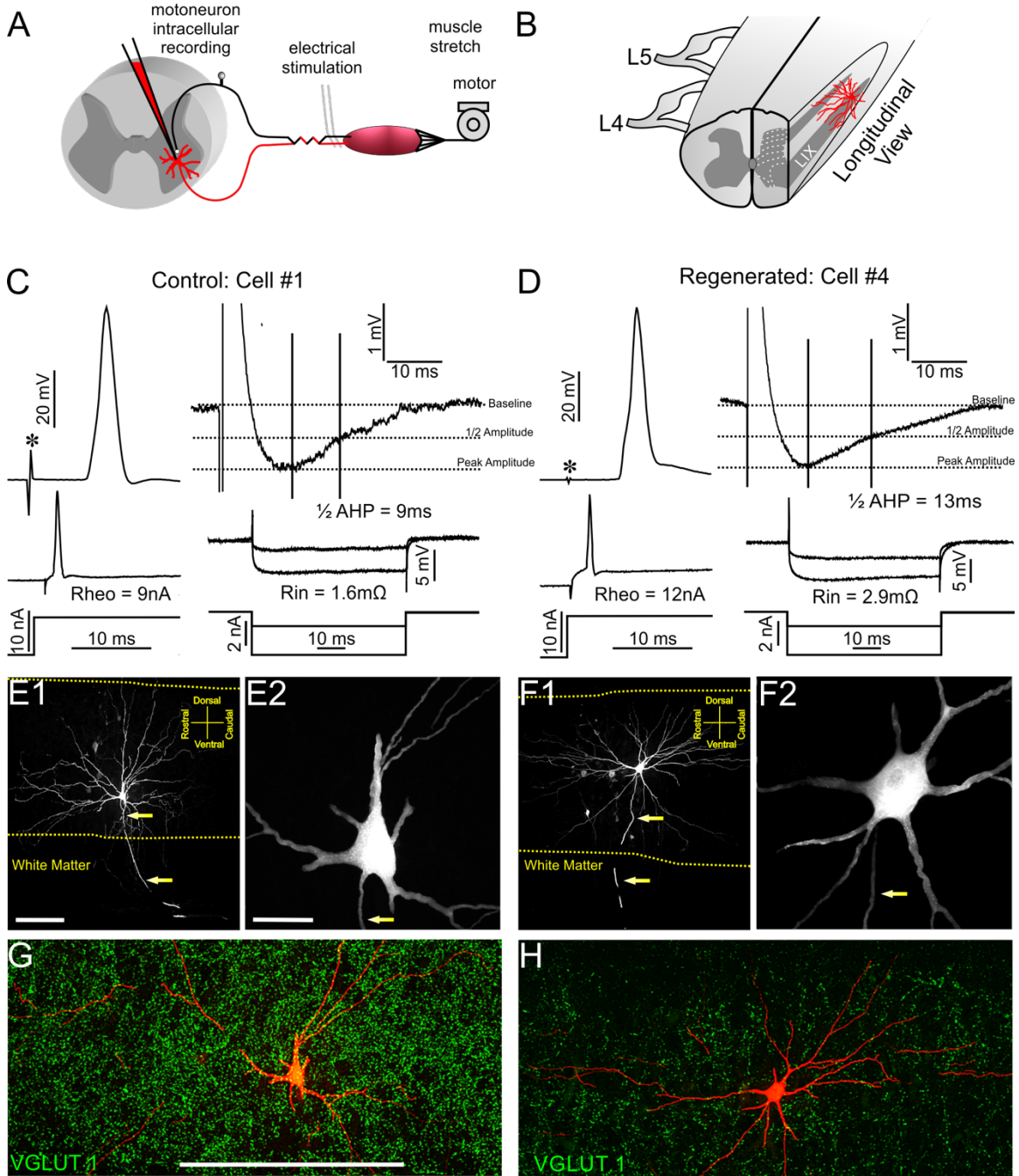


Figure 2.1: Control and regenerated medial gastrocnemius (MG) motoneurons (MNs) one year after nerve injury display similar general electrophysiological and morphological characteristics.

A) Schematic of experimental design. MNs were intracellularly recorded after identification using electrical stimulation from the MG nerve as search stimulus. The MG muscle was isolated, and its tendon attached to a motor for eliciting controlled stretches and recording muscle force. **B)** Diagram showing the location of filled MNs and section orientation. All recorded MNs were impaled between L5 and L4 segments and 75 μm -thick histological sections were obtained in the sagittal plane. The diagram shows the section profile and approximate location of MNs for orientation. **C, D)** Top left panels, antidromic action potentials (AP) elicited in a control (**C**) and a regenerated (**D**) MNs after stimulation of the MG nerve. There were no significant differences in latency onset of antidromic APs after the stimulus (asterisks) or in AP amplitude. Top right panels depict after hyperpolarizations (AHP) after eliciting single spikes through an intrasomatic current pulse. Horizontal dashed lines indicate baseline, $\frac{1}{2}$ amplitude and peak amplitude of the AHP. Vertical lines indicate time to peak and to $\frac{1}{2}$ AHP decay. Bottom panels, rheobase currents necessary to elicit firing (Rheo) and hyperpolarizing currents used to check input resistances (R_{in}) of control (**C**) and regenerated MNs (**D**). There were no differences in any of these properties between control and regenerated MNs (see Table 1). **E, F)** Low magnification partial reconstructions of a control (**E1**) and a regenerated (**F1**) MN. Images were constructed by superimposing wide-field epi-fluorescence

digital images from five consecutive 75 μm -thick serial sections. E2 and F2 are high magnification confocal images of 2D projections of all optical planes through the cell bodies of the same control (E2) and regenerated (F2) MNs. Dendritic branching, cell body size and number of primary dendrites did not significantly differ between control and regenerated MNs (see Table 2). Yellow dashed lines mark the border between white matter and gray matter. Arrows mark the trajectory of ventrally directed axons. **G, H**) 2D projections of all confocal planes through the 75 μm thick section containing the neurobiotin labeled cell bodies (red) of the same control (**G**) and regenerated (**H**) MNs. The sections were immunostained for VGLUT1 (green). After nerve injury there is dramatic reduction in VGLUT1-IR punctae in lamina IX regions containing the affected motor pools. Scale bars, E1: 300 μm (F1 is at the same magnification); E2: 50 μm (F2 is at the same magnification); G: 500 μm (H is at the same magnification).

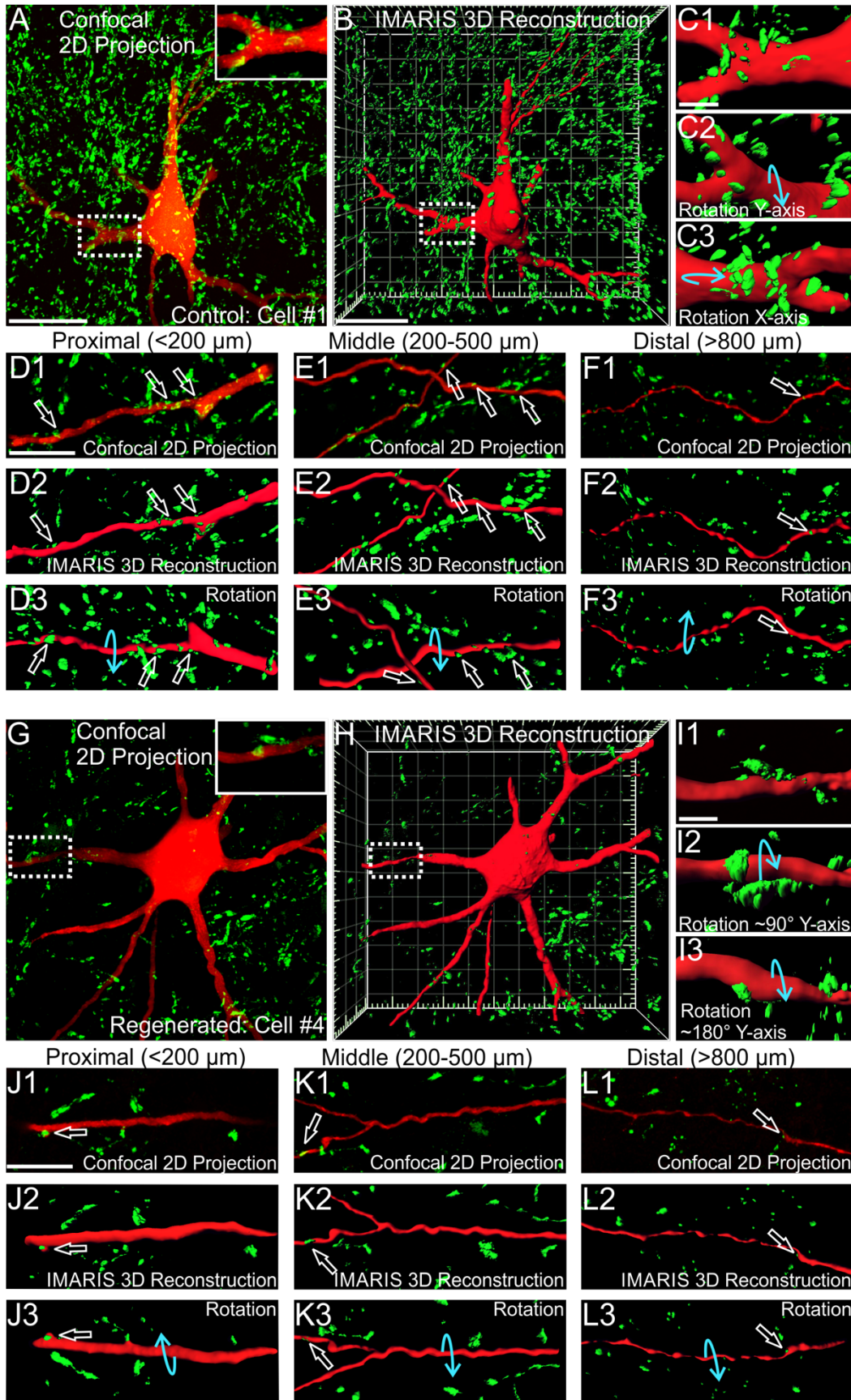


Figure 2.2: VGLUT1-IR contacts on cell bodies and different proximo-distal segments of dendrites.

A) Two-dimensional projection image of all VGLUT1-IR boutons contained in 10 confocal planes through the cell body of a control MN (obtained at 1 μm z-steps). **B)** Imaris 3D reconstruction of the full volume (75 μm thick) of the field of view shown in A. Note that in 3D projection views VGLUT1-IR contacts behind the filled cell body and dendrites are hidden. **C)** High magnification Imaris 3D rendering of the primary dendrite boxed in panels A and B. C1, C2, C3 display this dendrite segment in three rotations in the directions indicated by the blue arrows. Rotations confirm VGLUT1-IR contacts from all directions. **D)** VGLUT1-IR contacts (open white arrows) on a relatively proximal dendrite branch (less than 200 μm from the cell body) shown as 2D confocal projection (D1), IMARIS 3D rendered with no rotation (D2) and a 180° rotation in the Y-plane (D3). **E, F)** Similar image sequence but in dendrite branches located in mid-regions (200 to 500 μm from the cell body, E) or quite distally (>800 μm , F). Distal branches frequently become varicose. There is a reduction in the number of VGLUT1-IR contacts (open white arrows) from proximal to distal dendrite segments. **G-L)** Confocal 2D projection and Imaris 3D rendered images in different rotations of a regenerated MN showing VGLUT1-IR contacts (open white arrows) on the cell body and dendrite segments at different distances from the cell body. There is a large loss of synapses in regenerated MNs that is more pronounced around the cell body and proximal segments. Scale bars, A and B: 50 μm (G and H are at

the same magnification); C and I: 10 μm ; D and J: 50 μm (panels in E, F, K and L are at the same magnification).

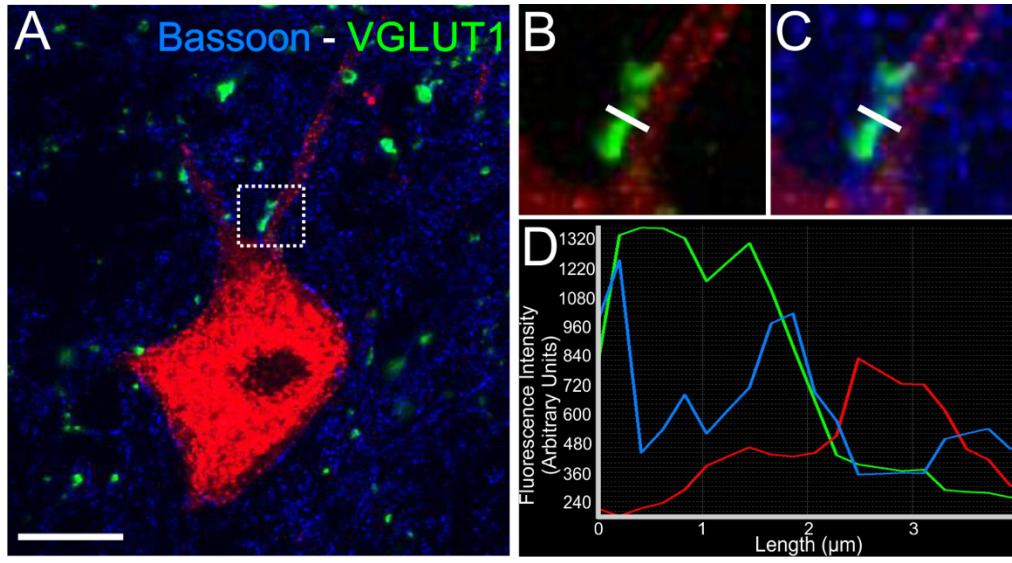


Figure 2.3: VGLUT1-IR contacts on MN dendrites display the active zone markers Bassoon.

A) Single confocal optical section through the cell body and proximal dendrite of a neurobiotin filled MN (*cell #7*). The section was counterstained for VGLUT1 (FITC, green) and bassoon (DyLight 649, blue). **B, C)** High magnification of the VGLUT1-IR contact inside the box in panel A. Bassoon immunoreactivity is detected in between the VGLUT1-IR contact and the MN dendrite. A line density profile was taken at the indicated position. **D)** Line profile density. A bassoon immunoreactivity peak (blue line) is present between the peak of VGLUT1-immunofluorescence (green line) and the neurobiotin-filled dendrite (red line). Scale bar in A is 20 μm .

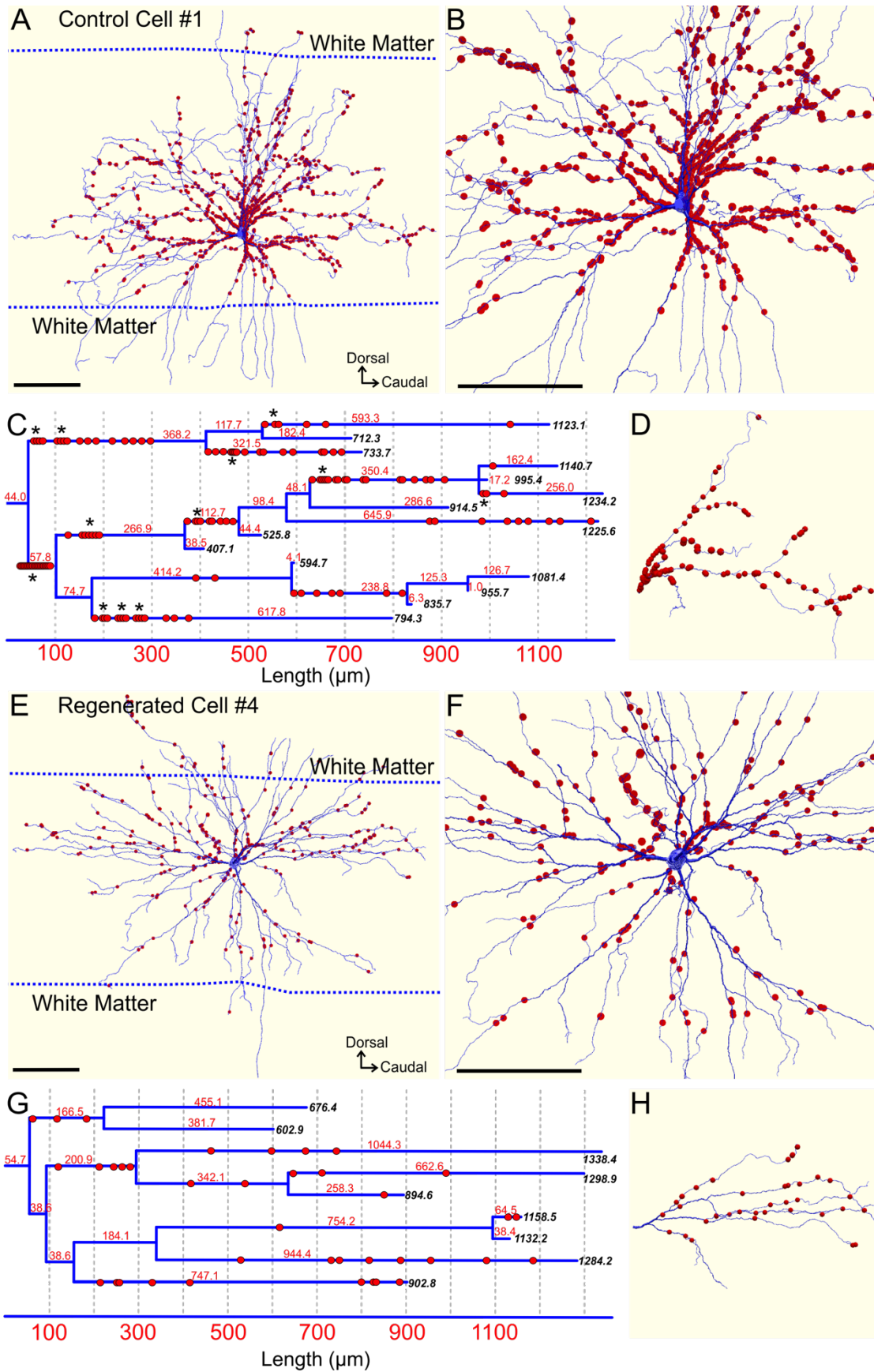


Figure 2.4: VGLUT1-IR synapses are lost along the dendrites of injured MNs; they also become de-clustered and more homogeneously distributed.

A, B) Three-dimensional reconstruction of a control MN (*cell #1*) with all VGLUT1-IR contacts marked as red dots. The white matter borders at the level of the cell body section are indicated with dashed lines. White matter dendrites receive almost no VGLUT1 synapses. Most VGLUT1-IR contacts are concentrated proximally, and panel B shows a close-up better illustrating their very high density in this region. **C, D)** Dendrogram in **C** of the dendrite shown in **D**. Numbers in black italics display the distance in microns to the dendrite ends. Numbers in red indicate the length in microns of each dendritic branch. VGLUT1-IR synapses (red dots) are distributed throughout the dendrites but with a higher concentration proximally. VGLUT1-IR synapses are highly clustered (asterisks). Clusters include a larger number of VGLUT1-IR synapses and are more frequent in the more proximal dendrites. **E, F)** Three-dimensional reconstruction of an injured MN after muscle reinnervation (*cell #4*) with its complement of VGLUT1-IR contacts (red dots). The close-up of proximal dendrites in panel E best reveals the significant loss of VGLUT1-IR synapses in this region. **G, H)** Dendrogram in **G** of dendrite shown in **H**. The dendrogram shows a loss of VGLUT1-IR contacts proximally, such that now they occur at a lower density and more uniformly along the dendrite. In addition, clusters of VGLUT1-IR contacts (i.e., >2 contacts spaced by less than 2-3 μm) are not present. Scale bars in A, B, E, F: 250 μm .

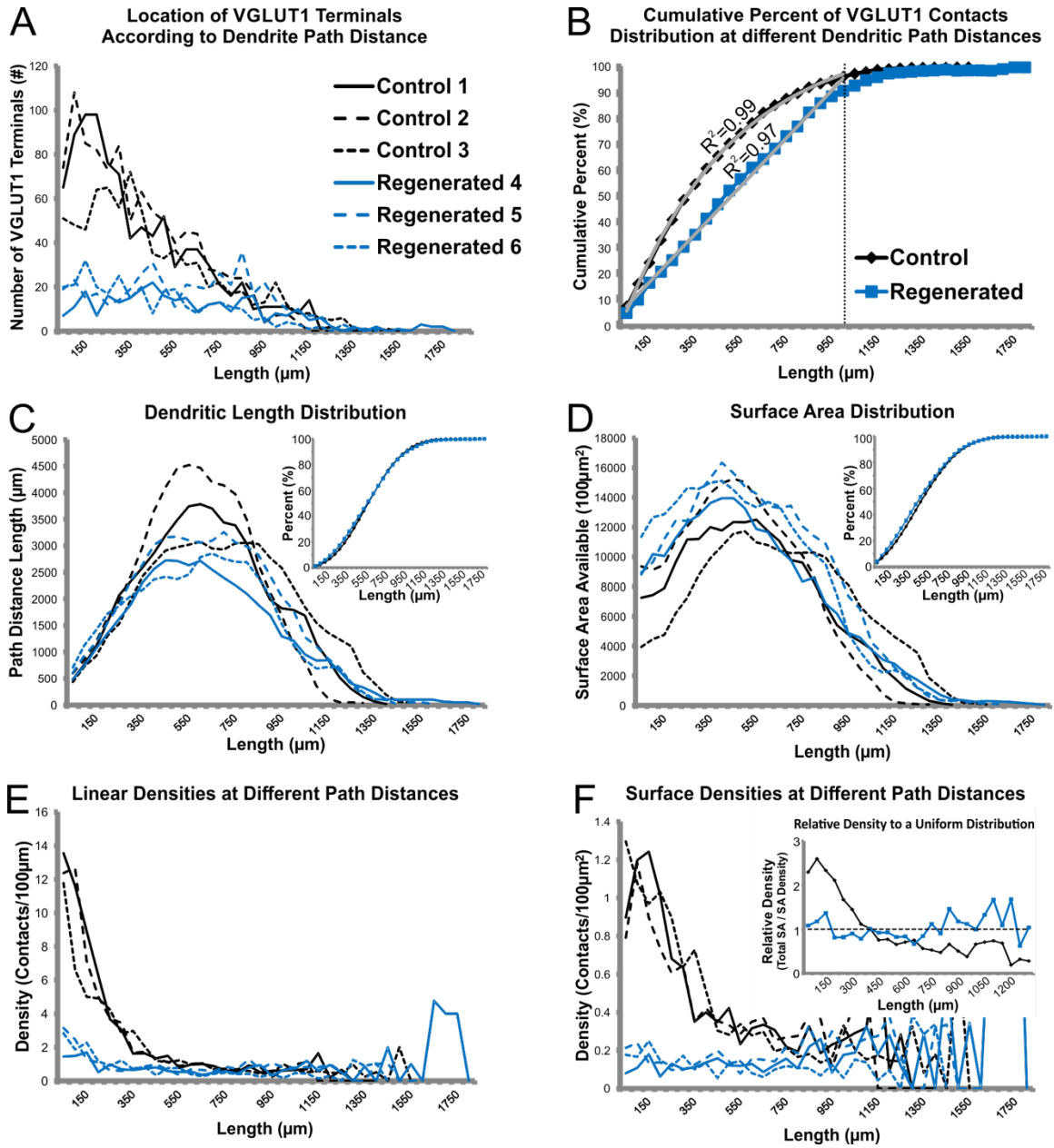


Figure 2.5: Quantification of VGLUT1-IR contact proximo-distal distribution in control and regenerated MNs.

A) Absolute number of VGLUT1-IR contacts found at different dendrite path distances from dendrite origins. Each cell is plotted separately. Most VGLUT1-IR synapses on control MNs occur adjacent to the cell body and then decrease in number with increased distance to the cell body. In contrast, similar numbers of VGLUT1-IR synapses are found at different distances on the dendrites of regenerated MNs, up to around 1000 μm distance from dendrite origins. In both control and regenerated MNs relatively few VGLUT1-IR synapses are found at distances beyond 1000 μm . **B)** Average cumulative distributions of VGLUT1-IR synapses along the dendritic arbor of control and regenerated MNs. Up to 1000 μm in the dendritic arbor (vertical line) the distribution of synapses in control MNs is best fitted by a single exponential function ($R^2=0.99$), suggesting a progressive decay in number of synapses with distance. In contrast, the distribution of synapses in regenerated MNs was well fitted by a linear polynomial function ($R^2=0.97$) with no fit improvement using exponential functions. This suggests a rather uniform distribution. **C)** Distribution of dendritic lengths at different distances from the cell body is best described by Gaussian curves with peaks between 500 and 700 μm path distance, where the maximum number of branches are concentrated. Curves describing regenerated MNs are always slightly below that of controls at all distances, but overall this decrease was not significant (see Table 2). Insets show the cumulative distribution of total dendritic length in control vs. regenerated MNs. Both distributions closely overlap

indicating that the relative proportions of dendritic segments at different distances from the cell body did not vary. **D)** Distributions of dendrite surfaces is shifted to the left compared to dendrite length because proximal dendrites are thicker and display larger surfaces. In contrast to the distribution of dendritic length, surface curves in experimental MNs were frequently above those from controls. This was due to an increase in dendrite thickness, particularly in the more proximal regions, that was reflected in very significant increases in total dendrite volume (see Table 2). However, the overall distribution of dendrite surface or their cumulative percent distribution (inset) did not reveal differences between control and injured MNs. **E)** Linear density of VGLUT1-IR contacts (i.e., number of VGLUT1-IR contacts per 100 μm of dendrite length) in the three controls and three regenerated MNs. In control MNs VGLUT1-IR contact density is very high adjacent to the cell body ($x=0$) and then declines abruptly, becoming lower and more uniform after approximately 400 μm path-distance from dendrite origins. In regenerated MNs a lower more uniform density is registered throughout the dendritic arbor. **F)** Surface densities (i.e., number of VGLUT1-IR contacts per 100 μm^2 of dendrite area) reveal a similar pattern. In this case the decrease in density with distance on control MNs is partially offset by dendritic tapering (which reduces available surface and thus partially compensate for the decrease in synapse number per unit length of dendrite). In regenerated MNs the density is low and uniform throughout the dendrite arbor. Beyond 1000 μm the estimates of VGLUT1-IR contact surface densities became highly variable because the number of dendritic segments in the gray matter is reduced and the extreme

tapering provokes large variations in calculated densities from just a few synapses. Inset, shows the average of control and experimental MN densities normalized against a uniform density calculated from the total number of synapses and dendritic lengths in each cell. While in control MNs densities greatly differ from the uniform average density (line at $y=1$), in regenerated MNs densities fluctuate around the uniform distribution throughout the total length of the dendritic arbor.

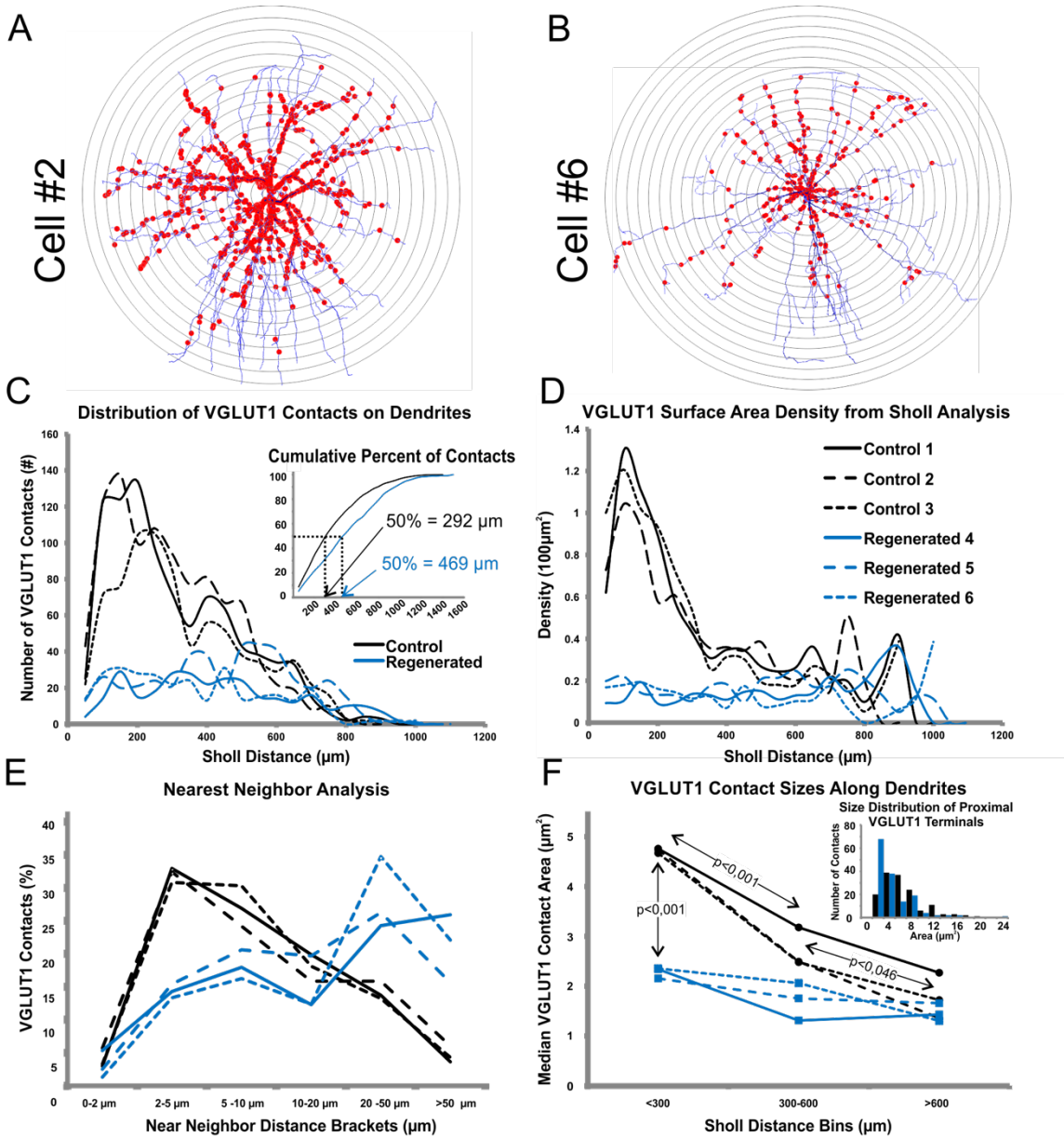


Figure 2.6: Sholl analyses also reveals a proximal bias in VGLUT1-IR contacts in control MNs and a preferential loss of proximal synapses in regenerated MNs.

A, B) Representation of Sholl bins placed on a control MN (*cell #2*, A) and an injured and regenerated MN (*cell #6*, B). The analyses were performed three-dimensionally so that each Sholl circle represents a sphere of increasing 50 μm radial distances from the center of the cell body. The dendritic length, surface and number of VGLUT1-IR contacts contained within each Sholl distance bin is then calculated. **C)** Distribution of VGLUT1-IR contacts in different Sholl bins. Most VGLUT1-IR contacts in control MNs are located close to the cell body and therefore in the first few Sholl bins, thereafter they gradually decrease in number with increasing Sholl distance. In regenerated MNs the numbers of VGLUT1-IR contacts remain relatively constant in all Sholl bins up to 800 μm radial distance from the center of the cell body. Inset shows the cumulative distributions of VGLUT1-IR contacts. The positions corresponding to 50% of terminals are indicated. **D)** Distribution of surface densities according to Sholl distances. In control MNs the surface density abruptly decreases proximo-distally while in regenerated motoneurons surface density is low and relatively constant in all Sholl bins. **E)** Near-neighbor analyses. The graph represents the percentage of VGLUT1-IR contacts with a near neighbor located within the distance brackets indicated in the x-axis. Distances are calculated as path-distance along the dendrite from the center of the apposition between VGLUT1-IR contact and dendrite for each synapse. The majority of VGLUT1-IR contacts in all three

control MNs have near neighbors located between 2 and 5 μm . Gradually longer near neighbor distances were found in progressively fewer VGLUT1-IR contacts in control MNs. In contrast, the nearest neighbors of most VGLUT1-IR contacts in regenerated MNs were located at distances of 20 μm or more along the dendrite.

F) VGLUT1-IR contacts significantly decreased in size in all three control MNs (black lines) with increasing distances to the cell body. Indicated are p-values for Bonferroni corrected t-tests comparing the average median values of VGLUT1-IR area from contacts sampled proximally ($<300 \mu\text{m}$ Sholl bin) , in mid-regions (300 to 600 μm) or distal ($>600 \mu\text{m}$) on dendrites of control MNs. In regenerated MNs (blue lines) the size of VGLUT1-IR contacts decreased and this was most dramatic in proximal regions where they become approximately half the size of controls ($p < 0,001$). This decrease in size of proximal VGLUT1-IR synapses abolished in regenerated MNs the size gradient according to VGLUT1-IR contact location. Differences in VGLUT1-IR size between control and regenerated MNs in mid and distal dendrite regions were not significant. Inset indicates the size distribution of VGLUT1-I contacts on the proximal dendrites of control (black bars) and regenerated (blue bars) MNs. In regenerated MNs there is an increase in the number of small boutons while the skewed tail of VGLUT1-IR contacts towards large sizes disappears (samples consist of 50 boutons measured in the proximal compartment in each of three regenerated and three control MNs).

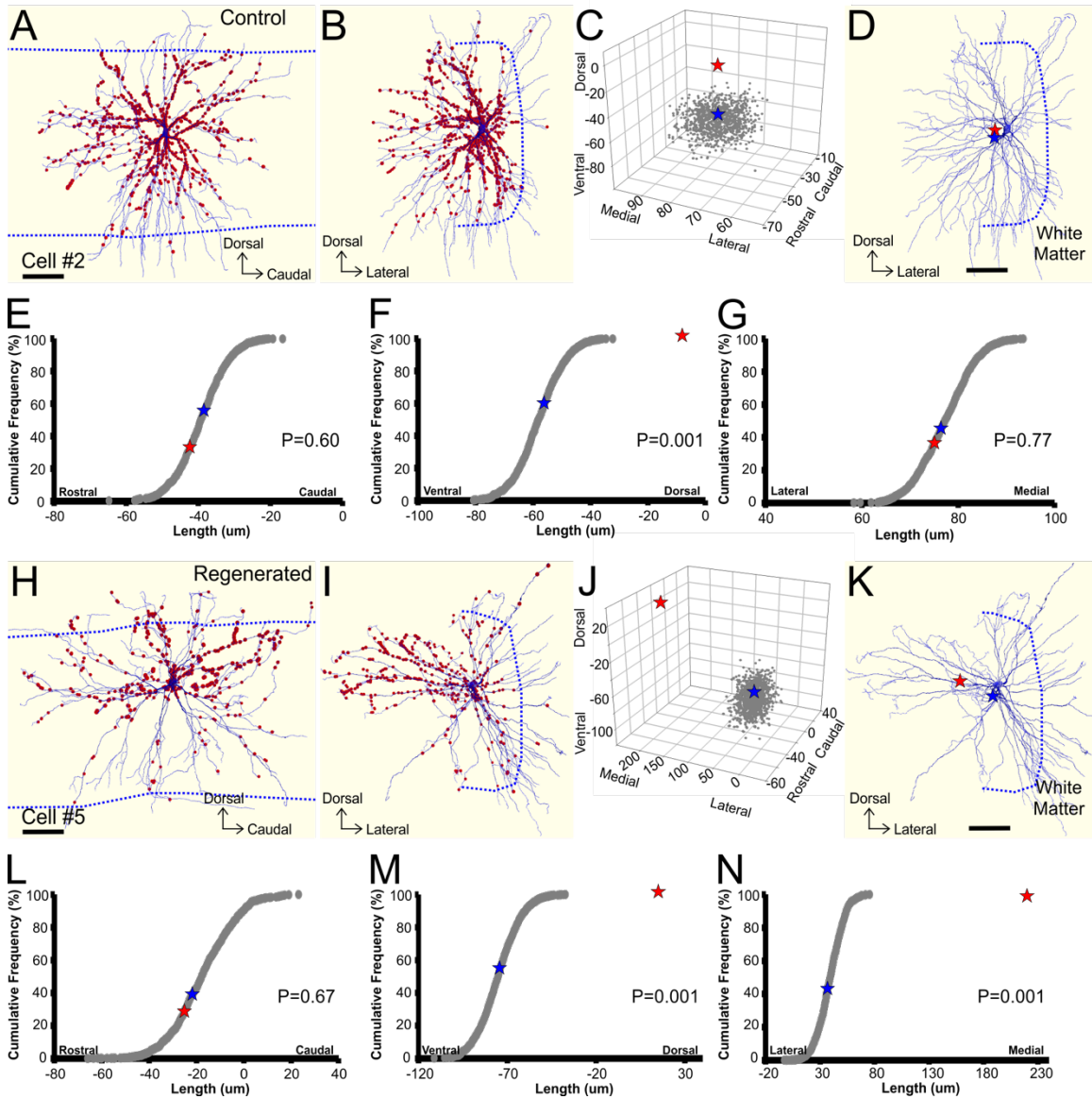


Figure 2.7: Center of Mass Analyses reveal a preferential loss of VGLUT1-IR in ventrolateral quadrants of the dendritic trees.

A-G and **H-N**) Center of Mass (COM) analyses in, respectively, a control (*cell #2*) and a regenerated MN (*cell #4*). **A, B**) NeuroLucida reconstruction of control MN *cell #2* and its VGLUT1-IR contacts in the original parasagittal plane (A) and rotated 90° degrees into a transverse plane (B). Dashed lines indicate the position of the white matter borders at the level of the section containing the cell body. **C**) Three-dimensional plots showing the position of the COM calculated from the distribution of VGLUT1-IR contacts (red star), the COMs of a thousand random synaptic distributions (gray dots) and the average of these random COMs (blue star). The cell body center has (0,0,0) coordinates and positive values indicate respectively caudal, dorsal and medial to the cell body. In this particular cell the COM calculated from the VGLUT1-IR synapse distribution is slightly more dorsal than random synapse distributions, but it is in approximately the same rostro-caudal and medio-lateral coordinates. **D**) Represents the location of the VGLUT1-IR contact COM (red star) and the average COM of the random synaptic distributions (blue star) on a transverse view of the dendritic arbor. **E-G**) Cum-sum plots of the rostro-caudal (**E**), dorso-ventral (**F**) and medio-lateral (**G**) coordinates of the thousand random synaptic distributions with the locations of the observed and average random COM coordinate (blue star). The cumulative probability of the VGLUT1-IR synapse distribution COM x, y and z coordinates is calculated by interpolation to the cum-sum curve. The probability that the observed COM is different to the computer generated random COM

coordinates is equal to 2 times (two-tail test) the y-coordinate value if this value is below 0.5 or 1 minus the y-coordinate if the COM coordinate value is above 0.5 (see Montague et al., 2013). In *cell #2* a significant difference for observed COM coordinates was only found for the dorso-ventral position, which is more positive and thus more dorsal, than expected for a random distribution of synapses. **H, I)** Parasagittal and transverse views of regenerated MN *cell #5*. Note a bundle of dorso-medially directed dendrites with more VGLUT1-IR contacts than dendrite segments travelling in other quadrants. **J)** Locations in space of random synaptic distributions COMs, their average COM and the COM calculated for the VGLUT1-IR contact distribution. In this case the observed COM is clearly more dorsal and medial than the random distributions. **K)** Locations of the VGLUT1-IR contact distribution COM (red star) and the random distributions average COM (blue star). **L-N)** Cum-sum plots used to calculate probabilities. In *cell #5* the observed distribution of VGLUT1-IR synapses is significantly more dorsal and medial than expected for random distributions.

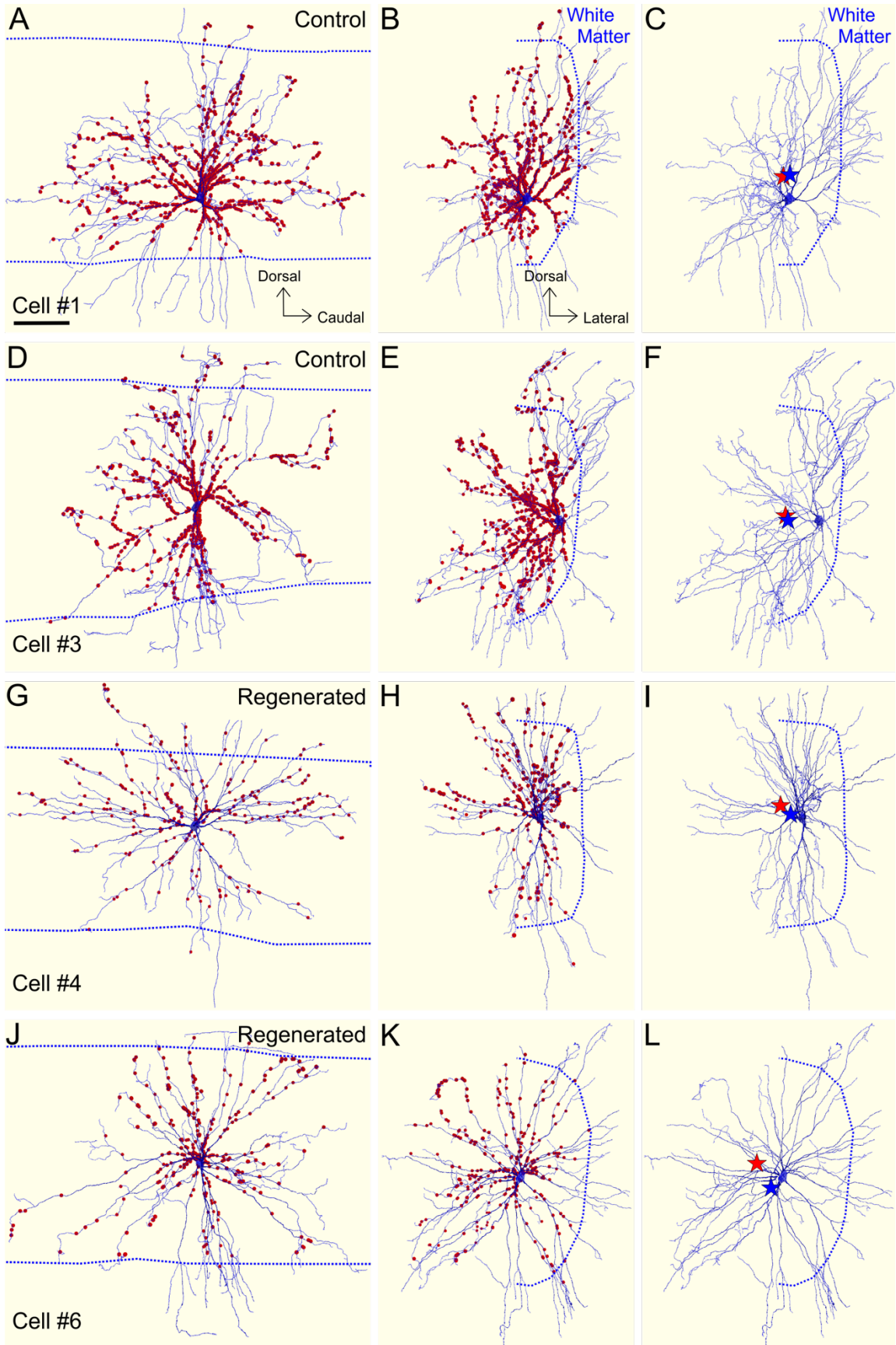


Figure 2.8: The COM of VGLUT1-IR synaptic distributions moves to dorso-medial positions in regenerated MNs.

A, D, G, J) NeuroLucida reconstructions of controls and regenerated MNs in their original longitudinal orientation and with all VGLUT1-IR contacts plotted. **B, E, H, K)** Rotation showing the same MNs and the distribution of VGLUT1-IR contacts in the transverse plane. **C, F, I, L)** Transverse view of the cells with VGLUT1-IR contact removed for better visualization of the dendritic tree. The calculated COM for the VGLUT1-IR contact distribution (red stars) and the average random synaptic COM (blue stars) are indicated. In all panels dashed lines indicate the position of the white matter. In control MNs both COMs are close together, with a slight shift of the VGLUT1-IR COM that is in part dependent on the amount of dendritic surface placed in white matter and that largely did not receive any VGLUT1-IR contacts. Because distal dendrites are usually small in relation to the total size of the neuron, they contribute little surface and therefore the shifts are small but can be statistically significant (see Table 3). In both regenerated MNs the VGLUT1-IR synaptic distribution moves dorso-medially with respect to random synaptic distributions in the available dendrite surface.

References:

- Abelew TA, Miller MD, Cope TC, Nichols TR (2000) Local loss of proprioception results in disruption of interjoint coordination during locomotion in the cat. *J Neurophysiol* 84:2709-2714.
- Alvarez FJ, Bullinger KL, Titus HE, Nardelli P, Cope TC (2010) Permanent reorganization of Ia afferent synapses on motoneurons after peripheral nerve injuries. *Ann N Y Acad Sci* 1198:231-241.
- Alvarez FJ, Titus-Mitchell HE, Bullinger KL, Kraszpulski M, Nardelli P, Cope TC (2011) Permanent central synaptic disconnection of proprioceptors after nerve injury and regeneration. I. Loss of VGLUT1/IA synapses on motoneurons. *J Neurophysiol* 106:2450-2470.
- Alvarez FJ, Villalba RM, Zerda R, Schneider SP (2004) Vesicular glutamate transporters in the spinal cord, with special reference to sensory primary afferent synapses. *J Comp Neurol* 472:257-280.
- Banks RW, Barker D (1989) Specificities of afferents reinnervating cat muscle spindles after nerve section. *J Physiol* 408:345-372.
- Bichler EK, Nakanishi ST, Wang QB, Pinter MJ, Rich MM, Cope TC (2007) Enhanced transmission at a spinal synapse triggered in vivo by an injury signal independent of altered synaptic activity. *J Neurosci* 27:12851-12859.
- Brown AG, Fyffe RE (1981) Direct observations on the contacts made between Ia afferent fibres and alpha-motoneurons in the cat's lumbosacral spinal cord. *J Physiol* 313:121-140.
- Bui TV, Ter-Mikaelian M, Bedrossian D, Rose PK (2006) Computational estimation of the distribution of L-type Ca(2+) channels in motoneurons based on variable threshold of activation of persistent inward currents. *J Neurophysiol* 95:225-241.
- Bullinger KL, Nardelli P, Pinter MJ, Alvarez FJ, Cope TC (2011) Permanent central synaptic disconnection of proprioceptors after nerve injury and regeneration. II. Loss of functional connectivity with motoneurons. *J Neurophysiol* 106:2471-2485.
- Burke RE, Glenn LL (1996) Horseradish peroxidase study of the spatial and electrotonic distribution of group Ia synapses on type-identified ankle extensor motoneurons in the cat. *J Comp Neurol* 372:465-485.
- Carlstedt T, Cullheim S (2000) Spinal cord motoneuron maintenance, injury and repair. *Prog Brain Res* 127:501-514.
- Chen HH, Hippenmeyer S, Arber S, Frank E (2003) Development of the monosynaptic stretch reflex circuit. *Curr Opin Neurobiol* 13:96-102.
- Chen XY, Wolpaw JR (1994) Triceps surae motoneuron morphology in the rat: a quantitative light microscopic study. *J Comp Neurol* 343:143-157.
- Collins WF, 3rd, Davis BM, Mendell LM (1988) Modulation of EPSP amplitude during high frequency stimulation depends on the correlation between potentiation, depression and facilitation. *Brain Res* 442:161-165.
- Collins WF, 3rd, Mendell LM, Munson JB (1986) On the specificity of sensory reinnervation of cat skeletal muscle. *J Physiol* 375:587-609.

- Cope TC, Bonasera SJ, Nichols TR (1994) Reinnervated muscles fail to produce stretch reflexes. *J Neurophysiol* 71:817-820.
- Cullheim S, Fleshman JW, Glenn LL, Burke RE (1987) Membrane area and dendritic structure in type-identified triceps surae alpha motoneurons. *J Comp Neurol* 255:68-81.
- Cullheim S, Thams S (2007) The microglial networks of the brain and their role in neuronal network plasticity after lesion. *Brain Res Rev* 55:89-96.
- Deardorff AS, Romer SH, Deng Z, Bullinger KL, Nardelli P, Cope TC, Fyffe RE (2013) Expression of postsynaptic Ca²⁺-activated K⁺ (SK) channels at C-bouton synapses in mammalian lumbar -motoneurons. *J Physiol* 591:875-897.
- Eccles JC, Eccles RM, Lundberg A (1957) The convergence of monosynaptic excitatory afferents on to many different species of alpha motoneurons. *J Physiol* 137:22-50.
- Eccles JC, Krnjevic K, Miledi R (1959) Delayed effects of peripheral severance of afferent nerve fibres on the efficacy of their central synapses. *J Physiol* 145:204-220.
- Elbasiouny SM, Bennett DJ, Mushahwar VK (2005) Simulation of dendritic CaV1.3 channels in cat lumbar motoneurons: spatial distribution. *J Neurophysiol* 94:3961-3974.
- Fleshman JW, Rudomin P, Burke RE (1988) Supraspinal control of a short-latency cutaneous pathway to hindlimb motoneurons. *Exp Brain Res* 69:449-459.
- Foehring RC, Sypert GW, Munson JB (1986a) Properties of self-reinnervated motor units of medial gastrocnemius of cat. I. Long-term reinnervation. *J Neurophysiol* 55:931-946.
- Foehring RC, Sypert GW, Munson JB (1986b) Properties of self-reinnervated motor units of medial gastrocnemius of cat. II. Axotomized motoneurons and time course of recovery. *J Neurophysiol* 55:947-965.
- Gallego R, Kuno M, Nunez R, Snider WD (1980) Enhancement of synaptic function in cat motoneurons during peripheral sensory regeneration. *J Physiol* 306:205-218.
- Goldring JM, Kuno M, Nunez R, Snider WD (1980) Reaction of synapses on motoneurons to section and restoration of peripheral sensory connexions in the cat. *J Physiol* 309:185-198.
- Grande G, Armstrong S, Neuber-Hess M, Rose PK (2005) Distribution of contacts from vestibulospinal axons on the dendrites of splenius motoneurons. *J Comp Neurol* 491:339-351.
- Grande G, Bui TV, Rose PK (2007) Effect of localized innervation of the dendritic trees of feline motoneurons on the amplification of synaptic input: a computational study. *J Physiol* 583:611-630.
- Haftel VK, Bichler EK, Wang QB, Prather JF, Pinter MJ, Cope TC (2005) Central suppression of regenerated proprioceptive afferents. *J Neurosci* 25:4733-4742.

- Hoke A, Brushart T (2010) Introduction to special issue: Challenges and opportunities for regeneration in the peripheral nervous system. *Exp Neurol* 223:1-4.
- Holtmaat A, Svoboda K (2009) Experience-dependent structural synaptic plasticity in the mammalian brain. *Nat Rev Neurosci* 10:647-658.
- Huyghues-Despointes CM, Cope TC, Nichols TR (2003) Intrinsic properties and reflex compensation in reinnervated triceps surae muscles of the cat: effect of movement history. *J Neurophysiol* 90:1547-1555.
- Inglis FM, Furia F, Zuckerman KE, Strittmatter SM, Kalb RG (1998) The role of nitric oxide and NMDA receptors in the development of motor neuron dendrites. *J Neurosci* 18:10493-10501.
- Ishizuka N, Mannen H, Hongo T, Sasaki S (1979) Trajectory of group Ia afferent fibers stained with horseradish peroxidase in the lumbosacral spinal cord of the cat: three dimensional reconstructions from serial sections. *J Comp Neurol* 186:189-211.
- Kalb RG (1994) Regulation of motor neuron dendrite growth by NMDA receptor activation. *Development* 120:3063-3071.
- Koerber HR, Mirnics K (1995) Morphology of functional long-ranging primary afferent projections in the cat spinal cord. *J Neurophysiol* 74:2336-2348.
- Lieberman AR (1971) The axon reaction: a review of the principal features of perikaryal responses to axon injury. *Int Rev Neurobiol* 14:49-124.
- Maas H, Prilutsky BI, Nichols TR, Gregor RJ (2007) The effects of self-reinnervation of cat medial and lateral gastrocnemius muscles on hindlimb kinematics in slope walking. *Exp Brain Res* 181:377-393.
- Mendell LM (1988) Physiological aspects of synaptic plasticity: the Ia/motoneuron connection as a model. *Adv Neurol* 47:337-360.
- Mendell LM, Henneman E (1971) Terminals of single Ia fibers: location, density, and distribution within a pool of 300 homonymous motoneurons. *J Neurophysiol* 34:171-187.
- Mendell LM, Munson JB, Scott JG (1974) Connectivity changes of Ia afferents on axotomized motoneurons. *Brain Res* 73:338-342.
- Mendell LM, Taylor JS, Johnson RD, Munson JB (1995) Rescue of motoneuron and muscle afferent function in cats by regeneration into skin. II. Ia-motoneuron synapse. *J Neurophysiol* 73: 662-673
- Mentis GZ, Blivis D, Liu W, Drobac E, Crowder ME, Kong L, Alvarez FJ, Sumner CJ, O'Donovan MJ (2011) Early functional impairment of sensory-motor connectivity in a mouse model of spinal muscular atrophy. *Neuron* 69:453-467.
- Mentis GZ, Siembab VC, Zerda R, O'Donovan MJ, Alvarez FJ (2006) Primary afferent synapses on developing and adult Renshaw cells. *J Neurosci* 26:13297-13310.
- Montague SJ, Fenrich KK, Mayer-Macaulay C, Maratta R, Neuber-Hess MS, Rose PK (2012) Non-uniform distribution of contacts from noradrenergic and serotonergic boutons on the dendrites of cat splenius motoneurons. *J Comp Neurol*.

- Navarro X (2009) Chapter 27: Neural plasticity after nerve injury and regeneration. *Int Rev Neurobiol* 87:483-505.
- Nicolopoulos-Stournaras S, Iles JF (1983) Motor neuron columns in the lumbar spinal cord of the rat. *J Comp Neurol* 217:75-85.
- Nishimune H, Sanes JR, Carlson SS (2004) A synaptic laminin-calcium channel interaction organizes active zones in motor nerve terminals. *Nature* 432:580-587.
- Pierce JP, Mendell LM (1993) Quantitative ultrastructure of Ia boutons in the ventral horn: scaling and positional relationships. *J Neurosci* 13: 4748-4763.
- Redman S (1979) Junctional mechanisms at group Ia synapses. *Prog Neurobiol* 12:33-83.
- Redman S, Walmsley B (1983a) Amplitude fluctuations in synaptic potentials evoked in cat spinal motoneurons at identified group Ia synapses. *J Physiol* 343:135-145.
- Redman S, Walmsley B (1983b) The time course of synaptic potentials evoked in cat spinal motoneurons at identified group Ia synapses. *J Physiol* 343:117-133.
- Sabatier MJ, To BN, Nicolini J, English AW (2011) Effect of slope and sciatic nerve injury on ankle muscle recruitment and hindlimb kinematics during walking in the rat. *J Exp Biol* 214:1007-1016.
- Siembab VC, Smith CA, Zagoraïou L, Berrocal MC, Mentis GZ, Alvarez FJ (2010) Target selection of proprioceptive and motor axon synapses on neonatal V1-derived Ia inhibitory interneurons and Renshaw cells. *J Comp Neurol* 518:4675-4701.
- tom Dieck S, Sanmarti-Vila L, Langnaese K, Richter K, Kindler S, Soyke A, Wex H, Smalla KH, Kampf U, Franzer JT, Stumm M, Garner CC, Gundelfinger ED (1998) Bassoon, a novel zinc-finger CAG/glutamine-repeat protein selectively localized at the active zone of presynaptic nerve terminals. *J Cell Biol* 142:499-509.
- Ulfhake B, Kellerth JO (1981) A quantitative light microscopic study of the dendrites of cat spinal alpha-motoneurons after intracellular staining with horseradish peroxidase. *J Comp Neurol* 202:571-583.
- Valero-Cabre A, Navarro X (2001) H reflex restitution and facilitation after different types of peripheral nerve injury and repair. *Brain Res* 919:302-312.
- Watt DG, Stauffer EK, Taylor A, Reinking RM, Stuart DG (1976) Analysis of muscle receptor connections by spike-triggered averaging. 1. Spindle primary and tendon organ afferents. *J Neurophysiol* 39:1375-1392.
- Webb CB, Cope TC (1992) Influence of synaptic identity on single-Ia-afferent connectivity and EPSP amplitude in the adult cat: homonymous versus heteronymous connections. *J Neurophysiol* 68:1046-1052.
- Zelená J. *Nerves and Mechanoreceptors: the Role of Innervation in the Development and Maintenance of Mammalian Mechanoreceptors*. Berlin: Springer, 1994.

CHAPTER 3:**Motor circuit synaptic plasticity after peripheral nerve injury depends on a central neuroinflammatory response and a CCR2 mechanism**

Currently under revisions after review at Journal of Neuroscience: Rotterman TM, MacPherson KP, Upad A, Tansey MG, Alvarez FJ (2018) Motor circuit synaptic plasticity after peripheral nerve injury depends on a central neuroinflammatory response and a CCR2 mechanism. J Neurosci: under revisions

Abstracts presented from this work:

1. Rotterman TM and Alvarez FJ. The removal of proprioceptive Ia afferents from motoneurons after injury occurs through a mechanism dependent on chemokine receptor CCR2. 2016 *Neuroscience Meeting Planner*. San Diego, CA: Society for Neuroscience, 2016, Program No. 6907 (online).
2. Rotterman TM and Alvarez FJ. Spinal cord neuroinflammatory responses are graded to the severity of peripheral nerve injuries and result in different amounts of synaptic plasticity. 2016 *Keystone Symposia: Microglia in the Brain*. Keystone, Colorado.
3. Rotterman TM and Alvarez FJ. The severity of the central neuroimmune response following peripheral nerve injury correlates with the amount of proprioceptive IA afferent loss from injured motoneurons. 2015 *Neuroscience Meeting Planner*. Chicago, Illinois: Society for Neuroscience, 2015, Program No. 2581 (online).

3.1: Abstract

Peripheral nerve injury results in persistent motor deficits regardless of successful nerve regeneration and muscle reinnervation. Lack of full functional recovery is partly explained by circuitry alterations that occur centrally triggered by the injury. One example is the permanent degradation, in the spinal cord ventral horn, of the projections of proprioceptive axons providing information about muscle length (Ia/II afferents). Consequently, Ia-mediated stretch reflexes are lost and importantly, the ventral horn is deprived of feedback information about muscles dynamics during motor actions. We hypothesized these synaptic modifications relate to the neuroinflammatory response that occurs around axotomized motoneurons. To study neuroinflammation we used mice that allow simultaneous visualization of microglia activation (CXCR1-GFP) and possible infiltration of peripheral myeloid cells (CCR2-RFP) and related them to Ia afferent synaptic losses (identified by their VGLUT1 content) on retrogradely labeled motoneurons. Microgliosis around axotomized motoneurons starts and peaks within the first week after nerve transection injuries and 2 weeks after injury this same region becomes infiltrated by various CCR2+ cells. Immunohistochemistry and flow cytometry demonstrated that these include T-cells, dendritic cells and monocytes. Only monocyte recruitment was dependent on CCR2 activation subsequent to microglia upregulation of CCL2. Axotomized motoneurons also make a minor contribution to local CCL2. Genetic elimination of CCR2 prevented CCR2+ monocyte entry and rescued VGLUT1 synapses on motoneuron dendrites. Moreover, CCR2+ cells entry was graded to the severity of the nerve

injury and correlated with the level of synaptic loss suggesting a mechanism to modulate plasticity of spinal motor circuits following nerve injuries.

3.2 Introduction

Long-term neural network plasticity occurs in undamaged brain and spinal cord regions in response to injury or dysfunction at remote interconnected locations. Similarly, neural plasticity is triggered centrally by peripheral nerve injuries (PNI) (Navarro et al., 2007; Davis et al., 2011; Mohanty et al. 2014) causing functional alterations that might contribute to life-long motor deficits in patients despite continuous improvements in nerve regeneration (Brushart, 2001; Lundborg, 2003; Mohanty et al., 2014). One example is the permanent loss of stretch reflexes (Cope et al., 1994; Haftel et al., 2005; Bullinger et al., 2011). Stretch-sensitive Ia afferents innervate muscle spindles and form the stretch reflex circuit establishing monosynaptic connections with motoneurons (MNs) (Burke et al., 1979; Brown and Fyffe, 1981). However, after nerve transection many Ia afferent axon branches and synapses are withdrawn from the ventral horn and never return, even after nerve regeneration and muscle reinnervation are completed (Alvarez et al., 2011; Rotterman et al., 2014). Consequently, the stretch reflex circuit is functionally disconnected (Bullinger et al., 2011). The absence of Ia input implies that ventral horn motor circuitries operate after nerve regeneration without feedback information about the lengths and dynamics of muscles and force signals from Ib Golgi organs become unopposed (Lyle et al., 2016). Thus, motor tasks involving high forces and/or rapid and large muscle

lengthening (steep slopes) show significant deficits (Abelew et al., 2000; Maas et al., 2007; Sabatier et al., 2011; Lyle et al., 2016). The mechanisms responsible for permanently removing Ia afferent synaptic arbors from the ventral horn after the peripheral branches of these same neurons are first injured and then regenerate, are unknown.

After PNI two temporarily coincident phenomena occur around cell bodies of axotomized MNs and sensory neurons: 1) microgliosis around MNs and immune cell recruitment around sensory neurons; 2) displacement of excitatory and inhibitory synapses from axotomized MNs (Blinzinger and Kreutzberg, 1968; Svensson et al., 1993; Aldskogius et al., 1999; Cullheim and Thams, 2007; Aldskogius, 2011; Niemi et al., 2013). Early studies showed that microglia proliferate and migrate towards MNs after PNI, and with electron microscopy they were found interposed between MN cell bodies and detaching synapses, suggesting an active role in synapse “lifting”. However, blocking microglia proliferation or activation did not prevent synaptic losses around MN cell bodies and thus, the possible role(s) of microglia in synapse plasticity after PNI remains debatable (Svensson and Aldskogius, 1993; Kalla et al., 2001; Perry and O'Connor, 2010; Berg et al., 2013). The loss of ventral horn Ia afferent synapses involves however a different process requiring active degradation of both Ia synapses and ventrally directed Ia axon collaterals (Alvarez et al., 2011). Similar degeneration of central projections has been described for other sensory afferents after PNI (Grant and Arvidsson, 1975; Aldskogius et al., 1985; Arvidsson et al., 1986), but its mechanisms and whether they involve microglia

are unknown. More recent studies showed that after certain types of nerve injuries the spinal cord is also infiltrated by peripheral myeloid cells, such as chemokine receptor 2 (CCR2) dependent monocytes/macrophages. Their significance in ventral horn function is unexplored, having been studied primarily in relation to dorsal horn pain mechanisms (Zhang et al., 2007; Echeverry et al., 2011; Echeverry et al., 2013; Gu et al., 2016). We therefore used mouse models to distinguish resident microglia (CX3CR1-GFP) from infiltrating myeloid cells (CCR2-RFP) (Mizutani et al., 2012; Parillaud et al., 2017) to analyze microglia reactivity and CCR2+ cells infiltration in relation to the loss of Ia afferent synapses, identified by Vesicular GLUtamate Transporter isoform 1 expression (VGLUT1) (Alvarez et al., 2004; 2011), during normal responses to PNI or after genetically blocking CCR2 activation. We demonstrate spinal cord infiltration after nerve transection by a heterogeneous population of CCR2+ cells, including T-cells and CCR2+ monocytes, some of which convert into microglia-like macrophages. The latter are recruited by CCL2 released primarily from activated microglia. CCR2 deletions prevented their entry and rescued ventral Ia synapses

3.3 Methods

All experiments were performed at Emory University and were approved by the Institutional Animal Care and Use Committee.

3.3.1: Transgenic models

All animal procedures were performed in adult mice (approximately 3 months of age; 20 - 25g) with comparable representation of males and females. We used several transgenic lines obtained from The Jackson Laboratory (Bar Harbor, ME) and maintained on a mixed C57Blk/6J and 6N background (Table 1). *Cx3cr1^{EGFP}* animals (RRID:IMSR_JAX:005582) carry an enhanced green fluorescent protein (EGFP) gene “knocked in” to replace the first 390 base pairs of the second exon region of the fractalkine receptor gene (Jung et al., 2000). In this model, strong EGFP is expressed in central microglia, and at various levels in subsets of peripheral myeloid cells. We also used *Ccr2^{RFP}* animals (RRID:IMSR_JAX:017586) to genetically label infiltrating peripheral myeloid cells after PNI. In these animals, red fluorescent protein (RFP) replaces the first 279 base pairs of the CCR2 open reading frame (Saederup et al., 2010). This model labels peripheral monocytes, T-cells, dendritic cells, and other small populations of myeloid-derived cells. Experimental mice were produced by crossing *Cx3cr1^{EGFP/EGFP}* with *Ccr2^{RFP/RFP}* mice to generate dual heterozygous *Cx3cr1^{EGFP/+}::Ccr2^{RFP/+}* mice. In both knock-in models the allele carrying the fluorescent protein gene is disrupted and therefore in homozygosis they are functional “KOs” for each respective receptor. Thus, in addition, we performed sciatic nerve injuries in *Ccr2^{RFP/RFP}* mice to determine if interfering with CCR2 mechanisms could prevent the loss of Ia afferent synapses on MNs. To investigate expression of the chemokine ligand 2 (CCL2, also known as MCP-1), a common CCR2 ligand, and obtain cell-specific CCL2 deletions to block or

diminish CCR2 activation specifically inside the spinal cord we used *Ccl2-RFP^{flox}* mice (RRID:IMSR_JAX: 016849). These mice contain *loxP* sites flanking exons 2 and 3 of *Ccl2* and exon 3 has been modified to incorporate an H2-2A cleavable mCherry (Shi et al., 2011). When these animals are not crossed to any Cre line they can be used to report *Ccl2* gene expression. When crossed with a cre line *Ccl2* is specifically deleted in Cre expressing cells. Lack of mCherry expression reports removal of the *Ccl2* gene. We used two cre lines to delete *Ccl2* from respectively MNs or microglia. For targeting MNs we used *Chat^{ires-cre}* mice (RRID:IMSR_JAX: 006410). In this mouse line an internal ribosome entry sequence (IRES) fused to cre recombinase sites was inserted after the ChAT stop codon (Rossie et al., 2011). When crossed to a R26-tdTomato reporter mouse (Ai9: RRID:IMSR_JAX: 007909) all spinal MNs were confirmed to express cre (not shown). For targeting microglia we used *Cx3cr1^{CreER}* mice (RRID:IMSR_JAX: 020940). In these mice, the *Cx3cr1* exon 1 was replaced by a cre recombinase and estrogen receptor ligand binding domain fusion gene (CreER) to allow for temporal control of Cre recombination in *Cx3cr1* expressing cells using tamoxifen (Yona et al., 2013). We used *Cx3cr1^{CreER}* animals to delete *Ccl2* from microglia after crossing with *Ccl2-RFP^{flox}* mice and following tamoxifen treatment. Alternatively, crossing *Cx3cr1^{CreER}* mice with the Ai9 R26-tdTomato reporter line we obtained a genetic permanent label of all resident microglia before nerve injury. This allowed us to search after injury for possible microglia derived from peripheral immune cells that will have escaped the tamoxifen-induced recombination event (see below). In uninjured mice, all Iba1+ microglia

expressed tdTomato after tamoxifen treatment suggesting 100% cre recombination efficiency.

3.3.2: Motoneuron labeling and peripheral nerve injury procedures

All animals were anesthetized with isoflurane until a surgical plane of anesthesia was achieved (induction: 4%; maintenance: 2%, both in 100% O₂) and given a subcutaneous injection of 0.05 – 0.10 mg/kg buprenorphine to reduce post-surgical pain. The left hindlimb was secured and the lateral gastrocnemius (LG) muscle exposed by making a posterior mid-line incision at the popliteal fossa level. The overlying biceps femoris was retracted to access the muscle. The muscle was then injected with 4-5 µl of 1.5% Fast Blue (Polysciences, Eppelheim, Germany) using a 10 µl Hamilton syringe. The skin was aligned and sutured back together. Animals recovered for approximately one week to allow sufficient retrograde transport of the tracer to MN cell bodies and dendrites before they underwent a second surgery in which either the tibial or the sciatic nerve was exposed, isolated and transected. A small piece of sterile silk was tied around the proximal nerve stump to prevent regeneration from occurring. In the case of tibial nerve injuries, the nerve was transected immediately after the trifurcation of the sciatic branch into the common peroneal, sural, and tibial nerves. The sciatic nerve was transected just distal to the top head of the femur. Once the appropriate nerve was transected and ligated, muscle and skin were closed using absorbable sutures.

In global and conditional knockout animals, we performed sciatic nerve cut-repair surgeries and the same procedure was done in parallel in heterozygous mice or control mice lacking cre expression for comparison. In this case, the sciatic nerve was exposed as above, and after a complete transection the proximal and distal nerve stumps were immediately aligned and joined using a fibrin glue mixture containing thrombin, fibronectin, and fibrinogen to repair the nerve and facilitate regeneration (Guest et al., 1997). This procedure results in >80% reinnervation of neuromuscular junctions by 8 weeks after injury (not shown). All animals were monitored daily for the first week after surgery; none of the animals exhibited signs of pain or distress.

In animals carrying *Cx3cr1^{CreER}* alleles and crossed to the Ai9 tdTomato or to *Ccl2-RFP^{flox}* animals, we induced recombination 5-6 weeks before nerve injuries after two intraperitoneal injections of 2 mg tamoxifen at P12 and P14. At the time of injection all CX3CR1 expressing cells (resident microglia and also some peripheral immune cells) would undergo Cre recombination. Given that microglia are long-lived with little turn over (Tay et al., 2017), and peripheral immune cells are fully replaced in a few weeks by non CX3CR1 expressing progenitors, then the only genetically cre-recombined cells remaining 5-6 weeks after tamoxifen injections correspond to resident microglia. This strategy to specifically target microglia has been fully validated in previous studies (Goldmann et al., 2013; Tay et al., 2017).

3.3.3: *Harvesting tissue for histological analysis*

Animals were allowed to survive from 3 days to 8 weeks after nerve injury, at which point they were deeply anesthetized with Euthasol (100 mg/kg) and transcardially perfused first with vascular rinse containing heparin followed by 4% paraformaldehyde in 0.1M phosphate buffer (PB, pH 7.4). The spinal cords were dissected out and post-fixed overnight in the same fixative solution at 4°C. The following day the spinal cords were rinsed with PB and cryoprotected in 30% sucrose solution at 4°C. Spinal segments L4-L5 were blocked out and 50 µm thick transverse sections cut on a freezing sliding microtome. Sections were collected and processed free floating.

3.3.4: *Histological processing and immunohistochemistry*

We performed triple immunocytochemical labeling using specific primary antibodies against GFP, RFP and VGLUT1, each raised in a different species. The sections were washed in 0.01M phosphate-buffer saline (PBS) with 0.3% Triton X-100 (PBS-Tx) and then blocked for one hour with 10% normal donkey serum (NDS) diluted in PBS-Tx. Sections were then incubated at room temperature with gentle agitation for approximately 24 hours in a primary antibody mixture containing chicken anti-GFP (1:1000, RRID#: AB_620519), rabbit anti-DsRed (1:1000, RRID#: AB_10013483) and guinea pig anti-VGLUT1 (1:1000, RRID#: AB_887878), all mixed in PBS-Tx. Immunoreactive sites were revealed with species-specific secondary antibodies raised in donkey (Jackson

ImmunoResearch Labs, West Grove, PA). Secondary antibodies (diluted 1:100 in PBS-Tx) were conjugated to either FITC (anti-chicken IgY, RRID#: AB_2340356) for EGFP amplification, Cy3 (anti-rabbit IgG, RRID#: AB_2307443) for enhancing RFP, or DyLight 647 (anti-guinea pig IgG, RRID#: AB_2340476) for immunodetection of VGLUT1. In *Ccr2* global and conditional KO mice we used rabbit anti-Iba1 (1:500, RRID#: AB_839504) revealed with donkey anti-rabbit IgG antibodies conjugated to FITC to detect microglia/macrophages in the CNS. To positively detect MNs and microglia in *Ccl2-RFP^{flox}* mice we used rabbit anti-Iba1 (see above) and goat anti-Chat (1:500, RRID#: AB_2079751), each revealed with fluorochrome-conjugated species-specific secondary antibodies, as above. These immunoreactions were used to detect CCL2-RFP expression in each of both cell types with or without cre recombination in either cell.

In some experiments infiltrating immune cells were tested for CD45 (general leukocyte marker) or CD3 ϵ immunoreactivity (T-cell marker). For CD45 immunodetection we used rabbit anti-CD45 (1:100; RRID#: AB_442810) and for T-cell immunodetection Syrian Hamster anti-CD3 ϵ antibodies (1:100, RRID#: AB_394727). In both cases we blocked sections with a mixture of 5% NDS and 5% normal goat serum (NGS). T-cell antibodies were mixed with rabbit anti-DsRed (1:1000, RRID#: AB_10013483). Immunoreactive sites were revealed with Cy3 (anti-rabbit IgG, RRID#: AB_2307443) for enhancing RFP and Alexa Fluor 647 (anti-Syrian Hamster IgG, RRID#: AB_2337482) for detection of either CD45 or CD3 ϵ immunoreactivity.

A summary of all antibodies sources and catalog numbers appears in Table 2. All immunoreacted sections were washed in PBS, mounted and coverslipped with Vectashield (Vector Labs, Burlingame, CA).

3.3.5: Densitometric analysis of VGLUT1 and GFP immunofluorescence

Six spinal cord sections per animal, all containing labeled LG MNs, were randomly selected and imaged on an Olympus FV1000 confocal microscope at low magnification (10x1, z-step: 1.5 μ m, N.A. 0.4). The sections were imaged on both sides with identical parameters. Confocal images were uploaded to ImageJ and a circular region of interest (ROI) with a diameter of 270 μ m was placed around the labeled motor pool on the injured side and a symmetrical ROI was placed on the non-injured side to measure the integrated pixel densities of VGLUT1 and GFP immunofluorescence (Fig. 2A, B; Fig. 3G, H). All measurements were done in a single optical plane per section and presented as a ratio between the two sides. Differences in fluorescence between both sides were estimated in each animal by averaging ratios obtained from six sections per animal.

3.3.6: Analysis of VGLUT1 of synaptic bouton densities on motoneurons

Retogradely labeled LG MNs were imaged at high magnification (60x1, z-step: 0.5 μ m, N.A. 1.35, oil-immersion) for VGLUT1 bouton quantification on MN surfaces. Motoneuron images were uploaded to the neural reconstruction

software Neurolucida (v.12.0, MicroBrightField, Burlington, VT). Cell bodies and proximal dendritic arbors contained within single sections were manually traced through all optical planes. VGLUT1 immunoreactive boutons in direct contact with the soma or dendrites were identified and a “marker” placed and attached to the corresponding position on the 3D tracing. The number of VGLUT1 terminals was obtained per cell body and their density calculated by dividing the number of VGLUT1 contacts by the total cell body surface ($\times 100 \mu\text{m}^2$). VGLUT1 contacts on dendrites were estimated as linear densities by dividing the number of VGLUT1 terminals by total dendritic length of the traced dendrites ($\times 100 \mu\text{m}$) (see also (Alvarez et al., 2011; Schultz et al., 2017). Sholl analysis was used to examine VGLUT1 distributions in dendrite segments at 25 μm bins of incremental radial distance from the center of the cell body. Average VGLUT1 densities in soma, dendrite or Sholl bins were obtained for each animal analyzed from 6 reconstructed MNs.

3.3.7: Quantification of microglia cells

The side of the spinal cord ipsilateral to the nerve injury was imaged with confocal microscopy at 20x magnification (z-step: 1.0 μm , N.A. 0.75) with automatic tiling. Each spinal cord hemi-section contained six stitched tiles. Stitched images were uploaded to Imaris 3D neural analysis software (Bitplane, Zurich, Switzerland) and we used the “spot function” to automatically detect and count the number of GFP+ cell bodies in 50 μm -thick spinal cord sections (Fig. 3I, J). We counted all GFP+ microglia cells in dorsal (data not shown) and ventral

horns. The ventral horn was “arbitrarily” defined as the region below a horizontal line traced from the dorsal tip of the central canal. Each animal estimate was the average of 6 hemisections.

3.3.8: Microglia morphological analysis

Twelve microglia cells (3 cells per animal, n = 4 animals per condition) were randomly sampled from confocal images containing retrogradely labeled motoneurons acquired at 60x (see above) from control animals and 14 days after tibial or sciatic nerve injury and uploaded into the Imaris program. All microglia analyzed were near and/or touching labeled MN cell bodies in lamina IX. We used the Imaris filament tracker module to reconstruct, in 3D, all the processes associated with individual cells and quantified overall filament lengths and total number of filaments per cell. We also performed a Sholl analysis for the number of filaments with each bin increasing by 10 μm from the center of the cell body. Finally, we digitally cropped all microglia processes and surface rendered the isolated cell body to calculate cell body volumes (μm^3).

3.3.9: Motoneuron cell body coverage by microglia cell processes

The total amount of MN cell body surface area covered by microglia cells in controls and 14 days after axotomy was also calculated. Only MNs with complete cell bodies were analyzed. We randomly selected 12 MNs from controls and 14 days after tibial or sciatic nerve injury. The MN soma surface

area was reconstructed using the “surface module” in the Imaris software. We then obtained surface reconstructions of all microglia cells touching the MN surface. A custom MATLAB script, provided by Bitplane, was used to compute the total surface of microglia cells (secondary surface) in direct contact with the MN cell body surface (primary surface). This allowed us to estimate the percent coverage of the MN surface covered by microglia processes.

3.3.10: RFP cell quantification

CCR2-RFP+ cells were counted manually using an Olympus epifluorescence microscope (BX52) at 20x magnification (N.A. 0.75). All 50 μm thick sections containing labeled LG MNs were included in the analysis and averaged to obtain an estimate in each animal (average of 23.2 sections per animal; $n = 4$ animals). To quantify the percent of CCR2+ cells expressing CD3 ϵ , six sections from dual heterozygous mice and CCR2 KO mice were randomly selected 21 days after sciatic nerve transection and ligation. The ventral horns were imaged with confocal microscopy at 20x magnification and images were then uploaded to Neurolucida for co-localization detection and cell counting.

3.3.11: Quantification of Iba1 cells after injury that are not derived from resident microglia

We crossed *Cx3cr1^{CreER}* homozygous mice with Ai9 R26 tdTomato reporter mice and injected the offspring with tamoxifen (2x, at postnatal day 12

and 14, 1 mg per injection dissolved in peanut oil) to induce Cre recombination allowing for expression of tdTomato. When mice were approximately 3 months of age, the LG muscle was then injected with Fast Blue as above. One week later the sciatic nerve was exposed, transected, and then ligated. Mice were allowed to survive for 21 days or 8 weeks before being perfused fixed. Control mice were injected with tamoxifen but had no surgical procedures performed on them. Spinal cords were then sectioned (50 μ m thick) and immunolabeled for Iba1 revealed with FITC-conjugated secondary antibodies (as above). All Iba1 cells derived from resident microglia are therefore expected to express tdTomato, while Iba1 cells derived from other sources should lack tdTomato. Tiled confocal microscope images of the entire ventral horn were obtained at 20X magnification (n = 4 mice, 6 sections per mouse). Image files were uploaded to NeuroLucida and all tdTomato+:Iba1+ dual expressing cells and Iba1+ only cells were manually counted within the ventral horn on both the ipsilateral and contralateral sides of the spinal cord. Since microglia numbers were quite different between sides because microgliosis in the ipsilateral side 21 days after the injury, we also obtained percentage estimates of the number of Iba1+ cells lacking tdTomato labeling.

3.3.12: Analysis of CCL2 expression inside the spinal cord after nerve injuries

We used *Ccl2-RFP^{flox}* mice in this study. These animals underwent retrograde labeling of the LG motor pool with Fast Blue (FB) and a sciatic nerve transection and ligation as explained before. Mice were perfused and the spinal

cord lumbar region collected 3 days, 7 days, 14 days, 21 days, and 8 weeks after injury. Three animals were prepared per time point. The L4-L5 region of the spinal cord was then sectioned at 50 μm on a freezing sliding microtome and sections were split equally into two vials to perform immunohistochemistry labeling for 1) DsRed (rabbit - RRID:AB_10013483) and ChAT (goat - RRID:AB_2079751) or 2) DsRed (rabbit - RRID:AB_10013483) and Iba1 (goat - RRID:AB_521594). We first quantified the number of MNs (ChAT+ cells) in the ventral horn that express CCL2. Ten randomly selected spinal cord sections from the L4-L5 region of the spinal cord were imaged at 20x (N.A = 0.75) using confocal microscopy. Images were uploaded to NeuroLucida and the total number of CCL2-RFP+:ChAT+ cells counted and averaged per section at each time point. We also obtained estimates of the percentage of FB labeled MNs expressing CCL2-RFP+. We then quantified the number of microglia (Iba1+ cells) in lamina IX containing FB labeled MNs. Six randomly selected L4-L5 ventral horns containing at least one FB+ MN were imaged at 20x using confocal microscopy. Image files were uploaded in NeuroLucida and an circular ROI (800 μm in diameter) was placed around the entire lateral motor column. All Iba1+ cells within the ROI were counted and the percent of Iba1+ cells that express CCL2 quantified and compared across all survival times.

3.3.13: Statistical analysis for histological analyses

For each injury type, genotype and time point we averaged data from 3 - 6 mice. We then used either a one or two-way ANOVA to reveal significant

differences according to injury type (sciatic, tibial or sham) and interactions with time after injury (3 days, 7 days, 14 days, 21 days, and 8 weeks). Significant differences were followed by Bonferroni post-hoc t-tests for pair-wise comparisons. In cases where normality failed, we used non-parametric Kruskal-Wallis one-way ANOVA on ranks followed by Dunn's Method post-hoc tests. In comparisons between different combination pairs of dual hets, controls and global or conditional KOs we used two-tailed t-tests. Specific tests used in each experiment are indicated in text. We pooled together data from males and females since we did not detect statistical significant differences in our measurements according to sex. All alpha values were set at 0.05. Sample sizes were set to power $1 - \beta = 0.80$ and varied according to sample variance and the size of the effect. If effect sizes were too small (less than 10% difference) we did not seek incrementing sample sizes but interpreted any change too small to be of relevance. "N" usually refers to number of animals (except when indicated) and inter-animal variability was usually kept low by performing repetitive measurements in each animal before obtaining one average per animal (for example, 6 motoneurons per animal estimating VGLUT1 densities; > 20 sections per animal for counts of CCR2 cells; 6 sections for microglia cell counts). Some genotypes occur at very low frequencies and in some cases "n" is necessarily low because it is unfeasible to obtain larger samples (situations in which we did not achieve the desired statistical power are indicated in the text).

3.3.14: *Peripheral blood mononuclear cell (PBMC) isolation and spinal cord tissue dissociation for myeloid cell analysis*

A total of 12 *Ccr2*^{RFP/+} heterozygous and 12 *Ccr2*^{RFP/RFP} KO mice were used for these experiments. All mice were subjected to a bi-lateral STL injury and were allowed to survive for 21 days. On the day of the experiment, each individual mouse was first subjected to a cheek bleed by using a blood lancet to puncture the submandibular vein. Approximately 200 μ l of blood was collected in a sterile tube and placed on ice. PBMCs were isolated by centrifuging blood samples mixed in Ficoll-Paque (GE Healthcare, Atlanta, GA). The upper plasma layer was selected and used for antigen labeling and flow cytometry analysis. Methods are as previously described in more detail (Kannarkat et al., 2015).

All mice were then anesthetized with isoflurane and decapitated to rapidly isolate the spinal cord. The entire lumbar enlargement was extracted and placed in a sterile petri dish containing 1x HBSS (Hank's Balance Salt Solution without calcium, Invitrogen, Carlsbad, CA) where it was finely minced using a scalpel. The tissue solution was transferred to an enzymatic DDP solution (DMEM/F12 media containing 1 mg/mL papain, Roche Diagnostics, Risch-Rotkreuz, Switzerland) and 220 U/mL DNase I (Invitrogen) for dissolution of tissue. The mixture was then incubated at 37°C for 20 mins before being neutralized with 10% Fetal Bovine Serum (FBS, Atlanta Biologicals, GA). The solution was centrifuged to create a tissue pellet and the supernatant was aspirated off. The pellet was homogenized in ice-cold 1xHBSS using a fine-tip glass pipette, filtered through a 70 μ m cell strainer, and then re-suspended in 37% Percoll (Percoll pH

= 8.5 – 9.5, Sigma Aldrich Co., St. Louis, MO) with a 70% Percoll layer below and a 1xHBSS layer on top. The Percoll gradient was centrifuged and the myeloid cell cloud was identified and collected between the 70% and 37% layer. Collected cells were washed 4x with 1xHBSS. Each individual blood sample was used for a single “n” in the analysis (CCR2 hets: n = 12 and CCR2 KO: n = 12). However, preliminary experiments showed a low yield of CCR2 cells in the spinal cord after injury, therefore 4 mice from each group were pooled together and analyzed as a single set (CCR2 hets: n = 3 (4 mice in each) and CCR2 KO: n = 3 (4 mice in each)).

3.3.15: *Flow cytometry*

Isolated myeloid cells from the spinal cord and PBMCs were stained with Live/Dead Fixable Aqua (1:2000, Invitrogen, L34957) and incubated with anti-mouse CD3 PE eFluor 610 (1:100, eBioscience, 61-0031), anti-mouse CD45 PerCP-CY5.5 (1:100, eBioscience, 45-0451), anti-mouse CD11b FITC (1:100, eBioscience, 11-0112), anti-mouse CD11c Alexa Fluor 700 (1:50, Biolegend, 117320), anti-mouse Ly6G PacBlue (1:100, Biolegend, 127611) and anti-mouse CD19 PE (1:100, BD Bioscience, 561736) all diluted in FACS buffer. Samples were run on an LSRII Flow Cytometer (BD Biosciences). The antibody panel was extensively validated by antibody titrations using blood and spleen (MacPherson et al., 2017). Background levels were set using antibody isotypes and FMO (fluorescence minus one) controls. Spherobeads are routinely used to set voltages and compensation settings between runs. The data was analyzed using

FlowJo software (v10.0.6, Ashland, OR). Isolated cells were gated for size (Forward Scatter Area, FSA) and granularity (Side Scatter Area, SSA) followed by Forward Scatter Height (FSH) vs FSA to select single cells. Live cells were detected with Fixable Aqua Live/Dead and gated for CD45 and CCR2-RFP and markers for B-cells (CD19), T-cells (CD3), neutrophils (CD11b^{high} Lys6G^{high}), monocytes/macrophages (CD45^{high} CD11b^{high}) and dendrite-like cells (CD11b^{high} CD11c^{high}). Microglia were identified as CD45^{low} CD11b^{high} and they were mostly CCR2(-). We obtained both raw cell counts and percentages for each cell type with respect to all CCR2 cells. Differences in cell numbers and percentages for each cell type between *Ccr2*^{RFP/+} heterozygous and 12 *Ccr2*^{RFP/+RFP} KO mice were statistically compared using t-tests independently in blood and spinal cord samples.

3.4: Results

3.4.1: Animal model and experimental design

To quantify the neuroinflammatory response inside the spinal cord after PNI we used dual heterozygous mice in which one *Cx3cr1* allele encodes for GFP (Jung et al., 2000) and one *Ccr2* allele for RFP (Saederup et al., 2010). CX3CR1 is the receptor for fractalkine and is known to be specifically expressed by microglia within the CNS (Mizutani et al., 2012) and at varying levels in peripheral immune cells such as circulating Ly6C^{negative} non-inflammatory monocytes, dendritic cells and natural killer cells (Harrison et al., 1998;

Papadopoulos et al., 1999; Huang et al., 2006). On the other hand, CCR2 is a chemokine receptor known to be expressed by T-cells and Ly6C^{positive} inflammatory monocytes and is involved in monocyte tissue trafficking in a variety of neurodegenerative diseases (Bonecchi et al., 1998; Ajami et al., 2011). It is also known to promote hyperalgesia in the spinal cord dorsal horn after PNI (Zhang et al., 2007). *Cx3cr1-GFP* and *Ccr2-RFP* alleles have their respective fluorescent protein constructs knocked into the coding regions of the target cytokine receptor gene resulting in their inactivation. In *Cx3cr1^{GFP/+}::Ccr2^{RFP/+}* dual heterozygotes one allele expresses the reporter protein while the other maintains expression of the receptors at functional levels. This animal model has been extensively used to differentiate resident microglia from blood-derived monocytes/macrophages in various neurodegenerative models (Ajami et al., 2011; Prinz et al., 2011; Shi and Pamer, 2011), after spinal cord injury (Donelley et al., 2011; Evans et al., 2014) or traumatic brain injury (Morganti et al., 2015, Katsumoto et al., 2018), and in one recent report to study dorsal horn pain mechanisms after PNI (Gu et al., 2016). This is the first study to use this dual-het dual-color model to study neuroinflammation in the ventral horn after PNI. To investigate the effect of loss of function of CCR2 on inflammation and VGLUT1 synapse plasticity after PNI we also used *Ccr2^{RFP/RFP}* homozygotes which are global CCR2 KOs. All mice were maintained on a C57Blk/6J and N mix genetic background to avoid variability in inflammatory responses and/or differences in synaptic plasticity after PNI, which are known to occur among different strains of mice (Sabha et al., 2008; Jinno and Yamada, 2011).

To focus analyses to just one motor pool, we retrogradely labeled motoneurons (MNs) projecting to the lateral gastrocnemius (LG) muscle with Fast Blue, at least one week prior to any nerve injury (Fig. 1A, B). CX3CR1-GFP microglia and CCR2+ cell infiltration were studied specifically in relation to spinal cord regions containing retrogradely labeled LG MNs (Fig. 1C, D). The same sections were also immunostained against VGLUT1 to study changes in the density of muscle spindle (Ia/II) afferent synapses (Fig. 1E). Previously, VGLUT1 synapses were analyzed after injuring the tibial nerve (TN) in Wistar rats (Alvarez et al., 2011; Rotterman et al., 2014). Our preliminary data in this mouse model (see below) indicated that VGLUT1 synapse depletions were of smaller amplitude compared to the rat after similar TN injuries. The difference might relate to species differences in neuroimmune responses since upregulation of pro-inflammatory mediators are known to be larger in Wistar rats compared to C57Blk/6 mice after brain injury (Schroeter et al., 2003). VGLUT1 synapse losses increased after transecting the sciatic nerve (SN), a more proximal nerve injury affecting a larger number of motor and sensory axons. Ia/II afferent axons that target LG MNs originate in the LG muscle and close synergists and travel through both the SN and TN. Thus, Ia/II afferents responsible for the VGLUT1 input onto LG MNs should be similarly axotomized after injuring either nerve. This suggest that the larger synaptic loss detected after SN injury is independent of the number of Ia/II axons giving input to LG MNs affected by the nerve injuries. One possibility is that the larger synaptic alterations after SN compared to TN injuries are caused by a greater local neuroinflammatory response resulting from

the larger overall number of injured MNs and sensory afferents (independent of their synaptic relations to LG MNs).

Finally, it is known that peripheral regeneration is increasingly impaired the more proximal and larger the injured nerve is because LG MNs and afferents might be misguided to a larger number of possible incorrect targets (Sunderland, 1968). Therefore, to avoid confounding factors related to differences in the efficiency and specificity of regeneration in the periphery after SN or TN injuries, we initially prevented regeneration in both nerves by placing a small ligature in the proximal end of the cut nerve. These two injury models are thus referred to as tibial or sciatic transection and ligation (TTL and STL). In these models we noted some cellular shrinkage of LG MNs after long-term survival (see below). To analyze resulting VGLUT1 synapse organization after regeneration (8 weeks survival) in KO models and avoid the confounding influence of cellular shrinkage we used in CCR2 KO animals a sciatic nerve cut and repair model (SNR, see methods) that allows motor axon regeneration, muscle reinnervation and prevents cellular shrinkage.

3.4.2: VGLUT1 synapse depletions on motoneurons following tibial or sciatic nerve injury in mice

To estimate VGLUT1 synaptic bouton depletions around injured motor pools we first compared changes in VGLUT1 immunofluorescence densities in the spinal cord ipsilateral and contralateral to the nerve injury. To obtain these

measurements we placed a region of interest (ROI) around the labeled LG MN pool on the side ipsilateral to the injury and a corresponding ROI on the contralateral side (Fig. 2A). ROI placement and measurements were performed in single optical planes of low magnification confocal images obtained with a 10X objective (N.A. = 0.4) and with an estimated optical thickness of $4.2 \mu\text{m}^1$. We calculated the integrated pixel density ratio for each pair of images. In sham control mice, the VGLUT1-immunofluorescence average ratio between the two sides was 1.05 ± 0.02 (\pm SE, $n = 4$ animals), indicating no differences between either side (Fig. 2B). After TTL or STL there was a decrease in VGLUT1 fluorescence in the ipsilateral side by 7 days post-injury that continued to decline up to 21 days and remained depleted 8 weeks after injury (two-way ANOVA, time: $F(5, 45) = 35.663$, $p < 0.001$) (Fig. 2B). The decrease in VGLUT1 immunofluorescence was significantly larger after STL compared to TTL (two-way ANOVA, type of injury: $F(1, 45) = 6.143$, $p = 0.018$; STL vs TTL at 8 weeks pot-hoc Bonferroni STL vs TTL comparison, t-test, $t = 2.479$, $p = 0.018$).

Changes in VGLUT1 immunofluorescence integrated pixel density can occur because synapses are lost, become smaller, or VGLUT1 content decreases (Hughes et al., 2004; Alvarez et al., 2011). To specifically analyze synaptic loss, we compared densities of VGLUT1 synaptic contacts on the surface of reconstructed LG MNs. We selected Fast Blue retrogradely labeled MNs with long and well stained dendrites for high magnification confocal imaging

¹ *equation to calculate optical thickness, $(dz = \frac{0.64 \times \lambda_{exc.}}{n - \sqrt{n^2 - NA^2}})$

(60x, N.A. = 1.35) and analysis (Fig. 2C). Cell bodies and proximal dendrites were reconstructed in Neurolucida to obtain surface estimates of cell bodies and dendritic lengths (Fig. 2D) (Table 2). VGLUT1 boutons in contact with the MN surface were identified and plotted along the soma and dendritic arbor (Fig. 2C, D). If necessary, bouton contacts on MN surfaces were confirmed with 3D visualization using Imaris (Fig. 2E). Motoneurons in sham control mice had, on average, a somatic density of 0.75 ± 0.03 (\pm SE) VGLUT1 contacts per $100 \mu\text{m}^2$ and overall dendritic linear density of 17.17 ± 0.72 VGLUT1 contacts per $100 \mu\text{m}$ of dendrite length ($n = 4$ animals; each estimate from 6 MNs per animal) (Fig. 2F, G). Eight weeks post injury, there was a significant depletion of VGLUT1 contacts on the soma of LG MNs following both TTL and STL (one-way ANOVA $F(2, 13) = 62.696$, $p < 0.001$; post-hoc Bonferroni t-tests vs control, TTL: $t = 7.504$, $p < 0.001$, STL: $t = 10.619$, $p < 0.001$). VGLUT1 somatic density depletions were significantly greater after STL compared to TTL (post-hoc Bonferroni TTL vs STL t-test, $t = 2.844$, $p = 0.048$). We also noticed that the cell bodies of LG MNs prevented from reinnervating muscle for 8 weeks tended to be smaller and had less surface area available for synaptic connections. Differences did not reach statistical significance compared to sham controls because increases in somatic size variability after injury (Table 2, one-way ANOVA $F(2, 13) = 3.563$, $p = 0.064$). Possible changes in surface area might underestimate synapse losses estimated as densities per unit surface. For this reason we also compared the absolute number of VGLUT1 contacts per cell body and found a significant 46% reduction with respect to control after TTL and 70% loss after STL (one-way

ANOVA $F(2, 13) = 55.619$, $p < 0.001$; post-hoc Bonferroni t-tests, TTL: $t = 6.654$, $p < 0.001$; STL: $t = 10.161$, $p < 0.001$). In conclusion, VGLUT1 bouton contacts are lost over MN cell bodies in both types of injuries and this is partially offset by variable cell body shrinkage 8 weeks after nerve injury when regeneration is prevented.

The majority of VGLUT1 synapses innervate the proximal dendritic arbor (Rotterman et al., 2014) and therefore this region best represents changes in total input. Overall dendritic VGLUT1 densities were significantly different when comparing sham controls, TTL and STL animals (one-way ANOVA $F(2, 13) = 5.410$, $p=0.026$), but while VGLUT1 dendrite densities after STL were significantly depleted (post-hoc Bonferroni t-test STL vs control, $t = 3.259$, $p = 0.023$), VGLUT1 densities after TTL were intermediate between STL and controls and did not reach statistical significance against either (post-hoc Bonferroni t-test, TTL vs control, $t = 1.713$, $p = 0.344$; TTL vs STL, $t = 1.411$, $p = 0.557$). To overcome interpretation problems due to differences in the lengths of the dendrites analyzed in different samples (Table 2) and to test whether VGLUT1 bouton contacts were preferentially lost along particular regions of the dendrite, we performed Sholl analysis with bin sizes increasing by 25 μm distance from the cell body center (Table 3, Fig. 2H). In the first 25 μm of dendrite there was a significant depletion in VGLUT1 linear density for both TTL and STL compared to sham controls (one-way ANOVA $F(2, 13) = 23.829$, $p < 0.001$; post-hoc Bonferroni t-tests vs control, TTL: $t = 2.332$, $p = 0.004$; STL: $t = 6.659$, $p < 0.001$). In the 25-50 and 50-75 μm bins there were significant depletions, compared to

sham control, following STL but not after TTL (one-way ANOVA 25-50 μm bin: $F(2, 13) = 7.996$, $p = 0.007$, post-hoc Bonferroni t-test vs control, TTL: $t = 2.493$, $p = 0.090$; STL: $t = 3.863$, $p = 0.008$; 50-75 μm bin: $F(2, 13) = 9.581$, $p = 0.004$; post-hoc Bonferroni t-test vs control, TTL: $t = 0.783$, $p = 1.000$; STL: $t = 4.260$, $p = 0.004$) (Fig. 2H). In conclusion, VGLUT1 densities in different dendritic regions after TTL were always intermediate between controls and STL with no significant differences detected between TTL and STL or TTL and controls at distances further than 25 μm from the cell body center.

The pattern of VGLUT1 synapse loss agrees with densitometry estimates highlighting a greater reduction in overall VGLUT1 immunofluorescence in STL compared to TTL (Fig. 2B), however, another variable that could impact these results is a change in the size of VGLUT1 puncta. To compare VGLUT1 sizes in different animals we used Imaris to surface-render VGLUT1 puncta contacting FB-labeled MNs 8 weeks after injury. Average surface areas were similarly reduced by 52-55% after TTL and STL injuries from a value of $12.89 \mu\text{m}^2 \pm 1.33$ (\pm SE) estimated in sham controls. This change was highly significant (one-way ANOVA $F(2, 11) = 16.876$, $p < 0.001$; post-hoc Bonferroni t-test vs control, TTL: $t = 5.347$, $p = 0.001$, STL: $t = 4.640$, $p = 0.004$). There was no difference between TTL or STL in VGLUT1 puncta size 8 weeks after injury (post-hoc Bonferroni t-test TTL vs STL, $t = 0.707$, $p = 1.000$) (Fig. 2I). In conclusion, the data suggest that VGLUT1 loss on LG MNs soma and proximal dendrites is greater after sciatic nerve injury compared to tibial nerve injury and both injuries resulted in similar reductions in VGLUT1 immunoreactive puncta size. The later might be the

result of ligation likely inducing long-term inactivity in these synapses in both injury models.

3.4.3: *Microglia responses differ between tibial and sciatic nerve injuries*

Both TTL and STL trigger a microglia response around injured motor pools (and in the dorsal horn) starting 3 days post injury (Fig. 3A-F). To quantitatively compare the microglia reaction, we first performed densitometry analyses comparing microglia GFP fluorescence (CX3CR1-GFP) ipsilateral and contralateral to the injury after either TTL or STL (Fig. 3G). Sections containing FB-labeled MNs were selected for analysis (n = 3-4 mice, 6 sections per animal) and ROIs were placed around the labeled motor pool ipsilateral to the injury and in a mirror-image area on the contralateral side to obtain ratios between both sides. The integrated pixel density ratio between both sides in sham control mice was 0.98 ± 0.01 suggesting no difference in microglia fluorescence between sides. After injury we detected an increase in microglia fluorescence ipsilateral to the injury that became significant 7 days after either injury (Fig. 3H) and returned to control levels by 8 weeks post-injury in both models (Kruskal-Wallis one-way ANOVA on Ranks; TTL: $H(5) = 19.312$, $p = 0.002$, post-hoc Dunn's Method, $Q = 3.041$, $p < 0.05$; STL: $H(5) = 20.170$, $p = 0.001$, post-hoc Dunn's Method, $Q = 3.500$, $p < 0.05$). Pairwise multiple comparisons (Bonferroni-corrected t-tests) between TTL and STL revealed significantly greater integrated pixel density ratios after STL at 7 days ($t = 4.435$, $p < 0.001$), 14 days ($t = 3.508$, $p = 0.001$) and 21 days ($t = 4.546$, $p < 0.001$) after injury.

The detected increases in GFP fluorescence could be due to higher numbers of microglia cells, an augmentation of CX3CR1 expression, or morphological changes that increased the area covered by CX3CR1-GFP expressing microglia. We therefore used the “spot function” algorithm in Imaris to automatically detect and quantify the number of GFP+ microglia present within the ventral horn (Fig. 3I) (n = 3-4 animals per condition, each animal estimated from 6 ventral horns). Sham control mice had an average of 200.8 ± 16.9 GFP+ microglia per single ventral horn in 50 μm thick sections (Fig. 3J). In both tibial and sciatic models there was a significant increase in the number of microglia cells with time after injury, but there were no significant differences between both injury types (two-way ANOVA, time: $F(5, 44) = 25.250$, $p < 0.001$, injury: (1, 44) = 1.701, $p = 0.201$). Also, by difference to GFP densitometry analyses, microglia numbers were significantly increased in both injury models by 3 days after injury (post-hoc Bonferroni t-tests vs control, $t = 6.136$, $p < 0.001$) and the number of cells remained significantly elevated 21 days post injury before returning to control levels by 8 weeks (Fig. 3J). These data suggest that regardless of the site of the nerve injury and degree of VGLUT1 synaptic loss, microglia proliferation in the spinal cord ventral horn is similar. However, the microglia response estimated by GFP fluorescence is more robust in the STL model compared to TTL. Next, we examined whether this was related to different morphological changes in activated microglia after each type of injury.

3.4.4: Microglia undergo similar morphological changes after sciatic or tibial nerve injuries but become more tightly associated to motoneuron cell bodies after sciatic injuries

Following PNI microglia undergo several morphological transformations. They become hypertrophic, their processes retract and become thicker and their cell bodies increase in volume. These morphological changes have been associated with “activation” (Kreutzberg, 1996; Nimmerjahn et al., 2005) and changes in cytokine production (Hanisch, 2002; Hu et al., 2015). To evaluate whether morphological changes are similar after tibial vs sciatic nerve injuries we compared randomly selected microglia in the neighborhood of LG MNs in controls or 14 days after either TTL or STL (n = 12 cells per condition, 3 microglia cells per animal). Individual microglia cells were reconstructed in Imaris using the filament tracker module and volumes of cell bodies were rendered using the surface module (see methods) (Fig. 4A-F). Using Imaris filament tracker we recorded microglia branches and extensions, not filopodia. Control microglia had an average cell body volume of $142.6 \mu\text{m}^3 \pm 11.58$ (\pm SE, n = 12) and after either TTL or STL cell body volumes significantly increased by 83% and 107%, on average, with respect to control (one-way ANOVA $F(2, 35) = 12.574$, $p < 0.001$; post-hoc Bonferroni t-test vs control, TTL: $t = 3.719$, $p = 0.001$; STL: $t = 4.773$, $p < 0.001$) (Fig. 4G). In controls, microglia have an average combined process length of $861.4 \mu\text{m} \pm 96.9$ and an average of 110.0 ± 17.4 individual filaments per microglial cell (Fig. 4 H, I). After both TTL and STL the processes were 51.6-52.6% significantly shorter in overall length (one-way ANOVA $F(2, 35) = 16.059$,

$p < 0.001$, post-hoc Bonferroni t-test vs control, TTL: $t = 4.859$, $p < 0.001$; STL: $t = 4.956$, $p < 0.001$) and the number of filaments was also significantly reduced by 59.0-57.2% compared to controls (one-way ANOVA $F(2, 35) = 11.378$, $p < 0.001$, post-hoc Bonferroni t-test vs control, TTL: $t = 4.194$, $p < 0.001$; STL: $t = 4.07$, $p < 0.001$).

We then performed a Sholl analysis on the number of processes present in defined bins from the cell body, increasing every 10 μm (Fig. 4J). In the first 10 μm bin from the cell body center we recorded more branches in both TTL and STL models compared to control (one-way ANOVA $F(2, 35) = 11.420$, $p < 0.001$, post-hoc Bonferroni t-test vs control, TTL: $t = 3.992$, $p < 0.001$, STL: $t = 4.271$, $p < 0.001$). In the 20 μm bin there was no difference between groups, but thereafter there were significantly fewer branches in microglia after TTL or STL compared to controls (one-way ANOVA $F(2, 35) = 17.871$, $p < 0.001$, post-hoc Bonferroni t-test vs control, TTL: $t = 4.873$, $p < 0.001$; STL: $t = 5.436$, $p < 0.001$). In conclusion, TTL and STL lesions caused similar process retraction and volume increase in ventral horn microglia, at least close to LG MNs. Thus, the larger increase in CX3CR1-GFP fluorescence after sciatic nerve injury compared to the tibial nerve is probably due to a more robust upregulation of CX3CR1 expression or perhaps more hypertrophic microglia cells further from MN cell bodies.

Next, we examined if there were differences in the spatial relationships between microglia and MNs after each type of injury. Following injury, microglia processes specifically surround the cell bodies of axotomized MNs with little detectable interactions with dendritic branches. To quantify this observation, we

calculated the percentage of MN cell body surface covered by microglia using a custom MATLAB script in the Imaris analysis program (see methods). We randomly selected 12 MNs from controls and 14 days post TTL or STL and reconstructed the soma and microglia surfaces in direct contact (Fig. 4K, L). In controls, only $3.2\% \pm 0.64$ (\pm SE, $n = 12$) of the soma surface was in direct contact with microglia, however 14 days after TTL an average of $19.15\% \pm 1.78$ of the MN surface was covered and $25.33\% \pm 2.10$ after STL, both increases were significant (one-way ANOVA $F(2, 35) = 48.957$, $p < 0.001$, post-hoc Bonferroni t-test vs control, TTL: $t = 6.908$, $p < 0.001$; STL: $t = 9.589$, $p < 0.001$) (Fig. 4M). Motoneuron microglia coverage following STL was significantly greater compared to TTL (post-hoc Bonferroni t-test, $t = 2.681$, $p = 0.034$) (Fig. 4M). Thus, although we did not detect morphological differences in activated microglia, they are more closely associated to the MN cell body surface after STL than after TTL.

3.4.5: The number of CCR2-RFP+ cells infiltrating the spinal cord ventral horn depends on the type of injury and is tightly correlated to overall VGLUT1 loss

Almost no CCR2-RFP+ cells were found in the spinal cord parenchyma in sham control mice (not shown). They average 1.3 cells ± 0.2 per $50 \mu\text{m}$ thick section (\pm SE, $n = 4$ animals) and most were elongated perivascular cells that also express weak CX3CR1-GFP. After nerve injury, many CCR2-RFP+ cells infiltrate the lumbar 4 and 5 segments of the spinal cord (Fig. 5A-F), more prominently the ventral horn, where they associate with injured motor pools,

sometimes contacting MN cell bodies. We estimated the numbers of CCR2-RFP+ cells in the ventral horns of 50 μm -thick spinal cord sections by counting all sections containing at least one FB-labeled MN (Fig. 5G) ($n = 3\text{-}4$ animals per time point and injury). There was a significant increase in CCR2-RFP+ cells with time after injury and also a significantly larger infiltration after STL compared to TTL (two-way ANOVA: time: $F(5, 43) = 74.099$, $p < 0.001$; injury type, $F(1, 43) = 27.930$, $p < 0.001$). The number of intra-parenchymal CCR2-RFP+ cells started to increase the first week after injury and although this infiltration was small 3 and 7 days after injury, it was nevertheless significant given the practically non-existence of these cells before the injury (post-hoc Bonferroni t-tests vs control, 3 days: $t = 3.728$, $p = 0.011$; 7 days: $t = 6.643$, $p < 0.001$). These cells greatly increased and peaked in numbers 14 days after injury and their number remained significantly elevated even 8 weeks after injury (post-hoc Bonferroni t-tests vs control, 14 days: $t = 14.179$, $p < 0.001$; 21 days: $t = 16.254$, $p < 0.001$; 8 weeks: $t = 6.522$, $p < 0.001$). After 14 days, 21 days, and 8 weeks post injury there were significantly more CCR2-RFP+ cells following STL compared to TTL (post-hoc Bonferroni t-tests STL vs TTL, 14 days: $t = 5.183$, $p < 0.001$; 21 days: $t = 4.739$, $p < 0.001$; 8 weeks: $t = 2.156$, $p = 0.039$).

Comparing the time courses of CX3CR1-GFP microglia reaction, CCR2-RFP cell infiltration and VGLUT1 loss (Fig. 5H) we found that in both STL and TTL nerve injuries microglia activation precedes infiltration of CCR2-RFP+ cells and the latter tightly associates with the time course of VGLUT1 decrease. The close association between CCR2-RFP+ cell infiltration and VGLUT1 loss

suggests a possible role for these cells in the permanent degradation of Ia/II afferents.

3.4.6: Heterogeneity of CCR2+ cells infiltrating the spinal cord after nerve injury

Infiltrating CCR2-RFP+ cells displayed a variety of phenotypes and relations with CX3CR1-GFP microglia. The majority had a ruffled round or ellipsoid morphology with no expression of CX3CR1. A minority co-expressed CCR2-RFP and CX3CR1-GFP (Fig. 6A1-5, B1-5, C1-5, D1-5). Dual labeled cells displayed variable morphologies, from round/ellipsoid (Fig. 6A1-5) to microglia-like with many processes (Fig. 6C1-5) and some intermediate (Fig. 6B1-5). RFP and GFP fluorescence were inversely correlated and varied according to morphology: rounded/elongated cells were CCR2-RFP^{high}, CX3CR1-GFP^{low}, while microglia-like cells were CCR2-RFP^{low}, CX3CR1-GFP^{high}. RFP+ intensity was reduced with increased size and number of processes, perhaps suggesting downregulation of CCR2 while establishing a CX3CR1 microglia-like phenotype. A similar CCR2 to CX3CR1 phenotypic transition was recently reported for monocytes recruited to injured liver tissues and found to be necessary for optimal repair (Del-Secco et al., 2015). A less abundant type of dual RFP/GFP labeled cell corresponds to elongated perivascular cells (Fig. 6D1-5). A few of these cells were present before the injury and slightly increased in number after nerve injury.

Round/ellipsoid CCR2-RFP+ “only” cells were frequently located close to microglia (Fig. 6E1-3) and sometimes they form large cell clusters with activated

microglia (Fig. 6F1-3). Many correspond to CD3 ϵ T-cells (Fig 6G1-2). Twenty-one days after STL 71.3% \pm 5.7 of ventral horn CCR2 $^{+}$ cells express CD3 ϵ (n = 4 animals, 6 sections with retrogradely labeled LG MNs analyzed per animal) and almost all CD3 ϵ^{+} cells express CCR2-RFP (87.1% \pm 1.7). This suggests that CCR2-RFP expression is relatively stable in infiltrated T-cells.

In contrast, dual labeled cells never expressed T-cell markers and their numbers and infiltration time-course pattern varied according to injury type (Fig. 6H). Their numbers significantly increased after both injuries (two-way ANOVA time: $F(5, 43) = 52.265$, $p < 0.001$, injury: $F(5, 43) = 14.631$, $p < 0.001$; post-hoc Bonferroni t-test vs control, TTL: $t = 4.42 - 7.15$, all time points $p < 0.001$; STL: $t = 4.94 - 13.73$, all time points $p < 0.001$), but showed a peak increase only 14 days after STL, more than doubling the number of cells present at 3 and 7 days post-injury. In contrast, their number remained relatively low from 3 days to 8 weeks after TTL. This difference according to injury type and time after injury was highly significant (two-way ANOVA time x injury: $F(5, 43) = 7.740$, $p < 0.001$). Correspondingly, pairwise comparisons showed significantly larger numbers of dual labeled cells at 14 and 21 days after STL (post-hoc Bonferroni t-tests: TTL vs STL, 14 days: $t = 6.627$, $p < 0.001$; 21 days, $t = 2.789$, $p = 0.009$). Since many of these cells seem to actively downregulate CCR2-RFP expression after entering the spinal cord, their numbers are best interpreted as a reflection of steady-state infiltration rates and not total cell accumulations.

The results suggest the possible presence of a dynamic population of CCR2-RFP cells converting into CX3CR1-GFP microglia-like cells, specifically

after STL injuries. To test whether a proportion of microglia after STL injuries are derived from peripheral cells we genetically labeled all resident microglia in neonates before any injury using *Cx3cr1^{creER}* mice crossed to Ai9 R26 tdTomato reporter mice. In the resulting mice tamoxifen drives tdTomato expression in microglia and several other CX3CR1 expressing peripheral immune cells. However, due to the fast replacement of peripheral immune cells compared to the low turnover of microglia (Tay et al., 2017), 4-5 weeks after tamoxifen injections only resident microglia remain labeled (Goldman et al., 2013). Tamoxifen was injected at postnatal days 12 and 14 and nerve injuries were performed at 3 months of age one week after retrogradely labeling LG MNs with Fast Blue. The spinal cord sections were immunolabeled for Iba1. In uninjured control animals almost 100% of Iba1+ cells are tdTomato labeled, corresponding to the resident microglia population, thus Iba1 cells lacking tdTomato after injuries were interpreted as derived from sources other than resident microglia (Fig. 6J1-2). tdTomato cells lacking Iba1-immunoreactivity were never observed. We analyzed 1 animal in each of three conditions: uninjured control, 21 days after STL and 8 weeks after STL (a total of 4 mice per condition has been prepared and are currently being analyzed). The preliminary results suggest a significant increase in Iba1 cells lacking tdTomato in the ventral horn on the side of the spinal cord ipsilateral to the injury. Interestingly, there is also an increase, albeit of smaller magnitude, in contralateral ventral horn. These cells were not found 8 weeks after the injury. The preliminary quantitative data suggest that around 5% of microglia are possibly derived from infiltrating immune cells 3

weeks after the injury and that these cells do not form a long-lived stable population detectable 8 weeks after the injury. Although 5% might appear a relatively low percentage, they represent a sizable number of cells given the intensity of microgliosis (around 20 cells per 50 μm thick ventral horn section). Frequently, they are found in direct contact with the surfaces of axotomized LG MNs (Fig. 6H).

In conclusion, CCR2⁺ cells entering the spinal cord after nerve injuries are heterogeneous and include T-cells and some cells that downregulate CCR2-RFP expression and might be converting into CX3CR1-GFP microglia-like cells. Because CCR2-RFP expression in infiltrated T-cells is long lived the majority of CCR2-RFP cells at any time point were CD3 positive. Dual labeled cells are preferentially present two weeks after STL injuries and might be related to “*de novo*” microglia that seem derived from sources other than resident microglia. The most likely origin of these cells are CCR2⁺ CD45^{high} CD11b^{high} Ly6C^{positive} inflammatory monocytes known to acquire the phenotype of resident macrophages of tissues they infiltrate (i.e., microglia in the spinal cord). To better identify these cells, we next performed flow cytometry analyses.

3.4.7: Flow cytometry characterization of CCR2⁺ cells

To further characterize the types of CCR2⁺ cells entering the spinal cord after STL we used flow cytometry (Fig. 7). We isolated leukocytes from spinal cords of CCR2-RFP animals 21 days after bilateral sciatic transections to

maximize recovery of CCR2⁺ cells within the spinal cord. The isolated cells were gated for size (Forward Scatter Area, FSA) and granularity (Side Scatter Area, SSA) to select the leukocyte population (Fig. 7A) and followed by Forward Scatter Height (FSH) vs FSA to select single cells (Fig. 7B). Live cells were detected with Fixable Aqua Live/Dead (Fig. 7C) and gated for CD45 to confirm leukocyte phenotype (Fig. 7D). The experiments were run in parallel for leukocytes isolated from spinal cord or blood of the same animals. Blood samples served as positive controls for expected cell numbers and proportions. In the spinal cord we detected CD45^{high} and CD45^{low} populations. Both CD45 populations were then gated for CCR2-RFP. Both the CD45 and CD45/CCR2 populations were then tested for markers of different types of leukocytes. These included markers for B-cells (CD19), T-cells (CD3) (Fig. 7E,F), neutrophils (CD11b^{high} Ly6G^{high}) (Fig. 7G,H), monocytes/macrophages (CD45^{high} CD11b^{high}) and dendrite-like cells (CD11b^{high} CD11c^{high}) (Fig. 7I,J). Microglia were identified as CD45^{low} CD11b^{high} (Fig. 7K), they were CCR2(-) (Fig. 7K). Inside the spinal cord we detected all types of cells, some like B cells (Fig. 7E,F) and neutrophils (Fig. 7G,H) were largely CCR2 negative. CCR2 positive cells were largely all CD45^{high} and included T cells, monocyte/macrophages and dendritic cells. Spinal microglia can also upregulate CD11c⁺ during myelinated axon degeneration (Wlodarczyk et al., 2014).

For quantitative comparisons a total of 12 *Ccr2*^{RFP/+} heterozygous and 12 *Ccr2*^{RFP/+RFP} KO mice were used, but preliminary experiments showed a low yield of CCR2 cells isolated from the spinal cord after injury. Therefore, while we

maintained each animal as an individual data point for analyses of CCR2⁺ cells in the blood, for spinal cord analyses 4 mice from each group were pooled together and analyzed as a single set (CCR2 hets: n = 3 (4 mice in each) and CCR2 KO: n = 3 (4 mice in each)). The numbers and proportions of each leukocyte population in blood samples were similar to previously published materials suggesting effective detection and discrimination (MacPherson et al., 2017). Also, interestingly there was a significant increase in blood neutrophils in CCR2 KOs (Fig. 7N). This compensatory increase in neutrophils has been reported before in CCR2 KOs (Saederup et al., 2010; Lindborg et al., 2017) and further confirms the KO phenotype and also the sensitivity of our methods. However, the percentage of CCR2⁺ cells defined as T-cells inside the spinal cord with flow cytometry is lower than estimated with immunocytochemistry (see above). This difference likely arises because by difference to histological preparations the spinal cord samples collected for flow cytometry originate from animals not exsanguinated by perfusion and therefore counted CCR2⁺ cells include those that infiltrated the spinal cord parenchyma and also all cells in spinal cord blood capillaries and meninges. The proportions of CCR2⁺ cells defined with flow cytometry as T-cells or monocytes/macrophages inside the spinal cord after injury were not significantly different (Fig. 7M). In CCR2 KOs there was a trend towards increased proportions of CCR2⁺ cells expressing a T-cell phenotype and a significant decrease of monocyte/macrophages (Het vs KO t-test; $t(4) = 3.050$, $p = 0.038$). In blood (Fig. 7N), we also detected a significant depletion of CCR2⁺ monocyte/macrophages (Het vs KO t-test; $t(22) = 8.346$, p

<0.001). Deficits in CCR2⁺ monocytes/macrophages in both spinal cord and blood occur because these cells are known to require CCR2 activation for infiltrating peripheral tissues (see above) and also exiting the bone marrow and into the blood (Serbina and Palmer, 2006). Blockade of either or both mechanisms will reduce infiltration into the spinal cord.

3.4.8: VGLUT1 synapses are preserved on motoneuron dendrites of CCR2 knockout mice

Next, we compared CCR2 KO mice (*Ccr2^{RFP/RFP}*) against dual heterozygous mice (*Cx3cr1^{GFP/+} :: Ccr2^{RFP/+}*) after transecting the sciatic nerve followed by repair (STR) (see methods) to avoid cell body shrinkage of disconnected MNs at long survival times and also to allow regeneration of motor and sensory axons in the periphery. We analyzed these animals 21 days after injury to assess microgliosis and CCR2⁺ cell infiltration and at 8 weeks after injury to analyze final VGLUT1 densities on regenerated MNs following muscle reinnervation (confirmed by re-occupancy of vacated neuromuscular junctions by motor end plates, not shown). In *Ccr2^{RFP/RFP}* animals we used Iba1 as a microglia marker as these animals do not express GFP driven by the *Cx3cr1* promoter. In preliminary analyses of control and injured animals we confirmed that 100% of spinal cord CX3CR1-GFP⁺ cells express Iba1⁺ and all Iba1⁺ cells are CX3CR1-GFP positive.

The number of Iba1+ microglia cells in the ventral horn of the spinal cord of CCR2 KO mice 21 days after STR was slightly decreased compared to the number of CX3CR1-GFP microglia cells in dual het mice (n = 4 animals per condition), but this difference did not reach significance (t-test, $t = 2.063$, $p = 0.085$) (Fig. 8A). There was also a slight decrease in the overall number of CCR2-RFP+ cells in CCR2 KOs that did not reach statistical significance either (t-test, $t = 1.256$, $p = 0.256$) (Fig. 8B), but when we compared the number of dual labeled RFP+/GFP+ cells in dual het mice to the number of RFP+/Iba1+ cells in CCR2 KOs we found a dramatic and significant decrease (Mann-Whitney Rank Sum Test $t = 26.000$, $p = 0.029$) (Fig. 8C). No differences were detected in the number of CD3 ϵ T-cells (t-test, $t = -1.394$, $p = 0.213$) (Fig. 8D). Since T-cell numbers overwhelm the CCR2+ population detected with immunohistochemistry inside the spinal cord parenchyma our statistics did not reach enough power to detect a small decrease in the total CCR2 population. Moreover, the depletion of microglia in CCR2 KOs might correspond with reduced numbers of CCR2+ monocytes infiltrating the spinal cord and available to transform into CX3CR1-GFP microglia, but since this population is also relatively small compared to the full microgliosis reaction, our statistics were underpowered. We need to increase samples sizes to (n > 4 animals) to detect statistical significance with enough power (these animals are currently prepared and waiting for analyses). Taken together with data from flow cytometry, the results suggest that in CCR2 KOs T-cell entry is not prevented but there is a specific reduction in CCR2+ monocyte

infiltration that is reflected in fewer cells found in the process of transforming into a microglia-like phenotype (Iba1/CCR2 or CX3CR1/CCR2 dual labeled cells).

Finally, we analyzed VGLUT1 densities on reconstructed LG MNs 8 weeks after STR (Fig. 8E-G). We first compared baseline somatic and dendritic VGLUT1 densities in sham operated CCR2 KO mice with their dual het counterparts and no significant differences were found in VGLUT1 densities on cell bodies (one-way ANOVA, $F(3, 17) = 31.267$, $p < 0.001$, post-hoc Bonferroni t-test dual het control vs CCR2 KO, $t = 1.334$, $p = 1.000$) or dendrites (one-way ANOVA, $F(3, 17) = 13.343$, $p < 0.001$, post-hoc Bonferroni t-test dual het control vs CCR2 KO, $t = 1.455$, $p = 1.000$). This suggests that lack of CCR2 has no impact on VGLUT1 synapse density on MNs in non-injured animals. After STR injury in dual het mice, we found, similar to STL, reduced somatic (post-hoc Bonferroni t-test dual het control vs dual het cut, $t = 8.804$, $p < 0.001$) and dendritic densities compared to sham controls (post-hoc Bonferroni t-test dual het control vs dual het cut, $t = 6.027$, $p < 0.001$). STR injury in CCR2 KO mice resulted in a significant loss in VGLUT1 density on MN cell bodies (post-hoc Bonferroni t-tests, sham vs injured CCR2 KOs, $t = 4.035$, $p = 0.007$). This loss was not significantly different to dual het mice after STR but trended towards some preservation (post-hoc Bonferroni t-tests of injured dual het vs injured CCR2 KOs, $t = 2.784$, $p = 0.088$). In contrast, VGLUT1 dendritic densities were preserved in CCR2 KOs. After STR all injured CCR2 KO animals showed dendritic VGLUT1 densities comparable to uninjured CCR2 KO mice and dual hets; VGLUT1 densities on dendrites after STR injury were thus significantly larger in CCR2 KOs compared to dual hets (post-hoc

Bonferroni t-test, $t = 4.848$, $p = 0.002$). In conclusion, CCR2 genetic deletion prevents CCR2⁺ monocyte infiltration after PNI and fully rescues VGLUT1 synapses on MN dendrites.

3.4.9: CCL2 is upregulated inside the spinal cord by axotomized motoneurons and activated microglia but with different time courses

The spinal sources of CCL2, a CCR2 ligand that could mediate entry of CCR2-dependent monocytes after PNI were analyzed using CCL2-RFP^{flox} animals (see methods). In these mice, and in the absence of cre recombination, all cells expressing *Ccl2* also express mCherry. CCL2 expression was analyzed 3, 7, 14, 21 days and 8 weeks after a STR injury (*currently n=1 animal per time point, 2 more animals have been prepared per time point*). Sections were immunolabeled against choline acetyltransferase (ChAT) or Iba1 to respectively label MNs and microglia (Fig. 8H-K). CCL2 expression was upregulated in both cells types but with different time courses (Fig. 8F). CCL2 expression in MNs had a fast onset after injury, peaking 7 days after the injury. In contrast, 3 and 7 days after the injury few microglia cells express CCL2, but then expression quickly upregulates and peaks 14 days after the injury, temporally coinciding with maximum entry of CCR2⁺ cells (see above). The pattern of mCherry labeling in microglia changed with time (Fig. 8G). While at 3 days after injury the cells had a few small spots of mCherry in their cytoplasm (partial labeling), they were filled with mCherry labeling by 14 days (full labeling) suggesting an increase in expression. After 14 days the proportion of microglia with full mCherry labeling

quickly decreased, however all cells retained RFP spots that at 8 weeks appear as intracellular inclusions in one side of the cell body. These bright inclusions might be reflective of non-degraded mCherry and not necessarily *Ccl2* gene expression. Nevertheless, their presence indicates that 100% of microglia in the area of analysis upregulated *cc/2* gene expression. In summary, although MNs and microglia upregulated CCL2 expression after injury, the temporal profile of microglia CCL2 expression fits better the time course of CCR2+ cells entry. The data also suggest that there is phenotypic switch in activated microglia towards a more pro-inflammatory phenotype 14 days after the injury and coinciding with the largest entry of CCR2+ cells.

3.5: Discussion

Our main findings include: 1) neuroinflammation after PNI is related to the loss of Ia/II afferents VGLUT1 synapses from axotomized MNs; 2) remodeling of VGLUT1 synapses on MN dendrites and cell bodies differ in their relation to neuroinflammation; 3) the neuroinflammatory response involves rapid microglia activation followed by infiltration of CCR2+ immune cells peaking two weeks after injury; 4) CCR2+ cells inside the spinal cord after nerve injury include T-cells and monocytes, only entry of the latter is CCR2 dependent; 5) sources of CCL2 within the spinal cord after injury include MNs and microglia, but the temporal profile of microglia CCL2 expression matches best CCR2 cell entry; 6) a population of microglia during peak microgliosis might derive from external sources and CCR2+ monocytes are the most probable source; 6) genetic

removal of CCR2 reduces entry of CCR2⁺ monocytes and rescues VGLUT1 synapses, on the dendrites of axotomized MNs; 7) neuroinflammation and VGLUT1 synapse plasticity are both graded to the proximity of the nerve injury. Taken together, the results suggest an association between VGLUT1 synapse removal and neuroinflammation, both modulated by injury severity. VGLUT1 synapses arise from Ia and II afferents, both extensively projecting to the ventral horn in rodents and synapsing directly onto MNs (Alvarez et al., 2011; Vincent et al., 2017). Hence, central neuroinflammation triggered by PNI is associated with permanent loss of spindle-derived information about muscle length in the ventral horn and this results in widespread deficits in joint coordination after nerve regeneration and muscle reinnervation (Cope et al., 1994; Abelew et al., 2000; Haftel et al., 2005; Maas et al., 2007; Bullinger et al., 2011; Sabatier et al., 2011; Lyle et al., 2017). The results also suggest that microglia activation is necessary for the permanent removal of VGLUT1 synapses from MN dendrites, but it is not sufficient since it is also required that microglia polarizes towards a CCL2-releasing proinflammatory phenotype that enhances local CCR2 activation and recruitment of peripheral CCR2-dependent monocytes.

3.5.1: Different mechanisms control plasticity of VGLUT1 synapses on dendrites and cell bodies of motoneurons and the role of microglia

In their pioneering study, Blinzinger and Kreutzberg (1968) found that after facial nerve injury, the cell bodies of facial MNs lose many synapses and become covered by microglia. Microglia were suggested to “lift” synapses from the MN

surface, a phenomenon named “synaptic stripping”, and thereafter extended to other cranial and spinal cord MNs after axotomy (Kerns and Hinsman, 1973; Sumner and Sutherland, 1973; Chen, 1978; Graeber et al., 1993; Brannstrom and Kellerth, 1998). Nevertheless, blocking microglia proliferation or activation, pharmacologically or genetically, failed to prevent “synaptic stripping” (Svensson and Aldskogius, 1993; Kalla et al., 2001; Heppner et al., 2005), casting doubt on the proposed mechanism (Perry and O'Connor, 2010). In contrast, we conclude that microglia activation and CCL2 release after PNI are critical for VGLUT1 synapse removal, in particular from dendrites. VGLUT1 synapse plasticity differs from “synaptic stripping” in time-course, fate of preterminal Ia/II afferent axons and lack of recovery (Alvarez et al., 2011). Moreover, “synaptic stripping” affects mainly synapses on the cell body, while VGLUT1 Ia/II afferent synapses are removed throughout the dendritic arbor (Rotterman et al., 2014). Importantly, VGLUT1 synapse removal depends on injury to the Ia/II afferent. Thus, while “stripping” involves local detachment and reattachment of synapses from uninjured presynaptic neurons on specifically postsynaptic axotomized MNs, VGLUT1 synapse removal involves die-back of Ia/II axons from the whole ventral horn, interestingly, while the peripheral branch of the same axon is regenerating. VGLUT1 synapse elimination is best related to “transganglionic anterograde degeneration” of sensory axons injured in peripheral nerves (Grant and Arvidsson, 1975; Aldskogius et al., 1985; Arvidsson, 1986). The fact that the affected central axons belong to sensory afferents injured elsewhere in the periphery, suggest the possibility of specific recognition by neuroimmune cells.

Interestingly, virally infected VGLUT1 synapses in adult hippocampus are specifically recognized and removed by a microglia and complement-dependent mechanism (Vasek et al., 2016). Our results indicate that neuroinflammation is directly related to the permanent removal of Ia/II VGLUT1 synapses from the ventral horn. This process involves loss of ventral horn Ia/II synapses and also die-back of preterminal Ia axon towards the dorsal horn (Alvarez et al., 2011). Removal of ventral horn Ia synaptic arbors thus affects synapses in both MN cell bodies and dendrites (Rotterman et al., 2014), as well as in other spinal targets, like uninjured MNs and ventral interneurons (Hortsman, 2012). The withdrawal of Ia afferent projections from the ventral horn likely also prevents their reestablishment after regeneration in the peripheral nerve is completed. Our results indicate that the removal mechanism requires CCR2 activation and entry of CCR2+ peripheral immune cells and microglia constitute the major local source of CCL2 after injury.

In contrast, synapse elimination around spinal cord MN cell bodies after sciatic nerve injury has been proposed to depend on cell-autonomous mechanisms intrinsic to the axotomized MN, more specifically upregulation of NO in axotomized MN cell bodies and NO destabilization of nearby presynaptic boutons (Sunico et al., 2005; Sunico et al., 2010; Sunico and Moreno-Lopez, 2010). This synaptic plasticity affects all types of synapses on the axotomized MN cell body, but preterminal axons are assumed not to degenerate since these synapses are readily reformed after the MN regenerates and reinnervates muscle targets. VGLUT1 synapses on the cell bodies of axotomized MNs are

likely also affected by this process explaining their removal in situations in which CCR2 mechanisms are blocked and VGLUT1 synapses on dendrites preserved. However, recovery of VGLUT1 synapses on the cell body of regenerated MNs seems impaired. We found higher microglia cell body coverage after injuries associated with maximal cell body VGLUT1 synapse loss. Therefore, the degree of microglia tropism towards the cell bodies of axotomized MNs could augment synapse removal (activated microglia can also release NO), or alternatively prevent their re-formation. In any case the bulk (>95%) of Ia/II VGLUT1 synapses target dendrites (Rotterman et al., 2014) and their partial loss from only the cell body is expected to have a relative smaller contribution to the functionality of the Ia input. Transient synaptic plasticity on cell bodies has been associated with a transient change of axotomized MNs to a “regenerative state” (Carlstedt and Cullheim, 2000) while permanent deletion of the Ia/II afferent input might reduce incongruence in central connectivity between sensory proprioceptors and MNs after both regenerate peripherally and reinnervate targets with more or less specificity (Schultz et al., 2017).

3.5.2: CCR2 monocyte entry is critical for VGLUT1 synapse plasticity

Microglia activation is followed by infiltration of CCR2+ blood-derived immune cells, the later temporally correlated with VGLUT1 synapse removal. Levels of CCR2+ cell recruitment and VGLUT1 synapse loss after different injuries co-vary, but not the number of activated microglia. Triggering graded spinal cord neuroinflammation by adjusting CCR2+ cell entry might therefore

modulate central Ia synaptic connectivity to possible novel innervation patterns after peripheral regeneration. This also indicates that microglia activation and proliferation are not alone sufficient for permanent removal of Ia/II VGLUT1 synapses. Using the CCR2-RFP allele we also found that CCR2⁺ cells infiltrate almost exclusively the ventral horn but not the dorsal horn, although dorsal microglia appears also activated. Microglia upregulation of CCL2 seems necessary to provoke peak entry of CCR2⁺ cells and we never found CCL2 expression in activated dorsal horn microglia suggesting differences in phenotypic activation of dorsal and ventral microglia after PNI. This might relate to our finding that while ventral horn synaptic collaterals of Ia/II afferents are removed, their dorsal horn branches and synapses are largely preserved (Alvarez et al., 2011). Motoneurons also contribute CCL2 in the ventral horn, but the temporal profile of expression does not match the period of extensive entry of CCR2⁺ cells. There are two possible interpretations of these data. First, that MNs do not release enough CCL2 for effective local CCR2 activation and recruitment of proinflammatory CCR2-dependent monocytes. Second, that microglia upregulation of CCL2 is coincident with phenotypic polarization that also mediates breakdown of the spinal cord blood brain barrier facilitating entry of blood-derived cells. Interestingly, CCL2-CCR2 activation has been reported to directly disrupt the blood brain barriers by acting directly on endothelial cells (Yao and Stirska, 2014), however, our data suggest further mechanisms are at play since CCR2 deletion affected infiltration specifically of CCR2-dependent monocytes and not of other blood-derived leukocytes like T-cells.

CCR2 is better known for its role in trafficking specific leukocytes into the CNS (Ransohoff, 2009). Specifically, entry of CD45^{high}Ly6C^{high} pro-inflammatory monocytes is CCR2-dependent and these cells then differentiate into local macrophages (Ma et al., 2002; Mahad and Ransohoff, 2003; Serbina and Pamer, 2006; El Khoury et al., 2007; Serbina et al., 2008; Ajami et al., 2011; Shi and Pamer, 2011; Shi et al., 2011). Interestingly, CCR2⁺ macrophages actively remove damaged axons in injured nerves and after spinal cord injuries they become the principal phagocytic cell responsible for secondary die-back of dorsal columns sensory afferent myelinated axons (Ma et al., 2002; McPhail et al., 2004; Evans et al., 2014). It is therefore possible that blood-derived macrophages infiltrating the spinal cord ventral horn after PNI are directly implicated in the removal of the central myelinated axon of Ia/II afferents. However, 2 weeks after PNI, CX3CR1 microglia are the principal cellular elements expressing the phagocytic marker CD68 (unpublished data, TM Rotterman and FJ Alvarez). One possibility is that CCR2⁺ monocytes differentiate into active phagocytic CX3CR1/Iba1 microglia-like cells and we have found evidence for this possibility by implementing lineage labeling strategies to reveal possible microglia-like cells derived from sources other resident microglia after PNI. Moreover, monocytes differentiating into local macrophages downregulate CCR2 (Dal-Secco et al., 2015) and therefore the spectrum of dual CCR2/CX3CR1 labeled cells found inside the ventral horn after PNI reflects the evolution from infiltrating CCR2⁺ monocytes to CX3CR1 local macrophages with microglia-like morphology. This population of cells was the most significantly

reduced in CCR2 knockouts in association with VGLUT1 synapse preservation on MN dendrites. Alternatively, CCR2⁺ monocyte entry might modulate phagocytic responses of resident microglia and even CCR2 expression. Both mechanisms are not exclusive of each other and future studies using CCR2-Cre lines might best resolve these different possibilities.

A variety of other cells also express CCR2, including natural killer cells and T-cells (Frade et al., 1997; Fife et al., 2000; Mack et al., 2001; Michen and Temme, 2016) and in fact most CCR2⁺ cells found in the ventral horn were T-cells. Their relative high percentage to the whole CCR2⁺ cell population in our histological analyses might be a consequence of better detectability due to the higher stability of CCR2-RFP expression in T-cells compared to CCR2⁺ monocytes. Nevertheless, flow-cytometry characterization also indicates T-cells represent a sizable population inside the spinal cord after sciatic nerve transections. They seem, however, not critical for Ia synaptic plasticity since they were not prevented from entry by blocking CCR2, a manipulation that rescued VGLUT1 synapses. In agreement with this conclusion, T-cells have been shown to infiltrate the facial nucleus after PNI using a CCL11/CCR3 signaling mechanism (Raivich et al., 1998; Jones et al., 2015) and predominantly express a CD4 phenotype that exerts neuroprotection on axotomized MNs (Jones et al., 2015) having no effects on synapse plasticity (Kalla et al., 2001). However, T-cell phenotypes entering the spinal cord after PNI also include CD8⁺ cells (not shown) and MHC I mechanisms have been related to certain types of synaptic

plasticity around MNs after PNI (Thams et al., 2008). Possible actions of T-cells on spinal synapses after PNI remain to be investigated.

In conclusion, transganglionic anterograde degeneration of the central branches of Ia/II afferents injured in peripheral nerves depends on CCR2 mechanisms and CCR2 monocyte infiltration in the ventral horn initiated by a phenotypic polarization of ventral horn microglia towards a CCL2-releasing phenotype. This mechanism might be modulated by injury severity regulating the extent of central spinal cord circuitry remodeling that occurs after different types of nerve injuries in the periphery.

Mouse	Jax#	Background	Donating Lab	Reference
CX3CR1 ^{EGFP}	005582	C57BL/6	Dr. Dan R. Littman, New York University	Jung et al., 2000
CCR2 ^{RFP}	017586	C57BL/6J	Dr. Israel F. Charo, Gladstone Inst of Cardiovascular Disease, UCSF	Saederup et al., 2010
Ccl2-RFP ^{flox}	016849	C57BL/6J	Dr. Eric G Pamer, Memorial Sloan- Kettering Cancer Center	Shi et al., 2011
Chat-IRES- Cre	006410	C57BL/6	Dr. Bradford B. Lowell, Beth Israel Deaconess Med Cntr. Harvard	Rossie et al., 2011
CX3CR1 ^{CreER}	020940	C57BL/6J	Dr. Steffen Jung, Weizmann Institute of Science	Yona et al., 2013
Ai9 R26- tdTomato	007909	C57BL/6J	Dr. Hongkui Zeng, Allen Institute for Brain Science	Madisen et al., 2010

Table 3.1: Transgenic mice.

Antigen	Immunogen	Host/Type	Manufacturer	RRID#	Dilution
EGFP	Recombinant GFP 6-his tag	Chicken/Polyclonal	Serotec Cat# obt1644	AB_620519	1:1000
DsRed	Variation of <i>Discosoma sp.</i>	Rabbit/Polyclonal	Clontech Cat# 632496	AB_10013483	1:1000
VGLUT1	Recomm. Protein (aa 456-560)	Guinea Pig/Polyclonal	Synaptic Systems Cat# 135 304	AB_887878	1:1000
Iba1	C-terminus of Iba1	Rabbit/Polyclonal	Wako Cat# 019-19741	AB_839504	1:500
Chat	Human placental Chat enzyme	Goat/Polyclonal	Millipore / Sigma Cat#ab144p	AB_207915	1:500
CD3ε	Clone 500A2 25-kDa ε chain	Syrian Hamster/ Monoclonal	BD Biosciences Cat# 553238	AB_394727	1:100
CD45	Synthetic peptide corresponding to Human CD45 aa 900-1000	Rabbit/Polyclonal	Abcam Cat#ab10588	AB_442810	1:100

Table 3.2: Antibodies used for immunohistochemistry

	Control	Tibial Ligation	Sciatic Ligation
Soma Surface Area (μm^2)	3118 \pm 142	2989 \pm 268	2377 \pm 239
Dendritic Length (μm)	431 \pm 28	324 \pm 55	249 \pm 45
Dendritic Surface Area (μm^2)	5014 \pm 292	3553 \pm 920	2044 \pm 364
# of VGLUT1 Contacts on Soma	23.2 \pm 1.0	12.6 \pm 1.6	7.0 \pm 1.3
# of VGLUT1 Contacts on Dendrites	71.6 \pm 4.8	45.0 \pm 6.7	28.0 \pm 4.8

Table 3.3: Morphological characteristics of reconstructed motoneurons and VGLUT1 numbers. Data is reported as averages from n=4 mice, 6 motoneurons per mouse \pm SE. Significant differences ($p = <0.05$), from controls, are highlighted in red.

	Control			Tibial Ligation			Sciatic Ligation		
	<u>25μm</u>	<u>50μm</u>	<u>75μm</u>	<u>25μm</u>	<u>50μm</u>	<u>75μm</u>	<u>25μm</u>	<u>50μm</u>	<u>75μm</u>
Dendritic Length (μm)	51.0 ± 3.7	177.9 ± 10.1	124.7 ± 11.8	52.1 ± 4.3	139.1 ± 14.6	54.7 ± 16.2	60.3 ± 4.8	140.2 ± 21.2	42.3 ± 15.9
# of VGLUT1	10.6 ± 0.9	33.2 ± 1.9	17.6 ± 1.9	7.6 ± 0.6	20.9 ± 2.8	10.3 ± 2.9	7.6 ± 1.2	16.9 ± 2.4	3.8 ± 1.4
Dendritic Density (per 100μm)	21.7 ± 0.8	19.2 ± 1.0	14.5 ± 0.5	14.6 ± 0.4	15.0 ± 0.8	13.1 ± 1.9	10.8 ± 2.0	12.7 ± 1.9	7.2 ± 1.5

Table 3.4: Sholl analysis

Motoneuron morphological details by increasing bins 25μm from cell body. Data is reported as averages from n = 4 mice, 6 motoneurons per mouse ± SE.

Significant differences (p = <0.05), from controls, are highlighted in red.

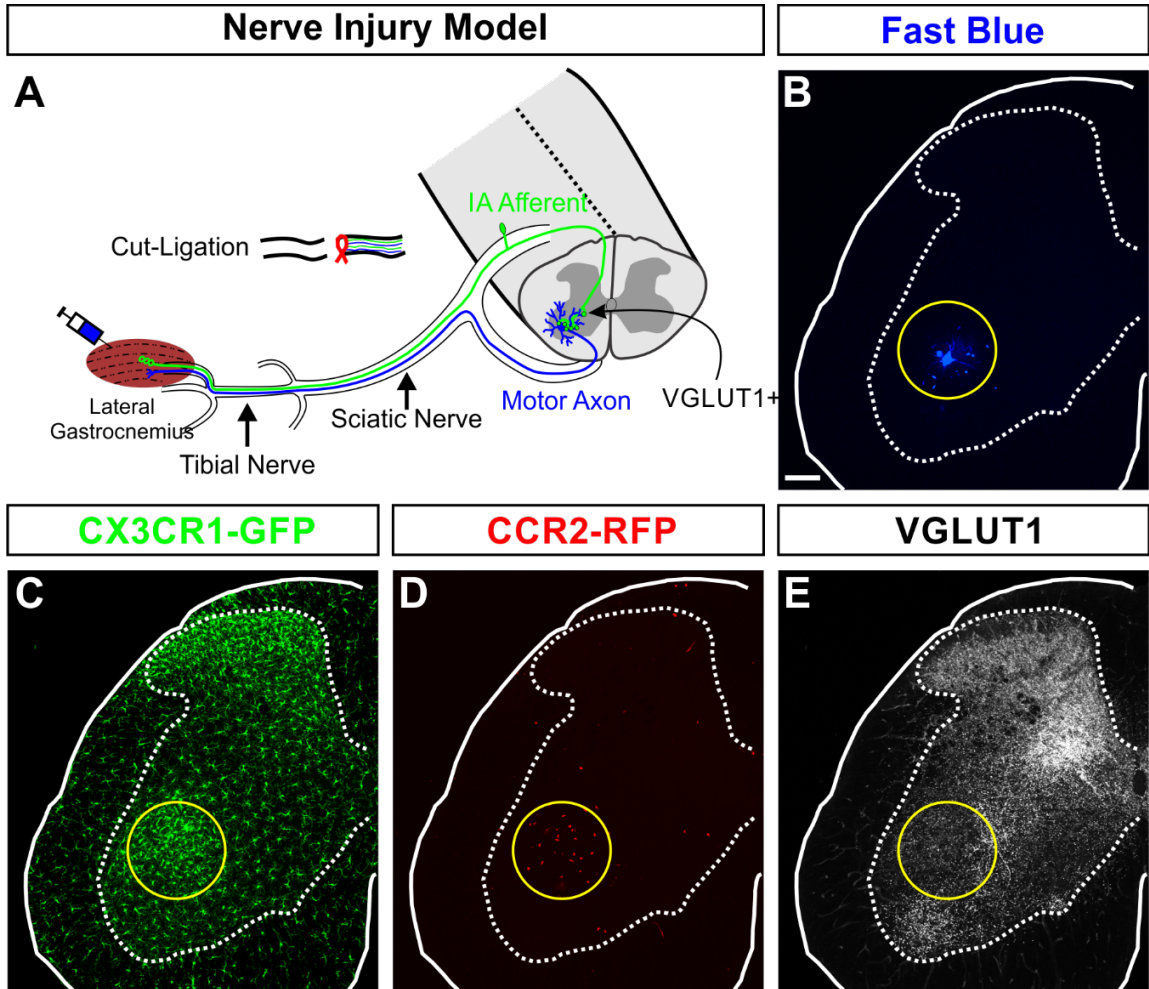


Figure 3.1: Peripheral nerve injury experimental design and mouse model.

A) The lateral gastrocnemius muscle of *Cx3cr1^{GFP/+}::Ccr2^{RFP/+}* dual heterozygous mice was injected with 1.5% Fast Blue to retrogradely label motoneurons (MNs) in the spinal cord. Then the tibial or sciatic nerve was completely transected and the proximal stump was ligated to prevent regeneration. Spinal cords were extracted and analyzed at different times after nerve injury ranging from 3 days to 8 weeks post injury. **B-E)** 2D projections of confocal image stacks through the 50 μ m spinal section thickness showing the four fluorescent signals: Fast Blue MNs (**B**), CX3CR1-GFP+ microglia (**C**), CCR2-RFP+ infiltrating myeloid cells (**D**) and VGLUT1-immunofluorescence (**E**) from an animal 14 days after a sciatic nerve transection. **B)** Spinal cord section outlined by a solid white line containing Fast Blue labeled MNs in lamina IX (blue). White/grey matter border indicated by a dotted white line. Yellow outline delimits the position of the sciatic motor column. **C)** Microglia express GFP under the *Cx3xr1* promoter (green) and after injury they accumulate in the dorsal horn and around axotomized sciatic motor pools in the ventral horn (yellow outline). **D)** Infiltrating myeloid cells express RFP under the *Ccr2* promoter (red) and accumulate within the area of ventral microgliosis (yellow outline). **E)** VGLUT1 immunoreactivity (white) is specifically depleted in the sciatic motor column (yellow outline) with high levels of microgliosis and CCR2+ cell infiltration. All spinal cord images are at the same magnification; scale bar in B: 100 μ m.

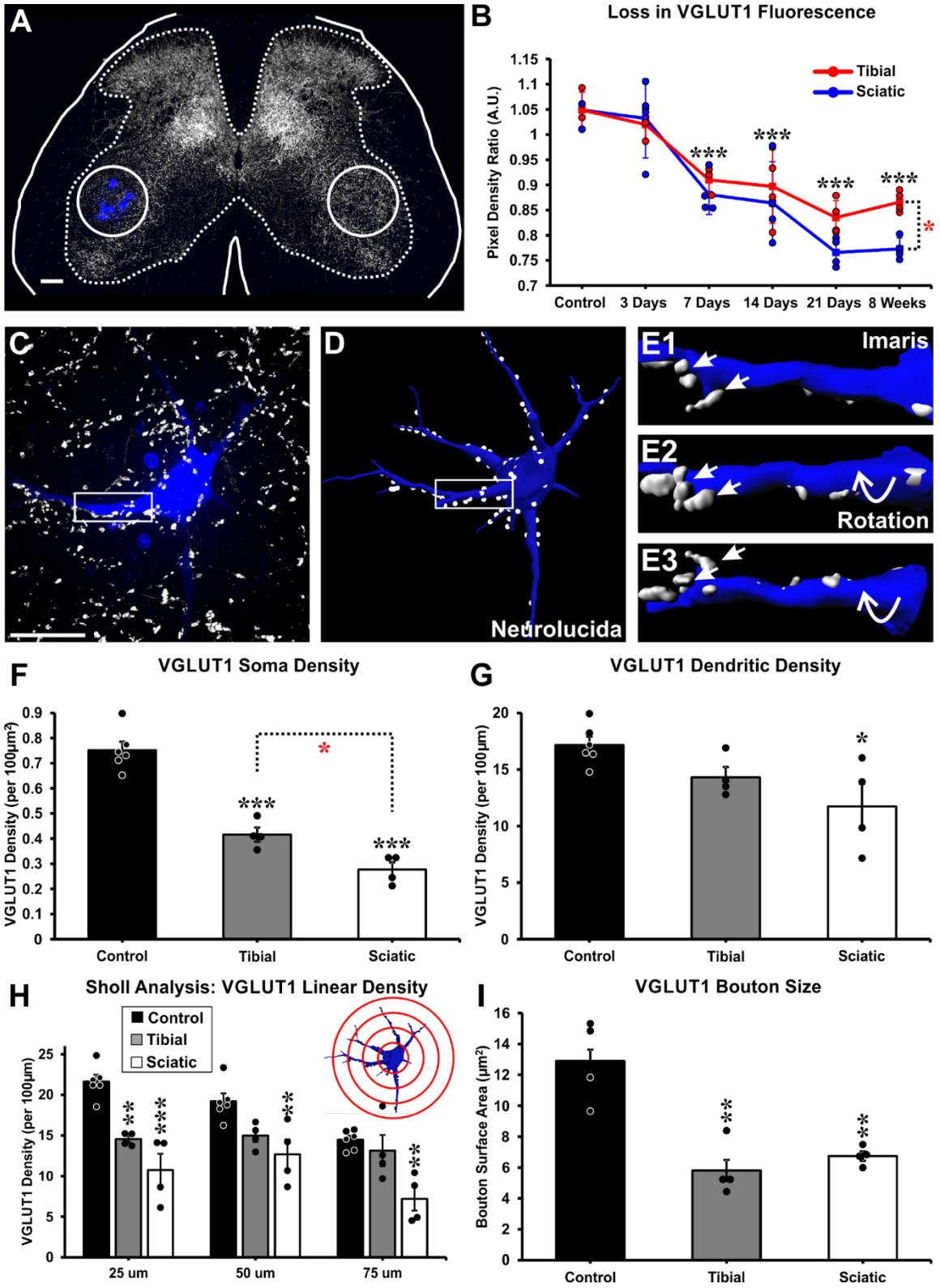


Figure 3.2: Permanent VGLUT1 synaptic loss on motoneurons after nerve injury.

A) VGLUT1 fluorescence densitometry. Region of interests (white circles) are placed on LG motor pools on both sides of the spinal cord and the integrated pixel density of VGLUT1 immunofluorescence measured. **B)** Time course of VGLUT1 fluorescence density changes. The data is presented as a ratio of the estimates ipsilateral vs contralateral to the injury. VGLUT1 fluorescence decreases ipsilateral to the injury after sciatic (blue line) or tibial (red line) nerve cut-ligation injuries. Y-axis = integrated pixel density ipsilateral / contralateral. Each dot represents estimates from one animal (n = 4 mice per time point per injury type). Lines indicate averages \pm SE at each time point. Black asterisks are comparisons to control (**p<0.001). Red asterisk at 8 weeks is a comparison between injuries (*p<0.05). **C)** High magnification confocal image of a retrogradely labeled LG MN (blue, Fast Blue) from a sham control animal receiving VGLUT1 synaptic inputs (white). **D)** NeuroLucida 3D reconstruction of the same LG MN with VGLUT1 contacts mapped along soma and dendrites. **E1-E3)** Imaris 3D surface renderings of dendritic segments shown in box highlighted in C and D. Rotations demonstrate VGLUT1 synapses attachment to the dendrite. **F)** VGLUT1 density in cell bodies is decreased both after tibial or sciatic nerve transection followed by ligation. Bars represent averages \pm SE, n = 4 mice, 6 motoneurons per mouse. Black asterisks are comparisons to control (**p<0.001) and the red asterisk compares the two injuries (*p<0.05). **G)** Dendrite linear densities of VGLUT1 contacts are significantly decreased only

after sciatic nerve injury (black asterisk; $*p < 0.05$). **H**) Sholl Analysis (bin size: 25 μm increments from cell body center): VGLUT1 densities along the dendritic arbor show significant decreases in the first 25 μm after both injuries, but at further distances depletions were significant only after sciatic nerve injury ($***p < 0.001$; $**p < 0.01$). **I**) VGLUT1 bouton surface area is similarly reduced after tibial or sciatic nerve injury compared to control VGLUT1 synapses. Scale bars, in A: 100 μm , in B: 50 μm .

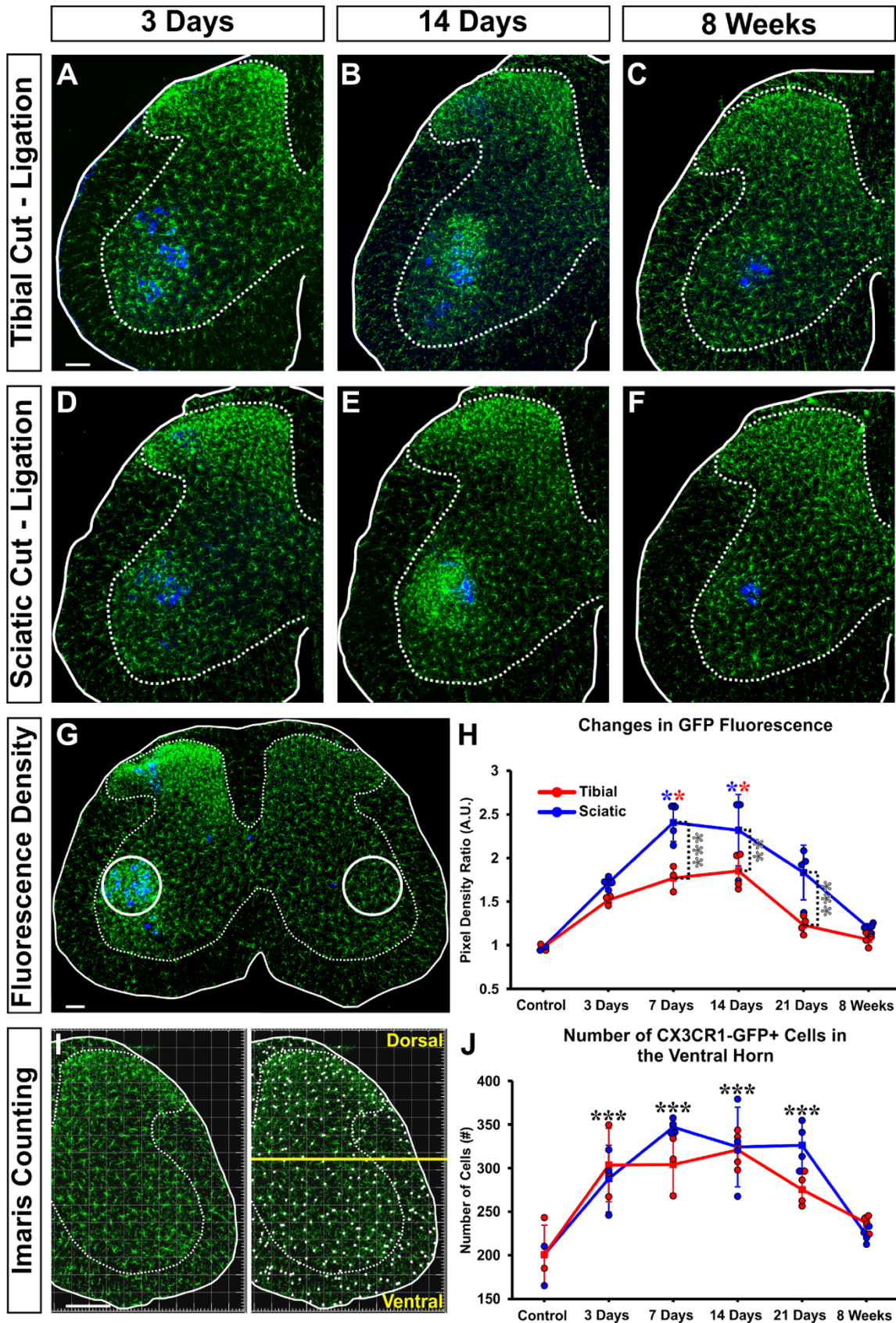


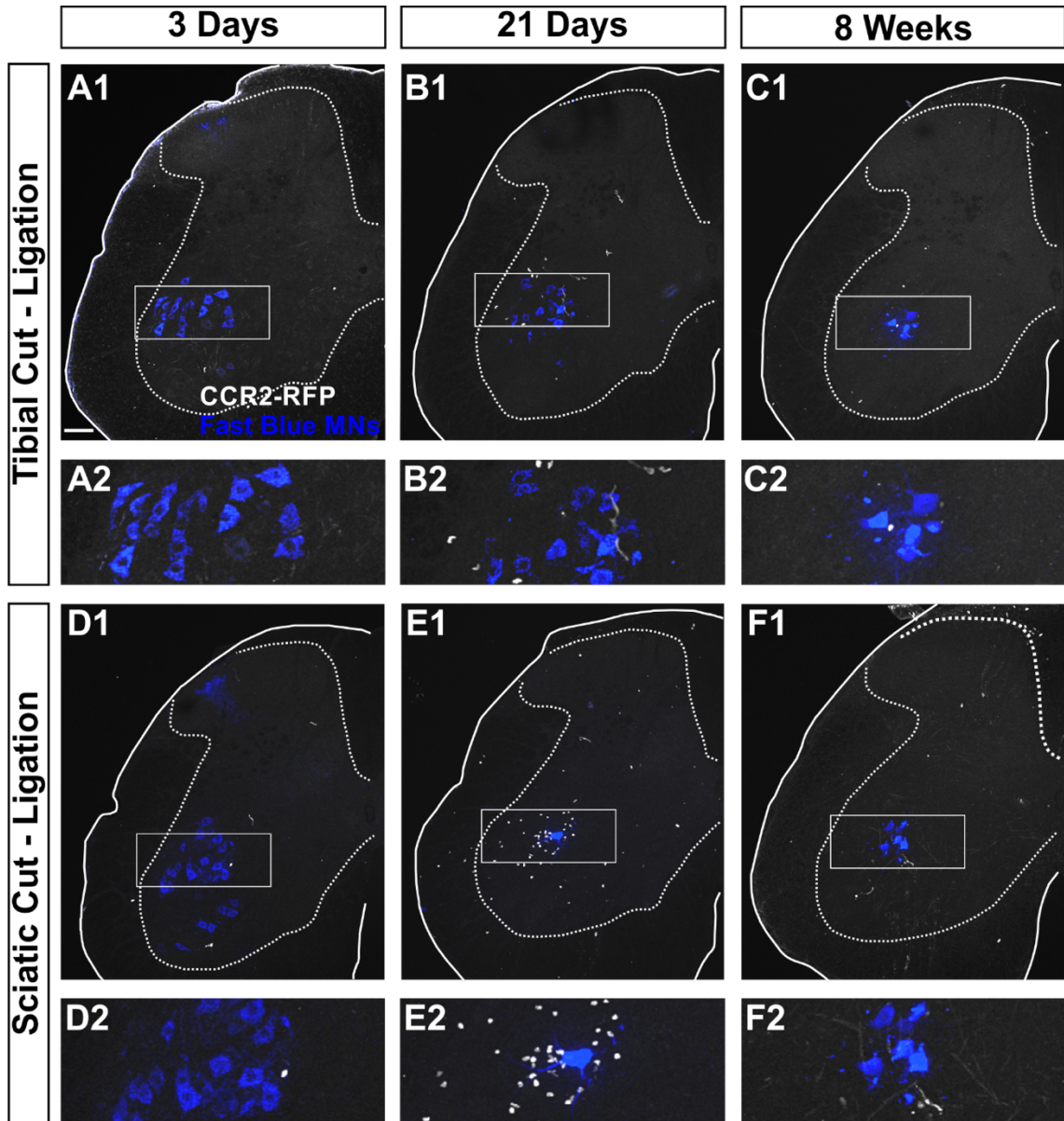
Figure 3.3: Microglia activation around injured motoneurons. A-F) CX3CR1-microglia (GFP, green) in the spinal cord 3 days (**A,D**), 14 days (**B,E**) and 8 weeks (**C,F**) after tibial (**A-C**) or sciatic (**D-F**) cut-ligation. LG motoneurons are labeled with Fast Blue (blue). **G)** Microglia CX3CR1-GFP integrated pixel densities were measured in the indicated ROIs (white circles) ipsilateral and contralateral to the injury. **H)** Changes in GFP fluorescence ipsilateral to contralateral ratios over time. A significant increase in GFP fluorescence was detected ipsilateral to the injury, 7 and 14 days post injury in both models (red asterisks tibial injury and blue asterisks sciatic nerve, both vs control and all $p < 0.05$). In addition, larger GFP fluorescence was detected after sciatic injury from 7 to 21 days post-injury (grey asterisks; $**p < 0.01$, $***p < 0.001$). GFP fluorescence returns to baseline control levels by 8 weeks. **I)** Imaris spot function used to automatically detect GFP+ cells in the spinal cord. Left panel, fluorescence; right panel, cell body identification. A line traced above the dorsal tip of the central canal separates dorsal from ventral regions. Data shown correspond to the ventral region. **J)** Number of GFP+ microglia per ventral horn in 50 μm thick sections. There is a significant increase in the number of GFP+ cells after both tibial and sciatic ligation between 3 and 21 days post injury ($***p < 0.001$ all vs control after either injury). Cells numbers return to baseline by 8 weeks post injury. By difference to GFP fluorescence intensity, no statistical differences were detected between sciatic and tibial nerve injury in GFP+ microglial cell numbers. Each data point represents one animal and the lines

show averages \pm SE at each time points (n = 4 mice, six spinal cords per mouse). A to F are at the same magnification; scale bar in A, G, I: 100 μ m

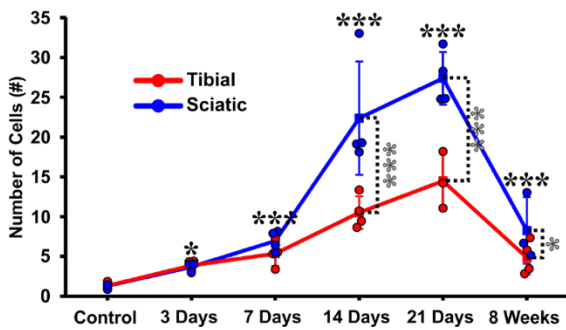
Figure 3.4: Microglia morphological changes around axotomized motoneurons.

A-C) 2D projections of confocal stacks of single microglia cells (CX3CR1-GFP) in control and 14 days after a tibial or sciatic nerve injury. **D-F)** Imaris filament tracker reconstructions superimposed on the confocal images. Inserts show the filament reconstructions alone. **G)** Microglia cell body volume show similar significant increases with respect to control after both nerve injuries (** $p < 0.01$; *** $p < 0.001$). **H)** Total microglia processes length and **I)** total number of filaments show also similar significant decreases compared to controls (*** $p < 0.001$). Each data point in G, H and I represent an individual microglia cell ($n = 12$ in each group) and error bars are SE. **J)** Sholl analysis comparing total number of microglia filaments in increasing 10 μm bins from the cell body center. In the first 10 μm , control microglia have significantly fewer processes than microglia in the injured conditions (blue asterisks). From 10 to 20 μm distance there are no differences, but past 20 μm there are significantly fewer microglia processes in injured animals. Asterisks show significant differences compared to control after sciatic (red) or tibial (green) nerve injury (*** $p < 0.001$). Microglia insert shows Sholl analysis bins (processes are colored coded based on branch distance from soma). **K)** Microglia-MN coverage analysis. Fast blue labeled MN cell body (blue) and all microglia in contact (green) were surface rendered in Imaris. **L)** Area of microglia coverage (red) on reconstructed MN soma (blue). **M)** Percent of MN soma surface covered by microglia 14 days after either tibial or sciatic nerve injury. After either injury, there is a significant increase in cell body surface

covered by microglia processes ($***p < 0,001$). but sciatic nerve injury resulted in significantly more coverage than tibial nerve injury ($*p < 0.05$). Each reconstructed MN is represented by an individual dot on the graphs ($n = 12$ in each group). Error bars are SE. Scale bars in A, B, C and K: $10 \mu\text{m}$. D, E and F are at the same magnification than respectively A, B and C. L is at the same magnification as K.



G Number of CCR2-RFP+ Cells in the Ventral Horn



H Time Course of Neuroinflammation and VGLUT1 Loss

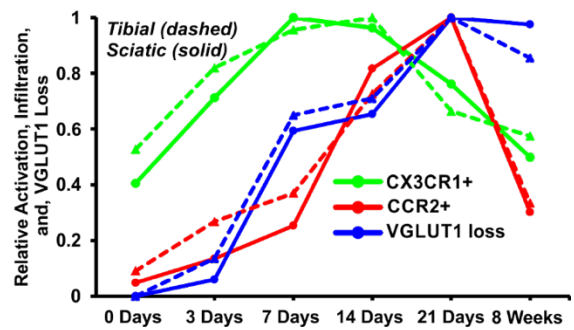


Figure 3.5: CCR2+ cells infiltrate the ventral horn of the spinal cord after nerve injury.

A-F) 2D projection confocal image stacks (50 μm thick) of CCR2+ cells (white cells) that infiltrated the spinal cord 3 days, 21 days, and 8 weeks after either injury to the tibial or sciatic nerve surround retrogradely labeled LG motoneurons (blue). Below each low magnification image the area highlighted in the rectangle is shown at higher magnification. **G)** Time course of CCR2+ cell infiltration after tibial (red line) or sciatic (blue line) nerve injury. Data is represented as average number of total RFP+ cells in the ventral horn of 50 μm thick spinal cord sections. Each data point represents the average from all L4-L5 sections in each mouse (average of 23.2 sections per animal). Lines represent the average of 3-4 mice per time point and error bars are SE. Significant increases in CCR2+ cells compared to control are found from 3 days to 8 weeks after injury for both injuries (black asterisks), while significant differences between STL and TTL are found at 14 days, 21 days, and 8 weeks after injury (grey asterisks) (* $p < 0.05$; *** $p < 0.005$). **H)** Time course of CX3CR1-GFP+ cell activation (green lines), infiltration of CCR2-RFP+ cells (red lines), and overall VGLUT1 loss after sciatic or tibial nerve injury (blue lines) normalized to maximum change for each condition and measurement. The time course of VGLUT1 loss overlaps with CCR2+ cell entry, both occur at a delay after the onset of microglia activation. Scale bar in A: 100 μm . B to F are at the same magnification.

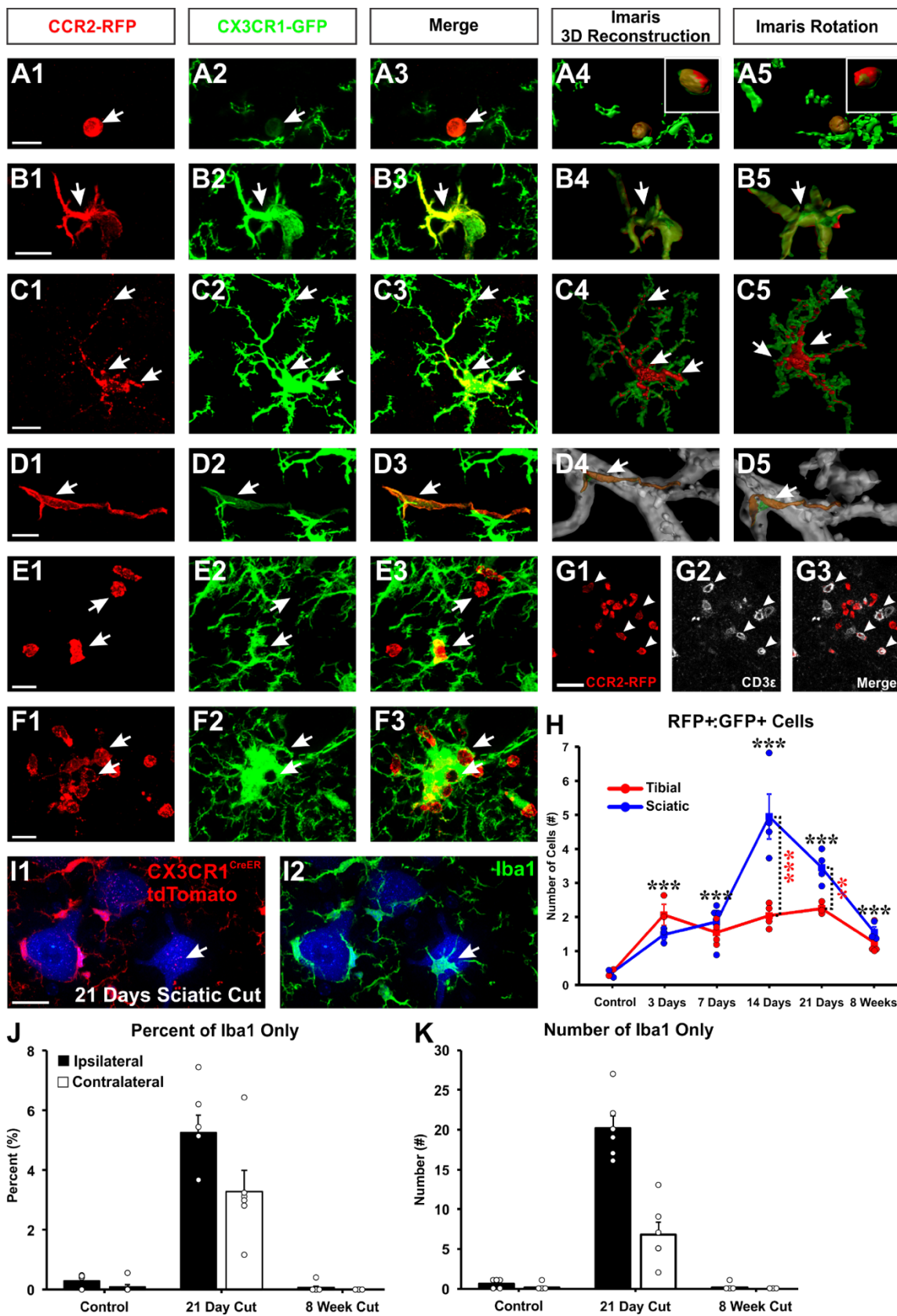


Figure 3.6: Heterogeneity of CCR2-RFP+ cells infiltrating the spinal cord ventral horn.

A1, B1, C1, D1, E1, F1) Different types of CCR2-RFP+ cells in the ventral horn of the spinal cord 14 and 21 days after sciatic nerve injuries. **A2, B2, C2, D2, E2, F2)** 2D projection confocal images showing CX3CR1-GFP expression and relationships with CX3CR1-GFP expressing cells. **A3, B3, C3, D3, E3, F3)** CCR2-RFP and CX3CR1-GFP merge images. **A4-5, B4-5, C4-5, D4-5)** Imaris surface reconstructions and 3D image rotations. CCR2-RFP cells in **A** to **D** show CX3CR1-GFP co-expression: **A** rounded cells with low CX3CR1 fluorescence; **B**, cell with few processes; **C**, cell with multiple process and high CX3CR1 fluorescence and microglia-like morphology. **D** perivascular cell. The blood vessel surface was rendered in D4 and D5. **E1-3, F1-3)** CCR2-RFP cells with no CX3CR1. Some of these cells are isolated (top arrow in **E** series), but more frequently interact with either single (bottom arrow **E** series) or macro clusters of CX3CR1-GFP microglia (arrows in **F** series). **G1-3)** Many CCR2-RFP cells express a CD3+ T-cell phenotype. **H)** Time course of CCR2-RFP / CX3CR1-GFP dual expressing cells presence after tibial (red line and dots) or sciatic (blue line and dots) injuries. Individual animals represented as data points (average of n = 23.2 sections per animal/data point). Lines are average at each time point and scale bars SE (n = 4 animals per time point). Black and gray asterisks represent significant differences with respectively controls or between injury types at individual time points (**p<0.01, ***p<0.001). A significant infiltration of dual labeled cells occurs after both injuries starting at 3 days and lasting for 8 weeks,

but a peak increase in entry specifically occurs after sciatic injuries. **I1-2)** Genetic lineage labeling demonstrating cells derived from resident microglia (Iba1 and tdTomato co-labeled) or sources other than resident microglia (labeled only with Iba1) 21 days after sciatic injuries. A proportion of microglia seem derived from extrinsic sources and these include cells in close apposition to MN cell bodies (arrow). **J, K)** Percent and total number of Iba1+ “only” cells. N = 1 animal, each dot represents estimates in different sections. All A-F scale bars are 10 μm . Scale bar in I, 20 μm .

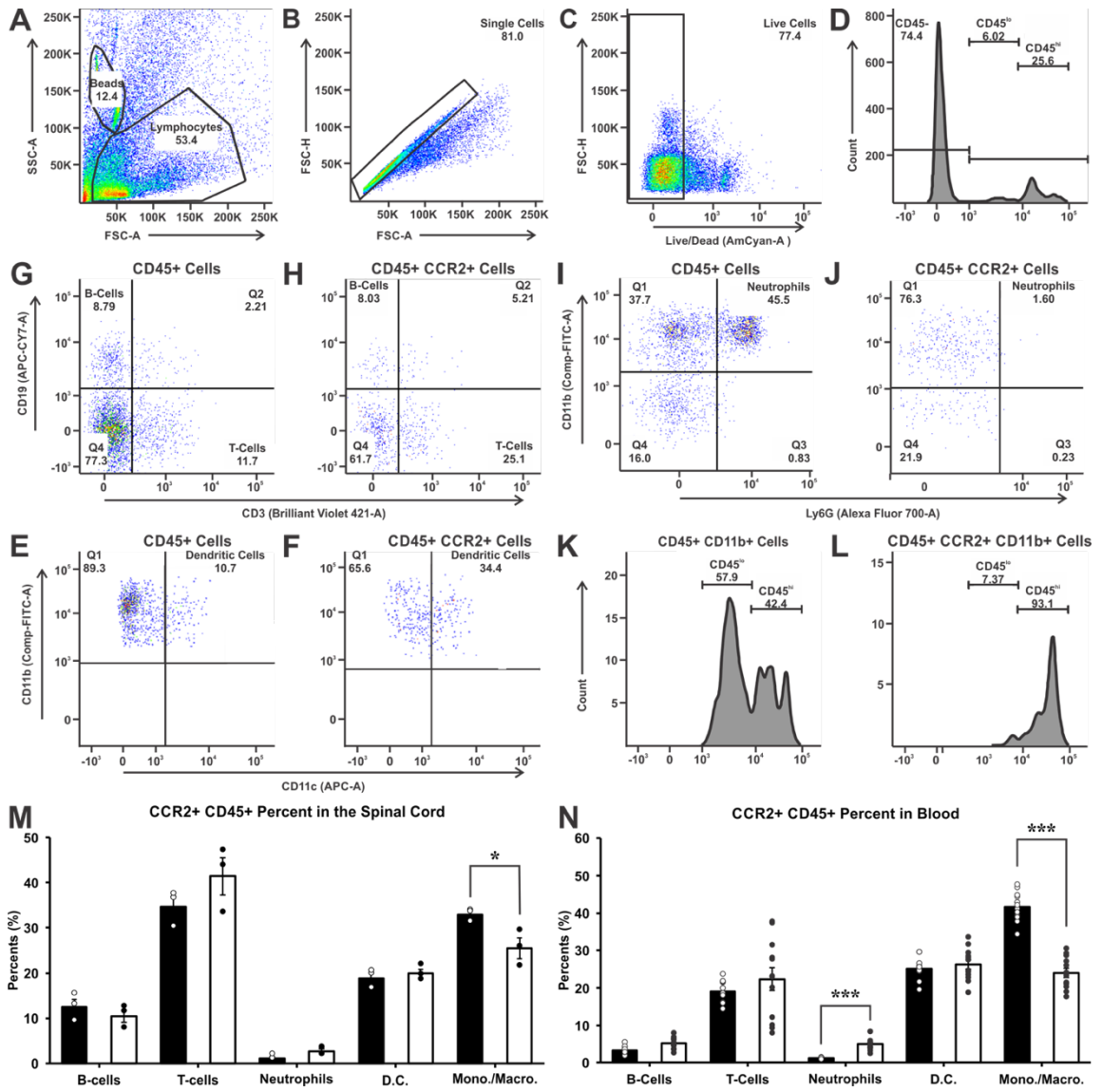


Figure 3.7: Flow cytometry analysis of CCR2+ cells inside the spinal cord and in the blood in CCR2 hets and CCR2 KOs 21 days after bilateral sciatic nerve injuries.

A-C) Gating for cell shape (**A**), single cells (**B**) and live cells (**C**). **D)** Resulting cells were CD45 negative, positive low or positive high. The CD45^{high} population was further gated for CCR2. **E-J)** Gating of the CD45^{high} or CD45^{high}:CCR2 cells for CD9 B and CD3 T cells (**E,F**), Ly6G neutrophils (**G,H**), CD11b monocytes/macrophages and CD11c dendritic cells (**I,J**). The results show all cell types represented in the spinal cord, but some like B cells, neutrophils and a proportion of CD11b cells (likely microglia) lack CCR2. CCR2+ subtypes include CD3 T-cells, CD11b monocytes / macrophages and CD11c dendritic cells. **K)** CD45/CD11b cells include CD45^{low} (likely microglia) and CD45^{high} populations. **L)** Only CD45^{high} CD11b cells express CCR2. **M)** Percentages of CCR2+CD45^{high} cells expressing different phenotypes in spinal cord 21 days after sciatic nerve injuries in CCR2 het (black bars) and CCR2 KO animals (white bars). Each data point represents pooling together 4 animals to increase CCR2 cell yield inside the spinal cord (n = 12 animals total, n = 3 for statistical comparisons; *p < 0.05 in t-tests). Error bars represent SE. The results show specific depletion of monocyte / macrophages with a trend toward increases in T-cell representation within CD45:CCR2+ cells. **N)** Different cell types in the blood of injured CCR2 hets (white bars) and CCR2 KOs (black bars). Each data point represents a different animal (n = 12 animals, *** p<0.001 in t-tests). The data shows the

expected reduced numbers of monocyte / macrophages and increased numbers of neutrophils in the blood of CCR2 KOs.

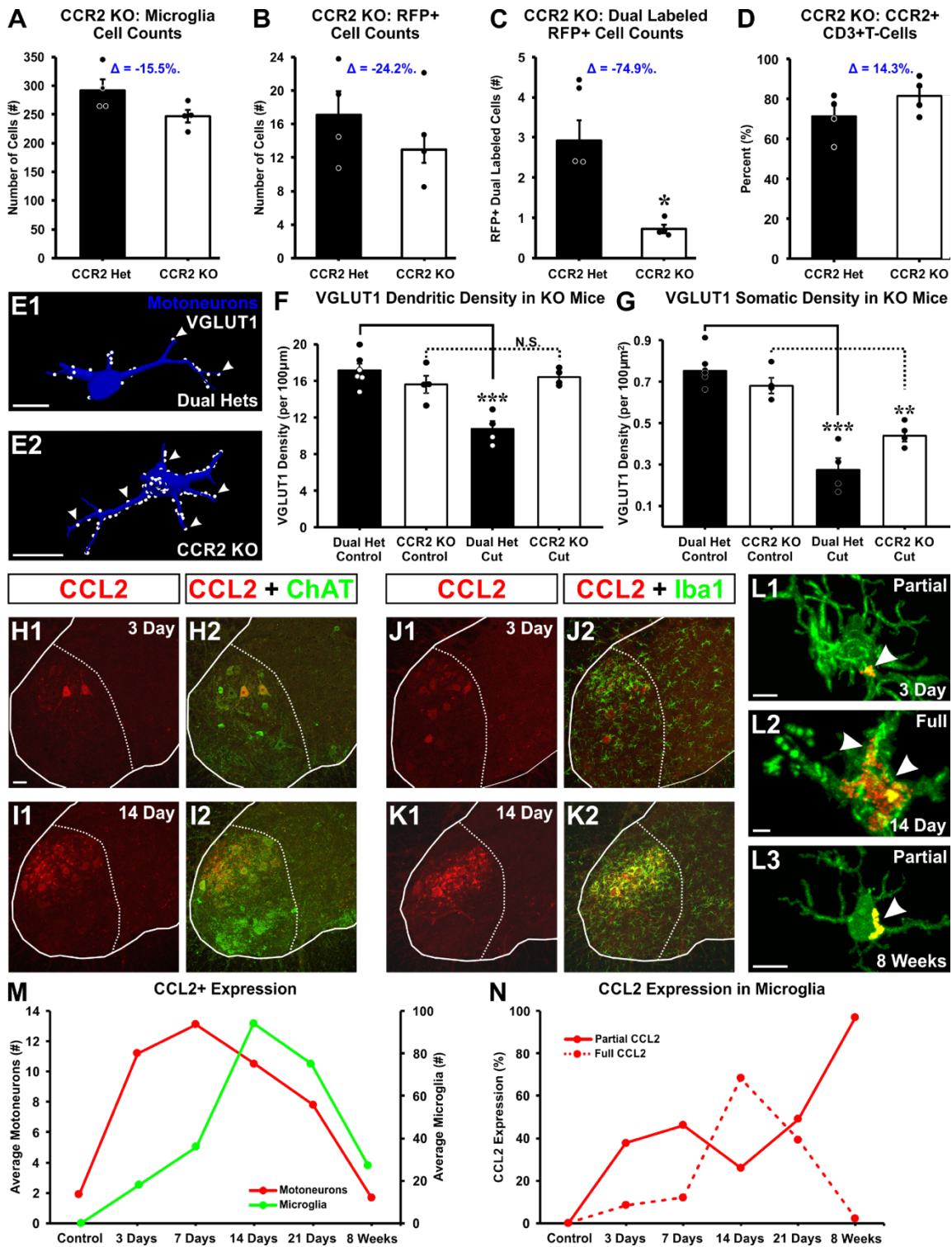


Figure 8: Microgliosis, CCR2-RFP cells and VGLUT1 synapses in CCR2 KOs after injury and sources of CCL2 within the spinal cord.

A-D) Change in microglia or CCR2-RFP cell numbers in CCR2 hets compared to CCR2 KOs 21 days after sciatic nerve injury and repair (STR). CCR2 hets are CX3CR1-EGFP:CCR2-RFP dual hets. In all cases $n = 4$ animals (each represented by a different dot), errors bars represent SE. * $p < 0.05$ in t-tests. Deltas are effect sizes. **A)** Non-significant small decrease in microglia cell number estimated by CX3CR1-GFP fluorescence in CCR2 hets and Iba1 immunoreactivity in CCR2 KOs. **B)** Non-significant small decrease in total RFP cells. **C)** Significant large decrease in dual CCR2-RFP/CX3CR1-GFP cells in CCR2 hets compared to dual CCR2-RFP/Iba1-IR cells in CCR2 KOs. **D)** Small non-significant increase in CCR2+ T-cells in CCR2 KO animals. **E1, E2)** Retrogradely labeled MNs reconstructed in NeuroLucida (blue) with VGLUT1 synapses indicated (white) in injured CCR2 het and CCR2 KO animals 8 weeks after STR. **F)** Dendrites VGLUT1 linear densities (per 100 μm). No significant differences found between sham control dual hets and CCR2 KO animals. There was a significant depletion in dual hets compared to their sham controls (** $p < 0.001$) while VGLUT1 synapses on dendrites were preserved in CCR2 KO mice. Each dot represents a single animal ($n = 4-6$ animals) and error bars are SE. **G)** VGLUT1 somatic densities (per 100 μm^2). Significant reductions were found in injured dual het and CCR2 KO animals compared to their respective sham controls (** $p < 0.001$, ** $p < 0.01$). There was also a trend towards partial preservation in CCR2 KOs ($p=0.088$, between injured dual hets and injured

CCR2 KO animals). **H-K**) CCL2 expression after STR reported by mCherry expression in *Ccl2-RFP^{fllox}* mice. **H** and **I** CCL2-RFP in ChAT MNs. **J** and **K** CCL2-RFP in Iba1 microglia. **H** and **J**, 3 days after injury. **I** and **K**, 14 days after injury. **L1-3**) Patterns of mCherry labeling in Iba1+ microglia different days after injury. **M**) Time course of CCL2 expression shows early onset and peak expression in MNs compared to microglia (n =1 animal per time point). **N**) Percentages of Iba1 microglia with either partial or full coverage by mCherry labeling. Scale bars, E and H1 are 50 μm ; L1-3, 5 μm .

References:

- Abelew TA, Miller MD, Cope TC, Nichols TR (2000) Local loss of proprioception results in disruption of interjoint coordination during locomotion in the cat. *Journal of neurophysiology* 84:2709-2714.
- Ajami B, Bennett JL, Krieger C, McNagny KM, Rossi FM (2011) Infiltrating monocytes trigger EAE progression, but do not contribute to the resident microglia pool. *Nature neuroscience* 14:1142-1149.
- Aldskogius H (2011) Mechanisms and consequences of microglial responses to peripheral axotomy. *Frontiers in bioscience* 3:857-868.
- Aldskogius H, Arvidsson J, Grant G (1985) The reaction of primary sensory neurons to peripheral nerve injury with particular emphasis on transganglionic changes. *Brain research* 357:27-46.
- Aldskogius H, Liu L, Svensson M (1999) Glial responses to synaptic damage and plasticity. *Journal of neuroscience research* 58:33-41.
- Alvarez FJ, Villalba RM, Zerda R, Schneider SP (2004) Vesicular glutamate transporters in the spinal cord, with special reference to sensory primary afferent synapses. *The Journal of comparative neurology* 472:257-280.
- Alvarez FJ, Titus-Mitchell HE, Bullinger KL, Kraszpulski M, Nardelli P, Cope TC (2011) Permanent central synaptic disconnection of proprioceptors after nerve injury and regeneration. I. Loss of VGLUT1/IA synapses on motoneurons. *Journal of neurophysiology* 106:2450-2470.
- Arvidsson J (1986) Transganglionic degeneration in vibrissae innervating primary sensory neurons of the rat: a light and electron microscopic study. *The Journal of comparative neurology* 249:392-403.
- Berg A, Zelano J, Thams S, Cullheim S (2013) The extent of synaptic stripping of motoneurons after axotomy is not correlated to activation of surrounding glia or downregulation of postsynaptic adhesion molecules. *PLoS one* 8:e59647.
- Blinzinger K, Kreutzberg G (1968) Displacement of synaptic terminals from regenerating motoneurons by microglial cells. *Zeitschrift für Zellforschung und mikroskopische Anatomie* 85:145-157.
- Bonecchi R, Bianchi G, Bordignon PP, D'Ambrosio D, Lang R, Borsatti A, Sozzani S, Allavena P, Gray PA, Mantovani A, Sinigaglia F (1998) Differential expression of chemokine receptors and chemotactic responsiveness of type 1 T helper cells (Th1s) and Th2s. *The Journal of experimental medicine* 187:129-134.
- Brannstrom T, Kellerth JO (1998) Changes in synaptology of adult cat spinal alpha-motoneurons after axotomy. *Experimental brain research Experimentelle Hirnforschung Experimentation cerebrale* 118:1-13.
- Brown AG, Fyffe RE (1981) Direct observations on the contacts made between Ia afferent fibres and alpha-motoneurons in the cat's lumbosacral spinal cord. *The Journal of physiology* 313:121-140.
- Brushart T (2011) *Nerve Repair*: Oxford University Press.
- Bullinger KL, Nardelli P, Pinter MJ, Alvarez FJ, Cope TC (2011) Permanent central synaptic disconnection of proprioceptors after nerve injury and

- regeneration. II. Loss of functional connectivity with motoneurons. *Journal of neurophysiology* 106:2471-2485.
- Burke RE, Walmsley B, Hodgson JA (1979) HRP anatomy of group Ia afferent contacts on alpha motoneurons. *Brain research* 160:347-352.
- Carlstedt T, Cullheim S (2000) Spinal cord motoneuron maintenance, injury and repair. *Progress in brain research* 127:501-514.
- Chen DH (1978) Qualitative and quantitative study of synaptic displacement in chromatolyzed spinal motoneurons of the cat. *The Journal of comparative neurology* 177:635-664.
- Cope TC, Bonasera SJ, Nichols TR (1994) Reinnervated muscles fail to produce stretch reflexes. *Journal of neurophysiology* 71:817-820.
- Cullheim S, Thams S (2007) The microglial networks of the brain and their role in neuronal network plasticity after lesion. *Brain research reviews* 55:89-96.
- Dal-Secco D, Wang J, Zeng Z, Kolaczowska E, Wong CH, Petri B, Ransohoff RM, Charo IF, Jenne CN, Kubes P (2015) A dynamic spectrum of monocytes arising from the in situ reprogramming of CCR2+ monocytes at a site of sterile injury. *The Journal of experimental medicine* 212:447-456.
- Davis KD, Taylor KS, Anastakis DJ (2011) Nerve injury triggers changes in the brain. *The Neuroscientist : a review journal bringing neurobiology, neurology and psychiatry* 17:407-422.
- Donnelly DJ, Longbrake EE, Shawler TM, Kigerl KA, Lai W, Tovar CA, Ransohoff RM, Popovich PG (2011) Deficient CX3CR1 signaling promotes recovery after mouse spinal cord injury by limiting the recruitment and activation of Ly6Clo/iNOS+ macrophages. *The Journal of neuroscience : the official journal of the Society for Neuroscience* 31:9910-9922.
- Echeverry S, Wu Y, Zhang J (2013) Selectively reducing cytokine/chemokine expressing macrophages in injured nerves impairs the development of neuropathic pain. *Experimental neurology* 240:205-218.
- Echeverry S, Shi XQ, Rivest S, Zhang J (2011) Peripheral nerve injury alters blood-spinal cord barrier functional and molecular integrity through a selective inflammatory pathway. *The Journal of neuroscience : the official journal of the Society for Neuroscience* 31:10819-10828.
- El Khoury J, Toft M, Hickman SE, Means TK, Terada K, Geula C, Luster AD (2007) Ccr2 deficiency impairs microglial accumulation and accelerates progression of Alzheimer-like disease. *Nature medicine* 13:432-438.
- Evans TA, Barkauskas DS, Myers JT, Huang AY (2014a) Intravital imaging of axonal interactions with microglia and macrophages in a mouse dorsal column crush injury. *Journal of visualized experiments : JoVE*:e52228.
- Evans TA, Barkauskas DS, Myers JT, Hare EG, You JQ, Ransohoff RM, Huang AY, Silver J (2014b) High-resolution intravital imaging reveals that blood-derived macrophages but not resident microglia facilitate secondary axonal dieback in traumatic spinal cord injury. *Experimental neurology* 254:109-120.
- Fife BT, Huffnagle GB, Kuziel WA, Karpus WJ (2000) CC chemokine receptor 2 is critical for induction of experimental autoimmune encephalomyelitis. *The Journal of experimental medicine* 192:899-905.

- Frade JM, Mellado M, del Real G, Gutierrez-Ramos JC, Lind P, Martinez AC (1997) Characterization of the CCR2 chemokine receptor: functional CCR2 receptor expression in B cells. *Journal of immunology* 159:5576-5584.
- Goldmann T, Wieghofer P, Muller PF, Wolf Y, Varol D, Yona S, Brendecke SM, Kierdorf K, Staszewski O, Datta M, Luedde T, Heikenwalder M, Jung S, Prinz M (2013) A new type of microglia gene targeting shows TAK1 to be pivotal in CNS autoimmune inflammation. *Nature neuroscience* 16:1618-1626.
- Graeber MB, Bise K, Mehraein P (1993) Synaptic stripping in the human facial nucleus. *Acta neuropathologica* 86:179-181.
- Grant G, Arvidsson J (1975) Transganglionic degeneration in trigeminal primary sensory neurons. *Brain research* 95:265-279.
- Gu N, Peng J, Murugan M, Wang X, Eyo UB, Sun D, Ren Y, DiCicco-Bloom E, Young W, Dong H, Wu LJ (2016) Spinal Microgliosis Due to Resident Microglial Proliferation Is Required for Pain Hypersensitivity after Peripheral Nerve Injury. *Cell reports* 16:605-614.
- Guest JD, Hesse D, Schnell L, Schwab ME, Bunge MB, Bunge RP (1997) Influence of IN-1 antibody and acidic FGF-fibrin glue on the response of injured corticospinal tract axons to human Schwann cell grafts. *Journal of neuroscience research* 50:888-905.
- Haftel VK, Bichler EK, Wang QB, Prather JF, Pinter MJ, Cope TC (2005) Central suppression of regenerated proprioceptive afferents. *The Journal of neuroscience : the official journal of the Society for Neuroscience* 25:4733-4742.
- Hanisch UK (2002) Microglia as a source and target of cytokines. *Glia* 40:140-155.
- Harrison JK, Jiang Y, Chen S, Xia Y, Maciejewski D, McNamara RK, Streit WJ, Salafranca MN, Adhikari S, Thompson DA, Botti P, Bacon KB, Feng L (1998) Role for neuronally derived fractalkine in mediating interactions between neurons and CX3CR1-expressing microglia. *Proceedings of the National Academy of Sciences of the United States of America* 95:10896-10901.
- Heppner FL, Greter M, Marino D, Falsig J, Raivich G, Hovelmeyer N, Waisman A, Rulicke T, Prinz M, Priller J, Becher B, Aguzzi A (2005) Experimental autoimmune encephalomyelitis repressed by microglial paralysis. *Nature medicine* 11:146-152.
- Hortsman G (2012) Limitation of functional recover of stretch reflex circuitry after peripheral nerve regeneration. In, p 184: Wright State University.
- Hu X, Leak RK, Shi Y, Suenaga J, Gao Y, Zheng P, Chen J (2015) Microglial and macrophage polarization-new prospects for brain repair. *Nature reviews Neurology* 11:56-64.
- Huang D, Shi FD, Jung S, Pien GC, Wang J, Salazar-Mather TP, He TT, Weaver JT, Ljunggren HG, Biron CA, Littman DR, Ransohoff RM (2006) The neuronal chemokine CX3CL1/fractalkine selectively recruits NK cells that modify experimental autoimmune encephalomyelitis within the central

- nervous system. *FASEB journal : official publication of the Federation of American Societies for Experimental Biology* 20:896-905.
- Hughes DI, Polgar E, Shehab SA, Todd AJ (2004) Peripheral axotomy induces depletion of the vesicular glutamate transporter VGLUT1 in central terminals of myelinated afferent fibres in the rat spinal cord. *Brain research* 1017:69-76.
- Jinno S, Yamada J (2011) Using comparative anatomy in the axotomy model to identify distinct roles for microglia and astrocytes in synaptic stripping. *Neuron glia biology* 7:55-66.
- Jones KJ, Lovett-Racke AE, Walker CL, Sanders VM (2015) CD4 + T Cells and Neuroprotection: Relevance to Motoneuron Injury and Disease. *Journal of neuroimmune pharmacology : the official journal of the Society on NeuroImmune Pharmacology* 10:587-594.
- Jung S, Aliberti J, Graemmel P, Sunshine MJ, Kreutzberg GW, Sher A, Littman DR (2000) Analysis of fractalkine receptor CX(3)CR1 function by targeted deletion and green fluorescent protein reporter gene insertion. *Molecular and cellular biology* 20:4106-4114.
- Kalla R, Liu Z, Xu S, Koppius A, Imai Y, Kloss CU, Kohsaka S, Gschwendtner A, Moller JC, Werner A, Raivich G (2001) Microglia and the early phase of immune surveillance in the axotomized facial motor nucleus: impaired microglial activation and lymphocyte recruitment but no effect on neuronal survival or axonal regeneration in macrophage-colony stimulating factor-deficient mice. *The Journal of comparative neurology* 436:182-201.
- Kannarkat GT, Cook DA, Lee JK, Chang J, Chung J, Sandy E, Paul KC, Ritz B, Bronstein J, Factor SA, Boss JM, Tansey MG (2015) Common Genetic Variant Association with Altered HLA Expression, Synergy with Pyrethroid Exposure, and Risk for Parkinson's Disease: An Observational and Case-Control Study. *NPJ Parkinsons Dis* 1.
- Katsumoto A, Miranda AS, Butovsky O, Teixeira AL, Ransohoff RM, Lamb BT (2018) Laquinimod attenuates inflammation by modulating macrophage functions in traumatic brain injury mouse model. *Journal of neuroinflammation* 15:26.
- Kerns JM, Hinsman EJ (1973) Neuroglial response to sciatic neurectomy. II. Electron microscopy. *The Journal of comparative neurology* 151:255-280.
- Kreutzberg GW (1996) Microglia: a sensor for pathological events in the CNS. *Trends in neurosciences* 19:312-318.
- Lindborg JA, Mack M, Zigmond RE (2017) Neutrophils Are Critical for Myelin Removal in a Peripheral Nerve Injury Model of Wallerian Degeneration. *The Journal of neuroscience : the official journal of the Society for Neuroscience* 37:10258-10277.
- Lundborg G (2003) Richard P. Bunge memorial lecture. Nerve injury and repair-- a challenge to the plastic brain. *Journal of the peripheral nervous system : JPNS* 8:209-226.
- Lyle MA, Nichols TR, Kajtaz E, Maas H (2017) Musculotendon adaptations and preservation of spinal reflex pathways following agonist-to-antagonist tendon transfer. *Physiol Rep* 5.

- Lyle MA, Prilutsky BI, Gregor RJ, Abelew TA, Nichols TR (2016) Self-reinnervated muscles lose autogenic length feedback, but intermuscular feedback can recover functional connectivity. *Journal of neurophysiology* 116:1055-1067.
- Ma M, Wei T, Boring L, Charo IF, Ransohoff RM, Jakeman LB (2002) Monocyte recruitment and myelin removal are delayed following spinal cord injury in mice with CCR2 chemokine receptor deletion. *Journal of neuroscience research* 68:691-702.
- Maas H, Prilutsky BI, Nichols TR, Gregor RJ (2007) The effects of self-reinnervation of cat medial and lateral gastrocnemius muscles on hindlimb kinematics in slope walking. *Experimental brain research Experimentelle Hirnforschung Experimentation cerebrale* 181:377-393.
- Mack M, Cihak J, Simonis C, Luckow B, Proudfoot AE, Plachy J, Bruhl H, Frink M, Anders HJ, Vielhauer V, Pfirstinger J, Stangassinger M, Schlondorff D (2001) Expression and characterization of the chemokine receptors CCR2 and CCR5 in mice. *Journal of immunology* 166:4697-4704.
- MacPherson KP, Sompol P, Kannarkat GT, Chang J, Sniffen L, Wildner ME, Norris CM, Tansey MG (2017) Peripheral administration of the soluble TNF inhibitor XPro1595 modifies brain immune cell profiles, decreases beta-amyloid plaque load, and rescues impaired long-term potentiation in 5xFAD mice. *Neurobiology of disease* 102:81-95.
- Mahad DJ, Ransohoff RM (2003) The role of MCP-1 (CCL2) and CCR2 in multiple sclerosis and experimental autoimmune encephalomyelitis (EAE). *Semin Immunol* 15:23-32.
- McPhail LT, Stirling DP, Tetzlaff W, Kwiecien JM, Ramer MS (2004) The contribution of activated phagocytes and myelin degeneration to axonal retraction/dieback following spinal cord injury. *The European journal of neuroscience* 20:1984-1994.
- Michen S, Temme A (2016) Genetically Engineered Natural Killer Cells as a Means for Adoptive Tumor Immunotherapy. *Crit Rev Immunol* 36:329-347.
- Mizutani M, Pino PA, Saederup N, Charo IF, Ransohoff RM, Cardona AE (2012) The fractalkine receptor but not CCR2 is present on microglia from embryonic development throughout adulthood. *Journal of immunology* 188:29-36.
- Mohanty CB, Bhat D, Devi BI (2015) Role of Central Plasticity in the Outcome of Peripheral Nerve Regeneration. *Neurosurgery* 77:418-423.
- Moreno-Lopez B, Sunico CR, Gonzalez-Forero D (2011) NO orchestrates the loss of synaptic boutons from adult "sick" motoneurons: modeling a molecular mechanism. *Molecular neurobiology* 43:41-66.
- Morganti JM, Jopson TD, Liu S, Riparip LK, Guandique CK, Gupta N, Ferguson AR, Rosi S (2015) CCR2 antagonism alters brain macrophage polarization and ameliorates cognitive dysfunction induced by traumatic brain injury. *The Journal of neuroscience : the official journal of the Society for Neuroscience* 35:748-760.
- Navarro X, Vivo M, Valero-Cabre A (2007) Neural plasticity after peripheral nerve injury and regeneration. *Progress in neurobiology* 82:163-201.

- Niemi JP, DeFrancesco-Lisowitz A, Roldan-Hernandez L, Lindborg JA, Mandell D, Zigmond RE (2013) A critical role for macrophages near axotomized neuronal cell bodies in stimulating nerve regeneration. *The Journal of neuroscience : the official journal of the Society for Neuroscience* 33:16236-16248.
- Nimmerjahn A, Kirchhoff F, Helmchen F (2005) Resting microglial cells are highly dynamic surveillants of brain parenchyma in vivo. *Science* 308:1314-1318.
- Papadopoulos EJ, Sasseti C, Saeki H, Yamada N, Kawamura T, Fitzhugh DJ, Saraf MA, Schall T, Blauvelt A, Rosen SD, Hwang ST (1999) Fractalkine, a CX3C chemokine, is expressed by dendritic cells and is up-regulated upon dendritic cell maturation. *European journal of immunology* 29:2551-2559.
- Parillaud VR, Lornet G, Monnet Y, Privat AL, Haddad AT, Brochard V, Bekaert A, de Chanville CB, Hirsch EC, Combadiere C, Hunot S, Lobsiger CS (2017) Analysis of monocyte infiltration in MPTP mice reveals that microglial CX3CR1 protects against neurotoxic over-induction of monocyte-attracting CCL2 by astrocytes. *Journal of neuroinflammation* 14:60.
- Perry VH, O'Connor V (2010) The role of microglia in synaptic stripping and synaptic degeneration: a revised perspective. *ASN neuro* 2:e00047.
- Prinz M, Priller J, Sisodia SS, Ransohoff RM (2011) Heterogeneity of CNS myeloid cells and their roles in neurodegeneration. *Nature neuroscience* 14:1227-1235.
- Raivich G, Jones LL, Kloss CU, Werner A, Neumann H, Kreutzberg GW (1998) Immune surveillance in the injured nervous system: T-lymphocytes invade the axotomized mouse facial motor nucleus and aggregate around sites of neuronal degeneration. *The Journal of neuroscience : the official journal of the Society for Neuroscience* 18:5804-5816.
- Ransohoff RM (2009) Chemokines and chemokine receptors: standing at the crossroads of immunobiology and neurobiology. *Immunity* 31:711-721.
- Rossi J, Balthasar N, Olson D, Scott M, Berglund E, Lee CE, Choi MJ, Lauzon D, Lowell BB, Elmquist JK (2011) Melanocortin-4 receptors expressed by cholinergic neurons regulate energy balance and glucose homeostasis. *Cell Metab* 13:195-204.
- Rotterman TM, Nardelli P, Cope TC, Alvarez FJ (2014) Normal Distribution of VGLUT1 Synapses on Spinal Motoneuron Dendrites and Their Reorganization after Nerve Injury. *The Journal of neuroscience : the official journal of the Society for Neuroscience* 34:3475-3492.
- Sabatier MJ, To BN, Nicolini J, English AW (2011a) Effect of axon misdirection on recovery of electromyographic activity and kinematics after peripheral nerve injury. *Cells, tissues, organs* 193:298-309.
- Sabatier MJ, To BN, Nicolini J, English AW (2011b) Effect of slope and sciatic nerve injury on ankle muscle recruitment and hindlimb kinematics during walking in the rat. *The Journal of experimental biology* 214:1007-1016.
- Sabha M, Jr., Emirandetti A, Cullheim S, De Oliveira AL (2008) MHC I expression and synaptic plasticity in different mice strains after axotomy. *Synapse* 62:137-148.

- Saederup N, Cardona AE, Croft K, Mizutani M, Cotleur AC, Tsou CL, Ransohoff RM, Charo IF (2010) Selective chemokine receptor usage by central nervous system myeloid cells in CCR2-red fluorescent protein knock-in mice. *PloS one* 5:e13693.
- Schroeter M, Kury P, Jander S (2003) Inflammatory gene expression in focal cortical brain ischemia: differences between rats and mice. *Brain research Molecular brain research* 117:1-7.
- Schultz AJ, Rotterman TM, Dwarakanath A, Alvarez FJ (2017) VGLUT1 synapses and P-boutons on regenerating motoneurons after nerve crush. *The Journal of comparative neurology* 525:2876-2889.
- Serbina NV, Pamer EG (2006) Monocyte emigration from bone marrow during bacterial infection requires signals mediated by chemokine receptor CCR2. *Nature immunology* 7:311-317.
- Serbina NV, Jia T, Hohl TM, Pamer EG (2008) Monocyte-mediated defense against microbial pathogens. *Annual review of immunology* 26:421-452.
- Shi C, Pamer EG (2011) Monocyte recruitment during infection and inflammation. *Nature reviews Immunology* 11:762-774.
- Shi C, Jia T, Mendez-Ferrer S, Hohl TM, Serbina NV, Lipuma L, Leiner I, Li MO, Frenette PS, Pamer EG (2011) Bone marrow mesenchymal stem and progenitor cells induce monocyte emigration in response to circulating toll-like receptor ligands. *Immunity* 34:590-601.
- Sumner BE, Sutherland FI (1973) Quantitative electron microscopy on the injured hypoglossal nucleus in the rat. *Journal of neurocytology* 2:315-328.
- Sunderland S (1968) *Nerves and nerve injuries*. Baltimore,: Williams and Wilkins Co.
- Sunico CR, Portillo F, Gonzalez-Forero D, Moreno-Lopez B (2005) Nitric-oxide-directed synaptic remodeling in the adult mammal CNS. *The Journal of neuroscience : the official journal of the Society for Neuroscience* 25:1448-1458.
- Sunico CR, Gonzalez-Forero D, Dominguez G, Garcia-Verdugo JM, Moreno-Lopez B (2010) Nitric oxide induces pathological synapse loss by a protein kinase G-, Rho kinase-dependent mechanism preceded by myosin light chain phosphorylation. *The Journal of neuroscience : the official journal of the Society for Neuroscience* 30:973-984.
- Svensson M, Aldskogius H (1993a) Infusion of cytosine-arabinoide into the cerebrospinal fluid of the rat brain inhibits the microglial cell proliferation after hypoglossal nerve injury. *Glia* 7:286-298.
- Svensson M, Aldskogius H (1993b) Synaptic density of axotomized hypoglossal motoneurons following pharmacological blockade of the microglial cell proliferation. *Experimental neurology* 120:123-131.
- Svensson M, Eriksson P, Persson JK, Molander C, Arvidsson J, Aldskogius H (1993) The response of central glia to peripheral nerve injury. *Brain research bulletin* 30:499-506.
- Tay TL, Savage JC, Hui CW, Bisht K, Tremblay ME (2017a) Microglia across the lifespan: from origin to function in brain development, plasticity and cognition. *The Journal of physiology* 595:1929-1945.

- Tay TL, Mai D, Dautzenberg J, Fernandez-Klett F, Lin G, Sagar, Datta M, Drougard A, Stempfl T, Ardura-Fabregat A, Staszewski O, Margineanu A, Sporbert A, Steinmetz LM, Pospisilik JA, Jung S, Priller J, Grun D, Ronneberger O, Prinz M (2017b) A new fate mapping system reveals context-dependent random or clonal expansion of microglia. *Nature neuroscience* 20:793-803.
- Thams S, Oliveira A, Cullheim S (2008) MHC class I expression and synaptic plasticity after nerve lesion. *Brain research reviews* 57:265-269.
- Vasek MJ et al. (2016) A complement-microglial axis drives synapse loss during virus-induced memory impairment. *Nature* 534:538-543.
- Vincent JA, Gabriel HM, Deardorff AS, Nardelli P, Fyffe REW, Burkholder TJ, Cope TC (2017) Muscle Proprioceptors in Adult Rat: Mechanosensory Signaling and Synapse Distribution in Spinal Cord. *Journal of neurophysiology:jn 00497 02017*.
- Wlodarczyk A, Lobner M, Cedile O, Owens T (2014) Comparison of microglia and infiltrating CD11c(+) cells as antigen presenting cells for T cell proliferation and cytokine response. *Journal of neuroinflammation* 11:57.
- Yao Y, Tsirka SE (2014) Monocyte chemoattractant protein-1 and the blood-brain barrier. *Cell Mol Life Sci* 71:683-697.
- Yona S, Kim KW, Wolf Y, Mildner A, Varol D, Breker M, Strauss-Ayali D, Viukov S, Guilliams M, Misharin A, Hume DA, Perlman H, Malissen B, Zelzer E, Jung S (2013) Fate mapping reveals origins and dynamics of monocytes and tissue macrophages under homeostasis. *Immunity* 38:79-91.
- Zhang J, Shi XQ, Echeverry S, Mogil JS, De Koninck Y, Rivest S (2007) Expression of CCR2 in both resident and bone marrow-derived microglia plays a critical role in neuropathic pain. *The Journal of neuroscience : the official journal of the Society for Neuroscience* 27:12396-12406.

Chapter 4:

The effect of axon regeneration efficiency in spinal motor circuit plasticity following peripheral nerve injury and the role neuroinflammation plays

Manuscript in preparation for submission: Rotterman TM, Chopra T, Fisher S, Franklin H, Alvarez FJ (2018) The effect of axon regeneration efficiency in spinal motor circuit plasticity following peripheral nerve injury and the role neuroinflammation plays.

Abstracts presented from this work:

1. Rotterman TM and Alvarez FJ. The severity of the central neuroimmune response following peripheral nerve injury correlates with the amount of proprioceptive IA afferent loss from injured motoneurons. 2015 *Neuroscience Meeting Planner*. Chicago, Illinois: Society for Neuroscience, 2015, Program No. 2581 (online).

4.1 Abstract

A peripheral nerve transection results in a central neuroinflammatory response that promotes the reorganization of essential spinal circuits necessary for proper motor control, such as the permanent degradation of Ia afferent inputs on axotomized MNs that form the stretch reflex. However, when a nerve is crushed, Ia inputs are not significantly lost and the stretch reflex is completely preserved. Here, we hypothesize that the permanency of Ia afferent loss is dependent on the duration of the neuroinflammatory reaction and the success of peripheral motor axon regeneration. We compared the overall loss in Ia afferent inputs on MNs and the neuroinflammatory response following a sciatic nerve crush or cut injury in mice expressing GFP in microglia cells (CX3CR1+) and RFP in peripheral myeloid cells (CCR2+). Furthermore, we compared the rate and specificity of motor axon regeneration and how it related to the recovery of Ia afferents. We found that following crush there was a temporary detachment of Ia afferent inputs by 21 days post injury, but these returned by 8 weeks. However, in the cut animals, these synapses detached and were permanently degraded. The recovery of synapses in crush related to a faster rate and greater specificity of motor axon regeneration in the periphery and an overall shorter microglia response in the ventral horn and no major infiltration of CCR2+ cells. However, following a cut-repair, motor axons regenerated much slower and had a significantly higher rate of reinnervation errors in the periphery. This related to a longer and more robust microglia reaction and a significant infiltration of CCR2+ cells in the spinal cord.

4.2 Introduction

The peripheral nerve is the conducting unit between the central nervous system (CNS) and the muscle (Sunderland, 1991), in which sensory information can be received, integrated into motor circuits in the ventral horn of the spinal cord and elicit an appropriate motor response. For example, Ia afferents axons innervate muscle spindles in the peripheral muscle and project directly into the spinal cord providing synaptic inputs on interneurons in lamina V/VI, VII (Jankowska and Lindstrom, 1972), and to motoneurons (MNs) in lamina IX (Brown and Fyffe, 1978; Alvarez et al., 2004; Vincent et al., 2017). These connections provide critical information to the CNS about limb position and provide one of the fundamental components of proprioception, by forming the stretch reflex circuitry with MNs (Liddell and Sherrington, 1924; Eccles et al., 1957; Lundberg and Winsbury, 1960; Mendell and Henneman, 1971). Following peripheral nerve injury (PNI) there is no longer a conducting unit between the periphery and the CNS, which results in the reorganization of spinal motor circuits, for example the loss in connectivity between Ia afferents and MNs (Alvarez et al., 2011; Rotterman et al., 2014) which has devastating consequences on proper motor control (Abelew et al., 2000; Bullinger et al., 2011; Hamilton et al., 2011). However, the severity and permanency of these changes may depend on the type of injury sustained and on the success of peripheral axon regeneration and targeted reinnervation.

When a nerve is completely severed and repaired both the sensory and motor axons degenerate distal to the injury and have the ability to regenerate.

However, severed axons enter the endoneurial tubes at random and can innervate different targets from the original source (Brushart and Mesulam, 1980; Brushart et al., 1983; Bodine-Fowler et al., 1997; Valero-Cabre et al., 2004). In contrast, when the nerve is crushed, the endoneurial tubes remain intact and both sensory and motor axons have greater success of regenerating and reinnervating their original targets (Nguyen et al., 2002). The functional consequences of these two injuries can also vary greatly. For example, complete nerve transection and repair results in a permanent and complete loss of the stretch reflex (Cope et al., 1994; Bullinger et al., 2011). This is explained by the degeneration of entire Ia afferent axon collaterals in lamina IX (Alvarez et al., 2011), resulting in the permanent detachment of boutons expressing the vesicular glutamate transporter 1 (VGLUT1), known to be specific for group Ia/II in the ventral horn (Alvarez et al., 2004; Vincent et al., 2017). However, in nerve crush there is actually an enhancement in the stretch-reflex (Prather et al., 2011) explained by better preservation of the Ia afferents on crushed MNs and a decrease in presynaptic inhibitory boutons (p-boutons) (Schultz et al., 2017).

Concurrently, axotomized sensory and motor axons release a host of different inflammatory signaling molecules, one of which is the colony stimulating factor 1 (CSF1), which result in the hypertrophy and proliferation of microglia cells in both the dorsal and ventral horn of the spinal cord (Raivich et al., 1994; Guan et al., 2016). The dorsal response has been analyzed mainly in relation to neuropathic pain mechanisms. In the ventral horn, hyperactive microglia cells surround axotomized and have been suggested to be involved in the stripping of

synaptic inputs from their surface (Blinzinger and Kreutzberg, 1968; Siskova et al., 2010; Kettenmann et al., 2013), though their direct role in synaptic removal remains a topic of debate (Svensson and Aldskogius, 1993; Svensson et al., 1993; Berg et al., 2013). Recently, we proposed an alternative explanation in which activated microglia release CCL2 and recruit infiltrating CD45^{high} CCR2+ cells, which are necessary for the permanent withdrawal of Ia afferent axons in the ventral horn and removal of these synapses from MN dendrites in mice that underwent a sciatic nerve transection. We also found that CCL2, the main ligand of CCR2, is upregulated in both MNs and microglia but with different time courses. CCL2 expression in microglia was better co-related temporarily with the infiltration of CCR2+ monocytes. Additionally, in CCR2 KO mice, we could significantly reduce the number of infiltrating CCR2+ monocytes in the spinal cord and that this resulted in preservation of Ia inputs on the dendritic arbor of axotomized MNs. These findings suggest that microglia activation and release of CCL2 recruits CCR2+ monocytes into the spinal cord and that both cellular mechanisms (microglia activation and CCR2+ monocyte infiltration) are necessary for the disappearance of Ia axon synapses from the ventral horn. This begs the question of how central neuroinflammation differs between injuries that induce permanent removal of Ia afferents from the ventral horn or not.

In the current study, we compared the neuroinflammatory response in sciatic nerve cut-repair (SR) and crush (SC) injuries in dual heterozygous transgenic mice that express EGFP under the CX3CR1 promoter to identify microglia cells (Jung et al., 2000) and RFP expression under the CCR2 promoter

to identify infiltrating myeloid cells (Saederup et al., 2010; Ajami et al., 2011; Ullrich et al., 2014; Rotterman et al., 2018). We hypothesized that the extent of this plasticity and permanency of Ia afferent connectivity is related to the severity of the nerve injury sustained and the success of peripheral regeneration as defined by the rate of axon regeneration and the specificity of targeted reinnervation. If this is the case, we predict that the properties of central neuroinflammation inside the spinal cord induced by different injuries might vary in either the degree of microglia activation and/or the extent of recruitment of peripheral CCR2+ monocytes into the spinal cord. If these hypotheses were validated this would provide evidence for a mechanism by which graded central neuroinflammatory responses mediate more or less circuit plasticity in the spinal motor network to adjust for the efficiency, speed and specificity of regeneration in the periphery.

4.3 Methods

All experiments were performed at Emory University and were approved by the Institutional Animal Care and Use Committee.

4.3.1: Transgenic mouse models:

All animal experiments were performed in adult C57Blk/6J and N mixed background mice (approximately 3 months of age; 20-25g). Both males and females were included in all experiments. All transgenic lines, unless otherwise stated, were purchased from the Jackson Laboratory (Bar Harbor, ME) and

colonies were generated and maintained at Emory University. We used the *Cx3cr1^{EGFP}* mouse (RRID: IMSR JAX:005582) to identify central microglia in the CNS. The *Ccr2^{RFP}* mouse (RRID: IMSR JAX:017586) was used to identify infiltrating myeloid cells, derived from the periphery, that had been recruited to the spinal cord. Dual heterozygous mice were created by crossing *Cx3cr1^{EGFP/EGFP}* mice with *Ccr2^{RFP/RFP}* to generate *Cx3cr1^{EGFP/+}::Ccr2^{RFP/+}* mice used for experimentation.

We used the *Ccl2^{RFP Flox}* mice (RRID: IMSR JAX:016849) to compare CCL2 expression between cut and crush injuries. This mouse expresses the mCherry protein under the *Ccl2* promoter, and flanking *loxP* sites around exons 2-3 of the CCL2 gene (Shi et al., 2011).

4.3.2: Motoneuron labeling and peripheral nerve injury procedures

Mice were anesthetized with isoflurane (induction: 4%; maintenance: 2%, both in 100% O₂) and were given a subcutaneous injection of buprenorphine (0.05 – 0.10 mg/kg) prior to the injury. The left lateral gastrocnemius (LG) muscle was exposed and injected with 5 µl of 1.5% Fast Blue (Polysciences, Eppelheim, Germany) or 5 µl of 0.1% Cholera Toxin subunit B conjugated to an Alexa Fluor 555 (CTB-555) using a 10 µl Hamilton syringe. The muscle and skin were realigned and sutured back together. Approximately one week later, after the retrograde tracer had been transported to the MNs in the spinal cord, mice underwent either a sciatic nerve cut followed by an immediate repair (SR) or a nerve crush (SC) injury. In sham controls, the sciatic nerve was exposed but not injured.

Mice were anesthetized and the left hindlimb was secured and a medial vertical incision was made, relative to the femur bone. The exposed biceps femoris muscle was retracted exposing the sciatic nerve. Surrounding connective tissue was bluntly dissected and a small silicone rubber scaffolding matrix (approximately 1mm², Dow Corning #501-1) was placed under the nerve. The nerve was then completely transected using fine surgical scissors, leaving only a piece of the epineurium intact. The nerve was then realigned and glued back together using a fibrin glue mixture composed of thrombin, fibronectin, and fibrinogen (Guest et al., 1997). For crush injuries, the sciatic nerve was exposed in the same manner. A fine pair of #5 forceps were used to compress the nerve for 10 seconds. Dissected muscle and skin were sutured back together using absorbable suture.

4.3.3: Harvesting tissue for histological analysis

Muscles and spinal cords were collected from mice at five different time points post injury: 3 days, 7 days, 14 days, 21 days, and 8 weeks. Mice were deeply anesthetized with Euthasol (≥100 mg/kg) and transcardially perfused with 10-15 ml of heparin vascular rinse followed by 25 mls of 4% paraformaldehyde (PFA) prepared in 0.1M phosphate buffer (PB, pH = 7.4). The LG muscle was collected from the left hindlimb and the spinal cord was dissected out of the spinal column. Both tissues were placed in 4% PFA overnight at 4°C. The tissues were rinsed with PB and cryo-protected in 30% sucrose at 4°C for at least 24 hours before being sectioned.

The lumbar regions 4 and 5 (L4-L5) of the spinal cord were blocked out and mounted on a freezing sliding microtome. We cut and collected 50 μm thick sections in 0.01M phosphate buffer saline (PBS) solution to process for immunohistochemistry (IHC) free floating. For muscle tissue sectioning, the LG was covered in an O.C.T. solution and frozen at -20°C . We cut 30 μm thick sections on a cryostat (ThermoFisher HM550) and collected directly on charged (+) slides. All muscle labeling and immunohistochemistry (IHC) was performed directly on the slide.

4.3.4 Histological processing and immunohistochemistry

For both spinal cord and muscle, we performed triple immunocytochemical labeling methods. All primary antibodies used in experiments are presented in table 1. We prepared a cocktail of antibodies containing chicken anti-EGFP (1:1000, RRID#: AB_620519) for CX3CR1-EGFP enhancement, rabbit anti-DsRed (1:1000, RRID#: AB_10013483) for CCR2-RFP enhancement, and guinea pig anti-VGLUT1 (1:1000, RRID#: AB_887878) for detection of Ia afferent synaptic inputs. Spinal cord sections were washed in 0.01M PBS with 0.3% Triton X-100 (PBS-Tx) and incubated in 10% normal donkey serum (NDS) blocking agent for one hour at room temperature (RT). Serum was aspirated off and a cocktail of primary antibodies, all prepared in PBS-Tx, were added. Sections were gently agitated at RT for approximately 24 hours. Primary antibodies were aspirated off and after tissue sections were washed in PBS-Tx, and a cocktail of specie specific secondary antibodies for immunofluorescence detection were added.

All secondaries were raised in donkey (Jackson ImmunoResearch Labs, West Grove, PA) and were diluted to 1:100 in PBS-Tx. We used FITC (anti-chicken IgY, RRID#: AB_2340356) for EGFP amplification, Cy3 (anti-rabbit IgG, RRID#: AB_2307443) for RFP enhancement, and DyLight 647 (anti-guinea pig IgG, RRID#: AB_2340476) for VGLUT1 immunodetection. After a two-hour incubation, the sections were washed in PBS, mounted on slides, and coverslipped with Vectashield (H-1000, Vector Labs, Burlingame, CA).

For muscle, the tissue was outlined with a pap pen and slides were placed in a hydration incubation chamber. The IHC procedures were the same as in spinal cord however all washes and incubation occurred directly on the slides with no agitation. We used chicken anti-neurofilament H (1:1000, RRID#: AB_2313552) for detection of peripheral motor axons and guinea pig anti-vesicular acetylcholine transporter (VACht) (1:100, RRID#: AB_10893979) for labeling the presynaptic motor axon terminals. We also used a bungarotoxin-555 (Btx-555, RRID#: AB_2617152) to stain post-synaptic nicotinic receptors at the neuromuscular junction (NMJ). Antibody reactive sites were revealed with FITC (anti-Chicken IgG, RRID#: AB_2340356) and Alexa Fluor 647 (anti-guinea pig IgG, RRID#: AB_2340476).

4.3.5: Densitometric analysis of VGLUT1 and GFP immunofluorescence

Six spinal cord sections were randomly selected that contained pre-labeled FB+ MNs, indicating they were from the L4-L5 region of the spinal cord. All sections were imaged at low magnification (10x1, N.A. 0.40, z-step: 1.5 μ m) on an Olympus FV1000 confocal microscope. Both the ipsilateral and

contralateral sides were imaged using identical parameters and stack sizes. Image files were uploaded to ImageJ and a region of interest (ROI) with a diameter of 270 μm was placed around the motor pool in the middle of the image stack on the ipsilateral side and on the contralateral side of the spinal cord. The VGLUT1 and GFP fluorescence integrated pixel densities were measured and compared between the two sides and presented as a ratio (Fig 1E).

4.3.6: Neuromuscular junction analysis

Fifty randomly selected NMJs were analyzed per animal (4 mice per condition). Each NMJ was imaged (20x, N.A. 0.75, z-step: 1.0 μm) on an Olympus FV1000 confocal microscope. Each image was uploaded to ImageJ and each Btx-555 labeled neuromuscular junctions were scored on two criteria: 1) was NF-H present in the NMJ (yes or no) and 2) was there VACHT immunoreactivity in the NMJ (fully, partially, or none). A percent was generated per total 50 NMJs based on these criteria.

4.3.7: Motoneuron reinnervation

The LG muscle was first injected with FB to pre-label the MNs in the spinal cord. Approximately one week later the sciatic nerve was either cut and repaired or crushed. Mice were allowed to survive 8 weeks at which point the LG muscle was injected with CTB-555. Mice survived another week before being perfused and processed. The entire lumbar segment from spinal cords were serially sectioned, collected on slides, and stained with Nissl-647 overnight at RT in a hydration chamber. Slides were washed in 0.01M PBS (no triton) and cover-

slipped with Vectashield. The slides were analyzed on an Olympus BX-53 wide-field fluorescence microscope NeuroLucida imaging system. A contour was drawn around each individual spinal cord section containing labeled MNs. Then, the number of FB+ only, CTB-555+ only, or dual labeled MNs were plotted for each section. When all sections had been analyzed each contour was uploaded in the NeuroLucida and we aligned each contour to create a 3D representation of the rostral-caudal distribution of MNs throughout the lumbar region. We also calculated and compared the percent of dual labeled MNs in each condition. MN cell counts were performed in 4 animals in each condition. We obtained a XY coordinate for each plotted MN. These data were uploaded to a custom Matlab script (a kind gift from the laboratory of Dr. Tom Jessell) to generate heat map plots to compare the changes in distribution of MNs before and after injury. Heat maps contain 9 contours with the innermost representing the 15th percentile and the outermost representing the 95th percentile.

4.3.8: EdU injections and Ki-67 labeling

After SR or SC, mice were injected with 5-ethynyl-2'-deoxyuridine (EdU, injected i.p., 50 mg/kg) at either 2 days post injury and perfused 24 hours later (3 day time point) or injected at 6 days post injury and perfused 24 hours later (7 day time point). We used the Click-iT EdU Alexa Fluor 647 imaging kit for EdU detection (ThermoFisher Scientific, cat# C10340) and processed the spinal cord sections according to the manufacturers protocol. Following the Click-iT reaction, spinal cord sections were incubated in a cocktail of primary antibodies consisting of chicken anti-EGFP (1:1000, RRID#: AB_620519) and mouse anti-Ki-67 (1:100,

RRID#: AB_393778) then revealed with FITC (anti-chicken IgY, RRID#: AB_2340356) and Cy3 (anti-mouse IgG, RRID#: AB_2340759). Ipsilateral L4-L5 spinal cord sections were selected at random and imaged using automatic tiling on an Olympus FV1000 confocal microscope (20x, N.A. 0.75, z-step: 1.0 μm). Each image consisted of six tiles stitched together using the Olympus multi-area time lapse module. These image files were then uploaded to NeuroLucida for analysis. We manually counted the number of CX3CR1+/EdU+ and CX3CR1+/Ki-67+ cells in the ventral horn of the spinal cord in six sections per animal.

4.3.9: Quantification of microglia cells

Randomly selected L4-L5 sections, containing FB+ MNs, were imaged and tiled on the Olympus confocal (20x, N.A. 0.75, z-step: 1.0 μm) (n = 4 mice, 6 sections per animal). Image files were then uploaded to the Imaris 3D neural analysis software (ver. 7.2.2, Bitplane, Zurich, Switzerland). We used the “spot function” algorithm to automatically detect and count the cell bodies of CX3CR1+ cells in the ventral horn of the spinal cord (both grey and white matter) in a 50 μm thick tissue section. The ventral horn was defined by an arbitrary horizontal line drawn directly above the central canal. We quantified six spinal cord sections from 4 animals at each time point.

4.3.10: CCR2-RFP cell quantification

We manually counted CCR2⁺ cells using an epifluorescence widefield Olympus BX52 microscope (20x, N.A. 0.75). Cell numbers are represented as the average number of cells per 50 μm thick section. For the CCR2⁺ cell time course, all sections containing at least one FB⁺ MN were quantified (n = 4 mice)

4.3.11: Experimental design and statistical analysis

In these experiments, both male and female animals were included. Three to four mice were analyzed at each time point in the time course experiments. We then used a two-way ANOVA to reveal significant differences between injury type (sham, cut, or crush) and time (3 days, 7 days, 14 days, 21 days, and 8 weeks). Post-hoc Bonferroni t-test were used for pair-wise comparisons. In cases where normality failed (indicated in the text) we used a non-parametric Kruskal-Wallis one-way ANOVA on ranks followed by a Dunn's Method post-hoc analysis. For experiments in which single time points were investigated comparing different injury types (sham, cut, and crush; VGLUT1 density, muscle reinnervation, and CSF1 experiments) we used a one-way ANOVA followed by a Bonferroni post-hoc pair-wise t-test to investigate differences. For two variable comparisons, we used a two-tailed Student's t-test. All alpha values were set at 0.05.

4.4: Results

4.4.1: VGLUT1 synapse depletion on motoneurons following sciatic nerve cut-repair or sciatic nerve crush

To analyze structural changes in the Ia afferent projection to the ventral horn after either sciatic crush (SC) or sciatic cut and repair (SR) we compared lamina IX VGLUT1 fluorescence, ventral horn VGLUT1 axon projections and VGLUT1 synapse densities on LG MNs after each type of injury. VGLUT1 fluorescence was estimated at different time points by measuring VGLUT1 integrated pixel density in low magnification confocal images (10x, N.A. 0.4) in regions of interest (ROI) around the Fast Blue (FB) retrogradely labeled LG motor pool in the spinal cord side ipsilateral to the injury (Fig. 1A1-A3) and a mirror-image ROI on the contralateral side. The ratio between the two sides was then calculated (Fig. 1B; $n = 4$ mice per time point / injury type, 6 sections per animal). Control mice showed no difference between both sides (*control values correspond to data from a previous analysis*). Similar to the changes described after sciatic nerve transection followed by ligation (*previous analyses*), lamina IX VGLUT1 fluorescence density was also significantly decreased ipsilateral to the injury 7, 14, and 21 days after SC or SR (two-way ANOVA, time: $F(5, 47) = 16.512$, $p < 0.001$, post-hoc Bonferroni t-test vs control, 7 day: $t = 3.656$, $p = 0.012$; 14 days: $t = 6.275$, $p < 0.001$; 21 days: $t = 7.303$, $p < 0.001$). The decrease was not significantly different between both injuries during the first three weeks after injury (t-test; 7 days: $t = 0.203$, $p = 0.840$; 14 days: $t = 0.680$, $p = 0.501$; 21 days: $t = 0.014$, $p = 0.989$). However, by 8 weeks there was no difference in

VGLUT1 lamina IX fluorescence between both sides after SC, although it remained significantly depleted in the ipsilateral side after SR. Thus, ipsi- vs. contralateral side ratios were no different to control animals after SC (t-test, $t = 1.004$, $p = 1.000$) but were significantly different after SR (cut t-test, $t = 5.477$, $p < 0.001$) (Fig. 1B). These data suggest that after SC there is a temporary decrease in VGLUT1 content in lamina IX around affected motor pools, but VGLUT1 returns by 8 weeks post injury. VGLUT1 fluorescence analyses can be influenced by regulation of VGLUT1 content. Previously, we reported that the loss of VGLUT1 in lamina IX is associated with the withdrawal of Ia axon collaterals (Alvarez et al., 2011). Therefore, we used VGLUT1^{Cre/+} animals crossed with Ai9R26 tdTomato reporter mice to genetically induce a permanent label of Ia axons and synapses. In these mice, tdTomato labels the projections of Ia fibers (and possibly type II fibers) in the ventral horn and the labeling, once induced by VGLUT1 expression during development, becomes independent of later fluctuations in VGLUT1 (Fig. 1C1). We found in these animals that 8 weeks after SR many VGLUT1 axon projections to lamina IX were removed (Fig. 1C2), but these were maintained after SC (Fig. 1C3).

The loss in VGLUT1 fluorescence intensity is also consistent with both a loss of synaptic boutons and with synaptic VGLUT1 clusters becoming smaller, as previously shown after nerve transections (Alvarez et al., 2011; previous chapters). To estimate VGLUT1 synapse losses we captured high magnification (60x, N.A. = 1.35) confocal image stacks of retrogradely labeled FB+ MNs, reconstructed the soma and proximal dendrites in Neurolucida and mapped all

VGLUT1-IR boutons in direct contact with the MN surface (Fig. 1D1-D4) to calculate a somatic and dendritic linear VGLUT1 density (n = 4 mice, 6 MNs per animal) (Fig. 1E, F). We estimated VGLUT1 densities on reconstructed MNs 21 days and 8 weeks after SC to test for possible transient losses while we analyzed MNs after SR only at 8 weeks after injury. We found that at 21 days there was a 32% decrease in VGLUT1 soma density compared to controls (post-hoc Bonferroni t-test vs control, $t = 4.336$, $p = 0.004$) and a 23% decrease in VGLUT1 linear density (post-hoc Bonferroni t-test vs control, $t = 3.883$, $p = 0.010$) (Fig. 1E, F), but both recover to control levels after eight weeks (post-hoc Bonferroni t-test vs control, somatic density: $t = 0.341$, $p = 1.000$, dendritic density: $t = 1.100$, $p = 1.000$). However, 8 weeks after SR there was a 63% depletion in somatic VGLUT1 synapses (post-hoc Bonferroni t-test vs control, SR: $t = 8.534$, $p < 0.001$) and a 34% drop in VGLUT1 dendritic linear density (post-hoc Bonferroni t-test vs control, SR: $t = 5.714$, $p < 0.001$). The results support the conclusion that following SC there is a transient detachment of VGLUT1 synapses that return by 8 weeks post injury, while complete transection induces a permanent loss of VGLUT1 synapses, likely because their axons are fully removed from the ventral horn preventing any possibility of synapse recovery in lamina IX.

To investigate any preferential loss in synapses along the dendrite, we performed a Sholl Analysis to calculate changes in VGLUT1 density at three different distances (25 μm , 50 μm , and 75 μm) along the dendrite 8 weeks after SC or SR compared to controls (Fig. 1G). At no distance was there any difference between sham controls and SC (one-way ANOVA; 25 μm : $F(2, 13) =$

20.659, $p < 0.001$, post-hoc Bonferroni t-test control vs SC, $t = 0.785$, $p = 1.000$; 50 μm : $F(2, 13) = 19.136$, $p < 0.001$, post-hoc Bonferroni t-test control vs SC, $t = 1.281$, $p = 0.679$; 75 μm : $F(2, 13) = 16.982$, $p < 0.001$, post-hoc Bonferroni t-test control vs SC, $t = 1.982$, $p = 0.219$) (Fig. 1G) . However, at all three distances along the dendritic the SR injury resulted in a significant depletion in VGLUT1 synapses (post-hoc Bonferroni t-test control vs SR, 25 μm : $t = 6.161$, $p < 0.001$; 50 μm : $t = 5.034$, $p = 0.001$; 75 μm : $t = 4.230$, $p = 0.004$) (Fig. 1G).

Previously, we found that nerve transection of the sciatic nerve caused a larger loss of VGLUT1 synapses compared to the same injury in the tibial nerve and we interpreted these different levels of VGLUT1 synapse plasticity in relation to the different numbers of MNs and sensory afferents affected by the injuries. We therefore counted the number of MNs expressing the immediate early gene activating transcription factor 3 (ATF3) after a SC or SR injury and calculated the percent of all pre-labeled FB+ LG MNs co-expressing ATF3, seven days after injury (Fig. 1H1, H2). ATF3 is only expressed after axotomy and is undetectable on the side contralateral to the injury or in sham controls (Tsujino et al., 2000). We found that in 50 μm thick spinal cord sections an average of 21.45 ± 1.33 (S.E.) MNs express ATF3 after SR and 19.08 ± 0.95 MNs after SC ($n = 4$ mice per condition) (Fig. 1I). These differences were not statistically significant (Student's t-test, $t(6) = 1.451$, $p = 0.197$). After SR, $93.1\% \pm 1.2$ of all FB+ MNs express ATF3 and $84.1\% \pm 5.1$ after SC, which was not significantly different either (Fig. 1J, Student's t-test, $t(6) = 1.735$, $p = 0.134$). Based on these data, we conclude that SR and SC injuries axotomize similar numbers of motor axons and

therefore difference in VGLUT1 axon and synapses plasticity between these two injury models are not related to different numbers of injured axons.

4.4.2: Rate and specificity of peripheral nerve regeneration and reinnervation predict the permanency of VGLUT1 loss

We compared peripheral nerve regeneration and reinnervation in both injuries based on two outcome measures. 1) Rate at which peripheral motor axons reinnervate vacated neuromuscular junctions (NMJs) and 2) how efficient motor axons reinnervate their original muscle target. To compare the time course of motor axon degeneration and reinnervation to the LG muscle, motor axons in muscle were identified by the expression of neurofilament-H (NFH) and the presence of a motor-end plate containing vesicular acetylcholine transporter (VACHT), both opposite to NMJs labeled by binding of α -bungarotoxin conjugated to an Alexa fluor-555 (BTX-555) to postsynaptic nicotinic receptors (Fig. 2A-B). Fifty randomly selected NMJs per animal (n = 4 mice per condition) were scored as either having NFH innervation or not and by the extent of coverage of the BTX-555 labeled NMJ by presynaptic VACHT (none, partial, full or complete). In sham control mice, 99% \pm 0.6 of NMJs were innervated by NFH motor axons and fully covered by presynaptic VACHT. After nerve injuries there was a significant drop in NFH motor innervation 3 and 7 days post SC and SR (Kruskal-Wallis one-way ANOVA on Ranks, SC: $H(5) = 19.829$, $p = 0.001$, post-hoc Dunn's Method; 3 day: $Q = 3.314$, $p < 0.05$, 7 day: $Q = 3.232$, $p < 0.05$; SR:

H(5) = 18.645, $p = 0.002$, 3 day: $Q = 3.102$, $p < 0.05$ 7 day: $Q = 3.310$, $p < 0.05$) (Fig. 2C) and essentially all presynaptic VAcHT labeling had disappeared (Kruskal-Wallis one-way ANOVA on Ranks, SC: H(5) = 20.280, $p = 0.001$, post-hoc Dunn's Method; 3 day: $Q = 3.571$, $p < 0.05$, 7 day: $Q = 3.440$, $p < 0.05$; SR: H(5) = 19.601, $p = 0.001$, 3 day: $Q = 2.711$, $p < 0.05$, 7 day: $Q = 3.128$, $p < 0.05$) (Fig. 2D). Remaining NFH axons showed signs of being in the process of degeneration (varicose, segmented...). Extensive re-innervation was obtained 14 days after SC injury. At this time point the percentages of NMJs with presynaptic NFH motor axons and presynaptic VAcHT+ motor-end plates that partially or fully occupied the BTX-555 NMJ receptor field were not significantly different to controls (for NFH innervation: $Q = 2.346$, $p > 0.05$; for partially or fully VAcHT-covered NMJs: $Q = 2.971$, $p < 0.05$). Re-innervation was slower after SR, between 14 and 21 days after SR some motor axons began to reinnervate vacated NMJs but were still significantly more depleted compared to SC and VAcHT+ motor end plates had not yet formed. By 8 weeks after either injury, >80% of BTX-555 labeled NMJs had a presynaptic axon and displayed a presynaptic VAcHT+ motor end-plate. Their frequency was not significantly different to controls. These data demonstrate that both injuries result in a similar degeneration of motor axons in the first week following injury, though SC injury results in a faster rate of motor axon regeneration and re-innervation compared to SR; extensive re-innervation occurs 2 weeks after SC, but not after SR.

To investigate the specificity of muscle target reinnervation we first injected the LG muscle with Fast Blue (FB) and one week later performed either

a SC or SR injury. We then waited 8 weeks until peripheral regeneration was near completeness in both injuries and then injected the LG with Cholera Toxin subunit B conjugated to an Alexa Fluor-555 (CTB-555). The distribution of MNs with each fluorochrome was mapped throughout the lumbar enlargement (lumbar 1 to 6) (Fig. 3). FB+ MNs represent the original LG motor pool, while CTB-555+ MNs represent MNs that reinnervated the LG after nerve injury. In control sham operated animals $81.4\% \pm 7.7$ (\pm SE) of FB+ MNs co-expressed CTB-555 (Fig. 3B). Some single labeled cells are always expected due to either poor uptake of either FB or CTB-555 tracer, or uncontrollable small leakage out of injected muscles with uptake in surrounding muscles. After SC there was a trend towards a lower percentage of FB+ MNs containing CTB-555 ($66.6\% \pm 6.7$), but it did not reach significance compared to controls ($t = 1.788$, $p = 0.335$). This suggests that regeneration after SC injuries does not result in major changes in the composition of the LG motor pool. However, 8 weeks after SR only $22.3\% \pm 2.1$ of FB+ MNs co-express CTB-555), suggesting a major significant change in the nature of MNs innervating the LG muscle after the injury (one-way ANOVA, $F(2, 10) = 29.411$, $p < 0.001$, post-hoc Bonferroni t-test, $t = 7.142$, $p < 0.001$).

The specificity of Ia afferent inputs is in large part defined by the spatial localization of the motor pools (Jessell et al., 2011). To investigate whether erroneous motor axon targeting in the periphery strongly disrupted motor pool spatial organization we compared the distribution FB+ and CTB-555+ MNs in transverse-section cell maps (Fig. 3C) and generated cell density contours to compare the distribution of LG MNs in the transverse plane prior to injury (FB+)

and 8 weeks after either SC or SR (CTB-555+) (Figs 3D-F). In addition, we compared the rostro-caudal distribution of labeled MNs before and after regeneration following the different injuries. A significant population of CTB-555 only labeled cells appeared after injury. After SC these were located slightly more lateral to original LG pool in regions that could correspond to other triceps surae pools, like medial gastrocnemius and soleus (Fig. 3C2). In contrast after SR we found CTB-555 MNs all around the original FB+ labeled pool. To estimate quantitatively differences in distribution we measured the area occupied by outermost cell density contours corresponding to 95% of labeled populations (Fig. 3D1, D2, E1, E2, F1, F2). We found no significant differences when comparing the FB+ and CTB-555 LG MNs in sham control mice (t-tests, area: $t(6) = 0.104$, $p = 0.921$) (Fig. 3G). Following regeneration after a SR injury the extension occupied by CTB-555 LG MNs expanded with respects to FB+ MNs and resulted in significant changes in area (t-test, $t(6) = -5.114$, $p = 0.002$). Interestingly, we also found a significant increase in area after SC (t-test, $t(6) = -5.114$, $p = 0.002$), however, this increase was significantly smaller compared to after SR (t-test, $t(6) = -3.152$, $p = 0.020$). We did not find significant differences in the rostro-caudal distribution of MNs labeled before or after in sham controls or after either injury (Fig. 3H, I). These data suggest that both crush and cut result in varying degrees of reorganization of the LG motor pool. The position of novel cell body locations innervating the LG after SC suggests confinement to close synergist in the triceps surae column. In contrast, after SR, CTB-555 MNs

surround the original FB+ pool in all directions and occupy a larger area (Fig. 3A3, C3).

In conclusion, regeneration after SR injuries result in delayed reinnervation of NMJs compared to SC and in a larger disorganization of motor pool maps inside the spinal cord.

4.4.3: The activation and proliferation of microglia cells in the ventral horn of the spinal cord after nerve injury

To compare the microglia response in the ventral horn following SC or SR we used CX3CR1-EGFP mice and performed densitometry analyses to compare average microglia EGFP fluorescence between the spinal cord sides ipsilateral and contralateral to the injury. We measured integrated pixel densities in a region of interest (ROI) defined by the retrogradely labeled LG motor pool (n = 3-4 mice, 6 sections per animal) (Fig. 4 A1-2, B1-2). By three and seven days after injury, we detected a significant increase in EGFP fluorescence in both SC and SR animals (Kruskal-Wallis one-way ANOVA on Ranks, SC: $H(5) = 19.975$, $p = 0.001$, post-hoc Dunn's Method; $Q = 3.393$, $p < 0.05$; SR: $H(5) = 21.526$, $p < 0.001$, post-hoc Dunn's Method; $Q = 3.393$, $p < 0.05$) (Fig. 4D). By 14 days post SC the microglia response returned to near control levels ($Q = 2.279$, $p > 0.05$) while the SR reaction remained significant higher than the controls ($Q = 3.899$, $p < 0.05$) and significantly higher compared to SC animals (t-test, $t(6) = -11.200$, $p < 0.001$) (Fig. 4D). By 21 days, the microglia response in the SR animals began

to return towards control levels, though the reaction was still significantly higher compared to SC mice (t-test, $t(6) = -4.449$, $p = 0.004$) (Fig. 4D). By 8 weeks the fluorescence values had returned to control levels in both injury types. This increase in fluorescence was parallel by similar increases in microglia cell numbers. We used the “spot function” algorithm in Imaris to automatically quantify the number of CX3CR1⁺ cells in the ventral horn of spinal cord sections imaged and tiled at 20x using confocal microscopy (n = 4 animals per condition, 6 spinal cords per animal) (Fig. 4C). Sham control mice had an average of 200.8 ± 16.9 CX3CR1⁺ cells per ventral horn in a 50 μm thick section (Fig. 4E). After SC or SR there was a significant increase in the number of cells at 3 days (SC: 288 ± 18.18 , SR: 277.71 ± 15.31 ; two-way ANOVA, time x injury: $F(5, 47) = 3.405$, $p = 0.013$, post-hoc Bonferroni t-test, SC: $t = 3.401$, $p = 0.008$; SR: $t = 2.998$, $p = 0.025$,) and 7 days post injury (SC: 301.92 ± 34.31 ; SR: 316.46 ± 10.89 ; SC: $t = 3.928$, $p = 0.002$; SR: $t = 4.493$, $p < 0.001$). There was no difference in microglia cell numbers between the two injury models at either time point (3 days: $t = 0.413$, $p = 0.682$, 7 days: $t = 0.565$, $p = 0.576$) (Fig. 4E). By 14 days, microglia cell counts return to near control levels after SC ($t = 1.105$, $p = 1.000$) while the number of CX3CR1⁺ cells in SR injured mice remained significantly greater compared to controls ($t = 5.491$, $p < 0.001$) and to the SC counts ($t = 4.386$, $p < 0.001$) (Fig. 4E). By 21 days post SR the number of CX3CR1⁺ cells returned towards control levels but were still significantly higher than controls ($t = 3.016$, $p = 0.023$) and to SC animals ($t = 3.540$, $p = 0.006$) (Fig. 4E). By 8 weeks post injury, the number of CX3CR1⁺ cells had returned to

values similar to controls after either injury (SC: $t = 0.178$, $p = 1.000$; SR: $t = 0.822$, $p = 1.000$).

To answer the question of whether the longer time course of the microglia reaction after SR compared to SC was due to an elongation of the proliferation period we performed either a SC or SR and injected mice with the thymidine homologue, 5-ethynyl-2'-deoxyuridine (EdU) 2 days post injury and perfused at 3 days or injected on day 6 post injury and perfused on day 7 to reveal EdU labeled proliferating microglia in the spinal cord ($n = 1$ mouse, 6 sections per animal) (Fig. 4F1, F2, G1, G2). In addition, we immunolabeled some sections with the "S-phase" cell cycle marker Ki-67 (Fig. 4H1, H2, I1, I2). Tiled confocal images of the ventral horn were uploaded to NeuroLucida and we manually quantified the percent of CX3CR1+ cells that expressed EdU or Ki-67. In these experiments, the level of microgliosis at 3 and 7 days replicated previous observations (Fig. 4J). Three days after SC, $40.07\% \pm 4.38$ of CX3CR1 cells were EdU+ (Fig. 4K) and $59.72\% \pm 1.67$ were Ki-67+ after injury (Fig. 4L). In the SR animals, $35.95\% \pm 6.30$ of all CX3CR1 cells were EdU positive (Fig. 4K) and $50.80\% \pm 3.18$ were Ki-67+ 3 days after injury (Fig. 4L). The majority of these dual labeled cells were located around the motor pool in lamina IX with very few dual labeled cells in the white matter area and in laminae VII, VIII, or X. The number of proliferating microglia dramatically decreases 7 days after either injury, estimated with either EdU or Ki67. In SC mice, $3.92\% \pm 0.94$ of CX3CR1+ cells were EdU+ and $4.34\% \pm 0.82$ were Ki-67+, a very significant decrease from 3 days post injury (EdU+: t-test, $t(10) = 18.583$, $p < 0.001$; Ki-67: t-test, $t(10) =$

29.759, $p < 0.001$) (Fig. 4K, L). By 7 days post injury in SR mice, only $4.84\% \pm 0.56$ of CX3CR1+ cells were EdU+ and $4.30\% \pm 0.46$ were Ki-67+, also a significant decrease from 3 days (EdU+: Mann-Whitney Rank Sum Test, $t = 57.000$, $p = 0.002$; Ki-67: Mann-Whitney Rank Sum Test, $T = 57.000$, $p = 0.002$) (Fig. 4K, L). These data suggest that microglia proliferation is very similar after SC or SR and does not explain the differences in the time course of microgliosis or the fact that peak microglia numbers occur one week later after SR (at 14 days) compared to SC (7days). The microglia reaction following SR is significantly more robust compared to SC at 14 and 21 days post injury. Therefore, the longer microglia response after SR must be due to delayed microglia apoptosis and migration (Tay et al., 2017).

4.4.4: The release of CCL2 and the recruitment of peripheral CCR2+ myeloid cells following sciatic injury

We previously found a significant infiltration of CCR2+ macrophages in the ventral horn of the spinal cord with a peak around 14-21 days following a complete transection and ligation of the sciatic nerve. The recruitment of these cells was dependent on expression and release of the CCL2 ligand from MNs and microglia after injury and was directly related to the loss of VGLUT1 synapses. We therefore compared CCL2 expression and infiltration of CCR2+ cells after both types of injuries.

We compared CCL2 expression in MNs and microglia 14 days after injury, a time point where MNs and microglia are known to express CCL2 after a sciatic nerve cut-ligation injury (Rotterman et al., 2018) in mice expressing mCherry under the CCL2 promoter. We found that both SR and SC resulted in expression of CCL2 from MNs (Fig. 5A1, A2, C1, C2), however microglia cells expressed CCL2 after SR injuries (Fig. 5B1, B2, D1, D2). We then analyzed infiltration of the spinal cord ventral horn by peripheral CCR2⁺ myeloid cells using CCR2-RFP mice. We counted all RFP⁺ cells in every spinal cord section (50 μ m thick) that contained at least one FB⁺ MN (n = 4 animals per condition) (Fig. 5E1, E2, F1, F2). There was a significant increase in CCR2-RFP⁺ cells inside the spinal cord after both injuries and significantly more cells after SR compared to SC (two-way ANOVA: time: $F(5, 46) = 31.031$, $p < 0.001$; injury type, $F(1, 46) = 48.143$, $p < 0.001$). CCR2⁺ cells began to infiltrate the spinal cord within the first week after injury and this was significant compared to controls given that there were essentially no CCR2⁺ cells in sham animals (post-hoc Bonferroni t-tests vs control, 3 days: $t = 3.413$, $p = 0.008$; 7 days: $t = 5.058$, $p < 0.001$) (Fig. 5G). The infiltration of these cells peaked at 14 days post injury with an average of 8.28 ± 1.72 cells in the SC (post-hoc Bonferroni t-tests vs control, $t = 4.996$, $p < 0.001$) and 25.12 ± 3.68 cells in the SR (post-hoc Bonferroni t-tests vs control, $t = 11.293$, $p < 0.001$) (Fig. 5G). The differences in CCR2⁺ cell number at 14 days were significant at 14 days (Bonferroni t-test, $t = 6.297$, $p < 0.001$) and thereafter (Fig. 5G).

These data demonstrate that following SC or SR, MNs increase expression of CCL2, however only in the completely transected animals do microglia express CCL2. Furthermore, while a small number of CCR2+ cells enter after crush, this number is significantly less compared to the robust infiltration detected in the SR animals.

4.5: Discussion

Based on these data our main conclusions are as follows: 1) the permanency of VGLUT1 loss is related to the speed and specificity of motor axon regeneration and reinnervation in the periphery. 2) SR results in a prolonged exaggerated microglia response compared to a SC injury. 3) SC does not result in a robust infiltration of peripherally derived CCR2+ myeloid cells. 4) Both SC and SR result in the release of CCL2 from MNs, however CCL2 is only released from microglia after SR injury. Taken together, the results suggest an association between the success of peripheral regeneration and the extent of neuroinflammation that is ultimately responsible for permanent VGLUT1 synaptic deletion.

4.5.1: Success of peripheral regeneration determines permanency of VGLUT1 loss

We found that SC resulted in the detachment and displacement of VGLUT1 synapses from the soma and proximal dendrites of LG MNs during the

first 3 weeks after injury, however these inputs returned by 8 weeks. The recovery of synaptic inputs coincided with a faster rate and greater specificity of muscle reinnervation after SC compared to SR. Faster innervation of muscle might occur because shorter delays at the injury site in pathfinding to find appropriate endoneurial tubes to regenerate through. Differences in targeting specificity have been previously explained by the maintenance of endoneurial tube infrastructure in the periphery, allowing the axons to be guided back to their original targets. Crush injuries nevertheless resulted in an expansion of the LG motor pool that appeared to occupy close synergist MNs in the triceps surae group (MG and soleus) (Nicolopoulos-Stournaras and Iles, 1983). This might suggest that while axon mixing can occur after our crush injuries, this might happen within individual axon fascicles inside the sciatic nerve (intrafascicular mixing), but that after nerve transection there is a large amount of interfascicular mixing. Individual nerve fascicles target closely related muscle groups, therefore any axon mixing after SC might be guided to close synergists, while after SR axons can be misguided to functionally unrelated muscle groups. After SR the motor pool significantly expands into regions associated with synergist but also antagonist muscle groups. This include regions that normally contain MNs associated with the hamstrings and the anterior crural group including tibialis anterior and extensor digitorum longus (Nicolopoulos-Stournaras and Iles, 1983). Therefore, the LG (preferentially an ankle extensor) might be innervated after regeneration by MNs that originally were preferentially related to knee flexion (hamstrings) or even antagonists involved in ankle flexion (tibialis anterior). The

functional consequences of motor pool expansion may not be as significant when it is related to re-innervation of close synergists. For example, in a study in humans undergoing ulnar or median nerve injuries it was found that orderly recruitment of motor units was preserved if regenerating MNs re-innervated the original muscle or close synergists, however, it was lost when a large number of misguided axons innervated unrelated muscle groups (Thomas et al., 1987). Preservation of orderly recruitment is a reflection of the organization of central spinal circuits controlling the patterned activation of MNs.

Similarly, following SR VGLUT1 synapses detach for MNs and VGLUT1 axons retract from the ventral horn, and they never return to the surface of the MN. This central circuit re-organization corresponds with a slower rate of muscle re-innervation and a higher rate of targeting errors compared to SC. Therefore, we propose that this permanent detachment and reorganization of the spinal motor circuitry may be a compensatory mechanism to account for the poor regenerative peripheral outcomes in SR animals. If the peripheral targets change drastically and the central connectivity is maintained there may be a higher rate of muscle co-contraction and inter-joint discoordination due to a miscommunication in sensory information and motor commands. This permanent removal of synapses in the SR model may functionally be the most appropriate response for the animal to maintain “near-normal” motor behavior.

One important factor that distinguishes the two injury models is also the timing of regeneration. A previous study by Ma et al., compared sciatic nerve crush and cut injuries and found that only cut resulted in permanent motor

deficits. However, when they genetically overexpressed a regenerative-associated protein, known as heat shock protein 27 (HSP27) in MNs, they could enhance the speed of peripheral axon regeneration after a complete transection and recovered motor function, as defined by a toe-spreading assay (Ma et al., 2011). These data suggest that timing of regeneration might be a key signal that allows preservation of motor circuits after injury. Intriguingly, the time point at which re-innervation after SC and SR is drastically different (14 days after injury) is also the time at which microgliosis starts to differ between both injuries resulting in upregulation of CCL2 and recruitment of CCR2+ cells. This might explain the preservation/recovery of VGLUT1 inputs found by enhancing speed of peripheral regeneration using exercise therapies (Brandt et al., 2015) (Brandt et al., 2015; Gordon, 2016; Gordon and English, 2016),.

4.5.2: CCL2 release from microglia results in a robust infiltration of peripheral CD45+ cells

Following a microglial reaction within the first two-weeks post SR injury, we observed a major infiltration of peripheral CCR2+ myeloid cells entering the spinal cord parenchyma 14 days post injury. However, in the SC model, the microglia reaction returned to control levels by 14 days, and we did not detect a major infiltration in CCR2+ cells. This lack of infiltration corresponds with a recovery of VGLUT1 synapses 8 weeks after injury.

While a number of peripheral immune cells can express CCR2 (Shi and Pamer, 2011), our previous work demonstrated that following a complete sciatic nerve transection, the two main CCR2 expressing cells that enter the spinal cord after sciatic nerve cut are T-cells (CD45^{Hi} CCR2⁺ CD3⁺) and macrophages (CD45^{Hi} CCR2⁺ CD11b⁺). However, when we performed SR injuries in CCR2 KO mice we did not significantly alter the infiltration of T-cells but significantly impaired the recruitment and infiltration of CCR2⁺ macrophages. This led us to conclude that these CCR2⁺ macrophages are responsible for promoting VGLUT1 loss (Rotterman et al., 2018), though the exact mechanism for removal remains to be elucidated.

Previously, we also found that MNs and microglia release the chemokine necessary for macrophage recruitment known as CCL2 following a sciatic cut-ligation injury, which led us to hypothesized that at 14 days there would be significantly greater expression of CCL2 in the spinal cord following a SR injury compared to SC. We found that at 14 days post injury MNs express low levels of CCL2 in both injury models. However, only in the SR mice did microglia cells express CCL2 while there was little to no detection of CCL2 production in microglia after crush. This led us to draw the conclusion that the release of CCL2 from MNs is not sufficient to recruit peripheral CCR2 macrophages. However, the more intense CCL2 released from microglia appears to be essential in the recruitment of peripheral CCR2⁺ macrophages. Furthermore, the release of CCL2 from microglia may be critical in the breakdown of the blood-spinal cord barrier (BSCB). Previous work by Echeverry et al., found that intrathecal delivery

of CCL2 (a.k.a. MCP-1) directly into the spinal cord of naïve rats could result in the downregulation of tight junction proteins responsible for maintaining the integrity of the BSCB (Echeverry et al., 2011), which results in leakage and the possibility for the infiltration of peripheral CCR2+ macrophage cells. The overwhelming CCL2 release from microglia in our model may serve dual roles; breaking down the BSCB and recruiting peripheral CCR2+ macrophages. The recruitments of these peripheral macrophages might be critical for the permanency of VGLUT1 synapse deletion by promoting the removals of Ia afferent axons in the ventral horn.

In conclusion, the differences in VGLUT1 synaptic plasticity after SC and SR might directly related to differences in the properties of the central neuroinflammatory response inside the ventral horn ipsilateral to the injury. These include a longer microglia reaction that allows these cells to phenotypically switch to a CCL2-releasing pro-inflammatory phenotype capable of attracting CCR2+ dependent myeloid cells. The exact mechanisms how these new cells promote the removal of Ia axons is not known but in our previous study blocking their entry was related with better preservation of VGLUT1 synapses in the ventral horn. Therefore, the characteristics of the neuroinflammatory reaction might be an adaptive mechanism to implement more or less plasticity in central spinal motor circuits depending on the efficiency of regeneration in the periphery. One critical signal appears to be whether or no motor axons are capable of significant muscle re-innervation by two weeks after injury.

Antigen	Immunogen	Host/Type	Manufacturer	RRID#	Dilution
EGFP	Recombinant GFP 6-his tag	Chicken/ Polyclonal	Serotec Cat# obt1644	AB_620519	1:1000
DsRed	Variant of <i>Discosoma</i> sp.	Rabbit/ Polyclonal	Clontech Cat# 632496	AB_10013483	1:1000
VGLUT 1	Recomm. Protein (aa 456-560)	Guinea Pig/ Polyclonal	Synaptic Systems Cat# 135304	AB_887878	1:1000
CD45	Synthetic peptide corresponding to Human CD45 aa 900-1000	Rabbit/ Polyclonal	Abcam Cat# ab10588	AB_442810	1:100
Iba1	Sequence: C-TGPPAKK AISELP	Goat/ polyclonal	Novus Cat#NB100-1028	AB_521594	1:500
Ki-67	Clone B56	Mouse/ Monoclonal	BD Biosciences Cat# 550609	AB_393778	1:100
NeuN	Clone A60	Mouse/ Monoclonal	Millipore Cat#MAB377	AB_2298772	1:500

Table 4.1: Antibodies used for immunohistochemistry

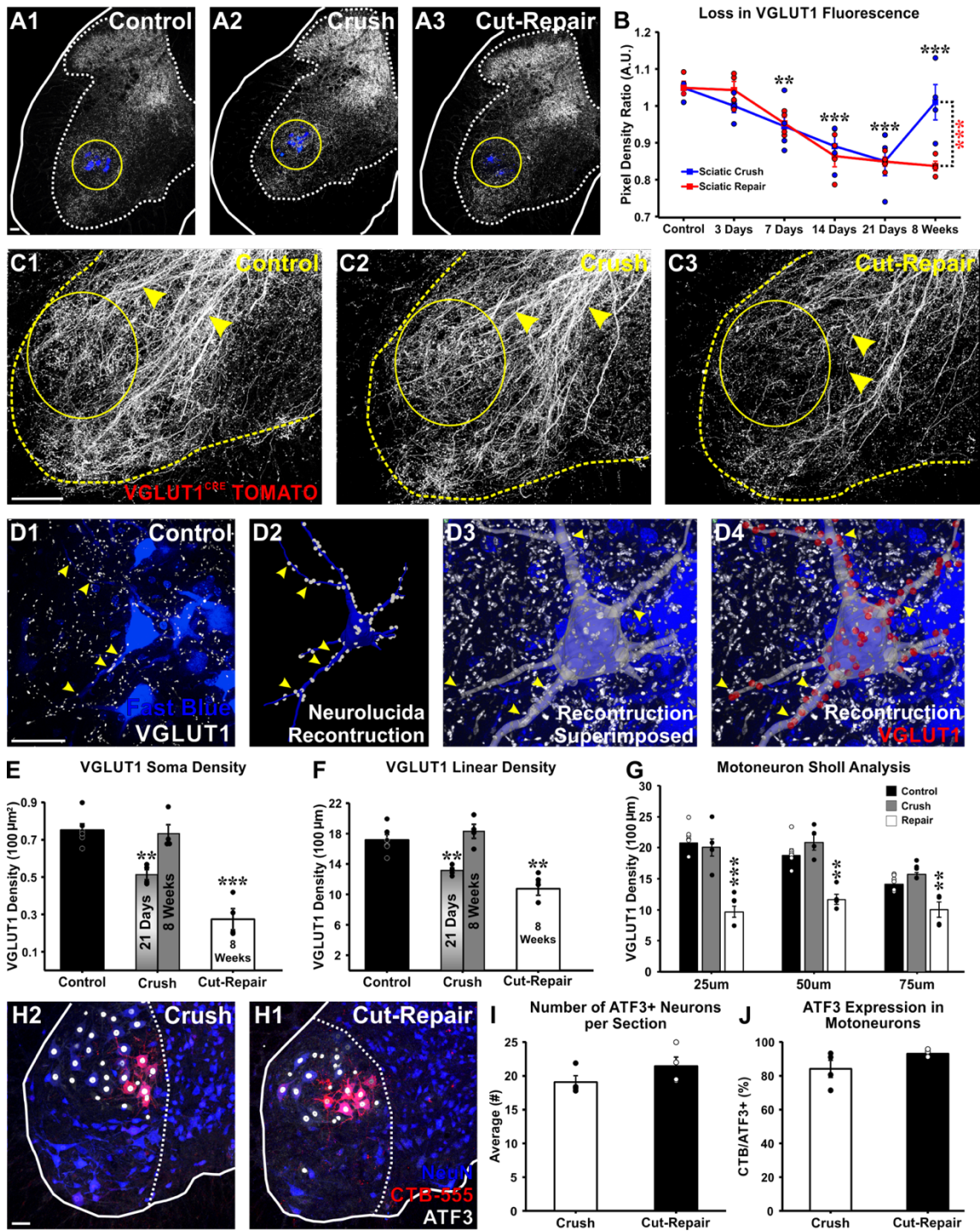


Figure 4.1: VGLUT1 synapses recover following a sciatic nerve crush but are permanently removed following a sciatic nerve cut

A1-A3) Low magnification (10x) confocal images of ipsilateral side of the spinal cord in sham controls (D1) and 8 weeks post sciatic crush (SC) (D2) or sciatic repair (SR) (D3). Retrogradely labeled FB+ MNs (blue) are shown in the ventral horn with VGLUT1 labeling (white). A region of interest (ROI, yellow circle) was placed around the motor pool to measure the VGLUT1 integrated pixel densities between the ipsilateral and contralateral sides of the spinal cord. **B)** Time course of changes in VGLUT1 fluorescence densities over time presented as a ratio between the ipsilateral and contralateral sides of the spinal cord after SR (red line) or SC (blue line). Y – axis = ipsilateral integrated pixel density / contralateral. Each dot represents an average from a single mouse (n = 4 mice per time point per condition, 6 spinal cord sections in each). Lines indicate averages \pm SE at each time point. Black asterisks are compared to controls (** p < 0.01, *** p < 0.001). Red asterisks at 8 weeks is a comparison between SR and SC (*** p < 0.001). **C1-C3)** Confocal images of the ipsilateral ventral horn in VGLUT1^{Cre/+}R26 tdTomato mice sham mice (C1) and 8 weeks after either SC (C2) or SR (C3). Yellow circles outline the motor pool where the permanent disappearance of projecting Ia afferent collaterals can be seen in SR mice (C3). **D1)** High magnification 60x confocal image of retrogradely labeled LG MN (Fast Blue, blue) from sham control mouse receiving VGLUT1 synaptic inputs (white). Arrow show several examples of VGLUT1 synapses along the dendritic arbor. **D2)** NeuroLucida 3D reconstruction of the same LG MN shown in D1 with VGLUT1

synapses mapped on the soma and proximal dendritic arbor. **D3)** NeuroLucida tracing superimposed on confocal image. Yellow arrows points to examples of VGLUT1 synapses. **D4)** Same image as D3 but with VGLUT1 synapses mapped in red. **E)** VGLUT1 somatic density is only a temporary loss in synapses at 21 days following SC and these return to control levels by 8 weeks, however there is a decrease in VGLUT1 synapses after SR and these do not return. Bars represent averages \pm SE (n = 4 – 6 mice per bar represented by individual dots, 6 MNs per animal). Black asterisks are in comparison to controls (** p < 0.01, *** p < 0.001). **F)** Dendritic VGLUT1 linear density is also significant decrease 8 weeks following SR, and only temporarily in SC at 21 days post injury. These synapses return by 8 weeks in the SC model. (** p < 0.01). **G)** Sholl Analysis: VGLUT1 densities along the dendritic arbor (bin size: 25 μ m, 50 μ m, and 75 μ m from cell body center) show no difference in any of the 3 bins following SC (grey bar) however there was significant decreases in each bin 8 weeks following SR (white bar). Comparisons were all relative to controls (black bar) (** p < 0.01, *** p < 0.001). **H1-2)** Confocal images (20x) of the ventral horn 7 days following SC or SR injury. Activating transcription factor 3 (ATF3) expression shown in white, neurons are labeled with NeuN (blue) and retrogradely labeled LG MNs were pre-labeled with CTB-555 (red). **I)** Average number of ATF3+ MNs in a 50 μ m thick spinal cord section and **J)** Percent of CTB+ MNs expressing ATF3 (represented by bars, \pm SE). Each individual dot is average from a single animal (n = 4 mice, 6 spinal cord sections per animal). These data demonstrate there is no significant difference in the number of MNs expressing ATF3 or the percent of

CTB MNs expressing ATF3 7 days after either SC or SR. Scale bars, A, D, H: 50 μm , C: 100 μm .

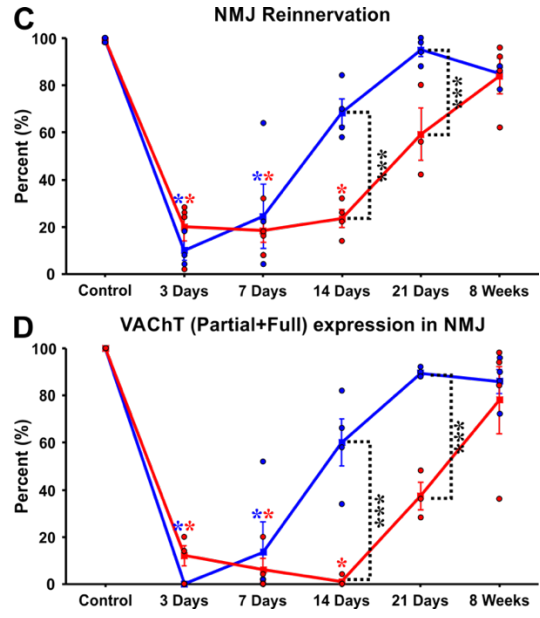
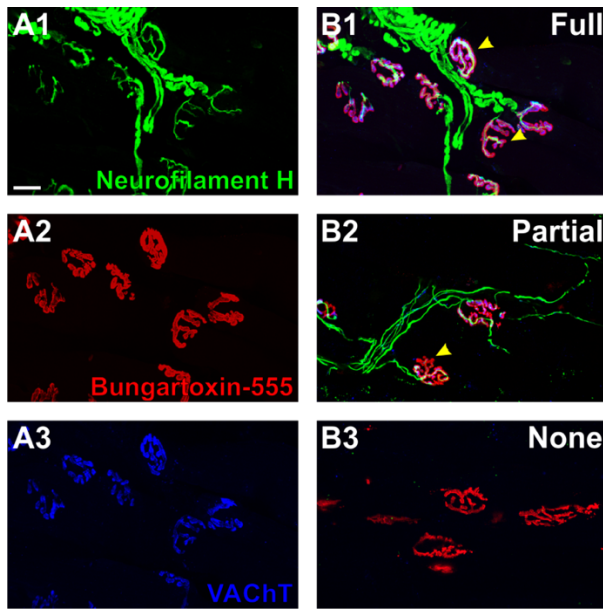


Figure 4.2: Motor axons regenerate faster after a SC compared to a SR injury

A1) High magnification (60x) confocal image of neurofilament-H expression (green) in the LG muscle in a sham control mouse. **A2)** Bungarotoxin conjugated to an Alexa Fluor 555 fluorochrome (bungx-555, red) staining of the LG muscle. **A3)** VACht expression (blue) in the presynaptic terminal of the motor axons. **B1)** Merge image of A1-A3 to demonstrate complete innervation of NFH into the motor end plate and full VACht expression (pointed out by yellow arrow). **B2)** Partial innervation of the NMJ by NFH+ axons and partial labeling of VACht in a motor endplate (yellow arrow) during the reinnervation period following nerve injury. **B3)** NMJ completely absent of motor axon innervation. Regardless, the post synaptic density (PSD) is maintained as demonstrated by bungx-555 expression by the presence of a basal lamina membrane. **C)** Time course of NFH presence in the NMJ. Both SC (blue line) and SR (red line) result in an immediate degeneration of the NMJ 3 and 7 days post injury. SC results in a recovery by 14 post injury and returns towards control values. NFH expression remains depleted 14 days post SR. Reinnervation begins between 14 and 21 days before returning to control levels by 8 weeks post injury. Y-axis = percent of NMJ innervated by NFH. **D)** Time course for presence of VACht in the NMJ. Partial and full expressions were combined plotted. The trend of VACht degradation follows a similar trend of the NFH innervation. For C) and D) each dot represents an average from one animals (3 – 4 mice per condition, 50 NMJs per animal). Lines indicate averages \pm SE at each time point. Color of asterisk

corresponds to line color compared to control (* $p < 0.05$). Black asterisks are comparisons between SR and SC (** $p < 0.001$) (see text for statistical description). Scale bar, A: 20 μm .

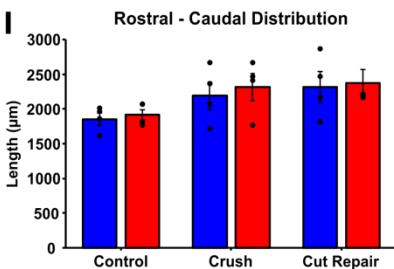
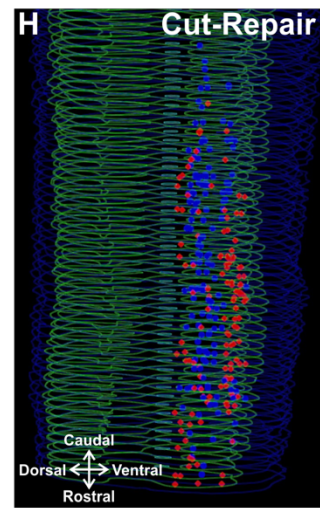
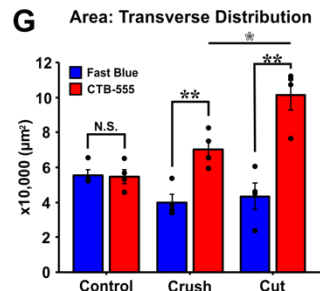
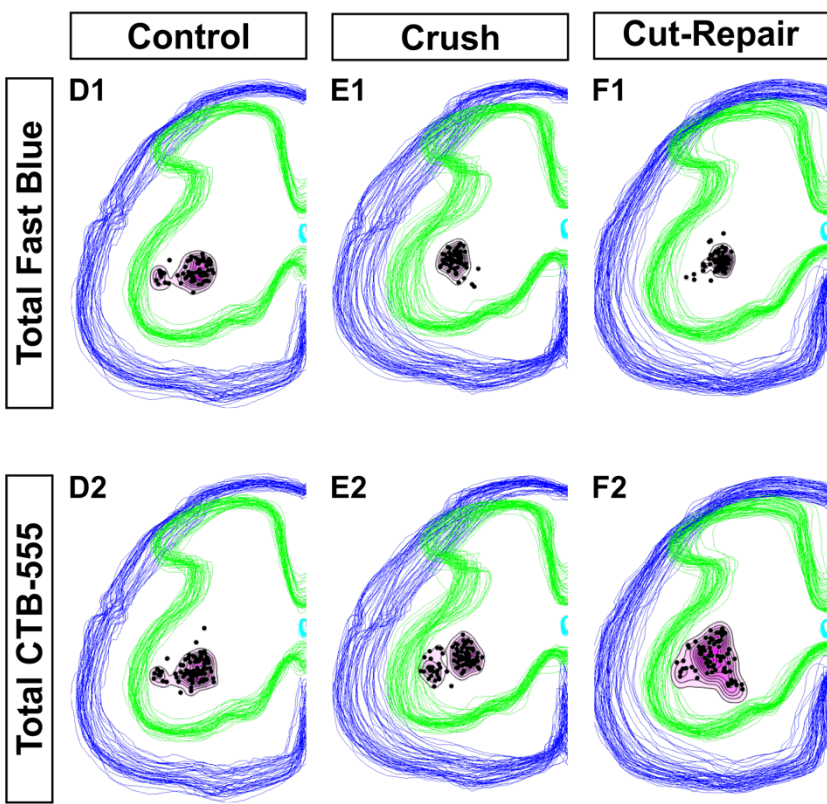
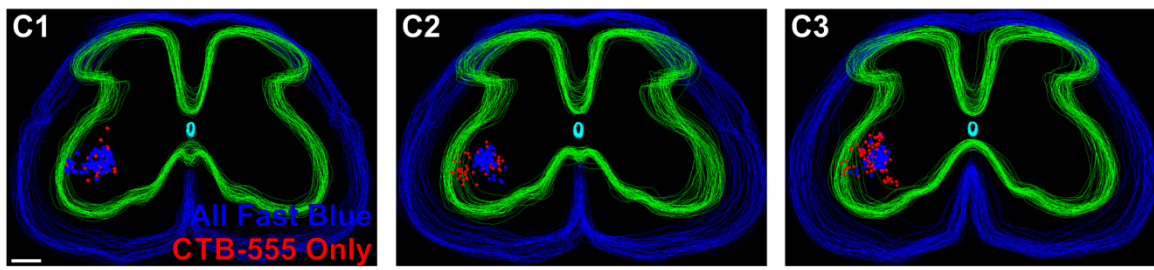
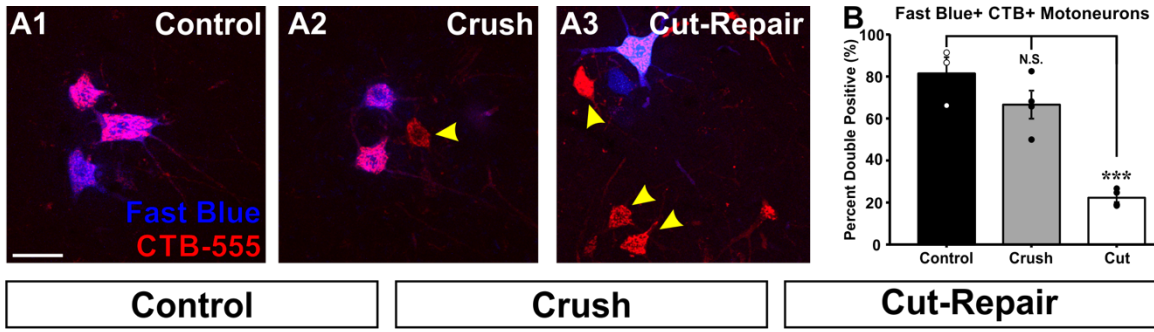


Figure 4.3: Motor axons regenerate with greater specificity after a SC compared to a SR injury

A1-A3) High magnification (60x) confocal images of spinal cord section in controls, and 8 weeks post SC or SR. LG MNs were pre-labeled with FB (blue) prior to injury and 8 weeks post injury the LG muscle was reinjected with CTB-555 (red). Mice were perfused one week after the second injection. Dual labeled MNs (pink) show MNs that have returned to the LG. Red only MNs are interpreted as newly acquired MNs innervating the LG. **B)** Graph represents the percent of all FB+ LG MNs that co-express CTB+. There was no difference found between control and SC mice however there was a significant decrease in the percent of dual labeled cells following SR (** $p < 0.001$). **C1-C3)** NeuroLucida reconstruction plots of serially collected spinal cord sections (43 sections in each plot). Blue line outlines the entire spinal cord section, green lines separate the grey and white matter boundary. Blue dots represent the entire FB+ MN population in all sections including single and dual labeled cells. Red dots represent CTB-555+ only cells. In sham controls there are very few red only cells (C1). In SC, there is an expansion of the CTB MNs that appear to occupy the territory of close synergist motor pools (C2). After SR, the CTB motor pool appears to spread in all directions (C3). **D11, D2, E1, E2, F1, F2)** Spinal cord outline plots taken from NeuroLucida reconstructions in panel C. The XY coordinate of each individual MN was uploaded to a custom Matlab script and plotted as individual points to create heat maps indicating the location and density in the dorso-ventral and medio-lateral direction. Each individual contour

represents a percentile ranging from 15% (innermost) to 95% (outermost). D1, E1, F1: individual plots for pre-labeled Fast Blue+ LG MNs with no obvious differences between controls, SR, or SC. D2, E2, F2: individual plots for post-labeled CTB-555+ MNs innervating the LG showing changes in the distribution in both cut and crush animals. Changes in **G**) contour surface area (95th percentile) of MNs distributed in the transverse plane. (black asterisks are comparisons against control ** $p < 0.01$, grey asterisk is comparison between crush and cut, * $p < 0.05$) **H**) Neurolucida reconstruction plot of all serial sections reconstructed that contained labeled FB+ and CTB+ MNs showing their distribution in the rostral-caudal direction. **I**) There were no differences found in the rostral-caudal distribution between FB and CTB-555+ MNs in controls, SC or SR mice. Scale bar, A: 50 μm , C: 200 μm .

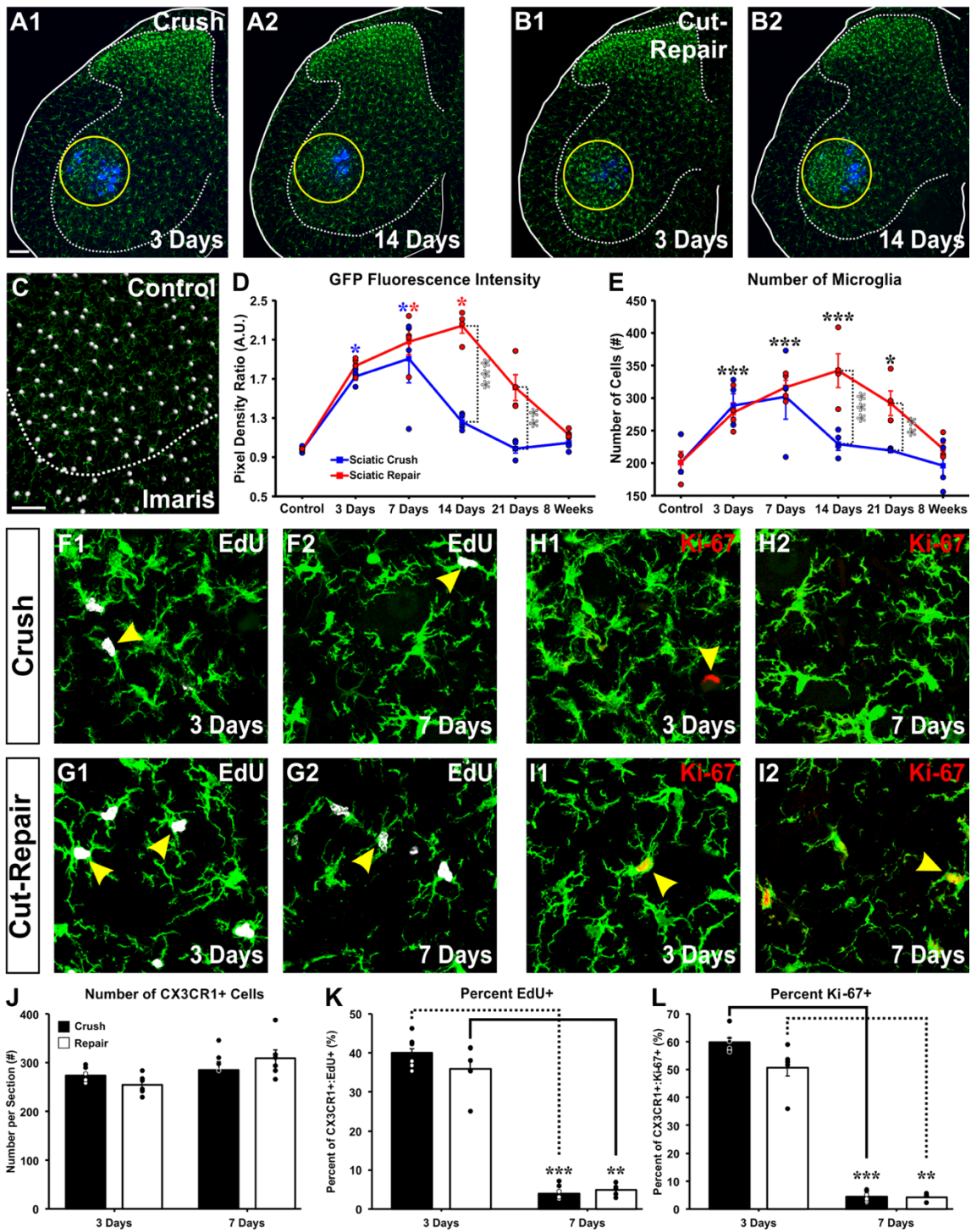


Figure 4.4: The microglial response in the ventral horn is longer following sciatic nerve cut compared to crush

A, B) CX3CR1-microglia (GFP, green) in the ventral horn of the spinal cord 3 days (A1) and 14 days (A2) after sciatic crush or repair (B1, B2). LG MNs were pre-labeled with Fast Blue (blue). Microglia CX3CR1-GFP integrated pixel densities were measured within the indicated ROI (yellow circle) ipsilateral (shown) and contralateral (not shown) to the injury and compared. **C)** Imaris “spot function” used to automatically quantify the number of CX3CR1-GFP+ cells in the ventral horn of the spinal cord. The white dashed line indicates the separation of the white and grey matter boundary. **D)** Changes in GFP integrated pixel fluorescence over time between the ipsilateral and contralateral sides of the spinal cord after SC (blue line) and SR (red line). There was a significant increase in the fluorescence in both SR and SC by 7 days post injury (* $p < 0.05$). However, by 14 days, the microglia fluorescence in the SC model returned near control levels, while the reaction remained significantly greater on the ipsilateral side 14 and 21 days following SR (* $p < 0.05$). Furthermore, the fluorescence reaction in SR was significantly greater than SC at both 14 and 21 days post injury (grey asterisks, ** $p < 0.01$, *** $p < 0.001$). GFP fluorescence returned to baseline levels by 8 weeks in both injury models. **E)** Time course of the number of GFP+ cells in the ventral horn of a 50 μm thick spinal cord section after either a SC or SR injury. There is a similar and significant increase in the number of microglia cells 3 and 7 days after SC and SR. By 14 days the number of microglia cells in the SC mice return towards baseline while the number of GFP+

cells in the SR mice remain significantly higher than controls and to SC mice at 14 and 21 days post injury. The number of cells return to control levels by 8 weeks post injury in both injury models (* $p < 0.05$, ** $p < 0.01$, *** $p < 0.001$). **F, G)** High magnification (60x) images of CX3CR1-GFP+ cells expressing EdU 3 and 7 days after a SC (F1, F2) or SR (G1, G2) injury. Arrows pointing to EdU expressing microglia. **H, I)** High magnification (60x) images of CX3CR1-GFP+ cells expressing Ki-67 3 and 7 days after a SC (H1, H2) or SR (I1, I2) injury. Majority of all EdU or Ki-67+ cell type detected inside the spinal cord parenchyma were CX3CR1+. Occasionally, we did detect a Ki-67+ cell that appeared to be lining the blood vessel as can be seen in H1 (yellow arrow). **J)** We manually counted the total number of Iba1+ cell 3 and 7 days after a SR or SC injury in NeuroLucida. Bars represent averages from one animal \pm SE. Each individual dot represents a single average per section (6 sections total per each bar from 1 animal). There were no significant differences between injury type or time point. **K, L)** Percent of all Iba1+ cells counted in the ventral horn that express either EdU (K) or Ki-67 (L). We found that more within the first 3 days after injury around 40% of all CX3CR1+ cells are EdU+ and around 50-60% are Ki-67+ in both injury models. However, by 7 days post injury less than 10% of all cells are EdU+ or Ki-67+. Scale bar, A, C: 100 μ m.

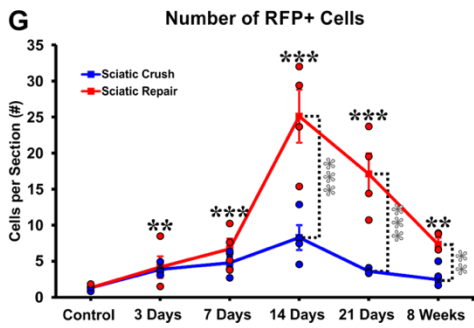
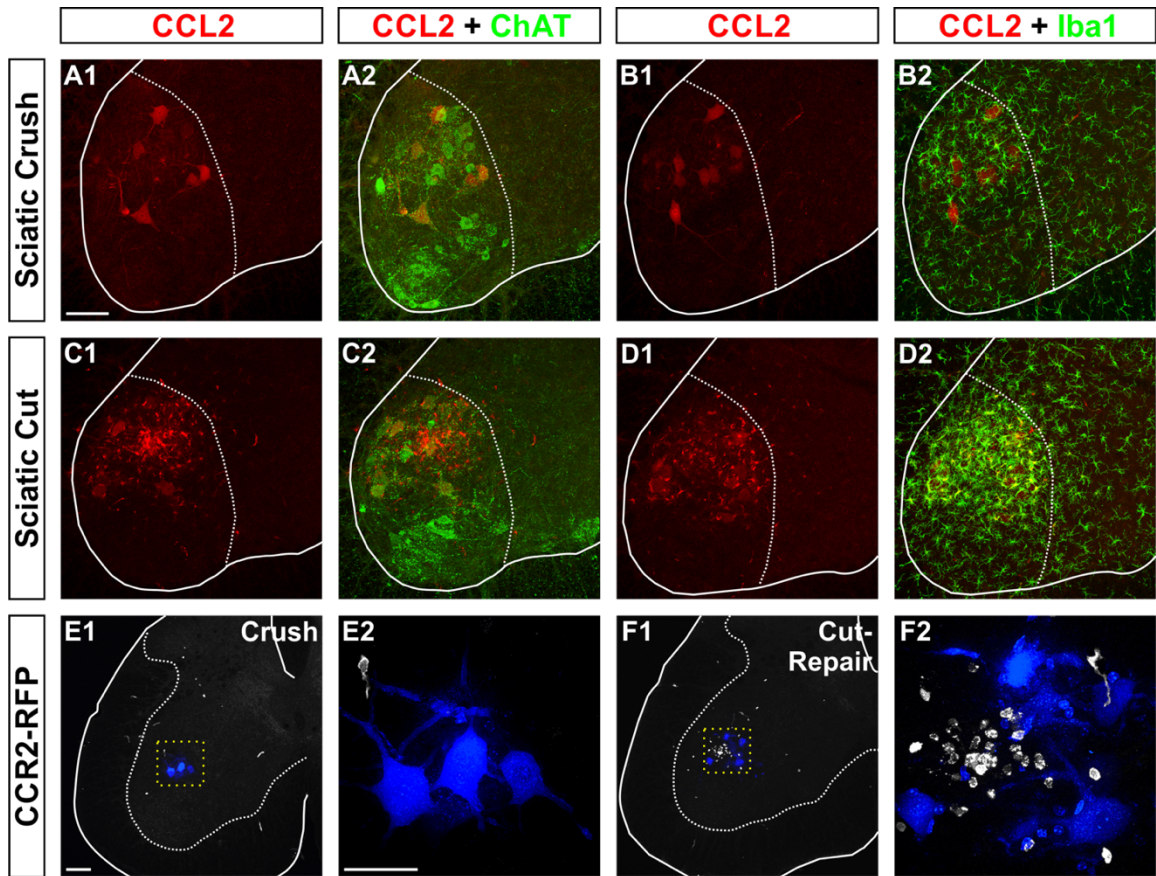


Figure 4.5: CCR2-RFP+ cells infiltrate the ventral horn following SR and are recruited by CCL2 release from microglia

A1, A2, C1, C2) a 20x confocal image stack of spinal cord sections 14 days after either a SC (A1) or a SR (C1) from a mouse expressing mCherry under the CCL2 promoter (red) merged with ChAT immunoreactivity (green) to identify MNs (A2, C2). These images show that MNs express CCL2 14 days post SC or SR injuries. **B1, B2, D1, D2)** 20x confocal image stack showing CCL2 expression (B1, D1) and Iba1+ immunoreactivity (green, B2, D2). These images show that microglia cells in the spinal cord only express CCL2 after SR but not after SC. **E1, F1)** 2D projection confocal image stacks (10x, 50 μm thick) of CCR2+ cells (white cells) that have infiltrated the spinal cord 14 days after either a SC (E1) or SR (F1) injury and migrate towards the ventral horn and surround retrogradely LG MNs (blue). E2, F2) High magnification (60x) collapsed confocal image stack of ventral horn outlined in A1 and B1 (yellow square). **G)** Time course of CCR2+ cell infiltration after SC (blue line) or SR (red line) injury. Data is represented as average number of total RFP+ cells in the ventral horn of a 50 μm thick spinal cord section (\pm SE). Each individual data point represents the average from all spinal cord sections quantified in the L4-L5 region of a single animal (3-4 mice per time point). There was a significant increase in the number of RFP+ cells at every single time point measured compared to controls (black asterisks), while SR resulted in significantly more CCR2 cells compared to SC at 14 day, 21 days, and 8 weeks post injury. (** $p < 0.01$, *** $p < 0.001$). Scale bar, A, E1, E2: 50 μm .

References:

- Abelew TA, Miller MD, Cope TC, Nichols TR (2000) Local loss of proprioception results in disruption of interjoint coordination during locomotion in the cat. *Journal of neurophysiology* 84:2709-2714.
- Ajami B, Bennett JL, Krieger C, McNagny KM, Rossi FM (2011) Infiltrating monocytes trigger EAE progression, but do not contribute to the resident microglia pool. *Nature neuroscience* 14:1142-1149.
- Alvarez FJ, Villalba RM, Zerda R, Schneider SP (2004) Vesicular glutamate transporters in the spinal cord, with special reference to sensory primary afferent synapses. *The Journal of comparative neurology* 472:257-280.
- Alvarez FJ, Titus-Mitchell HE, Bullinger KL, Kraszpulski M, Nardelli P, Cope TC (2011) Permanent central synaptic disconnection of proprioceptors after nerve injury and regeneration. I. Loss of VGLUT1/IA synapses on motoneurons. *Journal of neurophysiology* 106:2450-2470.
- Berg A, Zelano J, Thams S, Cullheim S (2013) The extent of synaptic stripping of motoneurons after axotomy is not correlated to activation of surrounding glia or downregulation of postsynaptic adhesion molecules. *PLoS one* 8:e59647.
- Blinzinger K, Kreutzberg G (1968) Displacement of synaptic terminals from regenerating motoneurons by microglial cells. *Zeitschrift für Zellforschung und mikroskopische Anatomie* 85:145-157.
- Bodine-Fowler SC, Meyer RS, Moskovitz A, Abrams R, Botte MJ (1997) Inaccurate projection of rat soleus motoneurons: a comparison of nerve repair techniques. *Muscle & nerve* 20:29-37.
- Brandt J, Evans JT, Mildenhall T, Mulligan A, Konieczny A, Rose SJ, English AW (2015) Delaying the onset of treadmill exercise following peripheral nerve injury has different effects on axon regeneration and motoneuron synaptic plasticity. *Journal of neurophysiology* 113:2390-2399.
- Brown AG, Fyffe RE (1978) The morphology of group Ia afferent fibre collaterals in the spinal cord of the cat. *The Journal of physiology* 274:111-127.
- Brushart TM, Mesulam MM (1980) Alteration in connections between muscle and anterior horn motoneurons after peripheral nerve repair. *Science* 208:603-605.
- Brushart TM, Tarlov EC, Mesulam MM (1983) Specificity of muscle reinnervation after epineurial and individual fascicular suture of the rat sciatic nerve. *J Hand Surg Am* 8:248-253.
- Bullinger KL, Nardelli P, Pinter MJ, Alvarez FJ, Cope TC (2011) Permanent central synaptic disconnection of proprioceptors after nerve injury and regeneration. II. Loss of functional connectivity with motoneurons. *Journal of neurophysiology* 106:2471-2485.
- Cope TC, Bonasera SJ, Nichols TR (1994) Reinnervated muscles fail to produce stretch reflexes. *Journal of neurophysiology* 71:817-820.
- Eccles JC, Eccles RM, Lundberg A (1957) Synaptic actions on motoneurons in relation to the two components of the group I muscle afferent volley. *The Journal of physiology* 136:527-546.

- Echeverry S, Shi XQ, Rivest S, Zhang J (2011) Peripheral nerve injury alters blood-spinal cord barrier functional and molecular integrity through a selective inflammatory pathway. *The Journal of neuroscience : the official journal of the Society for Neuroscience* 31:10819-10828.
- Gordon T (2016) Electrical Stimulation to Enhance Axon Regeneration After Peripheral Nerve Injuries in Animal Models and Humans. *Neurotherapeutics* 13:295-310.
- Gordon T, English AW (2016) Strategies to promote peripheral nerve regeneration: electrical stimulation and/or exercise. *The European journal of neuroscience* 43:336-350.
- Guan Z, Kuhn JA, Wang X, Colquitt B, Solorzano C, Vaman S, Guan AK, Evans-Reinsch Z, Braz J, Devor M, Abboud-Werner SL, Lanier LL, Lomvardas S, Basbaum AI (2016) Injured sensory neuron-derived CSF1 induces microglial proliferation and DAP12-dependent pain. *Nature neuroscience* 19:94-101.
- Guest JD, Hesse D, Schnell L, Schwab ME, Bunge MB, Bunge RP (1997) Influence of IN-1 antibody and acidic FGF-fibrin glue on the response of injured corticospinal tract axons to human Schwann cell grafts. *Journal of neuroscience research* 50:888-905.
- Hamilton SK, Hinkle ML, Nicolini J, Rambo LN, Rexwinkle AM, Rose SJ, Sabatier MJ, Backus D, English AW (2011) Misdirection of regenerating axons and functional recovery following sciatic nerve injury in rats. *The Journal of comparative neurology* 519:21-33.
- Jankowska E, Lindstrom S (1972) Morphology of interneurons mediating Ia reciprocal inhibition of motoneurons in the spinal cord of the cat. *The Journal of physiology* 226:805-823.
- Jessell TM, Surmeli G, Kelly JS (2011) Motor neurons and the sense of place. *Neuron* 72:419-424.
- Jung S, Aliberti J, Graemmel P, Sunshine MJ, Kreutzberg GW, Sher A, Littman DR (2000) Analysis of fractalkine receptor CX(3)CR1 function by targeted deletion and green fluorescent protein reporter gene insertion. *Molecular and cellular biology* 20:4106-4114.
- Kettenmann H, Kirchhoff F, Verkhratsky A (2013) Microglia: new roles for the synaptic stripper. *Neuron* 77:10-18.
- Liddell EGT, Sherrington CS (1924) Reflexes in response to stretch (myoatic reflexes). *Proc R Soc Lond B*:212-242.
- Lundberg A, Winsbury G (1960) Selective adequate activation of large afferents from muscle spindles and Golgi tendon organs. *Acta Physiol Scand* 49:155-164.
- Ma CH, Omura T, Cobos EJ, Latremoliere A, Ghasemlou N, Brenner GJ, van Veen E, Barrett L, Sawada T, Gao F, Coppola G, Gertler F, Costigan M, Geschwind D, Woolf CJ (2011) Accelerating axonal growth promotes motor recovery after peripheral nerve injury in mice. *The Journal of clinical investigation* 121:4332-4347.

- Mendell LM, Henneman E (1971) Terminals of single Ia fibers: location, density, and distribution within a pool of 300 homonymous motoneurons. *Journal of neurophysiology* 34:171-187.
- Nguyen QT, Sanes JR, Lichtman JW (2002) Pre-existing pathways promote precise projection patterns. *Nature neuroscience* 5:861-867.
- Nicolopoulos-Stournaras S, Iles JF (1983) Motor neuron columns in the lumbar spinal cord of the rat. *The Journal of comparative neurology* 217:75-85.
- Prather JF, Nardelli P, Nakanishi ST, Ross KT, Nichols TR, Pinter MJ, Cope TC (2011) Recovery of proprioceptive feedback from nerve crush. *The Journal of physiology* 589:4935-4947.
- Raivich G, Moreno-Flores MT, Muller JC, Kreutzberg GW (1994) Regulation of microglial proliferation: colony-stimulating factors and their receptors. *Neuropathology and applied neurobiology* 20:209-211.
- Rotterman TM, Nardelli P, Cope TC, Alvarez FJ (2014) Normal distribution of VGLUT1 synapses on spinal motoneuron dendrites and their reorganization after nerve injury. *J Neurosci* 34:3475-3492.
- Rotterman TM, MacPherson KP, Upad A, Tansey K, Alvarez FJ (2018) Motor circuit synaptic plasticity after peripheral nerve injury depends on a central neuroinflammatory response and a CCR2 mechanism. *Journal of Neuroscience Under Review*.
- Saederup N, Cardona AE, Croft K, Mizutani M, Cotleur AC, Tsou CL, Ransohoff RM, Charo IF (2010) Selective chemokine receptor usage by central nervous system myeloid cells in CCR2-red fluorescent protein knock-in mice. *PloS one* 5:e13693.
- Schultz AJ, Rotterman TM, Dwarakanath A, Alvarez FJ (2017) VGLUT1 synapses and P-boutons on regenerating motoneurons after nerve crush. *The Journal of comparative neurology* 525:2876-2889.
- Shi C, Pamer EG (2011) Monocyte recruitment during infection and inflammation. *Nature reviews Immunology* 11:762-774.
- Shi C, Jia T, Mendez-Ferrer S, Hohl TM, Serbina NV, Lipuma L, Leiner I, Li MO, Frenette PS, Pamer EG (2011) Bone marrow mesenchymal stem and progenitor cells induce monocyte emigration in response to circulating toll-like receptor ligands. *Immunity* 34:590-601.
- Siskova Z, Mahad DJ, Pudney C, Campbell G, Cadogan M, Asuni A, O'Connor V, Perry VH (2010) Morphological and functional abnormalities in mitochondria associated with synaptic degeneration in prion disease. *The American journal of pathology* 177:1411-1421.
- Sunderland S (1991) *Nerve Injuries and their Repair*. UK: Longman Group.
- Svensson M, Aldskogius H (1993) Synaptic density of axotomized hypoglossal motoneurons following pharmacological blockade of the microglial cell proliferation. *Experimental neurology* 120:123-131.
- Svensson M, Eriksson P, Persson JK, Molander C, Arvidsson J, Aldskogius H (1993) The response of central glia to peripheral nerve injury. *Brain research bulletin* 30:499-506.
- Tay TL, Mai D, Dautzenberg J, Fernandez-Klett F, Lin G, Sagar, Datta M, Drougard A, Stempfl T, Ardura-Fabregat A, Staszewski O, Margineanu A,

- Sporbert A, Steinmetz LM, Pospisilik JA, Jung S, Priller J, Grun D, Ronneberger O, Prinz M (2017) A new fate mapping system reveals context-dependent random or clonal expansion of microglia. *Nature neuroscience* 20:793-803.
- Thomas CK, Stein RB, Gordon T, Lee RG, Elleker MG (1987) Patterns of reinnervation and motor unit recruitment in human hand muscles after complete ulnar and median nerve section and resuture. *Journal of neurology, neurosurgery, and psychiatry* 50:259-268.
- Tsujino H, Kondo E, Fukuoka T, Dai Y, Tokunaga A, Miki K, Yonenobu K, Ochi T, Noguchi K (2000) Activating transcription factor 3 (ATF3) induction by axotomy in sensory and motoneurons: A novel neuronal marker of nerve injury. *Molecular and cellular neurosciences* 15:170-182.
- Ullrich PM, Lavela SL, Evans CT, Miskevics S, Weaver FM, Goldstein B (2014) Associations between perceptions of evidence and adoption of H1N1 influenza infection prevention strategies among healthcare workers providing care to persons with spinal cord injury. *Journal of advanced nursing* 70:1793-1800.
- Valero-Cabre A, Fores J, Navarro X (2004) Reorganization of reflex responses mediated by different afferent sensory fibers after spinal cord transection. *Journal of neurophysiology* 91:2838-2848.
- Vincent JA, Gabriel HM, Deardorff AS, Nardelli P, Fyffe REW, Burkholder TJ, Cope TC (2017) Muscle Proprioceptors in Adult Rat: Mechanosensory Signaling and Synapse Distribution in Spinal Cord. *Journal of neurophysiology:jn* 00497 02017.

Chapter 5:

General Discussion and Future Directions

5.1: Discussion

The theme of this thesis is to interrogate the involvement of neuroinflammation in the plasticity of neural circuits and synapses, a common phenomenon that occurs during neurodegeneration and injury. Here, we used peripheral nerve injury (PNI) as an experimental model to investigate our hypotheses, though the implications go well beyond the scope of this work as the inflammatory responses we describe and the consequences they have on synaptic connectivity are also of great relevance to CNS injury and disease (Streit et al., 2004; Trapp et al., 2007; Kettenmann et al., 2013; Wolf et al., 2017). The advantage of using PNI is that the injury is outside the CNS and does not result in secondary inflammatory effects due to large numbers of cell death directly related to injury or direct breakdown of the BSCB because of physical damage. Regardless, the MNs in the spinal cord and the sensory afferent cell bodies in the DRG release a host of factors resulting in an inflammatory reaction centrally, far away from the site of physical injury.

Another reason to study PNI is the persistent motor deficits that occur in this patient population. One of the significant consequences of nerve injury is deficiencies in proprioception, which is responsible for carrying sensory information into the CNS about positioning and dynamics of the skeleto-muscular system and is necessary for executing smooth, controlled movements through space. There are major impairments in motor control after nerve injury, and we believe they are in part due to a reorganization of spinal motor circuits. Here, we investigated one well studied spinal cord circuit that is anatomically and

functionally absent after a complete transection nerve injury, the stretch reflex circuit involving monosynaptic connections between Ia/II afferents and MNs. However, it is important to point out that removal of Ia afferents from the ventral horn also affects directly or indirectly many other spinal circuits, like for example reciprocal inhibition. Moreover, similar to the deletion of the central arbors of Ia afferents injured in the peripheral nerve, the central synaptic arbors of motor axons also injured peripherally are also permanently lost (not shown). This, of course, affects inter-neuronal circuits dependent on this input, like recurrent inhibition. Thus, the central changes that occur in the synaptic arbors of the motor and sensory axons injured peripherally cause significant re-organizations of motor circuits. These circuitries work in unison to promote smooth movement, and any disruption in one circuit can have drastic effects on the others.

Finally, another major theme of this thesis was to distinguish anterograde transganglionic degeneration of primary afferent central synapses from the classic synaptic stripping that occurs over axotomized MNs after nerve injury. Through the years the differences between these two phenomena have been blurred, and conflicting interpretations have contaminated the literature. Synaptic stripping was first described in 1968 by Blinzinger and Kreutzberg (Blinzinger and Kreutzberg, 1968) and is the process by which synaptic inputs, particularly glutamatergic synapses (Linda et al., 2000), temporarily detach from the cell body and very proximal dendrites of axotomized MNs but return once peripheral regeneration has occurred. The majority of these synapses come from sources not directly affected by the injury itself, and the inputs are removed specifically

from MNs with motor axons injured in the periphery. However, the less explored phenomenon of anterograde transganglionic degeneration occurs when the synapses inside the spinal cord of sensory axons axotomized in the periphery degenerate (Arvidsson, 1979; Arvidsson and Grant, 1979; Aldskogius et al., 1985; Arvidsson, 1986; Eriksson et al., 1993). A primary example of this is the sensory Ia afferent whose central terminations in the ventral horn are removed after their peripheral axons are injured in the peripheral nerve (Alvarez et al., 2011). This results in disconnection of Ia afferents from all ventral neuronal targets, including interneurons and heteronymous MNs, independent of injury to the postsynaptic neuron. Thus, while synaptic stripping is a phenomenon dependent on injury to the postsynaptic MNs, the synaptic removal we study here affects all ventral horn synapses of peripherally injured sensory afferents. In this thesis, we tried to distinguish these different outcomes and find novel mechanisms for the latter to provide some clarity to the literature.

5.1.1: Distribution of VGLUT1 synapses on motoneurons and their permanent loss after nerve injury

Hypothesis (1): Ia afferent synapses are permanently removed, by difference to synaptic stripping, throughout the dendritic arbor of MNs.

One of the fundamental findings of this thesis was mapping the distribution of Ia/II afferent inputs on the soma and proximal dendrites of rodent MNs, both in

uninjured and axotomized animals. Earlier studies had made predictions about the number of Ia inputs on MNs based on electrophysiological studies and single intra-axonal HRP fills (Brown and Fyffe, 1981; Redman and Walmsley, 1983b, a; Burke and Glenn, 1996). However, it was not technically feasible to directly quantify the total number of proprioceptive (Ia/II) synapses on a single MN. Furthermore, the majority of these early studies were performed in cats, and little was known about Ia/II afferent synaptic distribution in the rodent.

With the discovery of VGLUT1 expression in Ia/II synaptic boutons in the ventral horn (Alvarez et al., 2004), specific antibodies against this protein were used to identify and map Ia synaptic inputs on adult MNs before and after injury (Alvarez et al., 2011). However, these previous studies were based on retrograde tracing, and therefore only the first few hundreds of microns of dendrites were available to study. To obtain the entire synaptic distribution on rodent MNs individual cells were intracellularly filled with neurobiotin by the Cope lab to label the most distal dendritic tips. This was an advance over using retrograde tracers because we knew that the dendrites of rat MNs expanded over a millimeter in diameter in the spinal cord (Chen and Wolpaw, 1994) and that the Ia input preferentially targets the dendritic arbor (Brown and Fyffe, 1981).

Our study was the first to analyze and map VGLUT1 synapses across the entire dendritic arbor of intracellularly filled MNs. We found that approximately 50% of all VGLUT1 synapses were located within the first 300 μm of dendrite and that VGLUT1 density linearly decreased along the dendrites from proximal to distal. Interestingly, synapses tended to exist in clusters along the proximal

dendrite. This is also the region where persistent inward current (PIC) channels, such as voltage-gated calcium channels, are known to be distributed (Hultborn et al., 2003). The data suggest that the distribution of VGLUT1 synapses along the motoneuron dendrite and their organization may facilitate PIC-mediated amplification by providing a structural basis for spatial synaptic summation in dendrite regions known to be specially endowed with PIC-related channels.

Another critical finding in this study was the pattern of synaptic loss that occurred after tibial nerve transection. It had previously been shown that after PNI, 75-95% of Ia afferent inputs on the soma and around 50% on the proximal dendritic arbor detached and never returned (Alvarez et al., 2011). This resulted in a significant reduction in detectable stretch synaptic potentials in the MNs and a complete absence of the stretch reflex (Bullinger et al., 2011). However, the findings from these studies were limited in that the synaptic densities estimated were restricted to the first couple hundred microns of dendrite (since they were based on mapping synapses on retrogradely labeled MNs with reduced dendritic labeling) and the sections were quantified in the transverse plane, biasing the data to dendrites extending into lamina VII and not accounting for the dendritic branches extending in a rostral-caudal direction inside lamina IX, the lamina with the most extensive depletion of VGLUT1 synapses. We reconstructed and mapped VGLUT1 synapses on intracellularly filled axotomized MNs one year after injury.

We drew three major conclusions: 1) Approximately 77% of all proximal VGLUT1 synapses in the first 300 μm of dendrites were permanently removed

from the dendritic arbor resulting in a more uniform density of VGLUT1 synapses in proximal and distal dendrites. 2) The remaining VGLUT1 synapses became de-clustered suggesting that their functionality may be hindered by reduced spatial summation of postsynaptic currents and depolarizations. 3) The remaining VGLUT1 synapses, particularly the ones located proximally, also became significantly smaller. Smaller Ia synaptic boutons correlate with a fewer number of 'docked' synaptic vesicles and smaller presynaptic active zones (Pierce and Mendell, 1993), both affecting probability of synaptic release. In conclusion, the morphological data suggests not only a major loss in synapses but also disorganization of their spatial distribution on dendrites and changes at the single synapse level, all pointing to a weakening of this input.

Taken together, these data support our original **hypothesis (1)** as we successfully demonstrated a permanent deletion of VGLUT1 synapses (and weakening of remaining ones) from the soma and also throughout the dendritic arbor of MNs. This loss did not recover after the MN axons regenerate since all MNs studied were confirmed to have reinnervated muscle by eliciting motor unit muscle twitches when fired. This pattern of synaptic loss is different to what is expected from a purely synaptic stripping mechanism and suggested potential structural changes that could affect the efficacy of what remains of this input on regenerated MNs

The remaining parts of the thesis focused on finding a mechanism to explain this loss and gain a better understanding of how nerve injury severity can impact the permanency of this loss. Lastly, these data demonstrated that we

could capture a reasonable estimate of VGLUT1 synaptic changes by analyzing the proximal dendrites of MNs identified with retrograde tracers. This is because the most significant synaptic loss occurs over the proximal dendrite. Therefore, the rest of the study is based on retrogradely labeling MN cell bodies and proximal dendrites. Moreover, the lack of adequate and specific labeling and pharmacological tools to identify and manipulate immune cells intrinsic and extrinsic to the CNS suggested the optimal approach was to change animal model to mouse and implement global and cell-specific mutations to more specifically test mechanisms and identify different types of immune cells involved in this synaptic plasticity.

5.1.2: The permanent removal of Ia afferents is dependent on CCR2 mechanisms

Hypothesis (2): Sciatic nerve injuries causing more substantial loss of Ia afferent VGLUT1 synapses should correlate with stronger pro-inflammatory responses inside the spinal cord, assessed by microglia activation and infiltration CCR2+ immune cells.

Hypothesis (3): Preventing infiltration of CCR2+ peripheral macrophages preserves VGLUT1 synapses on MNs. Thus, a CCR2 mechanism is necessary for permanent removal of Ia afferent synapses.

There is a strong microglia reaction, which has been well characterized, in the ventral horn of the spinal cord following nerve injury, though the consequence of this reaction remains controversial (Blinzinger and Kreutzberg, 1968; Graeber et al., 1991; Svensson and Aldskogius, 1993; Aldskogius, 2011; Berg et al., 2013). Additionally, dorsal horn microglia become activated and are responsible for pain circuit modification (Coull et al., 2003), and recruitment, either directly or indirectly, of peripheral myeloid cells that promote hyperalgesia (Echeverry et al., 2011; Gu et al., 2016). Both of these cells have been shown to be involved in eliminating synapses in the CNS (Ransohoff, 2011; Schafer et al., 2012; Evans et al., 2014; Yamasaki et al., 2014), therefore both are possible candidates in the permanent deletion of Ia afferents.

To study the inflammatory response, we transitioned from a rat to a mouse model of nerve injury to utilize transgenic tools not available in the rat. We first performed a tibial nerve transection and quantified the VGLUT1 loss on retrogradely labeled LG MNs to compare these data to the rat. Surprisingly, the overall VGLUT1 loss 8 weeks after injury trended towards a decrease on the dendrites but was only significant on the MN soma. In other words, there was much better preservation of VGLUT1 synapses in mice compared to the rat. These results were intriguing because it is known that significant differences occur in neuroinflammatory responses between C57Blk/6 mice and Wistar Rats (Jinno and Yamada, 2011; Yamada et al., 2011).

We then cut the sciatic nerve and measured the changes in VGLUT1 density on LG MNs 8 weeks after injury. This resulted in a significant depletion of

VGLUT1 synapses on the soma and dendrites of LG MNs. One crucial factor to highlight is that in both cases all LG MNs were axotomized; however, the total number of severed motor and sensory axons was greater in the sciatic injury model. These data suggest that injury proximity can influence the degree of permanent Ia synaptic loss because a more substantial number of axotomized MNs could trigger a broader neuroimmune response.

We then compared the inflammatory response in the ventral horn between the two injury models using transgenic mice to distinguish central microglia (CX3CR1+) from infiltrating peripheral myeloid cells (CCR2+). We found that while both injuries resulted in a similar increase in the number of microglia cells, CX3CR1 fluorescence intensity was significantly greater after sciatic nerve cut compared to tibial nerve cut. Furthermore, microglia coverage of LG MNs somata was significantly greater 14 days after sciatic injury.

We also demonstrated that peripheral myeloid CCR2+ cells are recruited to the ventral horn of the spinal cord after injury with a peak 14 days following injury, and CCR2+ cell entry was significantly greater after sciatic injury compared to tibial nerve injuries. Interestingly, peak infiltration of CCR2+ cells occurred after the microglia reaction had occurred. To further characterize CCR2+ cells we collaborated with the Tansey lab to perform a flow cytometry experiment to determine the composition of the CCR2+ cells 21 days after the sciatic cut. We found that the majority of infiltrating CCR2+ cells were T-cells (CD3+) and macrophages (CD45^{High} CD11b+ CCR2+). We also performed these experiments in CCR2 KO mice and found T-cells entered the spinal cord

independent of CCR2. However, there was a significant decrease in the number of infiltrating macrophages. The results matched our immunohistochemistry analyses. Morphologically, we detected that most round CCR2⁺ cells inside the spinal cord were CD3⁺ T-cells. Also, we identified a population of dual-labeled CCR2 and CX3CR1 cells that had morphologies suggesting a transition from CCR2⁺ monocytes into CX3CR1 microglia-like cells. Interestingly, these cells were only found after injury and were mostly absent in CCR2 KO mice (while T-cell infiltration remained). One significant problem while interpreting these results is that they suggest that CCR2⁺ cells converting into local macrophages quickly downregulate CCR2 and become undetectable in our animals. To obtain further evidence about whether peripheral CCR2 monocytes were transforming into microglial cells we devised a lineage labeling method using CX3CR1-CreER mice to distinguish new microglia from microglia derived from the resident pool before the injury. The initial results confirmed the possibility that some microglia after the injury was derived from the periphery, although we still need to increase animal numbers in this experiment. However, this experiment does not give information about possible immune cells with downregulated CCR2 that do not upregulate CX3CR1 or transform into a microglia-like phenotype. This is an important point, and I will address strategies to address this issue in future directions.

Interestingly, VGLUT1 inputs seem preserved on the dendrites of regenerated MNs 8 weeks after the injury in CCR2 KO mice. These data suggest that the dendritic deletion of Ia afferent synapses depends on a CCR2 signaling

mechanism and likely on the entry of CCR2⁺ monocytes converting into CX3CR1 microglia-like cells. However, CCR2 is also upregulated after nerve injury in Schwann cells on the injured nerve (Chen et al., 2015) and the cell bodies of injured dorsal root ganglion cells (Niemi et al., 2013; DeFrancesco-Lisowitz et al., 2014). Both of these sites will be affected in global KO mice. Moreover, the exact source of CCL2 within the spinal cord was unknown. To more specifically locate a CCR2 mechanism within the spinal cord, we performed sciatic nerve transections in mice that express mCherry under the CCL2 promoter, a principal ligand that binds to CCR2 and activates this receptor. We found that CCL2 is expressed in MNs 3 days after sciatic cut and by microglia 14 days post-injury (more on this in the future directions). Qualitatively, fluorescence intensity is higher in microglia than in MNs, and also the timing of CCL2 upregulation in microglia correlates better with CCR2⁺ cell infiltration. These could suggest a more substantial influence of microglia-derived CCL2 in the recruitment of peripheral macrophages. We tentatively concluded (pending ongoing experiments) that microglia CCL2 is responsible for recruitment of CCR2⁺ monocytes/macrophages inside the spinal cord and that this entry is necessary for VGLUT1 synaptic losses on MN dendrites.

The data presented here support **hypothesis (2)** as we demonstrated a longer microglia reaction and a significantly higher rate of macrophage infiltration in the sciatic cut model compared to the more distal tibial injury. Ultimately, this difference resulted in a greater loss of VGLUT1 synapses after sciatic cut. These data also support **hypothesis (3)** by completely preventing the loss of dendritic

VGLUT1 synapses in the CCR2 KO mice. However, to adequately demonstrate that the relevant CCR2 mechanism involves explicitly the entry of CCR2 cells inside the spinal cord we are now performing conditional KO experiments in which we are deleting CCL2 from either microglia or MNs. In these experiments, CCL2-CCR2 signaling is preserved at the level of the dorsal root ganglia and in the peripheral nerve and should unequivocally test whether a spinal cord CCR2 activation mechanism is necessary for VGLUT1 synapse loss.

5.1.3: The importance of peripheral nerve regeneration efficiency and the permanency of Ia synaptic loss

Hypothesis (4): Nerve transection and nerve crush both results in activation of microglia cells in the ventral horn of the spinal cord, but only nerve transection (causing a more substantial permanent synaptic loss) will recruit CCR2 peripheral myeloid cells.

Once we had shown that VGLUT1 synapse loss is dependent on CCR2 activation and this in turn depends on the properties of neuroinflammation after nerve injury, the following question the significance of these different responses. One possibility is that graded neuroinflammatory responses are necessary to induce more or less central motor circuit plasticity depending on the degree of reinnervation specificity attained during peripheral nerve regeneration. For example, more synaptic plasticity might be necessary when MNs and Ia afferents

are directed to the wrong muscles since this will obviously affect function when preserving the original connectivity inside the spinal cord. This question can be directly answered by comparing a sciatic nerve crush to sciatic nerve transection. First, reinnervation efficacy and specificity is expected to be much higher after sciatic nerve crush (Bodine-Fowler et al., 1997; Nguyen et al., 2002). Second, in cats and rabbits it was shown that stretch reflexes recover after nerve crush but not after nerve transection (Barker and Young, 1947; Cope et al., 1994; Prather et al., 2011). However, as shown by our control data using ATF3 both injuries result in similar numbers of axotomized neurons.

Following nerve injury, sensory and motor axons can regenerate and reinnervate muscle. However, the success of returning to their original target is very much dependent on the type of injury sustained. For example, when a peripheral nerve is crushed the endoneurial tubes remain intact and can guide the axons back to their original target faster and more efficiently compared to a complete transection followed by repair. In this case, the nerve conduit is completely separated, and the axon regeneration process is slower and randomized as the endoneurial tubes are no longer in continuity with one another. We predicted that the success of peripheral regeneration would determine the degree and permanency of central Ia afferent loss.

We compared how each of these injuries, with different peripheral outcomes, influenced the loss of VGLUT1 synapses on MNs. We found that over the first three weeks after injury VGLUT1 fluorescence intensity decreases equally between the two injuries; however, in the crush model the fluorescence

intensity levels return to near controls levels 8 weeks after injury while in the complete transection model, there is no recovery. We reconstructed pre-labeled LG MNs and quantified differences in VGLUT1 density to determine if this trend reflected an actual reduction in the number of synapses on MNs. As the fluorescence data suggested, at 21 days following crush there is a significant decrease in somatic and dendritic VGLUT1 density compared to controls (although of smaller amplitude compared to the reduction after full nerve transection). However, these values returned to control levels by 8 weeks after injury. In the complete transection model, there was a more significant decrease in VGLUT1 density that did not return to control levels regardless of peripheral regeneration. This was correlated with a disappearance of the axonal projection of VGLUT1 afferents as shown within VGLUT1-cre-tdTomato animals in which both synapses and axons of VGLUT1 afferents are genetically labeled. The best interpretation of these results is that the withdrawal of synapses after nerve crush is partial and not accompanied by a die-back of Ia/II axons towards lamina V, thus allowing significant synapse recovery after both Ia afferents and MNs reinnervate muscle. This also correlates with faster and more efficient regeneration and recovery of original axons back to the LG muscle after sciatic nerve crush compared to transection.

We, therefore, hypothesized that the microglia reaction would be greater or more pro-inflammatory and the number of infiltrating CCR2+ cells would be larger in the cut model compared to crush. Interestingly, 3 and 7 days after injury the number of microglia in the ventral horn is very similar between the two

injuries; however, the response abruptly returns towards control levels by 14 days after crush and remains significantly elevated in the cut animals for 21 days before returning to control levels. We found no difference in initial microglia proliferation or migration towards the cell bodies of axotomized MNs between both injury models. We also found that while both injuries resulted in CCL2 upregulation in MNs, only after sciatic transection did microglia express CCL2. As expected, given the results above, we did not find a significant infiltration of peripheral CCR2⁺ cells in the crush model. These data further support the hypothesis that the infiltration of peripheral CCR2⁺ macrophages depends on microglia CCL2 and is necessary for the permanent removal of VGLUT1 synapses and axons from the ventral horn. It suggests that the phenotypic differentiation of microglia into a CCL2-expressing pro-inflammatory phenotype is necessary for the permanent loss of VGLUT1 synapses

In summary, the data presented here supports **hypothesis (4)**. Despite all these advances, many questions are remaining. What are the signals that maintain microglia activation past the second week after nerve transection? What signals induce microglia to change phenotype? Do CCR2 cells transform into microglia-like cells only or are there other phenotypes yet to be discovered? What cell type is directly responsible for the removal of the Ia afferent axon?

5.2: Future Directions

5.2.1: CCL2 Removal from MNs and microglia

Upon completion of my doctorate thesis, additional experiments will be added to support our hypotheses presented here. There are several key experiments that are currently in process. One experiment that needs to be completed is to genetically KO CCL2 production from MNs and microglia independently. Fortunately, the CCL2 mCherry mouse has exons 2-3 of the CCL2 gene flanked by loxp sites allowing for its removal in a cre dependent manner. We crossed ChAT cre mice with CCL2 mCherry mice to genetically eliminate CCL2 from MNs and we are in the process of crossing CX3CR1 creER mice with CCL2 mCherry mice to eliminate CCL2 from microglia. We will use these mice to quantify the infiltration of CD45 expressing leukocytes 14 days post-injury and then quantify the VGLUT1 somatic and dendritic density 8 weeks post-injury in both genetic KO animals. Based on our current findings we predict that eliminating CCL2 from microglia is key to preventing the infiltration of CD45+ cells and that this will result in the preservation of VGLUT1 synapses. The role of CCL2 release from MNs is not clear at this time. CCL2 is expressed after both sciatic cut and crush injuries in MNs, but this does not result in the infiltration of peripheral macrophages in the crush model. Only when CCL2 is produced by microglia does there appear to be any significant recruitment of these peripheral cells. One possibility is that MN CCL2 expression is too low to signal the recruitment of peripheral CCR2 cells as we detect stronger CCL2 fluorescence in microglia cells compared to MNs.

5.2.2: Microglia activation by CSF1

We are currently working on the signaling mechanism involved in triggering microglia activation and are using novel genetic tools to demonstrate their activation is necessary for the permanent loss of VGLUT1 synapses. Based on previous experiments, we predicted that axotomized MNs express colony stimulating factor 1 (CSF1), a key signaling mechanism for microglia activation. CSF1 release was found necessary for dorsal horn microglia activation (Guan et al., 2016) and mutant mice lacking the CSF1 receptor fail to activate microglia in the facial nucleus after injury (Kalla et al., 2001). We, therefore, deleted CSF1 specifically from MNs and performed sciatic nerve cut injuries. In these experiments, we did not have a genetic label for CCR2 cells, and therefore we utilized CD45 immunohistochemistry as a generalized marker of leukocytes. We found that CSF1 deletion from MNs strongly attenuated the microglia response and prevented the infiltration of peripheral CD45+ leukocytes. Although these experiments are still ongoing, the preliminary data suggests that nerve axotomy results in the release of CSF1 from MNs which initiates microglia activation in the ventral horn (dorsal horn microglia activation as not affected). A change in phenotype accompanies prolongation of microglia activation past 14 days into pro-inflammatory CCL2-releasing microglia that initiates recruitment of peripheral macrophages, perhaps converting into microglia-like cells. Both steps (microglia activation followed by CCR2 cell infiltration) are necessary for degradation and removal of afferent axons and synaptic inputs in lamina IX of the spinal cord. We are also producing CSF1 KO mice with an 8 week survival time point to quantify the VGLUT1 density on reconstructed MNs. Preliminary findings show complete

preservation of VGLUT1 synapses in these mice ($n = 1$). We therefore obtained data to support our hypothesis that preventing the microglia reaction and recruitment of macrophages will prevent the permanent degeneration of Ia afferent synapses in lamina IX of the spinal cord.

5.2.3: CCR2 lineage tracing experiments

To investigate the fate of CCR2+ cells inside the spinal cord, the Alvarez lab recently started the process of importing CCR2-CreERT2 animals (donated by Prof. Burkhard Becher, University of Zurich) that will allow labeling the cell lineage derived from CCR2 cells in the future. Although we have been discussing the need for these animals to discern better the fate of CCR2+ cells infiltrating the spinal cord they only very recently became available (Croxford et al., 2015). It is expected that these animals will more accurately detail in future experiments the fate of CCR2 cells inside the spinal cord.

5.2.4: Live cell imaging

Finally, we reasoned that the only experiment that can indeed demonstrate the cell types or types that directly remove Ia axons and synapses from the ventral horn is time-lapse two-photon microscopy of these cells while simultaneously genetically labeling VGLUT1 axons. I spent considerable time troubleshooting this technique and advances towards this goal are shown in the paper added in Appendix 2. The objective of these experiments is ultimately

perform time-lapse imaging of genetically labeled VGLUT1 afferents and CX3CR1 microglia and study their interactions directly. It is noteworthy that the only cell found expressing the phagocytic markers CD68 in the spinal cord are CX3CR1 microglia-like cells (not shown). If some of these cells are found responsible for deleting the VGLUT1 axons and synapses, then future experiments will need to investigate whether these are derived from resident microglia cells influenced by the entry of CCR2 cells, or if many are indeed derived from peripheral blood CCR2+ monocytes converting into local tissue CX3CR1 macrophages.

5.2.5: Physiology

Lastly, as I transition to my postdoctoral work, I will be using electrophysiological techniques to investigate the functional consequences of preserving the connectivity of the Ia afferents with MNs. We produced additional data (not presented in the thesis) in both rats (collaboration with the laboratory of Dr. Fyffe at Wright State University) and in mice demonstrating that administration of the anti-inflammatory drug, minocycline, prevents the loss of VGLUT1 synapses on axotomized MNs. The next logical step is to investigate the functional consequence of preserving these synapses. We hypothesize that the stretch synaptic potentials will return to near normal levels and that we will preserve the stretch reflex in drug-treated animals.

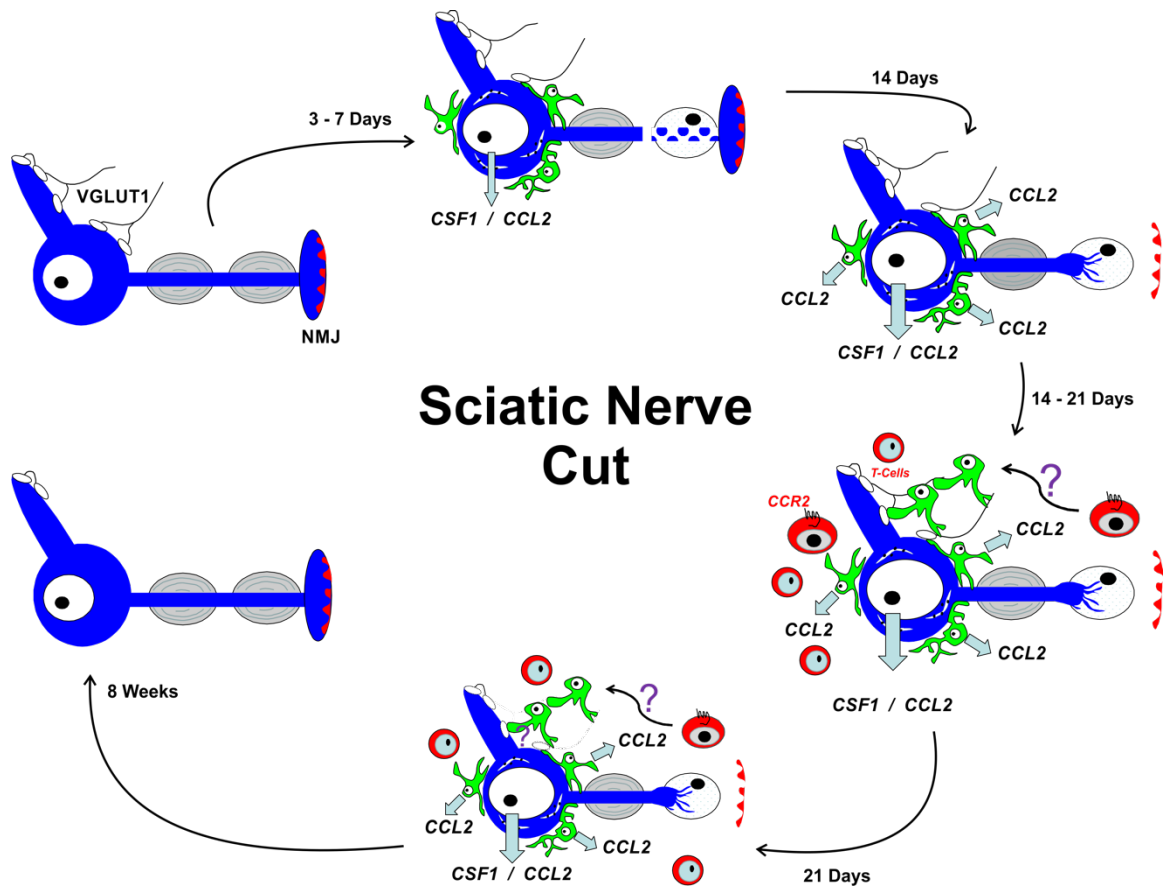


Figure 5.1: Mechanism of synaptic removal following a sciatic nerve cut

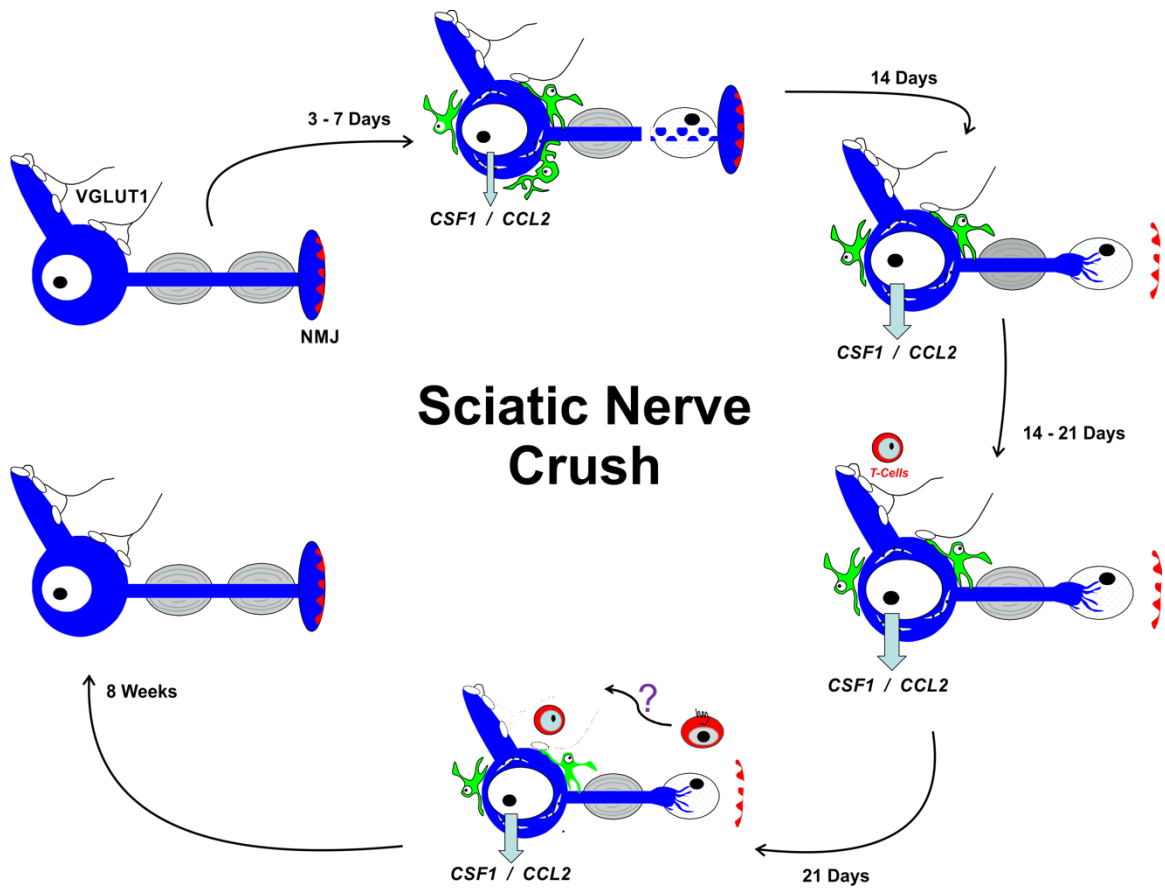


Figure 5.2: Mechanism for the recovery of synaptic inputs following a nerve crush.

References:

- Aldskogius H (2011) Mechanisms and consequences of microglial responses to peripheral axotomy. *Frontiers in bioscience* 3:857-868.
- Aldskogius H, Arvidsson J, Grant G (1985) The reaction of primary sensory neurons to peripheral nerve injury with particular emphasis on transganglionic changes. *Brain research* 357:27-46.
- Alvarez FJ, Villalba RM, Zerda R, Schneider SP (2004) Vesicular glutamate transporters in the spinal cord, with special reference to sensory primary afferent synapses. *The Journal of comparative neurology* 472:257-280.
- Alvarez FJ, Titus-Mitchell HE, Bullinger KL, Kraszpulski M, Nardelli P, Cope TC (2011) Permanent central synaptic disconnection of proprioceptors after nerve injury and regeneration. I. Loss of VGLUT1/IA synapses on motoneurons. *Journal of neurophysiology* 106:2450-2470.
- Arvidsson J (1979) An ultrastructural study of transganglionic degeneration in the main sensory trigeminal nucleus of the rat. *Journal of neurocytology* 8:31-45.
- Arvidsson J (1986) Transganglionic degeneration in vibrissae innervating primary sensory neurons of the rat: a light and electron microscopic study. *The Journal of comparative neurology* 249:392-403.
- Arvidsson J, Grant G (1979) Further observations on transganglionic degeneration in trigeminal primary sensory neurons. *Brain research* 162:1-12.
- Barker D, Young JZ (1947) Recovery of stretch reflexes after nerve injury. *Lancet* 1:704-707.
- Berg A, Zelano J, Thams S, Cullheim S (2013) The extent of synaptic stripping of motoneurons after axotomy is not correlated to activation of surrounding glia or downregulation of postsynaptic adhesion molecules. *PloS one* 8:e59647.
- Blinzinger K, Kreutzberg G (1968) Displacement of synaptic terminals from regenerating motoneurons by microglial cells. *Zeitschrift fur Zellforschung und mikroskopische Anatomie* 85:145-157.
- Bodine-Fowler SC, Meyer RS, Moskovitz A, Abrams R, Botte MJ (1997) Inaccurate projection of rat soleus motoneurons: a comparison of nerve repair techniques. *Muscle & nerve* 20:29-37.
- Brown AG, Fyffe RE (1981) Direct observations on the contacts made between Ia afferent fibres and alpha-motoneurons in the cat's lumbosacral spinal cord. *The Journal of physiology* 313:121-140.
- Bullinger KL, Nardelli P, Pinter MJ, Alvarez FJ, Cope TC (2011) Permanent central synaptic disconnection of proprioceptors after nerve injury and regeneration. II. Loss of functional connectivity with motoneurons. *Journal of neurophysiology* 106:2471-2485.
- Burke RE, Glenn LL (1996) Horseradish peroxidase study of the spatial and electrotonic distribution of group Ia synapses on type-identified ankle

- extensor motoneurons in the cat. *The Journal of comparative neurology* 372:465-485.
- Chen P, Piao X, Bonaldo P (2015) Role of macrophages in Wallerian degeneration and axonal regeneration after peripheral nerve injury. *Acta neuropathologica* 130:605-618.
- Chen XY, Wolpaw JR (1994) Triceps surae motoneuron morphology in the rat: a quantitative light microscopic study. *The Journal of comparative neurology* 343:143-157.
- Cope TC, Bonasera SJ, Nichols TR (1994) Reinnervated muscles fail to produce stretch reflexes. *Journal of neurophysiology* 71:817-820.
- Coull JA, Boudreau D, Bachand K, Prescott SA, Nault F, Sik A, De Koninck P, De Koninck Y (2003) Trans-synaptic shift in anion gradient in spinal lamina I neurons as a mechanism of neuropathic pain. *Nature* 424:938-942.
- Croxford AL, Lanzinger M, Hartmann FJ, Schreiner B, Mair F, Pelczar P, Clausen BE, Jung S, Greter M, Becher B (2015) The Cytokine GM-CSF Drives the Inflammatory Signature of CCR2+ Monocytes and Licenses Autoimmunity. *Immunity* 43:502-514.
- DeFrancesco-Lisowitz A, Lindborg JA, Niemi JP, Zigmond RE (2014) The neuroimmunology of degeneration and regeneration in the peripheral nervous system. *Neuroscience*.
- Echeverry S, Shi XQ, Rivest S, Zhang J (2011) Peripheral nerve injury alters blood-spinal cord barrier functional and molecular integrity through a selective inflammatory pathway. *J Neurosci* 31:10819-10828.
- Eriksson NP, Persson JK, Svensson M, Arvidsson J, Molander C, Aldskogius H (1993) A quantitative analysis of the microglial cell reaction in central primary sensory projection territories following peripheral nerve injury in the adult rat. *Experimental brain research Experimentelle Hirnforschung Experimentation cerebrale* 96:19-27.
- Evans TA, Barkauskas DS, Myers JT, Hare EG, You JQ, Ransohoff RM, Huang AY, Silver J (2014) High-resolution intravital imaging reveals that blood-derived macrophages but not resident microglia facilitate secondary axonal dieback in traumatic spinal cord injury. *Experimental neurology* 254:109-120.
- Graeber MB, Streit WJ, Kreutzberg G (1991) The glial response to motor neuron axotomy: role of microglia and astrocytes. In: *Proceedings of the XIth International Congress of Neuropathology, Supplement 4 pp 282-287. Kyoto: Japanese Society for Neuropathology*
- Gu N, Peng J, Murugan M, Wang X, Eyo UB, Sun D, Ren Y, DiCicco-Bloom E, Young W, Dong H, Wu LJ (2016) Spinal Microgliosis Due to Resident Microglial Proliferation Is Required for Pain Hypersensitivity after Peripheral Nerve Injury. *Cell reports* 16:605-614.
- Guan Z, Kuhn JA, Wang X, Colquitt B, Solorzano C, Vaman S, Guan AK, Evans-Reinsch Z, Braz J, Devor M, Abboud-Werner SL, Lanier LL, Lomvardas S, Basbaum AI (2016) Injured sensory neuron-derived CSF1 induces

- microglial proliferation and DAP12-dependent pain. *Nature neuroscience* 19:94-101.
- Hultborn H, Denton ME, Wienecke J, Nielsen JB (2003) Variable amplification of synaptic input to cat spinal motoneurons by dendritic persistent inward current. *The Journal of physiology* 552:945-952.
- Jinno S, Yamada J (2011) Using comparative anatomy in the axotomy model to identify distinct roles for microglia and astrocytes in synaptic stripping. *Neuron glia biology* 7:55-66.
- Kalla R, Liu Z, Xu S, Koppius A, Imai Y, Kloss CU, Kohsaka S, Gschwendtner A, Moller JC, Werner A, Raivich G (2001) Microglia and the early phase of immune surveillance in the axotomized facial motor nucleus: impaired microglial activation and lymphocyte recruitment but no effect on neuronal survival or axonal regeneration in macrophage-colony stimulating factor-deficient mice. *The Journal of comparative neurology* 436:182-201.
- Kettenmann H, Kirchhoff F, Verkhratsky A (2013) Microglia: new roles for the synaptic stripper. *Neuron* 77:10-18.
- Linda H, Shupliakov O, Ornung G, Ottersen OP, Storm-Mathisen J, Risling M, Cullheim S (2000) Ultrastructural evidence for a preferential elimination of glutamate-immunoreactive synaptic terminals from spinal motoneurons after intramedullary axotomy. *The Journal of comparative neurology* 425:10-23.
- Nguyen QT, Sanes JR, Lichtman JW (2002) Pre-existing pathways promote precise projection patterns. *Nature neuroscience* 5:861-867.
- Niemi JP, DeFrancesco-Lisowitz A, Roldan-Hernandez L, Lindborg JA, Mandell D, Zigmond RE (2013) A critical role for macrophages near axotomized neuronal cell bodies in stimulating nerve regeneration. *J Neurosci* 33:16236-16248.
- Pierce JP, Mendell LM (1993) Quantitative ultrastructure of Ia boutons in the ventral horn: scaling and positional relationships. *J Neurosci* 13:4748-4763.
- Prather JF, Nardelli P, Nakanishi ST, Ross KT, Nichols TR, Pinter MJ, Cope TC (2011) Recovery of proprioceptive feedback from nerve crush. *The Journal of physiology* 589:4935-4947.
- Ransohoff RM (2011) Microglia and monocytes: 'tis plain the twain meet in the brain. *Nature neuroscience* 14:1098-1100.
- Redman S, Walmsley B (1983a) The time course of synaptic potentials evoked in cat spinal motoneurons at identified group Ia synapses. *The Journal of physiology* 343:117-133.
- Redman S, Walmsley B (1983b) Amplitude fluctuations in synaptic potentials evoked in cat spinal motoneurons at identified group Ia synapses. *The Journal of physiology* 343:135-145.
- Schafer DP, Lehrman EK, Kautzman AG, Koyama R, Mardinly AR, Yamasaki R, Ransohoff RM, Greenberg ME, Barres BA, Stevens B (2012) Microglia sculpt postnatal neural circuits in an activity and complement-dependent manner. *Neuron* 74:691-705.

- Streit WJ, Mrak RE, Griffin WS (2004) Microglia and neuroinflammation: a pathological perspective. *Journal of neuroinflammation* 1:14.
- Svensson M, Aldskogius H (1993) Synaptic density of axotomized hypoglossal motoneurons following pharmacological blockade of the microglial cell proliferation. *Experimental neurology* 120:123-131.
- Trapp BD, Wujek JR, Criste GA, Jalabi W, Yin X, Kidd GJ, Stohlman S, Ransohoff R (2007) Evidence for synaptic stripping by cortical microglia. *Glia* 55:360-368.
- Wolf SA, Boddeke HW, Kettenmann H (2017) Microglia in Physiology and Disease. *Annu Rev Physiol* 79:619-643.
- Yamada J, Nakanishi H, Jinno S (2011) Differential involvement of perineuronal astrocytes and microglia in synaptic stripping after hypoglossal axotomy. *Neuroscience* 182:1-10.
- Yamasaki R et al. (2014) Differential roles of microglia and monocytes in the inflamed central nervous system. *The Journal of experimental medicine* 211:1533-1549.

Appendix I:

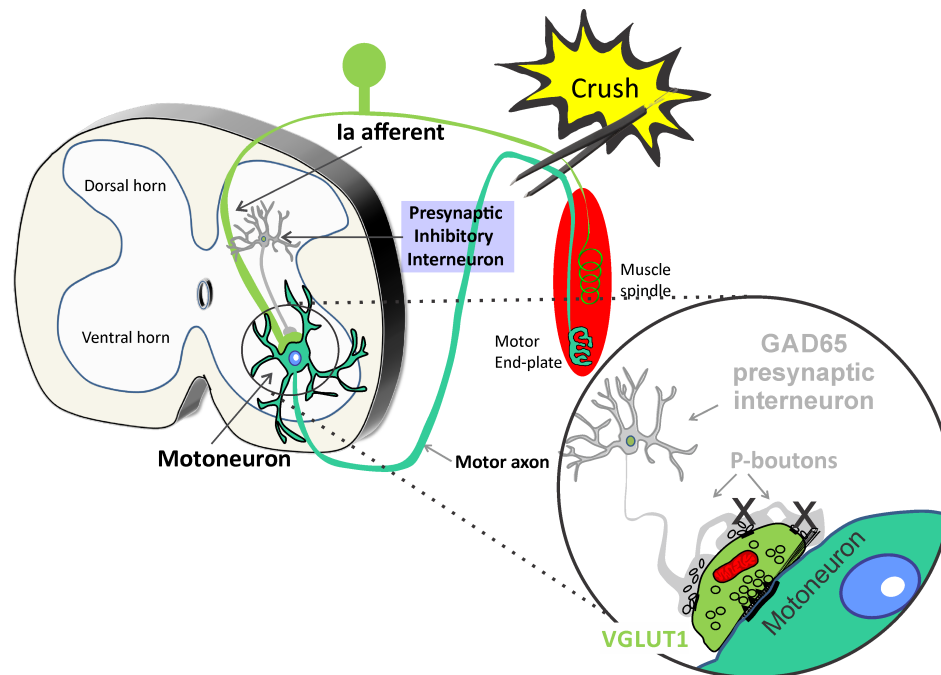
VGLUT1 synapses and p-boutons on regenerating motoneurons after nerve crush

Chapter Published: Schultz AJ, Rotterman TM*, Dwarakanath A, Alvarez FJ (2017) VGLUT1 synapses and P-boutons on regenerating motoneurons after nerve crush. The Journal of comparative neurology 525:2876-2889.*

*Co-first authors

Permission granted from publisher for reproduction:

license# 4290391172567, approved on 2/15/2018, full article



6.1: Abstract

Stretch-sensitive Ia afferent monosynaptic connections with motoneurons form the stretch reflex circuit. After nerve transection, Ia afferent synapses and stretch reflexes are permanently lost, even after regeneration and efficient re-innervation of muscle by motor and sensory afferents is completed in the periphery. This loss greatly affects full recovery of motor function. However, after nerve crush, reflex muscle forces during stretch do recover after muscle reinnervation and reportedly exceed 140% baseline values. This difference might be explained by structural preservation after crush of Ia afferent synapses on regenerating motoneurons and decreased presynaptic inhibitory control. We tested these possibilities in rats after crushing the tibial nerve and using Vesicular GLUtamate Transporter 1 (VGLUT1) and the 65 kDa isoform of glutamic acid-decarboxylase (GAD65) as markers of, respectively, Ia afferent synapses and presynaptic inhibition (P-boutons) on retrogradely labeled motoneurons. We analyzed motoneurons during regeneration (21 days post crush) and after they reinnervate muscle (3 months). The results demonstrate a significant loss of VGLUT1 terminals on dendrites and cell bodies at both 21 days and 3 months post-crush. However, in both cellular compartments the reductions were small compared to those observed after tibial nerve full transection. In addition, we found a significant decrease in the number of GAD65 P-boutons per VGLUT1 terminal and their coverage of VGLUT1 boutons. The results support the hypothesis that better preservation of Ia afferent synapses and a change in

presynaptic inhibition could contribute to maintain or even increase the stretch reflex after nerve crush and by difference to nerve transection.

6.2: Introduction

Peripheral nerve injuries may arise from a variety of trauma from nerve crush to complete lacerations and affect different types of nerves and body regions. Although nerve regeneration occurs in the periphery, overall recovery of motor function is generally disappointing; only 10% of adult patients regain near-normal function after median or ulnar injuries that require surgical repair, although outcomes are much better after milder injuries (Lundborg, 2003; Brushart, 2011). It is thus important to understand the neurobiological mechanisms that impair motor function recovery to different levels after different injuries.

Axon regeneration is fairly inefficient in patients with injuries in large nerve or that occur at long distances from their targets (for example, a brachial plexus injury). One problem is that the velocity of peripheral axon regeneration is slow (1-3 mm/day) (Sunderland, 1947) and regeneration capacity declines with time (Fu and Gordon, 1995a; Fu and Gordon, 1995b). In addition, pathfinding signals found in early development are not present in the adult and regenerating axons have difficulties finding the correct paths and can be misrouted to wrong muscles or targets (Brushart and Mesulam, 1980; Brushart et al., 1983; Allodi et al., 2012). Not surprisingly, much experimental attention has focused on

mechanisms that can improve the efficiency and specificity of regeneration in the periphery (Chan et al., 2014; Gordon and English, 2016). However, even when successful peripheral regeneration is achieved after surgical repair, persistent motor deficits remain. For example, full nerve transection and repair of small distal nerves projecting to single hind limb muscles (medial gastrocnemius nerve or quadriceps nerves) result in rapid and specific muscle reinnervation and full recovery of force within weeks, but stretch reflexes are permanently lost. This occurs even though stretch-sensitive sensory proprioceptors (that is, Ia afferents) efficiently reinnervate muscle spindle receptors and are capable of encoding and transmitting information about muscle length (Cope et al., 1994; Haftel et al., 2005; Bullinger et al., 2011; Lyle et al., 2016). Deficits in feedback information about muscle length manifest in abnormal inter-joint coordination during walking, higher than normal co-contraction of antagonists around single joints and errors in slope walking (Abelew et al., 2000; Maas et al., 2007; Sabatier et al., 2011). Some of these deficits are compensated by adjustments in the unaffected hind limb joints such that overall limb kinematics and general limb functions are preserved (Chang et al., 2009). However, feedback information about muscle length has many important roles during ongoing motor activity including opposing influences from force signals generated by Ib Golgi tendon organs in nearby muscles (Lyle et al., 2016). Their loss implies that tasks involving high forces and/or rapid and large muscle lengthening (steep downslopes) should predictably show significant deficits in performance after nerve regeneration (Abelew et al., 2000; Maas et al., 2007; Lyle et al., 2016).

Deficits in proprioceptive information relayed by stretch-encoding Ia afferents arise because their central synaptic arbors inside the spinal cord are removed from the ventral horn (Alvarez et al., 2010; Alvarez et al., 2011; Bullinger et al., 2011). This causes the loss of most synaptic collaterals from Ia afferents in lamina IX, and to lesser extent those in lamina VII, greatly denervating motoneurons. Motoneurons lose approximately 60-65% of synapses from Ia afferents on the dendritic arbor and 85-90% on the cell bodies (Rotterman et al., 2014). Functionally, single Ia afferents in normal un-injured animals give input to around 93% of the motor pool, but after injury and complete regeneration in the periphery they only innervate 17% of the pool motoneurons (Bullinger et al., 2011) and remaining synaptic potentials evoked by stretching the muscle are greatly diminished (Haftel et al., 2005; Bullinger et al., 2011). In summary, injured Ia afferent axons can regenerate in the periphery, reinnervate muscle and muscle spindles and become functional (Haftel et al., 2005), however their central branches do not reestablish the synapses lost in the ventral horn (Alvarez et al., 2010; Bullinger et al., 2011; Rotterman et al., 2014) causing a sensory insufficiency in the stretch reflex and in central processing of muscle length information that alters modulation of motoneuron activity and impairs motor performance.

Interestingly, the stability of the stretch reflex is dependent on the type of nerve injury. In a pioneering study prompted by the types of injuries sustained by British soldiers in World War II, D. Barker and J.Z. Young compared spinal reflexes in rabbits in which peripheral nerves were either fully transected or

crushed (Barker and Young, 1947). They found that while stretch reflexes were frequently small or not detectable after full nerve transections, they were fully recovered after nerve crush injuries. A more recent study (Prather et al., 2011), reported supranormal stretch reflexes in cats after recovery from medial gastrocnemius nerve crush. Interestingly, Prather and colleagues (2011) found 70% preservation of stretch-evoked excitatory synaptic potentials (strEPSPs) in medial gastrocnemius motoneurons and this contrasts with the large depression that occurs after complete transection of the same nerve (Haftel et al., 2005; Bullinger et al., 2011). These results predict that Ia afferent synapses should be retained to a larger extent after nerve crush compared to nerve transection.

Increased synaptic preservation is certainly a pre-requisite for the results described in Prather and colleagues (2011), however, additional factors need to be considered to explain why dynamic stretch reflex forces were increased by 145% or greater after nerve crush. This increase in reflex forces can, potentially, be explained by alternative changes in spinal cord circuitry. Presynaptic inhibition of cutaneous sensory afferent mechanoreceptor synapses is reduced in the dorsal horn following peripheral nerve injury, and this is associated with a loss of GABAergic synapses (Castro-Lopes et al., 1993; Horch and Lisney, 1981; Moore et al., 2002). The effect of crush injury on presynaptic inhibition of ventral proprioceptive Ia afferents is, however, less clear (Enriquez et al., 1996; Enriquez-Denton et al., 2004) and has not yet been analyzed at the structural level. Indeed, one potential explanation for the increased stretch-reflex is a loss

of presynaptic terminals (P-boutons) (Conradi, 1969). P-boutons on Ia afferents are GABAergic (Maxwell et al., 1990) and on VGLUT1 Ia afferent synaptic boutons they can be easily identified by their immunoreactivity to the 65kda isoform of glutamic decarboxylase (GAD65) (Hughes et al., 2005; Betley et al., 2009).

The goals of the present study are therefore to test whether after crush nerve injury: i) there is preservation of Ia afferent synapses on regenerating motoneurons using the Vesicular GLUamate Transporter 1 (VGLUT1) as an efficient marker to map these synapses on motoneuron dendrites (Alvarez et al., 2004; 2011; Rotterman et al., 2014); ii) GABAergic presynaptic control of VGLUT1 Ia afferent synaptic boutons is diminished. To accomplish these goals we analyzed VGLUT1 boutons and their GAD65 P-boutons on retrogradely labeled medial gastrocnemius motoneurons after tibial nerve crush and compared the results to previous data after tibial nerve transection (Alvarez et al., 2011). The results confirm that VGLUT1 synapses are better preserved after crush compared to complete nerve transections. Furthermore, a decrease in GAD65 P-bouton coverage of VGLUT1 terminals was also detected suggesting a possible decrease in GABAergic presynaptic control. These differences in structural remodeling of Ia afferent synapses after nerve crush compared to nerve transection contribute to explain the observations on the differential preservation of the stretch reflex in both types of injuries as originally reported by Barker and Young 70 years ago.

6.3: Methods

All studies were performed on adult female Wistar rats (225-300g). All animal procedures and nerve surgeries were performed at Wright State University and approved by the institutional laboratory animal use committees of Wright State University and Emory University. Collected tissues were sent to Emory University for processing and analyses.

6.3.1: Nerve injury and injections of retrograde tracers

Adult female Wistar rats were anesthetized with isoflurane until a surgical plane of anesthesia was obtained (induction 4-5%; maintenance 1-3%, both in 100% O₂). The tibial nerve (TN) was exposed at mid-thigh by a midline posterior incision (~1.5 cm) through the skin and underlying connective in the left hind limb. The TN was then crushed with fine #5 forceps for 10s. After washing with 0.9% sterile saline, the wound was closed in layers and the animals removed from anesthesia. Buprenorphine (subcutaneous, 0.1 mg/kg) was delivered immediately and every 12 hours after surgery prophylactically for 48 hours to alleviate any possible pain and distress. Signs of pain or distress (lethargy, vocalizations, weight loss, absence of grooming) were closely monitored but not observed in any animals. One week prior to the animals being euthanized, the medial gastrocnemius (MG) muscle of the left leg was exposed and injected with 10-20 µl of 0.1% Alexa 555 conjugated to recombinant cholera toxin subunit b (CTb-555, Invitrogen, ThermoFisher Scientific, Waltham, MA). The total volume was distributed throughout the muscle in four to five 2 to 5 µl injections. The

control group did not undergo any nerve surgeries prior to the CTb-555 injections.

6.3.2: Histology and immunocytochemistry

Control (n=4) and experimental animals (n=8) were deeply anesthetized with Euthasol and transcardially perfused with 4% paraformaldehyde in 0.1M phosphate buffer. Experimental animals were sacrificed 21 days or 3 months following nerve crush (n=4 in each group). These dates were chosen to compare VGLUT1 synaptic coverage on regenerating MG motoneurons at a time point prior to muscle reinnervation (21 days) or well after nerve regeneration and muscle reinnervation is completed (3 months). Spinal cords were collected and post-fixed overnight. Lumbar segments 4 and 5 (L4-L5) were extracted and 50 μ m thick sections were obtained in a freezing sliding microtome and processed “free-floating”. After washing the sections in 0.01M phosphate buffer saline (PBS) with 0.3% Triton-x-100 (PBS-Tx) they were blocked in 10% normal donkey serum in PBS-Tx for 1 hour. Sections were then incubated for 24 hours at room temperature in goat polyclonal anti-cholera toxin B subunit (1:1000, List Biological Laboratories, Campbell, CA; cat#7032A6; RRID: AB_2313637), rabbit polyclonal anti-VGLUT1 (1:1000, Synaptic Systems, Goettingen, Germany; cat# 135 303; RRID: AB_887875) and mouse monoclonal anti-GAD65 (1:200, Developmental Studies Hybridoma Bank, Iowa City, Iowa; RRID: AB_528264) both diluted together in PBS-Tx. The immunoreactive sites were revealed with a mixture of anti-goat, anti-rabbit and anti-mouse IgG secondary antibodies made

in donkey (1:100 dilution in PBS-Tx; Jackson ImmunoResearch, West Grove, PA) each tagged to a different fluorochrome (FITC for VGLUT1: RRID: AB_2315776; Cy3 for CTb: RRID: AB_2340411 and Cy5 for GAD65: RRID: AB_2340819).

6.3.3: *Antibody characterization*

The specificity of the rabbit polyclonal VGLUT1 antibody (Synaptic Systems, Goettingen, Germany; cat# 135 303; RRID: AB_887875) was confirmed in VGLUT1 knockout tissue using materials and procedures previously described (Siembab et al., 2016). This VGLUT1 antibody was raised against a Strep-Tag® fusion protein of rat VGLUT1 (aa 456-560). The mouse monoclonal GAD65 antibody used corresponds to the GAD-6 clone that has been amply characterized since it was generated in the mid-80's (Gottlieb et al., 1986). The antibody was generated against GAD partially purified from chicken brains. Clones producing antibodies recognizing GAD were selected thereafter. The antibody produced by clone 6 specifically recognizes an epitope localized between aa 545 and 585 in the lower molecular weight GAD65 isoform (Chang and Gottlieb, 1988; Richter et al., 1993) (Developmental Studies Hybridoma Bank, Iowa City, Iowa; RRID: AB_528264). It does not recognize GAD67. Finally the goat polyclonal antibody against the CTb subunit was raised against recombinant Cholera toxin B subunit (List Biological Laboratories, Campbell, CA; cat#7032A6; RRID AB_2313637) and it does not recognize any immunoreactivity sites in spinal cords lacking neural elements that have uptaken

CTb. No labeling was seen in the contralateral size that was not injected with CTb.

6.3.4: Confocal imaging and neuron reconstruction

Sections from each animal were imaged first at low magnification (20x, N.A. 0.70) in an Olympus FV1000 confocal microscope. CTb-labeled MG motoneurons with their cell bodies fully contained within the 50 μm -thick section and showing long dendrites were re-imaged at high magnification (60x, N.A. 1.35, oil immersion, 0.5 μm z-steps throughout the tissue thickness). Confocal images were obtained by author TMR and coded such that all quantitative analyses performed by AJS were blinded to the condition of the animal. The images were uploaded into NeuroLucida (MicroBrightField, Colchester, VT: RRID: nif_0000_10294) and the whole labeled dendrites traced and reconstructed. The position of each VGLUT1 synapse was “marked” and the GAD65 synapses in contact with marked VGLUT1 synapses were also plotted. VGLUT1 synapses targeting the cell body or dendrites were analyzed separately. Total path length and overall surface of the combined dendrites as well as the surface of the cell body were measured and compared to confirm similar sampling of motoneuron surfaces in all animals (see Table 1). The distribution and density of VGLUT1 synapses was analyzed by obtaining the following two measurements: (1) overall VGLUT1 synaptic densities calculated by dividing the total number of synapses by the total dendritic length (linear), total dendritic surface, or cell body surface; (2) Sholl analysis to examine VGLUT1 distributions in dendrite segments at 50

μm bins of incremental radial distance from the center of the cell body. Linear and surface densities of VGLUT1 contacts within each bin were then calculated. The distribution of GAD65 synapses on VGLUT1 contacts was analyzed also using two separate measurements: (1) the percentage of VGLUT1 contacts receiving contact from GAD65 synapses; (2) the density of contacts from GAD65 synapses was measured by calculating the average ratio of GAD65 to VGLUT1 synapses. We reconstructed and analyzed 40 motoneurons in each of three experimental groups (control, 21 day, 3 month), sampling 10 MNs per animal in each group (n=4 animals per group).

6.3.5: *Surface-to-surface analysis*

To analyze the percentage of surface contact between both types of boutons, confocal image stacks were loaded into Imaris (Bitplane, Concord, MA; RRID: nif-0000-00314) to obtain 3D surface renderings of VGLUT1 boutons and the GAD65 boutons contacting them (20 VGLUT1 terminals were randomly selected from three animals per condition; all VGLUT1 terminals were pooled together for statistical comparisons). VGLUT1 boutons of similar size were selected to avoid biasing trends on P-bouton coverage dependent on VGLUT1 size. For making surface renderings of the boutons, fluorescent level thresholds were determined based on control VGLUT1 terminals and then applied to the other conditions. Thereafter we used a custom MATLAB script to calculate the surface area of the VGLUT1 terminal contacted by GAD65-IR synapses. For this

determination we defined contact surface between the GAD65 and the VGLUT1 bouton as the region with 0 μm separation in the rendered surfaces.

6.3.6: Statistical analyses

All statistical tests were made using SigmaPlot 12.3 (Systat). We used one-way analysis of variance (ANOVAs) to compare VGLUT1 dendritic linear density, dendritic surface area density, and somatic density between control, 21 day crush, and 3 month crush animals. Bonferroni's post-hoc tests were used to determine significant differences between experimental groups with respect to control. In all these data sets normality criteria were fulfilled. Normality, however, failed in data comparing the percentage of VGLUT1 boutons associated with GAD65 P-boutons, the number of P-boutons per VGLUT1 or the coverage of VGLUT1 boutons by P-boutons. In this case we used Kruskal-Wallis One Way ANOVA followed by post-hoc Dunn's tests vs. control. These data sets are therefore displayed as whisker-box plots to better describe the data. Significance was set to $p < 0.05$ in all tests.

6.3.7: Figure composition

Figures were composed in CorelDraw (v. 16.0) and graphs were created in SigmaPlot (ver. 12.0; Jandel Scientific). Adjustments to images were made only for presentation and publication purposes. All quantification was carried out with unprocessed original images. Images in plates were adjusted for optimal contrast and brightness in Image Pro Plus (ver. 5.0; Media Cybernetics,

Bethesda, MD; RRID: nif_0000_00313). Some images were sharpened with a “high-gauss” filter. Manipulations were minimal, and the informational content was not altered.

6.4: Results

6.4.1: *Technical considerations and data interpretation*

Retrogradely labeled medial gastrocnemius (MG) motoneurons and their dendritic arbors were imaged first at low and then at high magnification (see methods) in single transverse spinal cord sections with the cell body centered in the field of view (Fig. 1). Only motoneurons with cell bodies larger than $485 \mu\text{m}^2$ in cross-sectional area were sampled. This cut-off excludes the smaller α -motoneurons that do not receive Ia/VGLUT1 inputs (Shneider et al., 2009). Motoneurons with long continuously labeled dendrites were selected for analyses and these were carried out blind to the condition of each motoneuron (see methods). Imaging, sampling and measurements were chosen to be similar to Alvarez et al. (2011) for optimal comparisons between tibial nerve (TN) crush (this study) and TN transection (previous study). The extension and size of motoneuron surfaces analyzed on dendrites and cell bodies are similar in both studies (compare Table 2 in this study with Table 2 in Alvarez et al., 2011). However, when compared to full reconstructions of complete motoneuron dendritic trees (Rotterman et al., 2014), the labeling and sampling procedure used here is known to be biased to proximal dendrites with principal trajectories

in the transverse plane. This is because imaged dendrite segments are limited to those contained inside the field of view and within the 50 μm deep transverse section. Therefore, dendrites with a preferential rostro-caudal orientation are cut and under sampled (Fig. 1C,G,K). Moreover, the longest dendrites extended beyond the field of view and frequently dendrite segments became disconnected because dendrites meander in and out the section. Our preparations contain many labeled dendrites originating in different motoneurons and it is not feasible to follow single dendrites through serial sections. Unfortunately, for the sample sizes used here, it is also not feasible either to generate enough complete full neuron reconstructions of single intracellularly neurobiotin-filled motoneurons imaged through serial sections and with extensive tiling of confocal stacks to sample the whole dendrite territory. Analyses of fully reconstructed motoneurons (Rotterman et al., 2014), however revealed that 50% and 75% of VGLUT1 contacts in uninjured animals are located, respectively, within the first 300 and 550 μm of the dendritic arbor and that the larger loss of VGLUT1 synapses in injured animals occurs within the first 300 μm of dendrite (Rotterman et al., 2014). The large majority (94.7%) of CTb-retrogradely labeled motoneurons analyzed here had dendritic arbors in which the further point was more than 100 μm distal from the cell body dendrite origins. On average, the more distal dendrite location analyzed was $132.8 \mu\text{m} \pm 13.6$ (\pm S.D.) for motoneurons in control animals ($n=4$), $131.2 \mu\text{m} \pm 17.1$, 21 days TN crush and $124.7 \mu\text{m} \pm 19.5$, 3 months TN nerve crush. Thus, the study is focused on VGLUT1 inputs in the cell body and the more proximal dendritic region.

CTb retrograde labeling appears increasingly punctate inside finer and more distal dendrites and this characteristic could affect surface estimates which depend on accurate measurement of dendrite diameters at each traced segment interval. We therefore calculated in addition to surface density estimates (number of VGLUT1 contacts per unit of dendrite surface in μm^2) the linear dendrite VGLUT1 densities (numbers of VGLUT1 contacts per unit length of dendrite in μm), which are unaffected by possible inaccuracies in dendrite diameter estimates. In summary, the analyses performed assess changes in VGLUT1 synapse densities in the proximal somato-dendritic region and are best compared to Alvarez et al. (2011) using similar methods. Previous studies that analyzed fully reconstructed motoneurons (Rotterman et al., 2014) suggest that these methods focus on the most relevant regions of the motoneuron showing major changes in VGLUT1 density.

6.4.2: Nerve crush causes only a small loss of VGLUT1 contacts on proximal dendrites and cell bodies of regenerating motoneurons

VGLUT1 bouton contact densities on the cell bodies and dendrites were estimated in Neurolucida 3D reconstructions of CTb-labeled motoneurons (Figs. 1A-C, E-G, I-K). When necessary, confocal images were imported into Imaris software for confirmation of VGLUT1-IR bouton “contacts” on the surface of CTb-labeled MG motoneurons rendered in three-dimensional space (Figs. 1D,H,L). All VGLUT1 bouton “contacts” were considered synapses since previous studies confirmed the presence of bassoon, a presynaptic active zone protein, in the

VGLUT1-IR bouton surfaces in contact with labeled motoneuron cell bodies or dendrites (Rotterman et al., 2014). Control motoneurons received on average 0.50 ± 0.04 (\pm S.D.) VGLUT1 contacts per $100 \mu\text{m}^2$ of cell body surface (Fig. 2). In both, 21 day and 3 month post-injury groups VGLUT1 contact density was significantly reduced, respectively, by 35.5% and 38.4% from control (One-Way ANOVA, $F(2,9)=10.909$, $p=0.004$; power for $\alpha = 0.05 : 0.931$; post-hoc Bonferroni corrected t-tests $t=4.196$, $p=0.07$ control vs 3 month and $t=0.179$, $p=0.011$ control vs 21 day crush in; for these and following comparisons $n=4$ animals per group with each animal data point estimated as average VGLUT1 density calculated from 9-10 motoneurons per animal; see Table 3; The number of reconstructed motoneurons augmented accuracy of individual animal estimates and reduced inter-animal variability for statistical comparisons). The magnitude of these depletions is less substantial than the loss reported on MG motoneuron cell bodies after TN transections (69.8% and 57.9% at 6 weeks and 6 months post-injury, respectively; from Alvarez et al., 2011).

VGLUT1 bouton contacts on the dendrites were also reduced to a lesser extent than after TN transection. VGLUT1 dendritic linear density (VGLUT1 density per $100 \mu\text{m}$ of dendrite segment, Fig. 3A) revealed significant depletions after nerve crush compared to control (One-Way ANOVA $F(2,9)=8.885$, $p=0.007$; power for $\alpha = 0.05 : 0.861$). Twenty-one days after crush, CTb-labeled motoneuron dendrites showed, on average, a significant 33.3% loss from control (control average = 12.5 ± 0.8 VGLUT1-IR bouton contacts per $100 \mu\text{m}$ of dendrite length, \pm S.D., post-hoc Bonferroni t-test, $t=3.990$, $p=0.009$ compared to control,).

The 3 month group also exhibited a significant 26.5% depletion from control (post-hoc Bonferroni t-test, $t=3.172$, $p=0.034$ compared to control,). VGLUT1 surface density was also found diminished in both the 21 day (by 21.5%) and 3 month (by 19.5%) groups compared to control values (average surface density in controls = 0.8 ± 0.16 VGLUT1 boutons per $100 \mu\text{m}^2$ of dendrite surface) (Fig. 3B), however, differences in VGLUT1 surface densities did not reach significance (One-way ANOVA, $F(2,9)=2.389$, $p=0.147$; power for $\alpha = 0.05$: 0.220). Smaller percentage changes and lack of statistical significance in VGLUT1 surface densities compared to linear densities might be due to changes in dendritic surface area caused by either variable levels of thinning of proximal dendrites in regenerating motoneurons or lesser uptake of the retrograde tracer CTb that might not fully fill the dendrite thickness. These factors would, in both cases, increase VGLUT1 surface densities estimates and reduce differences with control. Small differences, if they exist, could not be statistically detected with this number of observations. The power of the performed test (0.22) is below the desired power of 0.8. Nevertheless, the results confirm that changes in VGLUT1 synapses are small after TN crush compared to TN transection (Alvarez et al., 2011)

To examine if different dendrite compartments sustained different synaptic losses we divided the traced dendritic trees in three $50 \mu\text{m}$ bins of different distance to the cell body center (Fig. 3C). As previously described (Alvarez et al., 2011; Rotterman et al., 2014), Sholl analyses in control motoneurons revealed a significant and progressive reduction in VGLUT1 linear density with distance from

the cell body (One-Way ANOVA, $F(2,9)=9.306$, $p=0.006$; power for $\alpha = 0.05$: 0.879) while VGLUT1 surface density was maintained constant (One-Way ANOVA, $F(2,9)=0.0151$, $p=0.985$; power for $\alpha = 0.05$: 0.050; in this case power is too small to detect significant differences in surface VGLUT1 density because there is practically no difference between the three dendritic compartments: 0.70 ± 0.29 ; 0.73 ± 0.17 ; 0.71 ± 0.22 VGLUT1 contacts per $100 \mu\text{m}^2 \pm \text{S.D.}$). Surface densities are maintained despite changes in VGLUT1 synapse numbers (linear density) because dendrites taper as they extend from the cell body reducing their surface area. In control motoneurons decreases in number of VGLUT1 synapses along the dendrite match reductions in available surface thus keeping the synaptic surface density constant. After nerve crush, VGLUT1 density on motoneuron dendrites tended to decrease in all distance bins in both linear and surface density estimates. These ranged from 12% to 35%, but only one data point reached statistical significance compared to control (3 month crush in distance segment of 50-100 μm from the cell body center; post-hoc Bonferroni t-test $t=3.566$, $p=0.015$). Loss of significance compared to analyses in the full traced dendrites are likely due to the compound effects of the small differences with control and the increased variance caused by segmentation of the traced dendrites into smaller segments. As a result all comparisons among the same dendritic compartment from animals in the tree conditions (control, 21 days and 3 months after TN nerve crush) were underpowered (<0.8), nevertheless the results once again highlight that if any differences could be revealed by increasing the power of statistical analyses, these would be rather small. These

results are notably different from TN transection, in which there was a larger and significant loss in both linear and surface VGLUT1 density in the proximal dendrite compartments using similar sampling, measurements and Sholl analyses (Alvarez et al., 2011).

To investigate whether there was also a change in the size of VGLUT1 immunoreactive punctae we surface rendered 100 VGLUT1 immunoreactive clusters per condition (25 per animal) and estimated their total volume using Imaris software. In control animals VGLUT1-immunoreactive clusters had an average volume of $10.6 \mu\text{m}^3 \pm 0.8$ (\pm S.E.M.; $n=100$; median = 8.4) while 21 days after nerve crush their average volume was reduced by 33% to $7.1 \mu\text{m}^3 \pm 0.8$ ($n=100$; median = 4.4) and after 3 months there was a partial recovery to $8.2 \mu\text{m}^3 \pm 0.7$ ($n=100$; median = 6.1). Changes with respect to control values were only significant 21 days after crush (One-Way ANOVA on Ranks; $H(2)= 14.436$, $p<0.001$; post-hoc Dunn's test, $Q = 3.79$ $p<0.05$; in 21 day vs control comparison and $Q = 2.12$ $p>0.05$ in 3 month vs control comparison). Bouton size is important given the reported relationship between Ia afferent bouton size, active zone size and other structural parameters indicative of synaptic strength (Pierce and Mendell, 1993). Thus, neither VGLUT1 bouton density nor size are reduced after nerve crush to the levels identified after nerve transection.

6.4.3: Reduction in P-bouton coverage of VGLUT1 boutons following nerve crush

Large preservation of VGLUT1 synapses alone does not fully explain the enhancement of the stretch reflex after nerve crush (Prather et al., 2011). To

examine one possible mechanism that may contribute to disinhibition of the Ia-motoneuron synapse, and thus possibly the stretch reflex, we examined the effects of nerve crush on presynaptic GABAergic control of Ia afferents synapses by examining the incidence and density of GAD65 P-boutons on VGLUT1 synapses (Fig. 4).

We examined a total of 3,957 VGLUT1 boutons in contact with dendrites and 1,242 VGLUT1 boutons on the cell bodies of retrogradely labeled control MG motoneurons and these were compared to 2,686 and 774 VGLUT1 boutons on dendrites and cell bodies of MG motoneurons 21 days after TN crush and 2,694 and 737 VGLUT1 boutons, respectively, 3 months post injury (see Table 3 for the characteristics of the sample). The percentage of VGLUT1 boutons receiving presynaptic inhibition in controls (defined by receiving at least 1 contact from GAD65 P boutons) was 86.9% on both the dendrites and cell bodies. This estimate is remarkably similar to the 86% of Ia afferent synapses filled with HRP (n = 90) found to receive contacts from P-boutons in an exhaustive serial section electron microscopy analysis (Pierce and Mendell, 1993). In MG motoneurons 21 days after TN crush, 74.4 and 70.1% of VGLUT1 boutons on, respectively, dendrites and cell bodies were associated with P-boutons. These percentages partially recovered 3 months after the injury (80.1% and 76.5%). For statistical analyses we pooled together VGLUT1 contacts on dendrites and cell bodies in each motoneuron and compared the percentage of VGLUT1 contacts per cell with presynaptic inhibition in control (n=40 motoneurons), 21 days after crush (n=40 motoneurons) and 3 months (n=39 motoneurons). The data was not

distributed normally (skew towards lower values was apparent in a number of injured motoneurons; Fig. 4F) and therefore a Kruskal-Wallis One Way ANOVA was used resulting in significant differences among the three populations (control, 21 days, 3 months; $H(2)=41.158$, $p<0.001$). Post-hoc Dunn's comparisons revealed significant differences both at 21 days and 3 months with respect to control ($Q=6.315$ (21 days vs control) and $Q=4.118$ (3 months vs control), both $p<0.05$) (Fig. 4F).

In addition, the number of GAD65 boutons per VGLUT1 synapse was significantly decreased. VGLUT1 boutons associated with GAD65 P-boutons and contacting dendrites in the control group were surrounded by an average of 2.8 ± 0.2 (\pm S.D.) P-boutons and this was similar for those contacting the cell body (2.7 ± 0.2). Overall VGLUT1 boutons contacting retrogradely labeled motoneurons were associated with 2.7 ± 0.2 P-boutons (Fig. 4G). Larger VGLUT1 boutons had more P-boutons than smaller ones but this was not systematically analyzed (see also Pierce and Mendell, 1993). At 21 days after crush, the number of GAD65 P-boutons per VGLUT1 bouton was reduced by 32.8% from the control value. There was some recovery after 3 months such that the estimated reduction at this time point was then only 19% less than control. The reduction in number of P-boutons was significant at both times post-injury (Kruskal-Wallis One ANOVA on Ranks, $H(2)=65.508$, $p<0.001$; post-hoc Dunn's tests $Q=7.973$ (21 days vs. control) and $Q=5.170$ (3montsh vs. control), both $p<0.05$ in both injured groups vs. control) (Fig. 4G).

Given the known relationship between VGLUT1 size and P-bouton number, smaller boutons should be surrounded by fewer P-boutons. Although changes in bouton size were small after nerve crush (see above), we directly tested whether the reduction in P-boutons is independent of changes in VGLUT1 bouton size. For this we resampled VGLUT1 boutons by selecting only boutons of a typical average size and being careful to be blind to the GAD65 immunofluorescence in the same images (by blanking that channel). Then we rendered bouton surfaces in Imaris (Fig. 5A) and used a MATLAB script to calculate the total surface of the VGLUT1 boutons covered by GAD65 P-boutons (that is the region with 0 μm distance between both rendered surface reconstructions). We analyzed 20 VGLUT1 boutons in each of the three conditions (control, 21 days and 3 months after TN crush) and confirmed that the size of VGLUT1 boutons selected for analysis was rather similar (One-way ANOVA, $F(2,57)=0.298$, $p=0.744$; power for $\alpha = 0.050 : 0.049$) (Fig. 5B). The results show statistically significant differences in VGLUT1 surface covered by P-boutons among the three conditions (Kruskal-Wallis One-way ANOVA; $H(2)=9.418$, $p=0.009$). Control VGLUT1 boutons were covered on $14.3\% \pm 5.7$ ($\pm\text{S.D.}$) of their surface in average, while VGLUT1 boutons 21 days and 3 months after TN crush had $9.7\% \pm 6.9$ and $8.6\% \pm 5.6$ of their surface covered by P-boutons (both were statistically different to control VGLUT1 boutons, $p<0.05$, post-hoc Dunn's test; $Q=2.811$ comparing 3 months vs control and $Q=2.472$ comparing 21 days vs control) (Fig. 5C). Interestingly, the trend towards recovery of P-bouton numbers observed at 21 days was not confirmed when analyzing the

percentage of surface covered in a subsample of VGLUT1 boutons normalized for bouton size.

In summary, slightly fewer VGLUT1 boutons are associated with P-boutons after crush, and VGLUT1 synapses receiving presynaptic control after nerve crush are associated with fewer P-boutons and a significant reduction in VGLUT1 surface coverage. These structural changes in the relations between P-boutons and VGLUT1 synapses could suggest a possible alteration in presynaptic inhibitory control strength.

6.5: Discussion

The major findings of this study indicate that the loss of VGLUT1/Ia afferent input on the soma and dendritic arbor of MG MNs following TN crush is less severe than after complete TN transection (Alvarez et al., 2011) and that remaining synapses have reduced coverage by GABAergic P-boutons controlling the strength of synaptic transmission from Ia afferents. Notably, the ~30% reduction in VGLUT1/Ia synapses demonstrated here aligns well with functional data reporting also ~30% loss in the strength of stretch-evoked excitatory synaptic potentials (strEPSPs) in motoneurons that regenerated and reinnervated muscle after a nerve crush (Prather et al., 2011). However, as discussed below it is more difficult to relate the partial reduction in P-bouton coverage with the 140% increase in the strength of muscle stretch reflexes.

6.5.1: Differences in stretch reflex synaptic circuit plasticity after different kinds of nerve injury

The milder deficits in VGLUT1/1a synapses after nerve crush compared to complete nerve transection could be an adaptation to the more efficient reinnervation of peripheral targets after nerve crush. Regeneration and recovery from nerve crush injuries is fundamentally different from complete transections because continuity between regenerating axons and endoneurial tubes are better preserved after crush resulting in facilitation of axon growth and greater specificity of target reinnervation (Bodine-Fowler et al., 1997; Nguyen et al., 2002; Valero-Cabre et al., 2004). This difference impacts the specificity of connections established in the periphery. It is generally believed that erroneous growth of motor axons to sensory corpuscles or of sensory afferents to neuromuscular junctions is prevented by differential neurotropic and cell-cell adhesion interactions between regenerating axons and Schwann cells lining sensory and motor endoneurial tubes (Brushart, 1993; Martini et al., 1994; Hoke et al., 2006), but there are two other important sources of possible guidance errors. First, motor and sensory axons can enter inappropriate pathways targeting wrong muscles; sometimes the new target might have synergistic actions with the original muscle, but in other situations it might have opposite function. Second, the exact composition of sensory afferents and motor efferents re-innervating muscle spindles might differ from the original innervation.

After full nerve transection, particularly of multifascicular large nerves, regenerating axons enter endoneurial tubes in erroneous fascicles which are

then guided to muscles different from the original (Brushart and Mesulam, 1980; Brushart et al., 1983; Gillespie et al., 1986; Brushart, 1988; Bodine-Fowler et al., 1997; Valero-Cabre et al., 2004). Axon misdirection in the periphery disorganizes the spatial order of motor pools inside the spinal cord after nerve transection, but not after nerve crush (Brown and Hardman, 1987; Valero-Cabre et al., 2004). Importantly, the specific connectivity between Ia afferents and motoneurons is dependent on topographic matching the spatial distributions inside the spinal cord of motor pools and terminal synaptic arbors of Ia afferents from different muscles (Surmeli et al., 2011). Moreover, during regeneration Ia afferents themselves can also be misrouted in the periphery to novel muscle targets further amplifying the disorganization of Ia inputs to motoneurons centrally. Better preservation after nerve crush of regenerating axons specific targeting in the periphery, implies that functional inputs and modulation of motoneuron activities controlling different muscles and the specificity of muscle stretch information conveyed to spinal neurons might be less disrupted after nerve crush compared to nerve transection, thus requiring less structural synaptic plasticity.

Another important difference between a full nerve transection and nerve crush is the better reinnervation specificity of the muscle spindle apparatus by the original Ia afferents and α -efferents after nerve crush, as demonstrated in experimental situations in which errors in muscle targeting are prevented (Brown and Butler, 1976; Hyde and Scott, 1983; Barker et al., 1985). There is excellent reinnervation of muscle spindles and recovery of normal stretch responses and α -efferent modulation of spindle responses after crushing nerves, but full

transection of the same nerves results in abnormal increases in efferent innervation (Brown and Butler, 1976) and in the possibility that Ib afferents are partially responsible for the reinnervation of muscle spindles (Banks and Barker, 1989). Alterations in the source of afferents and efferents innervating muscle spindles would have consequences for both spindle sensitivity modulation during normal motor behaviors in awake animals and also reduce input from stretch-responsive afferents to motoneurons because Ib afferents do not monosynaptically innervate motoneurons in lamina IX.

In summary, central synaptic plasticity in the stretch reflex circuit to overcome unadaptive re-organizations of central motor control circuits resulting from miswired motoneurons, Ia afferents or muscle spindles might be more necessary after nerve transection compared to nerve crush. This suggests that VGLUT1 inputs should be better preserved in regenerating motoneurons after crush, a prediction that was confirmed in this study. Enhancing central synaptic plasticity inside the spinal cord after injuries causing major misrouting of motor axons in the periphery enhances motor recovery, but this is not necessary after nerve crush (Galtrey et al., 2007). Our work therefore suggests that endogenous intrinsic signals cause different levels of synaptic plasticity in stretch reflex circuits after different types of injuries. Their exact mechanisms are currently under active investigation. Preliminary data indicate that each type of nerve injury in the periphery induces a different type of neuroinflammatory response inside the spinal cord producing different levels of Ia afferent synapse and axon removal from the ventral horn (Rotterman and Alvarez, 2015). Different

inflammatory responses are associated with more or less removal of the pre-terminal Ia axons arborizing in the ventral horn. Ia afferent axons die-back towards lamina V after nerve transection (Alvarez et al., 2011), while much of the Ia axon remains in ventral lamina VII and IX after nerve crush (Rotterman and Alvarez, unpublished observations in VGLUT1-cre mice). Thus, the decrease in VGLUT1 inputs is more extensive and permanent after nerve transection compared to nerve crush.

Functionally, our results suggest that the milder functional deficits in the stretch reflex reported after nerve crush compared to nerve transection (Prather et al., 2011) may be the result of better preservation of the synaptic contacts of Ia afferents onto motoneurons. Interestingly, Prather and colleagues suggested that “roughly 70% of the spindle afferent population recovered function following nerve crush regeneration”, function being measured as the EPSP evoked in MG motoneurons following stretch of the MG muscle (strEPSP). Although there are obvious differences between both studies that include species (cat vs. rat), site of injury (MG nerve vs. TN) and survival (1 year vs. 3 months), it is significant that we found a matching 30% loss of VGLUT1 synapses on the cell bodies and dendrites of MG motoneurons.

6.5.2: Presynaptic inhibition of Ia afferents after nerve crush injuries

Despite small reductions in VGLUT1 synapses and strEPSPs, the stretch reflex is however augmented after recovery from nerve crush (Prather et al., 2011). This suggests that notwithstanding a small reduction in the strength of Ia

afferent synapses onto regenerated motoneurons, muscle stretch nevertheless results in increased motor unit firing and/or recruitment. There are several pre- and postsynaptic mechanisms that could be responsible for this response augmentation. These include changes in Renshaw cell mediated recurrent inhibition of motoneurons that is well known to modulate the monosynaptic Ia afferent reflex and alterations in persistent inward currents that amplify Ia afferent synaptic inputs (see Prather et al. 2011 for a more thorough review). While there is evidence of altered recurrent inhibition after nerve transection (Obeidat et al., 2012) it is unknown if a similar reorganization of this circuit happens after nerve crush. On the other hand, possible changes in the synaptic integratory properties of motoneurons after different kinds of nerve injuries are at present unknown. However, the well-established downregulation of presynaptic inhibition in skin afferents after nerve injury (Castro-Lopes et al., 1993; Horch and Lisney, 1981; Moore et al., 2002) prompted us to examine presynaptic inhibition of Ia afferents, which is known to effectively modulate the strength of the Ia-motoneuron synapse and motor unit recruitment by Ia afferent inputs (Rudomin and Schmidt, 1999). The possibility that presynaptic inhibition to Ia afferents is altered after nerve injury was further suggested by a recent study concluding that the formation of presynaptic GABAergic inhibitory terminals (P-boutons) and their strength on Ia afferent neurotransmission is regulated by activity-dependent release of glutamate and Brain Derived Neurotrophic Factor (BDNF) from Ia synapses (Mende et al., 2016). In un-injured animals, Ia afferents maintain a continuous discharge that is modulated up-or down according to muscle length,

therefore it is conceivable that disconnection of Ia afferents from muscle spindles causes diminished activity that could have dramatic effects on the maintenance of P-boutons on Ia afferent synapses. Indeed, our results suggest a significant change in P-bouton innervation of Ia afferents synapses.

Whether the recorded decrease in P-bouton number correlates with the reported functional impact of nerve crush on stretch-reflexes is more difficult to evaluate. Two previous studies analyzed primary afferent depolarization (PAD, a measurement of presynaptic GABAergic control) in group I afferents (Ia muscle spindle and Ib golgi-tendon organ afferents) after crushing hind limb nerves in the cat and allowing for regeneration and muscle reinnervation to be completed (Enriquez-Denton et al., 2004; Enriquez et al., 1996). Both studies concluded that PAD persisted in group I afferents after nerve regeneration in contrast to previous studies in cutaneous nerves (Horch and Lisney, 1981; Moore et al., 2002) and in agreement with the many VGLUT1 boutons we found associated with GAD65 P-boutons 21 days and 3 months after crush. However, the electrophysiological studies also reported a change in the organization of PAD to regenerated group I afferents. An extensive body of literature (reviewed in Rudomin and Schmidt, 1999) suggest that Ia, Ib and type II proprioceptors are specifically modulated by presynaptic interneurons that differ in inputs and modulation. While interneurons presynaptic to Ib afferents are excited by other Ib afferents and also by the reticular formation, the majority of Ia afferents receive PAD from interneurons with convergent excitation from Ia and Ib afferents and that are negatively modulated by the reticular formation. However, after nerve

crush PAD on Ia afferents becomes positively modulated by reticular formation inputs implying a change in P-boutons origins. It could be argued that the small change in VGLUT1 coverage by GAD65 P-boutons could be the result of an initial detachment and thereafter recovery of GAD65 P-boutons that result in both a change in PAD patterns and also a slight decrease in GAD65 P-bouton number and coverage. It is possible that these alterations might be enough to diminish basal presynaptic inhibitory tone and result in increased efficiency of the stretch reflex during natural stimulation (lengthening) of individual muscles like it was done in Prather et al. (2011). However, more work on new animals models are clearly needed to label P-boutons of different origins and confirm these hypotheses.

In summary, the structural changes we report after nerve crush suggest maintenance of VGLUT1 synapses and an alteration of presynaptic inhibition that could contribute to the enhanced neurotransmission between Ia afferents and motoneurons. These two phenomena likely contribute to the better preservation of stretch-evoked EPSPs after nerve crush and may be the supranormal stretch reflex forces. Future experiments should more directly test whether presynaptic disinhibition of Ia afferent synapses is a major contributor to the enhanced stretch reflex observed after nerve crush.

	Immunogen	Host (Ab type)	Company	RRID	Specificity
VGLUT1	Strep-Tag® fusion protein of rat VGLUT1 (aa 456-560)	Rabbit (polyclonal)	Synaptic Systems	AB_887875	No reaction in VGLUT1 KO tissue
GAD65 (GAD6 clone)	GAD partially purified from chicken brains	Mouse (monoclonal)	Developmental Hybridoma Bank	AB_528264	Chang and Gottlieb (1988); Richter et al. (1993)
Cholera toxin subunit B	Recombinant Cholera toxin B subunit	Goat (polyclonal)	List Biological Laboratories	AB_2313637	No reaction in tissue lacking CTb

Table 6.1: Primary Antibody Characteristics

	Controls (n=40 motoneurons)	21 Day TN Crush (n=40 motoneurons)	3 Month TN Crush (n=40 motoneurons)
Somatic surface area (μm^2)	6,150 \pm 525	6,163 \pm 591	6,232 \pm 525
Dendritic total length (μm)	802 \pm 59	837 \pm 155	774 \pm 87
Dendritic total surface (μm^2)	13,068 \pm 2,473	11,392 \pm 3,349	10,999 \pm 1,371

Table 6.2: Somatic and dendritic surfaces sampled in CTb-labeled MG motoneurons

Values are Mean \pm Standard Deviation. Differences between groups did not reach significance (ANOVA $p > 0.05$). CTb, cholera toxin b. MG, medial gastrocnemius. TN, tibialis nerve.

	Controls (n=40 motoneurons) (10 in each of 4 animals)	21 Day TN Crush (n=40 motoneurons) (10 in each of 4 animals)	3 Month TN Crush (n=39 motoneurons) (9-10 in each of 4 animals)
<i>On Cell bodies</i>			
Total number	1,242	774	737
Average / cell body	31.1 ± 10.3	19.4 ± 7.5	18.9 ± 7.5
Average / animal	310.5 ± 10.1	193.5 ± 47.4	184.3 ± 31.3
% with P-boutons	86.9 ± 8.2	70.1 ± 17.6	76.6 ± 12.2
<i>On Dendrites</i>			
Total number	3,957	2,686	2,694
Average / motoneuron	98.9 ± 19.6	67.15 ± 19.6	69.1 ± 16.3
Average / animal	989.3 ± 32.6	671.5 ± 143.6	673.5 ± 113.7
% with P-boutons	86.9 ± 5.0	74.4 ± 13.5	80.0 ± 9.2

Table 6.3: VGLUT1 boutons analyzed and percentage covered by GAD65 P-boutons

Averages as Mean ± Standard Deviation. % based on total number of boutons sampled in either dendrites or cell bodies. % not distributed normally; median and distribution properties are graphed in Figure 5A.

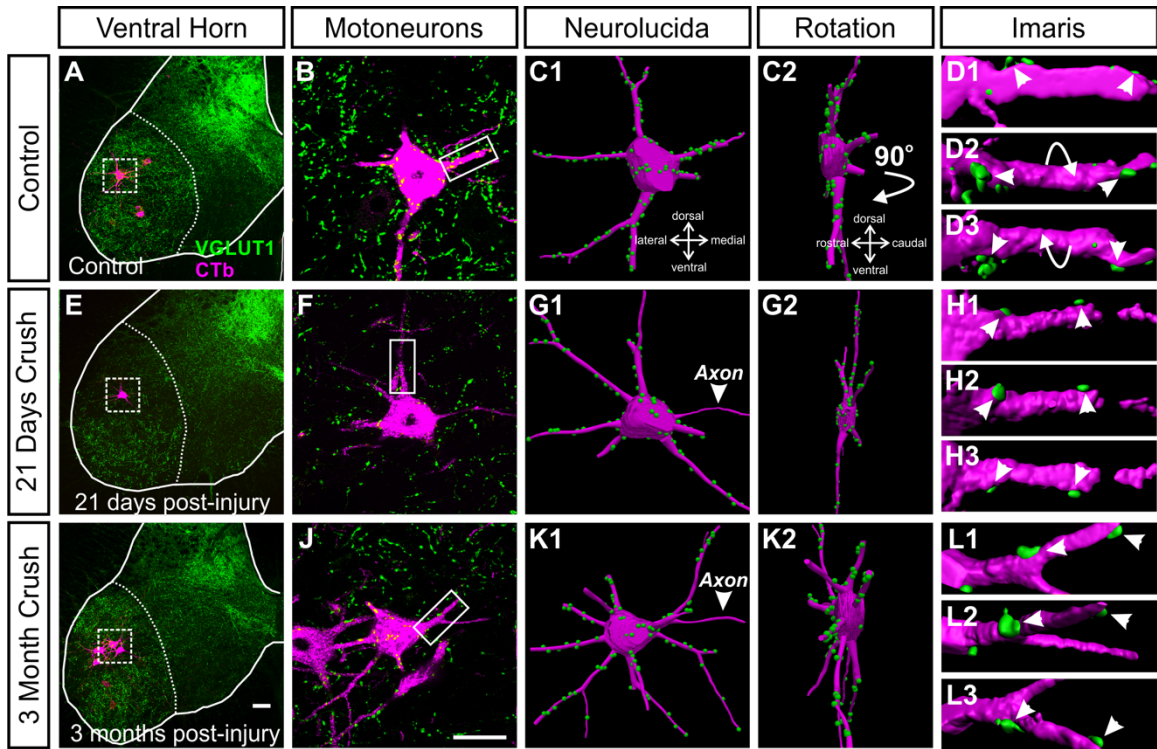


Figure 6.1: VGLUT1 inputs in control and regenerating motoneurons

A, E, I) Low magnification confocal images of VGLUT1 (FITC, green) and retrogradely labeled MG motoneurons (magenta neurons in boxes, CTb, amplified with Cy3 immunohistochemistry) in control (A), 21 days (E) and 3 months (I) after nerve crush. **B,F,J)** High magnification of CTb labeled motoneurons (magenta) and VGLUT1 contacts (green). **C1, G1, K1)** NeuroLucida 3D reconstructions of the motoneuron cell bodies, dendrites and VGLUT1 contacts on them within the field of view. **C2, G2, K2)** 90° rotations of motoneuron reconstructions showing in a perpendicular plane the dendritic arbor contained within the 50 µm thick section. **D1-3, H1-3, L1-3)** High magnification and surface rendered Imaris 3D reconstructions of VGLUT1 contacts (green) on dendrite segments (magenta) indicated by boxes in B, F and J. Arrows indicate rotations; Arrowheads indicate the same VGLUT1 contacts in different rotation views demonstrating attachment to the dendrites. The images show that by difference to previous work after a TN transection, TN crush causes limited loss of VGLUT1 synapses difficult to detect in single motoneuron examples. Scale bars: in I, 100 µm (A and E same magnification); in J, K1 and K2, 50 µm (B, F, C1-2, G1-2, K1-2 same magnification).

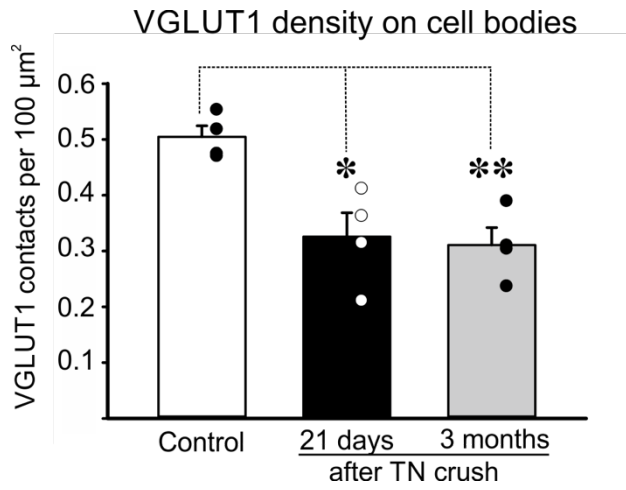
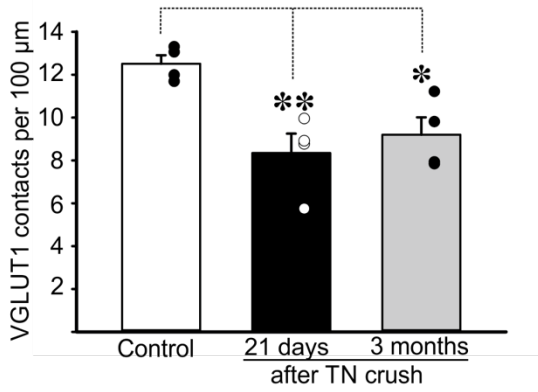


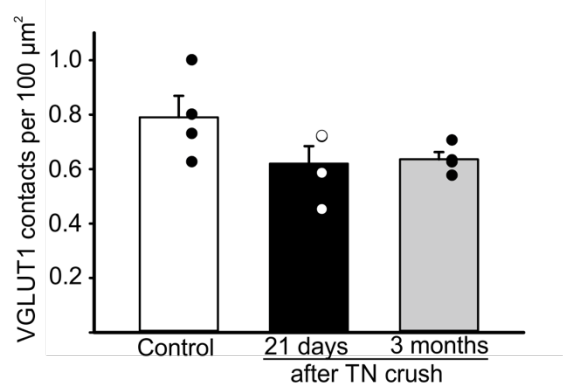
Figure 6.2: VGLUT1 synaptic density on the surface of control and regenerating motoneuron cell bodies

Averages \pm SEM, n = 4 animals analyzed per condition. Each dot represents the average in a different animal obtained from 10 motoneuron cell bodies fully reconstructed per animal. ** p<0.01, * p<0.05, *post-hoc* Bonferroni t-test comparisons to control.

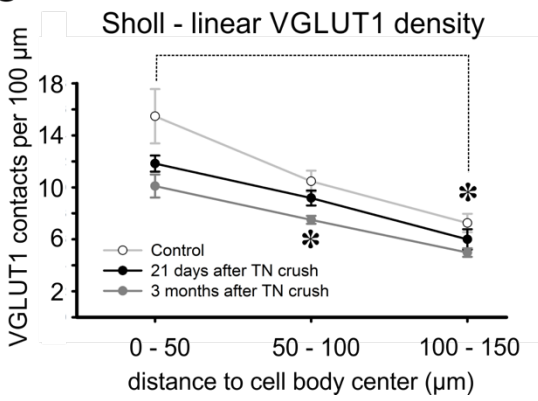
A “Linear” VGLUT1 density on dendrites



B “Surface” VGLUT1 density on dendrites



C Sholl - linear VGLUT1 density



D Sholl - surface VGLUT1 density

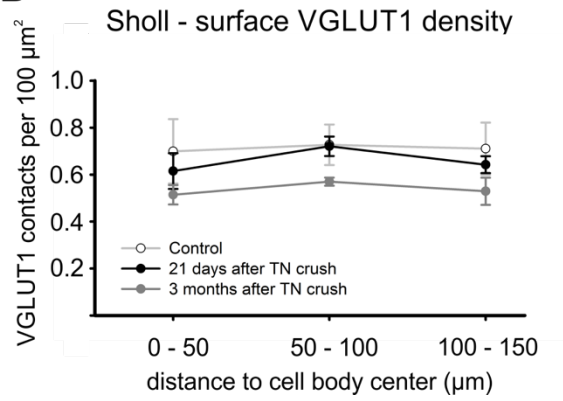
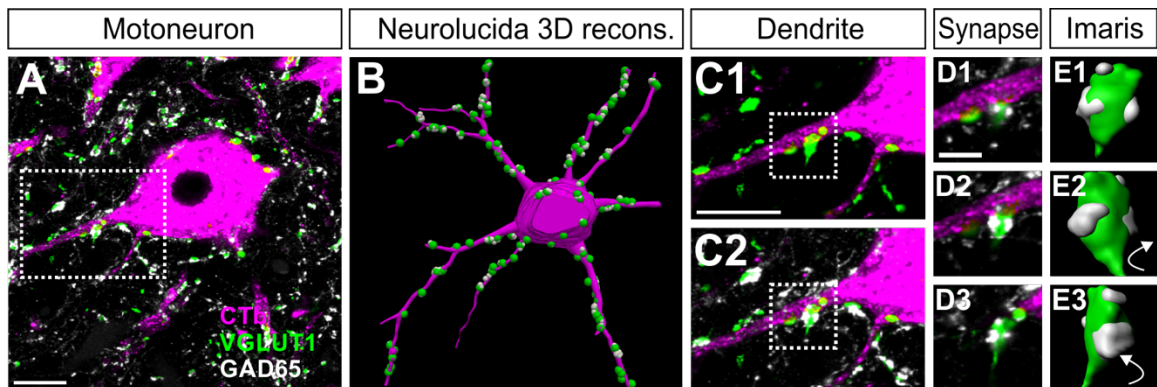
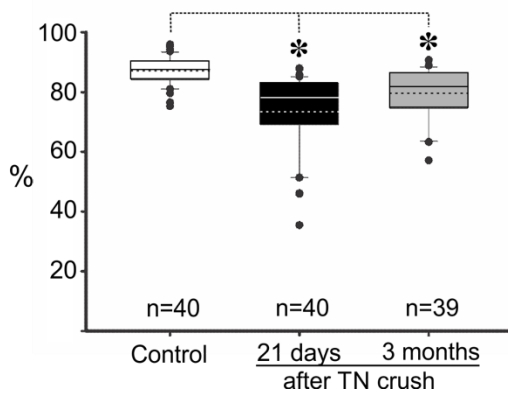


Figure 6.3: VGLUT1 synaptic densities on control and regenerating motoneuron dendrites

A, B) Linear and surface densities of VGLUT1 contacts on the traced dendrites (see table 1 for characteristics of the dendrites sampled). Averages \pm SEM, $n = 4$ animals analyzed per condition. Each dot represents the average in a different animal obtained from dendrite reconstructions of 10 motoneurons per animal. ** $p < 0.01$, * $p < 0.05$, *post-hoc* Bonferroni t-test comparisons to control. A significant depletion was detected in linear, but not in surface density. **C)** Density of VGLUT1 contacts per 100 μm distance in dendritic segments localized at different distances from the cell body (x-axis). Data points represent averages \pm SEM of estimates obtained in each of four animals. The number of VGLUT1 contacts decreased in a proximo-distal gradient (* $p < 0.05$, *post-hoc* Bonferroni t-test comparison of dendrite segments located at a distance of 100-150 μm from the cell body center with segments in the first 0 to 50 μm). Comparison between dendrite segments at the same location but in control or regenerating motoneurons was only significant for the 50-100 μm Sholl distance bin (asterisk). **D)** Density of VGLUT1 contacts per 100 μm^2 of dendrite surface. VGLUT1 surface density is maintained constant in all distance bins and no significant differences were detected between control dendrites and dendrites from regenerating motoneurons (ANOVA, $p > 0.05$).



F Percentage of VGLUT1 contacts with P-boutons



G Number of P-boutons per VGLUT1 contact

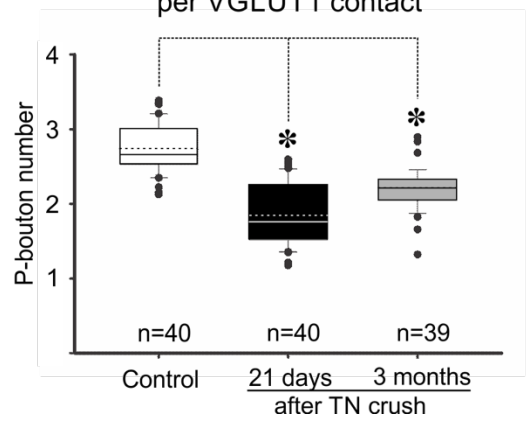


Figure 6.4: Presynaptic GAD65 P-boutons on VGLUT1 bouton contacts on retrogradely labeled motoneurons

A) High magnification of a single confocal image plane through the cell body and proximal dendrite of a retrogradely labeled MG motoneurons (magenta, CTb-555 amplified with Cy3 immunohistochemistry) receiving contacts from VGLUT1 terminals (green, FITC) associated GAD65 P-boutons (white, Cy5). **B)** NeuroLucida 3D reconstruction of motoneuron in A with all VGLUT1 contacts plotted on its surface and associated GAD65 boutons. **C)** High magnification confocal stack projection of dendrite with VGLUT1 contacts (green)(C1) and associated GAD65 P-boutons superimposed (C2). **D)** Higher magnification single confocal plane images (D1 to D3). **E)** Boutons shown in D surface reconstructed in Imaris and rotated in the Y plane. **F)** Whisker-and-box plots represent the distribution of the percentage of VGLUT1 contacts with P-boutons per motoneuron and in each condition. *Continuous lines*: median; *dashed lines*: average; *box*: 25 and 75% distribution percentiles; *whiskers*: 5 and 95 percentiles; *black circles*: outliers beyond the 5-95% distribution; n: number of motoneurons analyzed in each plot. Note skewedness towards lower values after injuries. *Asterisks*, $p < 0.05$ Dunn's post-hoc test. A significant, but small, reduction in the percentage of VGLUT1 contacts associated with P-boutons was detected. **G)** Number of P-boutons per VGLUT1 bouton was also diminished. Data presented as whisker-and-box plots as before; Normality test failed. *Asterisks*, $p < 0.05$ Dunn's post-hoc test. The number of P-boutons in VGLUT1 contacts

diminished after nerve crush and did not recover. Scale bars: in A and C1, 20 μm ; in D, 5 μm .

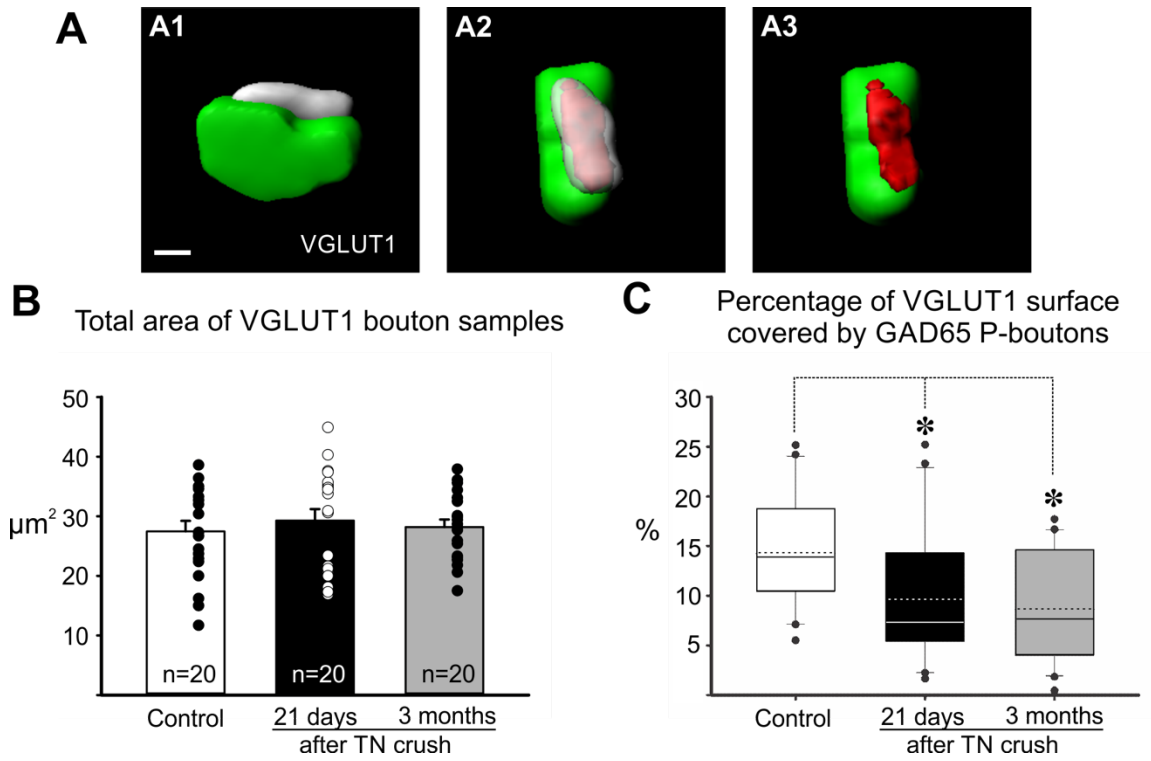


Figure 6.5: Coverage of VGLUT1 boutons by GAD65 P-boutons

A) Imaris 3D surface reconstruction of a VGLUT1 bouton and associated GAD65 P-bouton (A1). After rotations to visualize the contact “en face” (A2) a surface of contact is generated. A3 shows this surface on the VGLUT1 bouton to obtain a percentage coverage on the total VGLUT1 surface covered by the GAD65 P-bouton. **B)** VGLUT1 terminals selected for analysis were of similar size.

Histograms represent average total surface area and error bars represent standard errors of the mean. Data points are plotted to the side. **C)** Percentage of VGLUT1 surface area covered by P-boutons. Data did not distribute normally and is represented as whisker-box plots. *Continuous lines*: median; *dashed lines*: average; *box*: 25 and 75% distribution percentiles; *whiskers*: 5 and 95 percentiles; *black circles*: outliers; *n*: as in B. There was a statistically significant decrease in surface coverage after crush compared to control (ANOVA $p < 0.001$; *asterisks*: post-hoc Dunn’s tests vs. control $p < 0.05$).

References:

- Abelew, T. A., Miller, M. D., Cope, T. C., & Nichols, T. R. (2000). Local loss of proprioception results in disruption of interjoint coordination during locomotion in the cat. *J Neurophysiol*, 84(5), 2709-2714.
- Allodi, I., Udina, E., & Navarro, X. (2012). Specificity of peripheral nerve regeneration: interactions at the axon level. *Prog Neurobiol*, 98(1), 16-37.
- Alvarez, F. J., Bullinger, K. L., Titus, H. E., Nardelli, P., & Cope, T. C. (2010). Permanent reorganization of Ia afferent synapses on motoneurons after peripheral nerve injuries. *Ann N Y Acad Sci*, 1198, 231-241.
- Alvarez, F. J., Titus-Mitchell, H. E., Bullinger, K. L., Kraszpulski, M., Nardelli, P., & Cope, T. C. (2011). Permanent central synaptic disconnection of proprioceptors after nerve injury and regeneration. I. Loss of VGLUT1/IA synapses on motoneurons. *J Neurophysiol*, 106(5), 2450-2470.
- Alvarez, F. J., Villalba, R. M., Zerda, R., & Schneider, S. P. (2004). Vesicular glutamate transporters in the spinal cord, with special reference to sensory primary afferent synapses. *J Comp Neurol*, 472(3), 257-280.
- Banks, R. W., & Barker, D. (1989). Specificities of afferents reinnervating cat muscle spindles after nerve section. *J Physiol*, 408, 345-372.
- Barker, D., Scott, J. J., & Stacey, M. J. (1985). Sensory reinnervation of cat peroneus brevis muscle spindles after nerve crush. *Brain Res*, 333(1), 131-138.
- Barker, D., & Young, J. Z. (1947). Recovery of stretch reflexes after nerve injury. *Lancet*, 1(6456), 704-707.
- Betley, J. N., Wright, C. V., Kawaguchi, Y., Erdelyi, F., Szabo, G., Jessell, T. M., & Kaltschmidt, J. A. (2009). Stringent specificity in the construction of a GABAergic presynaptic inhibitory circuit. *Cell*, 139(1), 161-174.
- Bodine-Fowler, S. C., Meyer, R. S., Moskovitz, A., Abrams, R., & Botte, M. J. (1997). Inaccurate projection of rat soleus motoneurons: a comparison of nerve repair techniques. *Muscle Nerve*, 20(1), 29-37.
- Brown, M. C., & Butler, R. G. (1976). Regeneration of afferent and efferent fibres to muscle spindles after nerve injury in adults cats. *J Physiol*, 260(2), 253-266.
- Brown, M. C., & Hardman, V. J. (1987). A reassessment of the accuracy of reinnervation by motoneurons following crushing or freezing of the sciatic or lumbar spinal nerves of rats. *Brain*, 110 (Pt 3), 695-705.
- Brushart, T. M. (1988). Preferential reinnervation of motor nerves by regenerating motor axons. *J Neurosci*, 8(3), 1026-1031.
- Brushart, T. M. (1993). Motor axons preferentially reinnervate motor pathways. *J Neurosci*, 13(6), 2730-2738.
- Brushart, T. M., & Mesulam, M. M. (1980). Alteration in connections between muscle and anterior horn motoneurons after peripheral nerve repair. *Science*, 208(4444), 603-605.

- Brushart, T. M., Tarlov, E. C., & Mesulam, M. M. (1983). Specificity of muscle reinnervation after epineurial and individual fascicular suture of the rat sciatic nerve. *J Hand Surg Am*, 8(3), 248-253.
- Bullinger, K. L., Nardelli, P., Pinter, M. J., Alvarez, F. J., & Cope, T. C. (2011). Permanent central synaptic disconnection of proprioceptors after nerve injury and regeneration. II. Loss of functional connectivity with motoneurons. *J Neurophysiol*, 106(5), 2471-2485.
- Castro-Lopes, J. M., Tavares, I., & Coimbra, A. (1993). GABA decreases in the spinal cord dorsal horn after peripheral neurectomy. *Brain Res*, 620(2), 287-291.
- Chan, K. M., Gordon, T., Zochodne, D. W., & Power, H. A. (2014). Improving peripheral nerve regeneration: from molecular mechanisms to potential therapeutic targets. *Exp Neurol*, 261, 826-835.
- Chang, Y. C., & Gottlieb, D. I. (1988). Characterization of the proteins purified with monoclonal antibodies to glutamic acid decarboxylase. *J Neurosci*, 8(6), 2123-2130.
- Chang, Y. H., Auyang, A. G., Scholz, J. P., & Nichols, T. R. (2009). Whole limb kinematics are preferentially conserved over individual joint kinematics after peripheral nerve injury. *J Exp Biol*, 212(Pt 21), 3511-3521.
- Conradi, S. (1969). Ultrastructure of dorsal root boutons on lumbosacral motoneurons of the adult cat, as revealed by dorsal root section. *Acta Physiol Scand Suppl*, 332, 85-115.
- Cope, T. C., Bonasera, S. J., & Nichols, T. R. (1994). Reinnervated muscles fail to produce stretch reflexes. *J Neurophysiol*, 71(2), 817-820.
- Enriquez, M., Jimenez, I., & Rudomin, P. (1996). Changes in PAD patterns of group I muscle afferents after a peripheral nerve crush. *Exp Brain Res*, 107(3), 405-420.
- Enriquez-Denton, M., Manjarrez, E., & Rudomin, P. (2004). Persistence of PAD and presynaptic inhibition of muscle spindle afferents after peripheral nerve crush. *Brain Res*, 1027(1-2), 179-187.
- Fu, S. Y., & Gordon, T. (1995a). Contributing factors to poor functional recovery after delayed nerve repair: prolonged axotomy. *J Neurosci*, 15(5 Pt 2), 3876-3885.
- Fu, S. Y., & Gordon, T. (1995b). Contributing factors to poor functional recovery after delayed nerve repair: prolonged denervation. *J Neurosci*, 15(5 Pt 2), 3886-3895.
- Galtrey, C. M., Asher, R. A., Nothias, F., & Fawcett, J. W. (2007). Promoting plasticity in the spinal cord with chondroitinase improves functional recovery after peripheral nerve repair. *Brain*, 130(Pt 4), 926-939.
- Gillespie, M. J., Gordon, T., & Murphy, P. R. (1986). Reinnervation of the lateral gastrocnemius and soleus muscles in the rat by their common nerve. *J Physiol*, 372, 485-500.
- Gordon, T., & English, A. W. (2016). Strategies to promote peripheral nerve regeneration: electrical stimulation and/or exercise. *Eur J Neurosci*, 43(3), 336-350.

- Gottlieb, D. I., Chang, Y. C., & Schwob, J. E. (1986). Monoclonal antibodies to glutamic acid decarboxylase. *Proc Natl Acad Sci U S A*, 83(22), 8808-8812.
- Haftel, V. K., Bichler, E. K., Wang, Q. B., Prather, J. F., Pinter, M. J., & Cope, T. C. (2005). Central suppression of regenerated proprioceptive afferents. *J Neurosci*, 25(19), 4733-4742.
- Hoke, A., Redett, R., Hameed, H., Jari, R., Zhou, C., Li, Z. B., . . . Brushart, T. M. (2006). Schwann cells express motor and sensory phenotypes that regulate axon regeneration. *J Neurosci*, 26(38), 9646-9655.
- Horch, K. W., & Lisney, S. J. (1981). Changes in primary afferent depolarization of sensory neurones during peripheral nerve regeneration in the cat. *J Physiol*, 313, 287-299.
- Hughes, D. I., Mackie, M., Nagy, G. G., Riddell, J. S., Maxwell, D. J., Szabo, G., Todd, A. J. (2005). P boutons in lamina IX of the rodent spinal cord express high levels of glutamic acid decarboxylase-65 and originate from cells in deep medial dorsal horn. *Proc Natl Acad Sci U S A*, 102(25), 9038-9043.
- Hyde, D., & Scott, J. J. (1983). Responses of cat peroneus brevis muscle spindle afferents during recovery from nerve-crush injury. *J Neurophysiol*, 50(2), 344-357.
- Lundborg, G. (2003). Richard P. Bunge memorial lecture. Nerve injury and repair--a challenge to the plastic brain. *J Peripher Nerv Syst*, 8(4), 209-226.
- Lyle, M. A., Prilutsky, B. I., Gregor, R. J., Abelew, T. A., & Nichols, T. R. (2016). Self-reinnervated muscles lose autogenic length feedback, but intermuscular feedback can recover functional connectivity. *J Neurophysiol*, 116(3), 1055-1067.
- Maas, H., Prilutsky, B. I., Nichols, T. R., & Gregor, R. J. (2007). The effects of self-reinnervation of cat medial and lateral gastrocnemius muscles on hindlimb kinematics in slope walking. *Exp Brain Res*, 181(2), 377-393.
- Madison, R. D., Archibald, S. J., & Brushart, T. M. (1996). Reinnervation accuracy of the rat femoral nerve by motor and sensory neurons. *J Neurosci*, 16(18), 5698-5703.
- Martini, R., Schachner, M., & Brushart, T. M. (1994). The L2/HNK-1 carbohydrate is preferentially expressed by previously motor axon-associated Schwann cells in reinnervated peripheral nerves. *J Neurosci*, 14(11 Pt 2), 7180-7191.
- Maxwell, D. J., Christie, W. M., Short, A. D., & Brown, A. G. (1990). Direct observations of synapses between GABA-immunoreactive boutons and muscle afferent terminals in lamina VI of the cat's spinal cord. *Brain Res*, 530(2), 215-222.
- Mende, M., Fletcher, E. V., Belluardo, J. L., Pierce, J. P., Bommarreddy, P. K., Weinrich, J. A., Kaltschmidt, J. A. (2016). Sensory-Derived Glutamate Regulates Presynaptic Inhibitory Terminals in Mouse Spinal Cord. *Neuron*, 90(6), 1189-1202.

- Moore, K. A., Kohno, T., Karchewski, L. A., Scholz, J., Baba, H., & Woolf, C. J. (2002). Partial peripheral nerve injury promotes a selective loss of GABAergic inhibition in the superficial dorsal horn of the spinal cord. *J Neurosci*, 22(15), 6724-6731.
- Nguyen, Q. T., Sanes, J. R., & Lichtman, J. W. (2002). Pre-existing pathways promote precise projection patterns. *Nat Neurosci*, 5(9), 861-867.
- Obeidat, A.Z., Rotterman, T.M., Alvarez, F.J., Cope, T.C. (2012). Global changes in recurrent inhibition after peripheral nerve repair. Program No. 789.12. 2012 Neuroscience Meeting Planner. New Orleans, LA: Society for Neuroscience, 2012. Online
- Pierce, J. P., & Mendell, L. M. (1993). Quantitative ultrastructure of Ia boutons in the ventral horn: scaling and positional relationships. *J Neurosci*, 13(11), 4748-4763.
- Prather, J. F., Nardelli, P., Nakanishi, S. T., Ross, K. T., Nichols, T. R., Pinter, M. J., & Cope, T. C. (2011). Recovery of proprioceptive feedback from nerve crush. *J Physiol*, 589(Pt 20), 4935-4947.
- Richter, W., Shi, Y., & Baekkeskov, S. (1993). Autoreactive epitopes defined by diabetes-associated human monoclonal antibodies are localized in the middle and C-terminal domains of the smaller form of glutamate decarboxylase. *Proc Natl Acad Sci U S A*, 90(7), 2832-2836.
- Rotterman, T. M., Nardelli, P., Cope, T. C., & Alvarez, F. J. (2014). Normal distribution of VGLUT1 synapses on spinal motoneuron dendrites and their reorganization after nerve injury. *J Neurosci*, 34(10), 3475-3492.
- Rudomin, P., & Schmidt, R. F. (1999). Presynaptic inhibition in the vertebrate spinal cord revisited. *Exp Brain Res*, 129(1), 1-37.
- Sabatier, M. J., To, B. N., Nicolini, J., & English, A. W. (2011). Effect of axon misdirection on recovery of electromyographic activity and kinematics after peripheral nerve injury. *Cells Tissues Organs*, 193(5), 298-309.
- Shneider, N. A., Brown, M. N., Smith, C. A., Pickel, J., & Alvarez, F. J. (2009). Gamma motor neurons express distinct genetic markers at birth and require muscle spindle-derived GDNF for postnatal survival. *Neural Dev*, 4, 42.
- Siembab, V. C., Gomez-Perez, L., Rotterman, T. M., Shneider, N. A., & Alvarez, F. J. (2016). Role of primary afferents in the developmental regulation of motor axon synapse numbers on Renshaw cells. *J Comp Neurol*, 524(9), 1892-1919.
- Sunderland, S. (1947). Rate of regeneration in human peripheral nerves; analysis of the interval between injury and onset of recovery. *Arch Neurol Psychiatry*, 58(3), 251-295.
- Surmeli, G., Akay, T., Ippolito, G. C., Tucker, P. W., & Jessell, T. M. (2011). Patterns of spinal sensory-motor connectivity prescribed by a dorsoventral positional template. *Cell*, 147(3), 653-665.
- Valero-Cabre, A., Tsironis, K., Skouras, E., Navarro, X., & Neiss, W. F. (2004). Peripheral and spinal motor reorganization after nerve injury and repair. *J Neurotrauma*, 21(1), 95-108.

Appendix II:

Two-photon live imaging of microglia dynamics after nerve injury in an adult spinal cord slice

Manuscript in preparation for the Journal of Neuroscience Methods: Rotterman TM & Alvarez FJ (2018) Two-photon live imaging of microglia dynamics after nerve injury in adult spinal cord slice. Journal of Neuroscience Methods.

7.1: Abstract

Microglia cells throughout the central nervous system are constantly in motion surveying the parenchyma around them sensing for any disruptions in homeostasis. These cells respond rapidly to any disturbance in their environment and readily become activated where they retract their extensive processes and swell in size. This phenotypic change is generally associated with changes in cytokine production and phagocytosis. One specific example of this change is their response to peripheral nerve injury. When a peripheral axon is severed these cells become activated and surround the injured motoneurons in the ventral horn of the spinal cord. However, their exact role and function after injury is an ongoing debate. We propose in this study that one of their roles may be in promoting the degradation of central projecting Ia afferent inputs onto motoneurons. To investigate this, we performed a sciatic nerve transection in adult transgenic mice that express GFP in microglia (CX3CR1+) and RFP in Ia afferents (VGLUT1-Cre). We then created an adult spinal cord slice preparation in which we imaged microglia cells in real time using two-photon microscopy and investigated their interactions with injured MNs and axotomized Ia afferent terminals. We found that 7 days after injury these microglia cells increase the number of contacts they make with MNs and the dwell time they spend on individual Ia afferent terminals. However, we have not yet witnessed direct removal of these synapses and are continuing experiments to quantify these interactions.

7.2: Introduction

Microglia are neuroimmune cells specific to the central nervous system (CNS) that extend thin processes densely covered by filopodia and act as micro-sensors of the surrounding parenchyma. While at “rest” and in surveying mode microglia processes and filopodia display high motility establishing transient contacts with surrounding neurons and synapses (Nimmerjahn et al., 2005; Gyoneva and Traynelis, 2013; Gyoneva et al., 2014b) Though these contacts microglia are believed to interact with a number of surface and local chemical signals to detect disruptions in homeostasis due to changes in activity, injury or infection (Kettenmann et al., 2011). One of the many roles these cells have is recognizing inactive, aberrant or unnecessary synapses. Once “activated” they can display a variety of phenotypes and behaviors (Kreutzberg, 1996), including “lifting” synaptic boutons from specific postsynaptic targets (Blinzinger and Kreutzberg, 1968) or more permanent synapse, axon or neuron phagocytosis (Schafer et al., 2012). For example, early in development or during injury and disease, microglia adopt an amoeboid morphology and macrophage-like phenotype and are involve in sculpting neural circuitry by synaptic pruning weakened synapses or even removing entire neurons (Berg et al., 2012; Morris et al., 2013; Michailidou et al., 2015; Vasek et al., 2016). To fully understand these states and the dynamics of microglia interactions with neurons, axons and synapses a number of preparations were developed to visualize their dynamics in real time. This include two-photon imaging through cranial windows capable of visualizing microglia at the brain surface (Nimmerjahn et al., 2005; Wake et al.,

2009; Marker et al., 2010) or brain slices to visualize microglia in deeper regions (Haynes et al., 2006; Gyoneva et al., 2014a; Gyoneva et al., 2016). Fewer studies focused on methods to investigate these cells in the spinal cord; nevertheless, microglia are key players in a large variety of spinal pathologies that include spinal cord injury, peripheral nerve neuropathies, chronic pain, multiple sclerosis, amyotrophic lateral sclerosis and spinal muscular atrophy (Perry et al., 2010; Perry and Holmes, 2014; Gomez-Nicola and Perry, 2015).

We investigate the dynamics of activated spinal cord microglia after peripheral nerve injury (PNI). In this model, ventral horn motoneurons (MNs) axotomized in the injured nerve, release signals that result in local microglia activation in the spinal cord such that ventral horn microglia switch to an amoeboid shape, proliferate and migrate towards the cell bodies of axotomized MNs (Rotterman 2018, under review). It was first reported that microglia surrounding axotomized MNs (originally facial MNs after facial nerve injury) were responsible for “stripping” synapses from MNs. During this process microglia extensions interpose in between synaptic boutons and MNs cell bodies “lifting” the synapses from the MN surface (Blinzinger and Kreutzberg, 1968); eventually, these synapses re-attach after microglia move away from the MN cell surface as MNs reinnervate muscle following regeneration of their axons in the peripheral nerve (Alvarez et al., 2011). However, blocking microglia proliferation or using genetic animal models that inhibited microglia activation did not prevent synaptic loss around the cell bodies of axotomized MNs (Svensson and Aldskogius, 1993), casting doubt on the exact roles microglia play in the ventral horn after

PNI (Berg et al., 2013), and in particular the significance of their tight spatial relations with the cell bodies of axotomized MNs. In addition, there is microglia activation after PNI in the dorsal horn where the central branches of many sensory afferents, also axotomized in the peripheral nerve, undergo central degradative changes through a process denominated “transganglionic anterograde degeneration” (Arvidsson, 1979; Aldskogius et al., 1985; Arvidsson, 1986), but whose exact mechanisms are all but unknown. This process is not exclusive of dorsal horn sensory axons, since muscle proprioceptors (Ia and II afferents) projecting to the ventral horn also dye back after certain types of nerve injuries (Alvarez et al., 2011). Finally, the microglia reaction in the most superficial lamina after PNI has been related to development of hyperalgesia and chronic pain by altering the electrophysiological properties of neurons residing in these laminae (Coull et al., 2003). In conclusion, spinal microglia activation after PNI relate with a number of different alterations in different spinal cord laminae, but we know little about the significance and mechanisms of many of these processes (with exception perhaps of their role in hyperalgesia). To investigate spinal microglia dynamics, we developed an adult spinal cord slice preparation that in combination with novel genetic approaches allows to directly image interactions with MNs and sensory afferents using two-photon microscopy. One advantage of this preparation is that nerve injury is induced unilaterally, permitting in the same slice comparison of the spinal cord side ipsilateral to the injury with the control side, contralateral to the injury.

7.3: Methods

7.3.1: Animals

All animal experiments were approved and complied with Emory University's Institutional Animal Care and Use Committee (IACUC). Adult (≥ 3 months old) male and female transgenic mice in a C57Blk/6J and N (mixed background) were used.

Microglia cells were identified by expression of enhanced green fluorescent protein (EGFP) under the chemokine receptor promoter, *Cx3cr1* (Jung et al., 2000) (RRID:IMSR_JAX:005582). Ia afferent axon collaterals and synaptic boutons were identified by crossing mice that expressed Cre under the VGLUT1 promoter (RRID:IMSR_JAX:023527) with Rosa26 reporter mice that had a loxP-flanked STOP cassette in front of the td tomato reporter gene (RRID:IMSR_JAX:007914). VGLUT1-expressing axons and synapses in the ventral horn are proprioceptive afferents (Alvarez et al., 2004; 2011). We back crossed these mice with $CX3CR1^{EGFP/EGFP}$ mice to get a final genotype of $VGLUT1^{Cre/+}::R26^{tdTomato/+}::CX3CR1^{EGFP/+}$ to allow us to visualize microglia interactions directly with Ia afferent axons and synaptic boutons. In other experiments, we pre-labeled lateral gastrocnemius (LG) MNs in a cohort of $CX3CR1$ heterozygous mice by injecting 5 μ l of 0.1% cholera toxin subunit B conjugated to an Alexa Fluor 555 (CTB-555) directly into the LG muscle with a Hamilton syringe. Injections were performed one week prior to any nerve injury.

7.3.2: Injury model

Mice were anesthetized with isoflurane until a surgical plane of anesthesia was achieved (induced: 4-5%; maintained: 2-3%, both in 100% O₂) and were given a subcutaneous injection of 0.05 – 0.10mg/kg buprenorphine to reduce any post-surgical pain. Once animals were anesthetized, a posterior hindlimb incision was made on the left side. The biceps femoris muscle was bluntly dissected and the sciatic nerve exposed, dissected free of connective tissue, and completely transected with surgical scissors. A small piece of 5/0 sterile silk was tied around the proximal nerve stump to prevent regeneration from taking place. Both the dissected muscle and skin were sewn shut with absorbable suture. All animals were closely monitored daily for the first week post-operation for any signs of surgical complications or distress. Mice were allowed to survive for 3 – 7 days post injury.

7.3.3: aCSF preparation

We prepared dissection aCSF (DaCSF) and imaging (recording) aCSF (IaCSF) (supplementary table 1) optimized to preserve the health and integrity of adult spinal cord slices (Mitra and Brownstone, 2012). Osmolarity of both aCSF solutions ranged between 305-315 mOsm/kg of H₂O and a pH between 7.3 – 7.4 and were bubbled (strongly) with 95% O₂ / 5% CO₂ for at least 30 minutes prior to any procedure.

7.3.4: Spinal cord dissection

Mice were injected with ≥ 50 mg/kg of Euthasaol until a deep plane of anesthesia was reached but with the heart still beating. Mice were then placed in an ice bath (*head above water*) to lower the core temperature and were monitored closely until breathing almost ceased. At this point the mice were quickly decapitated and the spinal column rapidly removed (about 2-3 mins) and placed in a petri dish with a Sylgard base filled with ice cold oxygenating DaCSF under a dissection microscope. The spinal cord was carefully removed and the meninges peeled off with a fine pair of #5 forceps. Then, the entire lumbar region was cut out and transferred to a beaker containing pre-warmed 35°C DaCSF and incubated at room temperature (RT) for 15 minutes (*note: warm the DaCSF on a hot plate then place beaker on top of the lab bench right before placing the spinal cord inside. Keep oxygen flowing). This procedure reduces the spinal shock from the dissection.

7.3.5: Sectioning

While the tissue incubates, prepare fresh low-melting 4% agarose (Sigma, cat# A9414) and mix in oxygenated DaCSF. Place the agar on a heat plate (low setting), stir continuously, and monitor temperature. When there is 1 min left of tissue incubation, pour the agar in a 15mm petri dish placed on ice. Once the tissue is added, place the petri dish in a -20°C freezer for about 5 mins to expedite agar solidification (note: only pour agar over cord when agar has cooled

to approximately 37°C). Once the agar has solidified, pop it out of the petri dish and use a razor blade to cut the tissue out leaving only a small layer of agar on all sides of the cord.

Glue the spinal cord vertically, with the caudal end up, in the cutting tray of a vibratome (Leica VT1000P). Fill the chamber with ice cold oxygenated DaCSF. Cut 350 µm thick transverse sections and collect them with a fire polished glass pipet. Place the sections in 30% polyethylene glycol (PEG, pre-heated to 35°C, mixed in dH₂O and oxygenated) for 1 – 2 mins. Wash sections 2x with 35°C DaCSF (note: we used a 12 well culture plate for the PEG incubation and washes). Transfer sections to a 35°C incubation chamber filled with DaCSF with constant oxygenation for 30 mins. Finally, transfer the sections to another chamber filled with laCSF at room temperature. Let sections adjust for 30 mins before imaging. In our preliminary analyses, we found that slices should be recorded, conservatively, within the first 4 hours after slicing to obtain microglia recordings of activity the least affected by the sectioning process.

7.3.6: Imaging parameters

Sections were secured in a slice chamber with a harp to prevent movement and placed on top of stage platform under a HC-Fluotar-L 25x immersion objective (NA = 0.95) (Figure 1A). A circulating bath of laCSF was set up to deliver oxygenated solution to the sections in between imaging sets. We stopped the flow during the actual imaging procedure to prevent ripples in the

bath. Video data sets were captured using a Leica SP8 two-photon microscope equipped with a Coherent Chameleon Vision II laser tuned to 920nm and at 2-5% strength to capture both GFP and RFP (or CTB-555) using two independent and high sensitive external gallium-arsenide HyD detectors (BrightR, green, gain = 110, red: gain = 40). All imaging was done with a water immersion 25X objective of NA 1.35. Digital zoom strength was set up at different levels depending on the size of the field of view necessary for the different structures that we wanted to image. We set up z-stacks to a 1.5 μm step size to scan volumes of approximately 45 μm average thickness of. Scan speed was set up at 400 Hz. Each stack was captured approximately every 30 seconds with little or no dwell time between scans. Total recording times lasted 30 – 45 mins. Longer time-lapses frequently resulted in altering microglia morphology and activity.

7.3.7: Analysis

Time-lapse data sets were analyzed in Imaris (Bitplane, Zurich, Switzerland, version 7.2.2) and 4D renderings were created using the surface area (SA) module. Changes in microglia SA and volume were tracked over time for cells on the contralateral (control) and ipsilateral (injured) side of the spinal cord. Data sets containing MNs (CTB-555) and primary afferent (VGLUT1-tomato) were reconstructed and qualitatively analyzed in Imaris as well.

7.3.8: Statistics

Changes in SA and volume were compared between microglia from the control and the axotomized sides of the spinal cord. The percent change reported is an average of the absolute value and is in regard to the change from each frame to the next. We performed a t-test and set the alpha value at 0.05. Statistics are reported by test, t-score, and p-value. N = 3 per group.

7.3.9: Tips and tricks

Make sure all solutions are prepared and oxygenating before starting the spinal cord dissection. It is best to have a designated thermometer for each beaker/flask of solution. Store the Sylgard dissection dishes in the -20°C and only remove from freezer right before the dissection starts. Have agarose powder already weighed out and in flask prior to procedure. When you glue the agar block, sprinkle sodium bicarbonate powder around the base after you place the cord in the glue, this speed glue hardening immediately and secures the cord instantaneously. Rinse excess powder off with DaCSF before filling the reservoir.

7.4: Results

Following sciatic nerve transection, microglia cells become amoeboid in shape and surround axotomized MNs within the first few days after injury. We describe these cells as becoming phagocytic by their increase in CD68

expression (Schafer et al., 2012) (Fig. 1B, C). This marker is not expressed by surveying microglia and is a good indicator of the “activation state” of microglia. We first validated the integrity of the spinal cord slices by performing a time course analysis of CD68 expression in control slices fixed every hour, for up to six hours, after sectioning (Suppl. Fig. 1). We found that there was no increase in CD68 expression for up to six hours after sectioning and no major changes in microglia morphology, suggesting that the slicing technique itself does not induce a functional change in microglia within hours after sectioning. This agrees with results in brain slices that showed that increased expression of cytokines suggesting microglia reaction to slicing does not start until 5 hours after sectioning (Gyoneva and Traynelis, 2013). Taken together these results suggest that the spinal cord slice is a viable preparation for imaging microglia dynamics close to their “in situ” behavior.

We then performed a sciatic transection and ligation injury on the left side of CX3CR1-GFP heterozygous mice and imaged individual microglia cells using time-lapse two photon microscopy specifically in the ventral horn, on the contralateral control side (Fig. 1A, D1-D4) and on the ipsilateral injured side (Fig. 1E1-E4) for approximately 30 – 45 mins. CX3CR1-GFP microglia in the control side displayed extensions and filopodia with normal dynamics. Interestingly, process extensions and retractions seem matched (when one process extends another retracts) predicting little change in total cell surface and size with time. However, this behavior was totally different in microglia located in the ventral horn ipsilateral to the injury. In this case microglia processes were characterized

by the presence of transient phagocytic cups and process extension that were unmatched with retraction such that the cell will constantly change in morphology and size. Phagocytic cups extend from the cell body outward and produce a “claw-like” structure that appears to be grabbing debris in the neuropil and bringing it back to phagosomes inside the process and travelling towards the cell body where they become large (Fig. 1 E1-E4). The formation of these cups, as well as the presence of phagosomes, was rarely detected in control microglia cells.

Microglia cell surfaces and volumes were estimated in surface renderings obtained with Imaris and changes in both surface area and volume plotted over time (Fig. 1 F1-G2), however for statistical analyses, we compared the absolute value of SA and volume change over time between microglia from the two sides. We found the average percent change in SA for control microglia was 1.74 ± 0.40 (SE, $n = 3$) from one frame (approximately 30 seconds) to the next and percent change in volume was 1.39 ± 0.20 (SE, $n = 3$). The average change for microglia on the injured side was 4.35 ± 0.52 (SE, $n = 3$) and the percent change in volume was 2.87 ± 0.42 (SE, $n = 3$). Changes in both SA and volume were significantly greater in microglia ipsilateral to the injury (t-test, SA: $t(4) = -3.982$, $p = 0.016$; Vol: $t(4) = -3.220$, $p = 0.032$). These data show that as early as three days after nerve injury, ventral microglia around axotomized MNs display significantly different behavior and dynamics.

We then qualitatively, visualized the interactions between microglia cells and MNs in both control and axotomized animals. We injected the left LG muscle

of CX3CR1-GFP heterozygous mice with CTB-555. One week after the injection, the sciatic nerve was transected, and the spinal cord slice preparation was performed 7 days after injury. In sham control mice, microglia cells do not surround MNs and make very few contacts with the soma over time (Figure 2 A1-A10). However, following transection, microglia become highly active and increase their rate of interactions with MNs. They continuously extend and retract their processes and appear to become intimate with the MNs by continuously “massaging” the surface of the cells.

Lastly, we qualitatively investigated the interactions between microglia processes and primary sensory Ia afferent axonal branches and synaptic terminals. We genetically labeled Ia afferents by crossing a VGLUT1-Cre/+ mouse with a R26 tdTomato reporter line to generate VGLUT1^{Cre/+}:R26^{tdTomato/+} mice. This line was then crossed to a CX3CR1-GFP homozygous mouse and we generated VGLUT1^{Cre/+}:R26^{tdTomato/+}:CX3CR1^{GFP/+} mice which allowed us to visualize both the microglia and Ia afferents in a single spinal cord slice. In sham control mice, microglia, again, are constantly surveying the environment and make brief interactions with Ia afferent synapses with short dwell times (Figure 2 C1-C10). Data. However, in the axotomized mice, microglia completely engulf VGLUT1 labeled synapses and spend more time surrounding individual synaptic terminals (Figure 2 D1-D10). An increase in time of interactions has been correlated with a mechanism for synaptic removal (Tremblay et al., 2010).

7.5: Discussion

We propose here an innovative technique to visualize microglia cells in real time in regions of the CNS that are not readily visible with cranial or spinal windows, as previously reported in the cortex or dorsal horn of the spinal cord (Nimmerjahn et al., 2005). Furthermore, with the appropriate genetic reporters and/or tracers, this method allows investigators to explore the function of microglia in synaptic removal in health and in disease of adult animals, which, to the best of our knowledge, the combination has not been done before.

We found that following PNI microglia cells have significantly greater changes in SA and volume over time with the formation of phagocytic cups compared to cells on the contralateral side. The most likely reason for this is that the rate at which a single filament extends and retracts significantly enhances in activated microglia. As a phagocytic cup extends out the SA and volume increase and when the cup retracts both parameters decrease resulting in an overall greater rate of change.

Additionally, we show that the microglia cells are attracted to the surface of the MN soma following axotomy. One possibility is that activated microglia cells are actively phagocytosing perineuronal nets (PPNs), which are extracellular matrix structures necessary for maintaining synaptic inputs on the cell body. In order to have synaptic plasticity these PPNs must be degraded. Another possibility is that these microglia recognize damaged synapses coming from Ia afferent axons and are targeting them for removal. In fact, we found a much greater rate of microglia process interactions with single VGLUT1

synapses on the axotomized side of the spinal cord in which entire synapses were engulfed by a microglia cell. These observations could indicate a direct removal of Ia synapses providing, for the first time, a direct role for the microglia reaction around injured MNs.

Lastly, one area of major improvements that needs to be pursued is optimizing the analysis, specifically for microglia on the axotomized side of the spinal cord. Due to the dynamic nature of these cells and the constant change in structure, doing individual filament tracking overtime proved difficult and unreliable and therefore was not reported in this study. Regardless, we developed a technique to image microglia essentially anywhere in the CNS using an adult spinal cord slice preparation that could potentially tell us about the different roles microglia play in promoting, or perhaps ameliorate, neurodegenerative conditions.

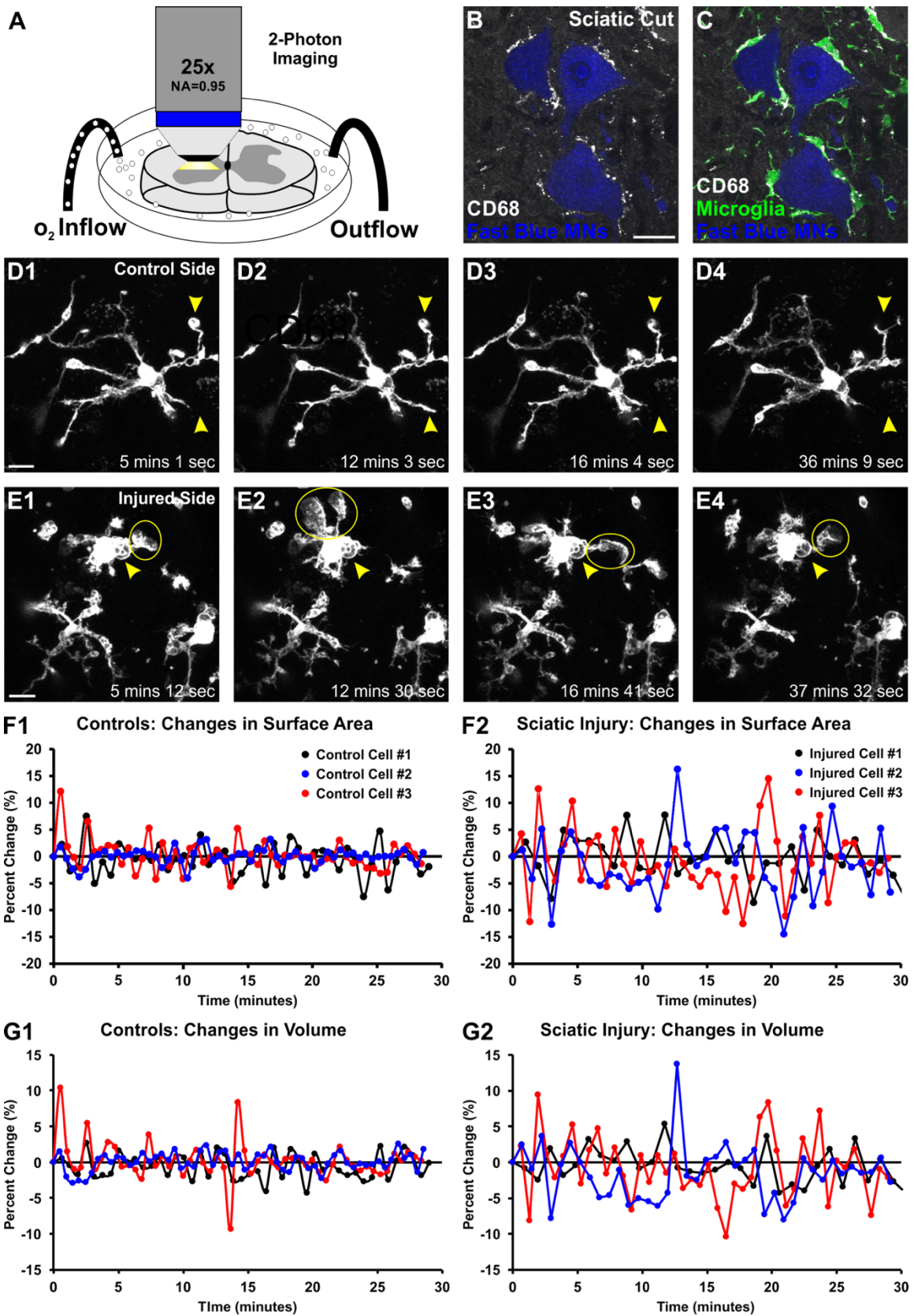


Figure 7.1: Imaging and quantification of microglia dynamics in an adult spinal cord slice preparation using two photon microscopy

A) Preparation set up for imaging. Spinal cord slices were placed in an imaging chamber, equipped with a circulating bath, filled with oxygenated laCSF. **B)** Confocal image of a fixed spinal cord slice (perfused animal) 7 days after sciatic nerve transection. Motoneurons are in blue (Fast Blue) and phagocytic marker CD68 immunoreactivity (IR) in white. Image demonstrates peripheral axotomy results in an increase in CD68 expression; **C)** specifically, in microglia cells (CX3CR1, green). **D1-D4)** Individual frames from a 45min imaging experiment in the ventral horn on the contralateral side of the spinal cord to the injury. Yellow arrows show individual filaments over time. **E1-E4)** Individual frames from a 45min imaging experiment in the ventral horn on the ipsilateral side of the spinal cord 3 days after sciatic nerve transection. Microglia cells become much more active and form phagocytic cups (yellow circles) continuously expanding and contracting in the parenchyma. **F1, F2, G1, G2)** Changes in surface area (SA) and volume over time (between each frame) from Imaris reconstructed individual microglia cells in controls (F1, G1) or in response to axotomy (F2, G2). These data show, in response to injury, microglia have much greater changes in SA and volume over time compared to those on the non-injured side. Scale bars, B: 20 μ m, D1, E1: 10 μ m.

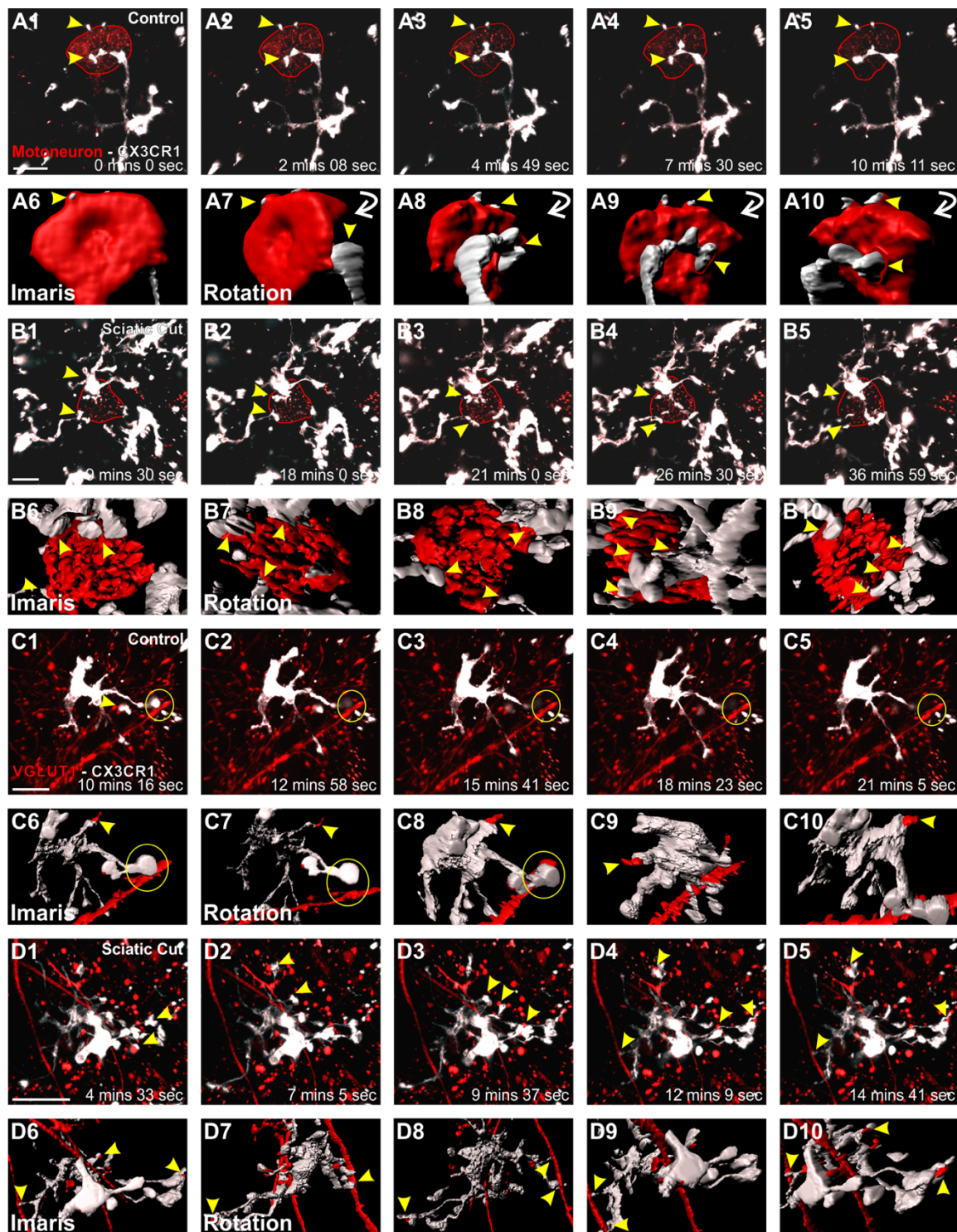


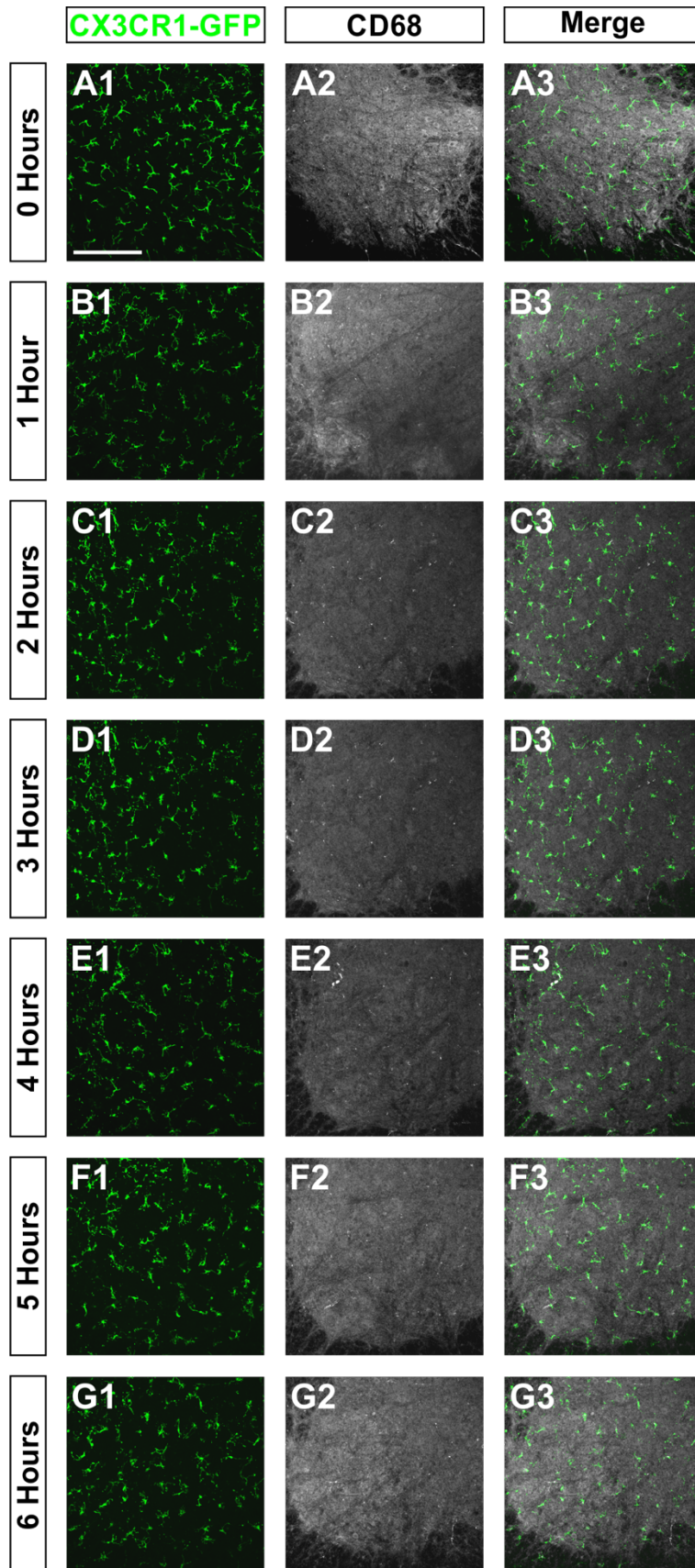
Figure 7.2: Microglia interactions with axotomized motoneurons (MNs) and sensory Ia afferent axons/synapses in the ventral horn of the spinal cord

A1-A5) Microglia interactions with a control pre-labeled (CTB-555) LG MN in the ventral horn of the adult spinal cord. The MN surface is outlined in red. There were only brief contacts over a small amount of surface in these MNs. **A6-A10)** Imaris reconstructions and rotation of a single time frame in a control MN. Yellow arrows show confirmed contacts between an individual microglia cell and the MN surface. **B1-B5)** Microglia interactions with a MN 3 days after sciatic nerve axotomy. These images demonstrate a greater number of interactions and prolonged dwell times between microglia and the MN soma. **B6-B10)** Imaris reconstruction and rotations of a single time point. Images demonstrate that there is much greater MN surface area coverage by microglia compared to control. **C1-C5)** Control microglia (white) interactions with VGLUT1-IR boutons and axon collaterals genetically labeled with tdTomato (red). Images show a low rate of individual events between microglia and Ia afferents. Yellow circle shows one brief event between an individual Ia afferent and a single axon collateral. **C6-C10)** Imaris reconstruction and rotations of a single control microglia cell and Ia axon collateral at one single time point. Yellow circle shows an apparent contact between a microglia cell and a Ia afferent, however in the rotation images it is clear there is no contact between the two. These images emphasize the importance of 3D visualization. Yellow arrow shows a contact between a single microglia process and VGLUT1 bouton. **D1-D5)** Time lapse imaging of a microglia cell and VGLUT1 synapses/axon in response to a PNI. These images

show a greater rate of interactions between microglia and Ia afferents and VGLUT1 synapses after injury. **D6-D10**) Imaris reconstructions and rotations, from a single frame, demonstrating the number of interactions between microglia and Ia afferents in 3D. Yellow arrows show a greater number of VGLUT1 synapses contacted by a single microglia cell. Scale bars: 20 μ m

Dissecting aCSF (DaCSF)		Imaging aCSF (IaCSF)	
Concentration (mM)	Compound	Concentration (mM)	Compound
191	Sucrose	121	NaCl
0.75	K-gluconate	3	KCl
1.25	KH ₂ PO ₄	1.25	NaH ₂ PO ₄
26	Choline bicarbonate (80%)	25	NaHCO ₃
4	MgSO ₄	1.1	MgCl ₂
1	CaCl ₂	2.2	CaCl ₂
20	Dextrose	15	Dextrose
1	(+) sodium L-ascorbate	1	(+) sodium L-ascorbate
5	Ethyl pyruvate	5	Ethyl pyruvate
3	Myo-inositol	3	Myo-inositol
2	Kynurenic acid <u>sodium salt</u>		

Supplemental Table 7.1: The artificial cerebral spinal fluid (aCSF) recipe for the dissection (DaCSF) and imaging (IaCSF) necessary for the viability of the adult spinal cord slice. DaCSF should have a pH=7.3 and an osmolarity of 305-315 mosmol/kgH₂O and the IaCSF should have a pH=7.4 and an osmolarity of 305-315 mosmol/kgH₂O. Both solutions were continuously bubbled with carbogen. Recipe was adopted from *Mitra et al., 2012*.



Supplemental Figure 7.1: Spinal cord quality control experiment. Slice preparation was performed in a control CX3CR1-GFP heterozygous mouse. A single section was dropped in 4% paraformaldehyde (PFA) immediately after slicing and every hour after that for up to six hours. Sections were washed and immunostained for CD68, a marker of phagocytosis and an indicator of the health of the section. **A1, B1, C1, D1, E1, F1, G1**) Show microglia (green) morphology over time. These images show no major microglia reaction after slicing. **A2, B2, C2, D2, E2, F2, G2**) CD68 immunoreactivity over time. These images show that CD68 is not upregulated within the first 6 hours after slicing. **A3, B3, C3, D3, E3, F3, G3**) Merge images show microglia are not expressing CD68 after slicing. These images provide quality control of the preparation and support the viability of adult spinal cord slicing.

References:

- Aldskogius H, Arvidsson J, Grant G (1985) The reaction of primary sensory neurons to peripheral nerve injury with particular emphasis on transganglionic changes. *Brain research* 357:27-46.
- Alvarez FJ, Titus-Mitchell HE, Bullinger KL, Kraszpulski M, Nardelli P, Cope TC (2011) Permanent central synaptic disconnection of proprioceptors after nerve injury and regeneration. I. Loss of VGLUT1/IA synapses on motoneurons. *Journal of neurophysiology* 106:2450-2470.
- Arvidsson J (1979) An ultrastructural study of transganglionic degeneration in the main sensory trigeminal nucleus of the rat. *Journal of neurocytology* 8:31-45.
- Arvidsson J (1986) Transganglionic degeneration in vibrissae innervating primary sensory neurons of the rat: a light and electron microscopic study. *The Journal of comparative neurology* 249:392-403.
- Berg A, Zelano J, Thams S, Cullheim S (2013) The extent of synaptic stripping of motoneurons after axotomy is not correlated to activation of surrounding glia or downregulation of postsynaptic adhesion molecules. *PLoS one* 8:e59647.
- Berg A, Zelano J, Stephan A, Thams S, Barres BA, Pekny M, Pekna M, Cullheim S (2012) Reduced removal of synaptic terminals from axotomized spinal motoneurons in the absence of complement C3. *Experimental neurology* 237:8-17.
- Blinzinger K, Kreutzberg G (1968) Displacement of synaptic terminals from regenerating motoneurons by microglial cells. *Zeitschrift für Zellforschung und mikroskopische Anatomie* 85:145-157.
- Coull JA, Boudreau D, Bachand K, Prescott SA, Nault F, Sik A, De Koninck P, De Koninck Y (2003) Trans-synaptic shift in anion gradient in spinal lamina I neurons as a mechanism of neuropathic pain. *Nature* 424:938-942.
- Gomez-Nicola D, Perry VH (2015) Microglial dynamics and role in the healthy and diseased brain: a paradigm of functional plasticity. *The Neuroscientist : a review journal bringing neurobiology, neurology and psychiatry* 21:169-184.
- Gyoneva S, Traynelis SF (2013) Norepinephrine modulates the motility of resting and activated microglia via different adrenergic receptors. *The Journal of biological chemistry* 288:15291-15302.
- Gyoneva S, Swanger SA, Zhang J, Weinshenker D, Traynelis SF (2016) Altered motility of plaque-associated microglia in a model of Alzheimer's disease. *Neuroscience* 330:410-420.
- Gyoneva S, Shapiro L, Lazo C, Garnier-Amblard E, Smith Y, Miller GW, Traynelis SF (2014a) Adenosine A2A receptor antagonism reverses inflammation-induced impairment of microglial process extension in a model of Parkinson's disease. *Neurobiology of disease* 67:191-202.

- Gyoneva S, Davalos D, Biswas D, Swanger SA, Garnier-Amblard E, Loth F, Akassoglou K, Traynelis SF (2014b) Systemic inflammation regulates microglial responses to tissue damage in vivo. *Glia* 62:1345-1360.
- Haynes SE, Hollopeter G, Yang G, Kurpius D, Dailey ME, Gan WB, Julius D (2006) The P2Y₁₂ receptor regulates microglial activation by extracellular nucleotides. *Nature neuroscience* 9:1512-1519.
- Jung S, Aliberti J, Graemmel P, Sunshine MJ, Kreutzberg GW, Sher A, Littman DR (2000) Analysis of fractalkine receptor CX₃CR1 function by targeted deletion and green fluorescent protein reporter gene insertion. *Mol Cell Biol* 20:4106-4114.
- Kettenmann H, Hanisch UK, Noda M, Verkhratsky A (2011) Physiology of microglia. *Physiol Rev* 91:461-553.
- Kreutzberg GW (1996) Microglia: a sensor for pathological events in the CNS. *Trends in neurosciences* 19:312-318.
- Marker DF, Tremblay ME, Lu SM, Majewska AK, Gelbard HA (2010) A thin-skull window technique for chronic two-photon in vivo imaging of murine microglia in models of neuroinflammation. *Journal of visualized experiments : JoVE*.
- Michailidou I, Willems JG, Kooi EJ, van Eden C, Gold SM, Geurts JJ, Baas F, Huitinga I, Ramaglia V (2015) Complement C1q-C3-associated synaptic changes in multiple sclerosis hippocampus. *Annals of neurology* 77:1007-1026.
- Mitra P, Brownstone RM (2012) An in vitro spinal cord slice preparation for recording from lumbar motoneurons of the adult mouse. *Journal of neurophysiology* 107:728-741.
- Morris GP, Clark IA, Zinn R, Vissel B (2013) Microglia: a new frontier for synaptic plasticity, learning and memory, and neurodegenerative disease research. *Neurobiology of learning and memory* 105:40-53.
- Nimmerjahn A, Kirchhoff F, Helmchen F (2005) Resting microglial cells are highly dynamic surveillants of brain parenchyma in vivo. *Science* 308:1314-1318.
- Perry VH, Holmes C (2014) Microglial priming in neurodegenerative disease. *Nature reviews Neurology* 10:217-224.
- Perry VH, Nicoll JA, Holmes C (2010) Microglia in neurodegenerative disease. *Nature reviews Neurology* 6:193-201.
- Schafer DP, Lehrman EK, Kautzman AG, Koyama R, Mardinly AR, Yamasaki R, Ransohoff RM, Greenberg ME, Barres BA, Stevens B (2012) Microglia sculpt postnatal neural circuits in an activity and complement-dependent manner. *Neuron* 74:691-705.
- Svensson M, Aldskogius H (1993) Synaptic density of axotomized hypoglossal motoneurons following pharmacological blockade of the microglial cell proliferation. *Experimental neurology* 120:123-131.
- Tremblay ME, Lowery RL, Majewska AK (2010) Microglial interactions with synapses are modulated by visual experience. *PLoS Biol* 8:e1000527.
- Vasek MJ et al. (2016) A complement-microglial axis drives synapse loss during virus-induced memory impairment. *Nature* 534:538-543.

Wake H, Moorhouse AJ, Jinno S, Kohsaka S, Nabekura J (2009) Resting microglia directly monitor the functional state of synapses in vivo and determine the fate of ischemic terminals. *J Neurosci* 29:3974-3980.